Exploring of the Role of Ionic Liquids and Electrolyte Additives on the Electrochemical Performance of Potassium-Ion Batteries

Tianyi Shi
University College London

Primary Supervisor: Prof. Robert Palgrave
Second Supervisor: Dr. Yang Xu

A thesis submitted to University College London in partial fulfillment of the requirements for the degree of Doctor of Chemistry

November 26, 2024

Declaration

I, *tianyi Shi* confirm that the work presented in my thesis is my own. Where information has been derived from other sources, I confirm that this has been indicated in the thesis

Abstract

This study examines the possibility of potassium-ion batteries (PIBs) as alternatives to lithium-ion batteries (LIBS), with a focus on the effectiveness of ionic liquids as safe electrolytes and as additives to carbonate electrolytes, in comparison to traditional carbonate-based electrolyte designs. The long-term performances of various electrolyte designs are compared to evaluate the reliability of different electrolytes for extended cycling of traditional Graphite anode and 3,4,9,10-perylene-tetracarboxylic-dianhydride (PTCDA) cathode materials. The degradation of a specific electrolyte for a given graphite electrode in potassium-ion batteries is analyzed through capacity failure analysis of the materials and interfaces. The accumulation of the key nanoscale solid-electrolyte interface (SEI) on graphite electrodes is primarily analyzed through surface analysis methods, mainly X-ray Photoelectron Spectroscopy (XPS). Through capacity failure analysis, we can understand the correlation between a stable SEI layer and extended cycling life of graphite in potassium-ion batteries. Furthermore, the electrolytes were tested with the PTCDA electrode to verify the integrity of the electrolyte design. In general, the electrochemical and failure analysis can offer guidelines for selecting suitable electrolytes for to enhance long-term performance of conventional electrodes in potassium-ion batteries

Impact statement

This work primarily focuses on evaluating the feasibility of developing potassium-ion batteries (PIBs) as an alternative to the well-established lithium-ion batteries (LIBs). The potential replacement of LIBs with PIBs could significantly alleviate the issue of lithium resource scarcity, given the abundance and sustainability of potassium on Earth. Moreover, lithium mining often results in considerable water waste, whereas the extraction of potassium is a more environmentally friendly process, making PIBs a more promising technology from both commercial and ecological perspectives.

Since PIBs are still under development, material selection remains a critical area of research. Among available materials, graphite stands out as a commercially viable and environmentally friendly option. The use of graphite electrodes can substantially lower the cost of PIBs compared to other alkali-ion batteries, such as sodium-ion batteries (NIBs), which are incompatible with graphite electrodes. To understand the cycling performance of graphite electrodes, we conducted a capacity failure analysis to investigate the degradation mechanisms of graphite anodes in PIBs. This failure analysis provides valuable insights that can help address the production challenges PIBs may face in future commercial applications.

Another major challenge in developing PIBs is the selection of appropriate electrolytes, which serve as a crucial link between electrode performance and overall battery efficiency. Ionic liquid electrolytes are considered safer than traditional commercial organic electrolytes. In this thesis, we explored the potential of traditional ionic liquid electrolytes and applying ionic liquids as additives in organic carbonate electrolytes to enhance the long-term cycling performance of PIBs, while also ensuring a safer electrolyte design.

Acknowledgement

I would like to express my sincere gratitude to many people who have supported me over the past four years. First and foremost, I want to thank my primary supervisor, Prof. Robert Palgrave, for giving me the opportunity to pursue a PhD in Chemistry, for his guidance, motivation, and scientific assistance throughout my research on interface chemistry. Additionally, I extend my heartfelt thanks to my second supervisor, Dr. Yang Xu, who provided invaluable scientific advice for the electrochemical research aspect of my work. The research journey over these four years has been long, but every challenge has been worthwhile.

I would also like to thank the members of Robert's group, including Tim, Roxanna, Natalie, Yuhan, Prajna, Lana, Firas, Avishek, Lina, Charles, and Gogulan, who provided friendship and useful scientific discussions that helped me navigate various challenges. My gratitude also goes to the members of Yang's group, including Runzhe Wei, Pan He, Yupei Han, Yi Lu, Wanjun Ren, Yudong Luo, Charlie, Harry, and Ajay, who have been supportive colleagues and offered much-needed experimental assistance.

I would like to acknowledge the invaluable support from the staff at the Harwell XPS campus, especially Dr. Mark Isaacs and Dr. Arthur Graf, for their assistance in booking XPS slots and providing technical help, which was instrumental in obtaining the crucial results for this thesis. I am also grateful to Dr. Tim Evans for his insights into ionic liquids and for his assistance with Thermogravimetric Analysis. Furthermore, I am thankful to Dr. Andrew Stewart and Dr. Xueming Xia for providing training in Scanning Electron Microscopy and Transmission Electron Microscopy, as well as to Dr. Jamie Gould for his guidance on X-Ray Diffraction techniques.

Finally, but by no means least, I wish to thank my family—my mum and dad—who have always stood by me during the most challenging times.

Despite being in different countries on opposite ends of the Earth, our hearts have always been connected, especially when facing difficulties. I cannot express enough gratitude to them—they have given me life and helped me navigate through the most difficult paths in my journey.

Acronyms

PIBs Potassium-Ion Batteries

LIBs Lithium-Ion Batteries

NIBs Sodium-Ion Batteries

K Potassium

SEI Solid Electrolyte Interface

CEI Cathode Electrolyte Interface

SEM Scanning Electron Microscopy

XRD X-Ray Diffraction

TEM Transmission Electron Microscopy

XPS X-Ray Photoelectron Spectroscopy

CV Cyclic Voltammetry

EIS Electrochemical Impedance Spectroscopy

GCD Galvanostatic Charge-Discharge

OCV Open Circuit Voltage

FWHM Full-Width at Half-Maximum

BE Binding Energy

PTCDA 3,4,9,10-perylene–tetracarboxylicacid–dianhydride

PVDF Polyvinylidene Fluoride

NMP N-Methyl-2-Pyrrolidone

EC Ethylene Carbonate

PC Propylene Carbonate

DMC Dimethyl Carbonate

DEC Diethyl Carbonate

IL Ionic Liquid

LiFSI Lithium Bis(fluorosulfonyl)imide

LiTFSI Lithium Bis(trifluoromethanesulfonyl)imide

KFSI Potassium Bis(fluorosulfonyl)imide

KTFSI Potassium Bis(trifluoromethanesulfonyl)imide

KPF_6 Potassium Hexafluorophosphate

$Pyr_{13}FSI$ N-Propyl-N-methylpyrrolidinium Bis(fluorosulfonyl)imide

$Pyr_{14}FSI$ N-Butyl-N-methylpyrrolidinium Bis(fluorosulfonyl)imide

$Pyr_{13}TFSI$

N-Propyl-N-methylpyrrolidinium Bis(trifluoromethanesulfonyl)imide

ES Ethylene Sulfite

FEC Fluoroethylene Carbonate

DTD 1,3,2-Dioxathiolane 2,2-Dioxide

Publications

In preparation:

The role of ionic liquid anions for controlling graphite surface electrolyte interphase chemistry in potassium ion batteries. **Tiani Shi**, Avishek Dey, Yuhan Liu, Mark Isaacs, Pan He, Yang Xu, Robert G. Palgrave
This work has been drafted as a manuscript and is intended for submission

Table of Contents

Chapter 1 Introduction, Literature Review and Aims

1.1. Development of PIBs

In recent years, lithium-ion batteries (LIBs) have become the primary energy storage technology for electronics devices and electric vehicles. Commercial lithium-ion batteries offer several key advantages, including high energy density and long cycling life. However, with the growing demand for lithium-ion batteries, concerns have arisen regarding the limited supply of lithium resources, rising costs, and the environmental impact of lithium mining. These challenges have driven the search for more abundant, cost-effective, and environmentally friendly alternative materials. Potassium-ion batteries (PIBs) have become one promising substitute technology for Lithium-ion batteries.[1, 2] Unlike lithium, potassium is abundantly available in the Earth's crust, making it a more cost-effective option for large-scale energy storage applications. This abundance, combined with the high compatibility of potassium ions with carbon-based materials, including graphite, significantly reduces material costs in PIBs. Additionally, potassium metal has a standard redox potential of -2.93 V (versus SHE), which is close to that of lithium metal (-3.04 V). This similarity in redox potential implies that PIBs can achieve relatively high voltage, laying the foundation for competitive energy density.[3]

However, the PIBs are facing a few technical challenges. For instance, the higher ionic radius of the potassium ion (1.4 Å compared with Li ion 0.76 Å) and the its relatively reactive chemical nature of potassium ions can give rise to higher stress accumulation on the electrode material during the continuous insertion/extraction process.[2] The electrode material will experience the significant volume expansion and structural degradation,

the whole battery life will be shortened.[4, 5] In addition, the higher reactivity of potassium metal will enhance the irreversible side reactions, accelerating the decomposition of the electrolytes and forming the more unstable solid electrolyte interface (SEI) with cycles, the entire cycling life is impacted by interface failure on graphite electrodes when traditional electrolytes are used. [1, 6, 7] To achieve stability comparable to that of affordable commercial graphite electrodes in lithium-ion batteries, electrolyte design has been a primary research focus over the years.

To identify an optimal electrolyte design, capacity failure analysis is crucial when comparing PIBs with different electrolytes, especially under extended cycling conditions. Understanding the primary causes of capacity degradation during prolonged cycling is essential. By examining the impact of different electrolytes on the capacity retention of PIBs with commonly used commercial materials, optimized solvent design strategies can be developed. This approach has the potential to enable commercial PIBs with significantly reduced capacity degradation, enhancing their viability for practical applications.

1.2. Common Configuration of PIBs

To understand the crucial role of electrolytes in the cycling of PIBs, it is essential to first examine the coin cell configuration of these batteries. In basic lithium-ion batteries, full cells consist of a current collector, anode, electrolyte, separator, and cathode, with SEI and cathode-electrode interface (CEI) protective layers formed by electrolyte decomposition.[8] The cathode materials are high-voltage materials chosen for their high compatibility with potassium ions. Aluminum foil, valued for its high conductivity and corrosion resistance at high voltage, is chosen as the current collector for cathode materials. The separator in PIBs should

possess high porosity to enable effective potassium-ion diffusion, as well as robust mechanical stability to accommodate the gradual expansion of electrodes and resist potassium dendrite formation, ensuring greater safety. Glass fiber has shown promise in meeting these requirements widely for PIBs.[6, 9-11] Anode materials should have a working voltage similar to the SHE of potassium and exhibit strong structural stability to support the reversible intercalation process. Copper foil, with its excellent low-voltage electrochemical stability, ionic conductivity, and mechanical strength, is an effective current collector for the anode. In addition to the basic materials, electrolytes play a crucial role in connecting the electrode materials and serve as the primary source for the nanoscale SEI for anode materials and CEI for cathode materials, which are formed through electrolyte decomposition.

To verify electrolyte compatibility with a specific target electrode (anode or cathode), the half-cell configuration is commonly used to eliminate interference from the opposite electrode. A metal counter electrode serves as a reference, stabilizing the redox potential to K/K^+ (-2.93 vs.SHE). This design of PIBs offers advantages like stable reference electrodes, simplified operation, and consistent cycling conditions, making half-cells ideal for evaluating the feasibility of promising new materials (figure 1.1). In battery failure analysis, half-cell configurations are useful for assessing key electrochemical parameters such as initial capacity, coulombic efficiency, and cycling stability of a specific electrode. For a targeted electrolyte design, direct cycling performance can reveal the electrolyte's long-term compatibility with a specific electrode over extended cycles. Material failure analysis can be conducted at specific cycles, particularly when significant capacity fluctuations along with SEI/CEI interfacial changes and material deterioration happen. This approach enables us to assess whether a given electrolyte design can meet the requirements for

the safe stable cycling performances, based on the view of the interfacial chemistry.

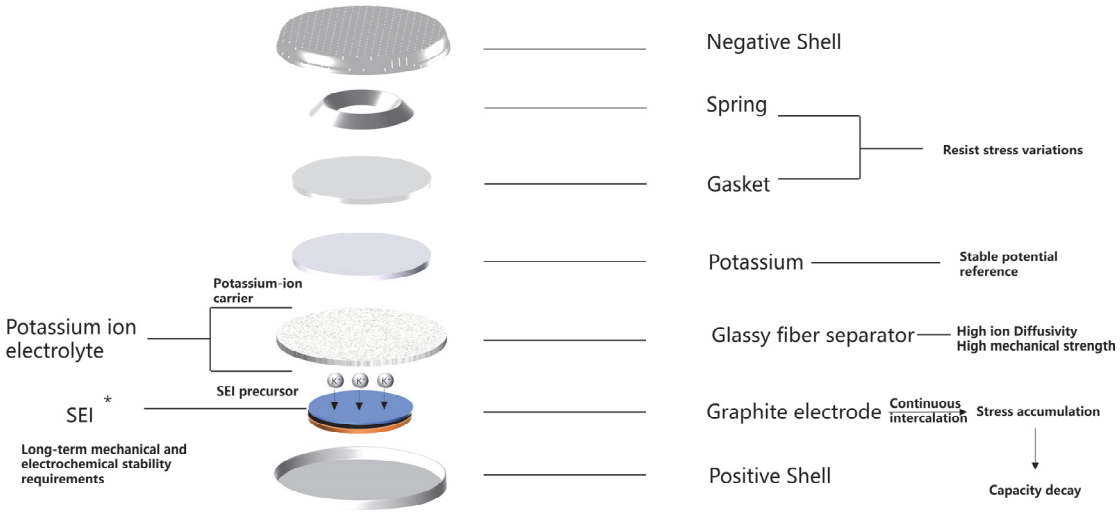

Figure 1.1. The configuration of potassium half-cells for one promising electrolyte for graphite electrodes in PIBs.

1.3. Development of Electrodes for PIBs

1.3.1. Conventional Anode electrodes for PIBs

The development of electrodes for PIBs presents several key challenges. As previously noted, the larger ionic radius of potassium can lead to significant lattice expansion and thus stress accumulation. During extended cycling, stress accumulation increases mechanical strain and challenges the elasticity of anode electrodes, often leading to capacity degradation in PIBs. Anode materials face a risk of capacity failure in PIBs unless optimized.[1, 4] Therefore, the primary criterion for anode materials is to maintain the long-term cycling stability. Carbon-based anode materials hold great potential for PIBs due to their excellent conductivity and structural stability. These qualities make carbon materials a preferred

choice for anodes in lithium-ion, sodium-ion, and PIBs. As the most mature carbon materials, the graphite electrodes are known for the outstanding properties, low cost and complete production process. Although there are large hindrances of the potassium intercalation behavior, the strong K-C bond and adaptability of the interlayer spacing of the graphite provide the possibility of the intercalation behavior of potassium ions into the graphite interlayer[12], provide the high theoretical capacity of 279 mAh/g for fully intercalated KC_8.[1, 5] However, the intercalation process of potassium ions into the graphite layer can cause the large interlayer expansion. The interlayer distance of fresh graphite is 3.35 Å, which increases to 5.35 Å upon complete intercalation of KC_8, which is significantly larger than that of lithiated LiC_6 (3.706 Å).[5] The greater intercalation distance leads to increased stress accumulation, which contributes to intrinsic changes affecting interfacial and graphite material stability during prolonged cycling.[13] To develop the graphite electrodes into commercial electrodes for PIBs, the capacity decay of the graphite electrodes needs to be reduced. Since graphite was introduced as an anode material for PIBs in 2015, capacity decay has been significantly greater with conventional carbonate electrolytes than in typical lithium-ion batteries.[1, 2] The failure of carbonate electrolytes is intensified under extended cycling and high current conditions for natural graphite electrodes.[4-6, 14] When selecting electrolytes, it is crucial to enable efficient intercalation and deintercalation of potassium ions into the graphite electrode layers for long cycles. When there is no capacity failure behavior, the high reversible intercalation process from 0.4V to 0.01V ($C \rightarrow KC_{36} \rightarrow KC_{24} \rightarrow KC_8$) of potassium-ion into the graphite electrode can be maintained normally at low current of the initial cycles.[1] In previous research, the rate capability and cycling stability have been significantly limited with traditional carbonate electrolytes. Polarization behavior at 0.1 V during the KC_8 formation process, arising from capacity

failure, leads to an incomplete intercalation process that worsens with extended cycling. [1, 2]To deal with the capacity decay problems for long cycles, the solvent-design work is always viewed as the most vital part to maintain the long cycling life of the graphite electrodes. In order to the provide guidelines

for the solvent design, there is a need to focus not only on the initial cycle performance but place greater emphasis on long-term cycling stability, as maintaining extended cycling stability is essential for the electrochemically active PIBs.

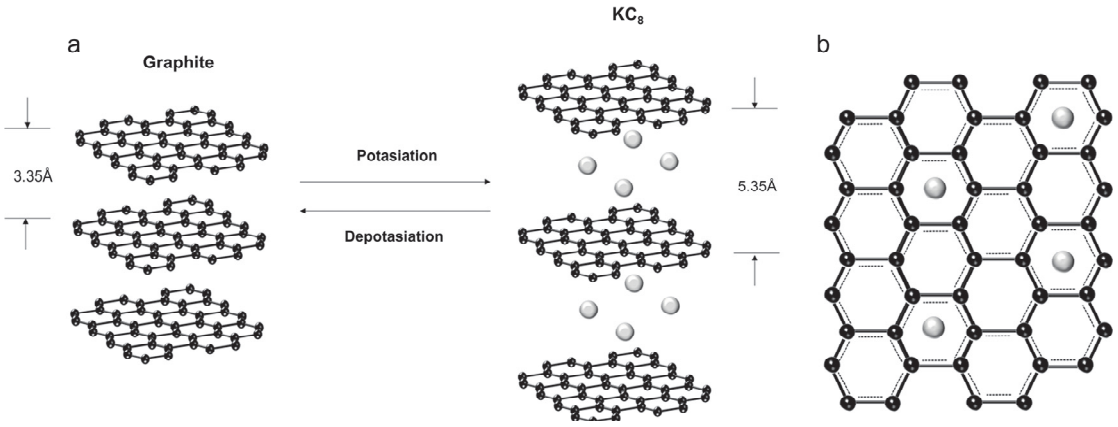

Figure 1.2. (a) A diagram illustrating the potassiation/depotassiation process of graphite, highlighting its theoretical capacity of 279 mAh/g, along with the significant interlayer expansion from 3.35 Å to 5.35 Å.(b) diagram of the in-plane pattern of KC_8.[5]

1.3.2. Conventional Cathode Electrodes for PIBs

Contrary to the almost universal use of graphite electrodes in PIBs, the selection of the cathode materials is quite competitive. Prussian-blue cathodes[15], layered oxide materials[16], PTCDA organic electrodes[17] are widely analyzed for promising materials. Compared to other cathode materials, PTCDA electrodes offer a low-cost, environmentally friendly

option with excellent flexibility and adjustability. The mature production technology of the PTCDA electrode makes it become the most traditional electrode in PIBs. To assess the feasibility of an electrolyte, PTCDA electrodes serve as a fundamental base, functioning as traditional high-voltage electrodes. [1, 7, 17, 18] Although solvent-regulation methods have been employed to improve PTCDA/graphite full cells, failure surface analysis of specific electrolytes for PTCDA electrodes is less emphasized compared to graphite electrodes.[19, 20] The failure analysis is limited by the more complex additional PTCDA dissolution phenomenon into the electrolytes, which will increase the difficulty of analysis of the material failure.[21, 22] In addition, the capacity of PTCDA electrodes in carbonate electrolytes may be reduced due to the combined effects of an unstable CEI and significant dissolution.[23] To meet the stability requirements of PTCDA electrodes, a suitable electrolyte design is essential to enhance the performance of both PTCDA and graphite electrodes. Cycling PTCDA electrodes alongside graphite electrodes can provide a more comprehensive understanding of failure mechanisms in PIBs.

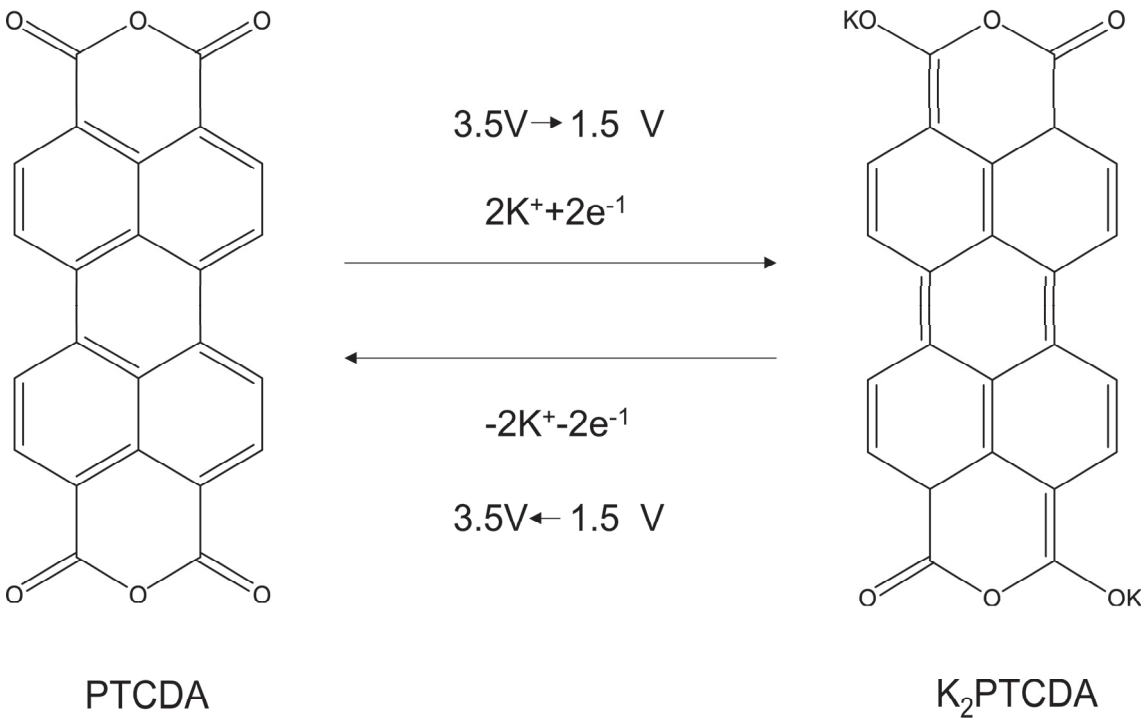

Figure 1.3. (a) The electrochemical reaction mechanism of the PTCDA electrodes as cathodes in PIBs with the theoretical capacity of 131mAh/g.[17]

1.4. Development of Electrolytes for PIBs

Since the early studies on PIBs, electrolytes have played a crucial role in overall cycling performance. Given the prominent role of graphite electrodes in PIBs, ensuring the cycling stability of specific electrolytes is essential. Given the greater volume expansion of commercial graphite electrodes in PIBs compared with LIBs, electrolytes must be specifically designed to meet the higher performance requirements of these systems. To adapt conventional carbonate electrolytes for commercial use in PIBs, various electrolyte design strategies have been developed with a focus on optimizing performance for graphite electrodes.

1.4.1. Conventional Carbonate Electrolytes for Potassium Ion Batteries

To tolerate the long-term drastic volume expansion, suitable SEI layers with much better mechanical stability and chemical stability are necessary to the long-term cycling life. This requirement implies that electrolyte formulations suitable for lithium-ion batteries may not be directly applicable to PIBs. As noted earlier, the instability of conventional carbonate electrolytes contributes to the failure of graphite electrodes in PIBs.[1, 5, 6]

In lithium-ion batteries, EC, PC, DEC, DMC carbonate organic electrolytes are achieving good electrochemical stability, good lithium-ion solubility and mature commercial use. The application of carbonates can be enhanced by blending electrolytes to modify viscosity and improve low-temperature performance.[24]

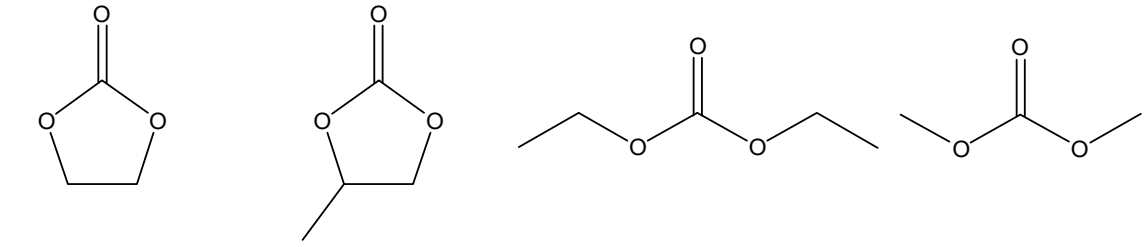

Ethylene carbonate **EC** | **Propylene carbonate** **PC** | **Diethyl carbonate** **DEC** | **Dimethyl carbonate** **DMC**

Figure 1.4. Common carbonate solvent used in alkali-ion batteries.

To improve conventional carbonate electrolytes in PIBs, understanding their decomposition process is essential. In lithium-ion batteries, the high-voltage stability of carbonate electrolytes helps form a uniform and dense SEI layer during lithium intercalation into the graphite layers.

EC-containing carbonates are considered effective for improving SEI stability. Notably, the ECPC electrolyte in a 1:1 volume ratio is recognized for its high oxidative stability and excellent low-temperature performance. The decomposition process of ECPC serves as a fundamental example of carbonate electrolyte decomposition. In standard ECPC organic electrolytes, the decomposition of ECPC primarily generates larger organic decomposition products like $(CH_2OCO_2K)_2$, K_2CO_3 and C_2H_4. C_2H_4 which

are thought of as unstable species among the SEI layers in LIBs. They can be the further decomposed into alkane species during extended cycling and then ruin the SEI structure. In addition, the evolution of C_2H_4 gas can cause the battery swelling phenomenon, thus give rise to the safety problems when the cycling is long. Thus, ECPC decomposition inherently produces unstable organic decomposition products into the SEI layers. The decomposition mechanism of typical carbonate solvents, such as EC and PC, during initial reduction to form SEI layers:[24, 25]

Decomposition mechanisms of EC:

$$2(CH_2O)_2CO+2K^++2e^-\rightarrow(CH_2OCO_2K)_2+C_2H_4 \quad (1)$$

$$2(CH_2O)_2CO+2K^++2e^-\rightarrow K_2CO_3+C_2H_4 \quad (2)$$

Decomposition mechanisms of PC:

$$CH_3CHCH_2OCOO +2K^++2e^- \rightarrow CH_3CH(OCO_2K)CH_2OCO_2K+ CH_3CH=CH_2 \quad (3)$$

$$CH_3CHCH_2OCOO+2K^++2e^-\rightarrow K_2CO_3+CH_3CH=CH_2 \quad (4)$$

Given the challenges with carbonate electrolytes, ether-based electrolytes have been tested in PIBs but still show capacity decay with low capacity when salts are used at typical commercial concentrations (≤1.0 M).[6, 26] The additional observed co-intercalation issues in ether-based electrolytes necessitate either high salt concentrations[27-29] or specific solvent designs[9, 30] to mitigate co-intercalation behavior. In PIBs, the control of co-intercalation behavior has increased research interest in carbonate electrolytes within the field of organic electrolytes.

Typical stable SEI layers which are electrochemically stable and ion conductive, are normally composed of organic-inorganic mixed species.[31] The inorganic-rich SEI layers have been proved as the key features for long-term cycling stability for carbon materials in PIBs.[10, 11, 32] Lack of

inorganic species can give rise to a few unaccepted outcomes like poor ion conductivity, fragile mechanical stability, weak electrochemical and chemical stability to the SEI layers. To increase the inorganic content in SEI layers of specific carbonate electrolytes, classic techniques like salt regulation and additive incorporation are used to modify SEI composition.[24] The primary aim is to artificially transform the SEI layer to contain more inorganic species, thereby enhancing the overall cycling performance of graphite electrodes.

1.4.2. Conventional Potassium Salts for PIBs

To enhance the stability of SEI layers, researchers are attempting to regulate the inorganic species within the layers by modifying the types of salts used. In common electrolyte design strategies, the salts are important constituent parts to adjust the inorganic salts in the SEI layer. The most commonly used salt is $LiPF_6$, which is widely employed in lithium-ion batteries.[33-35] The high oxidative stability of PF_6^- up to 5.1 V ensures its stability with high-voltage cathode materials.[36, 37] Due to its high voltage stability, its decomposition at low voltage to form the SEI on graphite electrodes is mainly analyzed. The decomposition of PF_6^- mainly can produce the inorganic decomposition species, involving POx and the LiF. In PIBs, the formation of salts can be undertaken with the same procedure.[24] Thus, the decomposition of KF and KPO_x^- can be the most possible decomposition products in PIBs. However, the PF_6^-can be chemical unreactive at high temperature to produce PF5- and further react with the H_2O to produce high acidic HF, which can corrode the electrode materials.[38] For PIBs, KPF_6 was initially considered a promising salt when graphite was first used as an electrode in PIBs.[1, 2] However, it was viewed

to be a poor choice, as severe capacity degradation occurs with standard carbonate electrolytes. The unstable SEIs formed by KPF_6 in carbonate electrolytes, which fail to accommodate long-term volume changes, are considered the primary cause of capacity degradation.[6] Therefore, to accommodate the significant volume changes of graphite electrodes during cycling, conventional PF_6^- additives are insufficient to meet the demands of long-term cycling in PIBs. Researchers are exploring fluorine-containing alternative salts to help design SEI layers with more stable inorganic species. Fluorosulfonyl salts, such as Bis(fluorosulfonyl)imide **(**FSI) and bis(trifluoromethanesulfonyl)imide (TFSI) are used in PIBs to promote the formation of more stable inorganic species within the SEI on graphite electrodes.[39] This design of salts come from the promising LiFSI and LiTFSI salts for graphite stablizing in Lithium-ion industry.

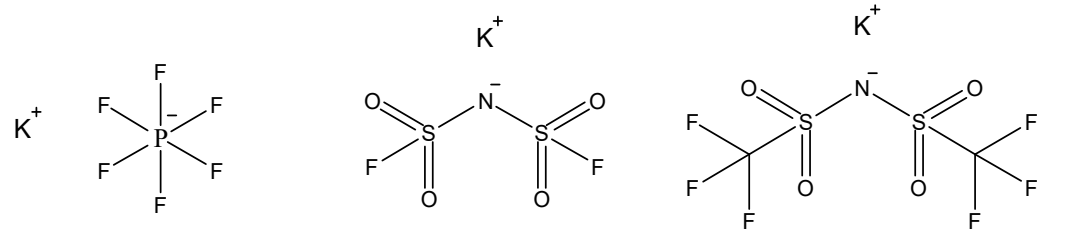

Figure 1.5. Common fluorine-containing salts in PIBs.

The decomposition of the FSI and TFSI anions can produce sulfide salts and fluorine salts. The primary difference between FSI and TFSI salts lies in their inorganic decomposition products, which can be explained by their distinct decomposition mechanisms. The decomposition processes of FSI (Eq.5) and TFSI (Eq.6-8) anions reveal significant differences in the inorganic species produced by each anion at low voltage:[40]

Decomposition mechanisms of FSI anion

$KN(SO_2F)_2+4K^++4e^-\rightarrow KSO_2N(K)SO_2K+2KF$ (5)

Decomposition mechanisms of TFSI anion

$KN(SO_2CF_3)_2+6e^-+6K^+\rightarrow K_3N+K_2S_2O_4+KF+C_2F_5K$ (6)

$K_2S_2O_4+4e^-+4K^+\rightarrow K_2SO_3+K_2S+K_2O$ (7)

$KN(SO_2CF_3)_2+e^-+K^+\rightarrow KNCF_3SO_2+CF_3SO_2K$ (8)

This difference in inorganic species give rise to different potassium intercalation process. As some of the most promising salts, KFSI combined with KTFSI is used at varying concentrations in different organic electrolytes for graphite electrodes in PIBs. KFSI-based salts achieve higher capacity performance and better retention compared to KTFSI-based salts and KPF_6.[39, 41] The plating process of KFSI salts is more efficient due to the stable SEI formed on potassium metal, compared to common KFSI and KTFSI salts.[42]

Although KFSI is widely used as an SEI-stabilizing salt, the typical concentration (1.0 M) of KFSI in carbonate electrolytes fails to form stable SEI layers necessary for long-term cycling.[14, 22, 43, 44] The common concentration in lithium-ion batteries cannot meet the high cycling stability requirements in PIBs. Thus, KFSI salts in organic electrolytes for PIBs are adjusted to high concentrations to enhance the stability of SEI layers. In order to control the organic species of the SEI layer, the high concentration salts are viewed as the promising methods for organic electrolytes in PIBs.[10, 45] Particularly, high-concentration KFSI in EC:EMC carbonate electrolyte is utilized in PIBs to create an inorganic-rich SEI layer, enhancing the long-term cycling stability of graphite electrodes at C/3 (C = 279 mA/g). The results reveal a correlation between the FSI-dominated environment and the development of a more inorganic SEI layer, which is crucial for stable, extended cycling performance.[11] While increasing salt concentration can help stabilize SEI layers over long cycles, it is often

considered wasteful and significantly raises costs, creating challenges for industrial applications of these electrolytes. In addition, the reduced amount of free solvent increases viscosity in carbonates, which slows ion diffusion and can lead to uneven distribution of ions on graphite electrodes.[46, 47] This may, in certain cases, cause partial failure of the graphite electrodes. For these reasons, various solvent regulation strategies should be considered to optimize electrolytes in PIBs for graphite electrodes.

1.4.3. Ionic liquid Electrolytes for PIBs

Due to the limitations of common carbonate electrolytes, researchers are exploring nonflammable electrolytes that promote stable SEI layers to ensure the long-term stability and safety of graphite electrodes in PIBs.
Ionic liquids solvent with high chemical stability have gained significant attention from researchers. Ionic liquids, composed of cations and anions, remain in a liquid state at room temperature. The delocalized structures of low-symmetry cations and anions with large volume hinder ion packing, reduce Coulombic forces between ions, and consequently lower the melting points of ionic liquids.[48] Low-symmetry ionic liquid cations, such as non-aromatic and aromatic azacycles, with a focus on pyrrolidinium and imidazolium salts, are primarily chosen for use in PIBs.[49-51] The non-aromatic pyrrolidinium cation stands out among cations for its thermal stability, high ionic conductivity, and strong electrochemical stability at high voltages, as well as its ability to form a stable SEI layer.[49] These advantages make pyrrolidinium cations the most popular choice for ionic liquid electrolytes in PIBs. Pyrrolidinium-based ionic liquid electrolytes with KFSI salts show potential for achieving stable SEI layers on graphite electrodes during cycling.[15, 43, 52] When we consider the SEI layers formed

by the ionic liquid electrolytes, the SEI layers formed is believed to be the anion-derived SEI layers covered on the graphite electrodes. The specific feature is answered by the unique solvation structure of potassium ions in the ionic liquid electrolytes with anion-dominating environment.

The structure of ionic liquid cations can be designed by adjusting the length of flexible carbon chains attached to the cation main group, allowing for specific physical property requirements in various applications. In ionic liquid electrolytes, the carbon chain length of the cations should be shorter to reduce van der Waals forces and steric hindrance between molecules, thereby lowering viscosity.[48] Due to these factors, N-Propyl-N-methylpyrrolidinium cation (Pyr_{13}^+) has become the traditional choice for achieving both low viscosity and cycling stability. In addition to cations, the choice of anions in ionic liquid electrolytes is crucial for maintaining the cycling stability of the SEI. Among the options, the fluoride-based anions TFSI and FSI are commonly selected as promising choices for ionic liquid electrolytes due to their strong potential to form the stable SEI layers.

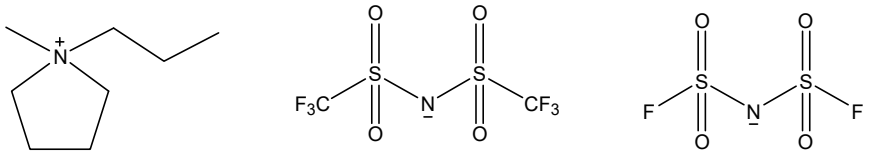

Figure 1.6. Promising pyrrolidinium cation and fluorosulfonyl anions of ionic liquids for electrolyte designs in PIBs.

The anion-derived SEI layers formed by ionic liquids significantly impact cycling stability, making anion selection crucial. Since the initial use of KFSI/[Pyr_{13}]FSI ionic liquid electrolytes in PIBs, FSI-based pyrrolidinium ionic liquid electrolytes have been regarded as promising alternatives to conventional carbonate electrolytes.[15, 43, 53] In contrast, TFSI-based pure

ionic liquid electrolytes are considered poor electrolytes for graphite electrodes.[54, 55] The chemical reasons behind these opposite behaviors are still not well understood, the decomposition pathway of one specific ionic liquid electrolyte become one large barrier. For example, with pyrrolidinium cations, decomposition is closely associated with carbon radicals, which can further react with sulfides and fluorides to produce organic-based decomposition products.[56, 57]Due to the high activity and fast reaction rate of radicals, the decomposition products of radicals are flexible and uncertain. Contrary to the well-defined $CH_2OCO_2^-$and CO_3^{2-} decomposition species from the carbonate electrolytes, there is not one definite product of the cations of ionic liquids based on the clear mechanistic study. In addition, whether the predicted decomposition products SEI layers formed by the ionic liquid electrolytes can be easily dissolved is also not understood. The unclear research makes the failure analysis of the SEI layers very important for pyrrolidinium ionic liquids electrolytes in PIBs.

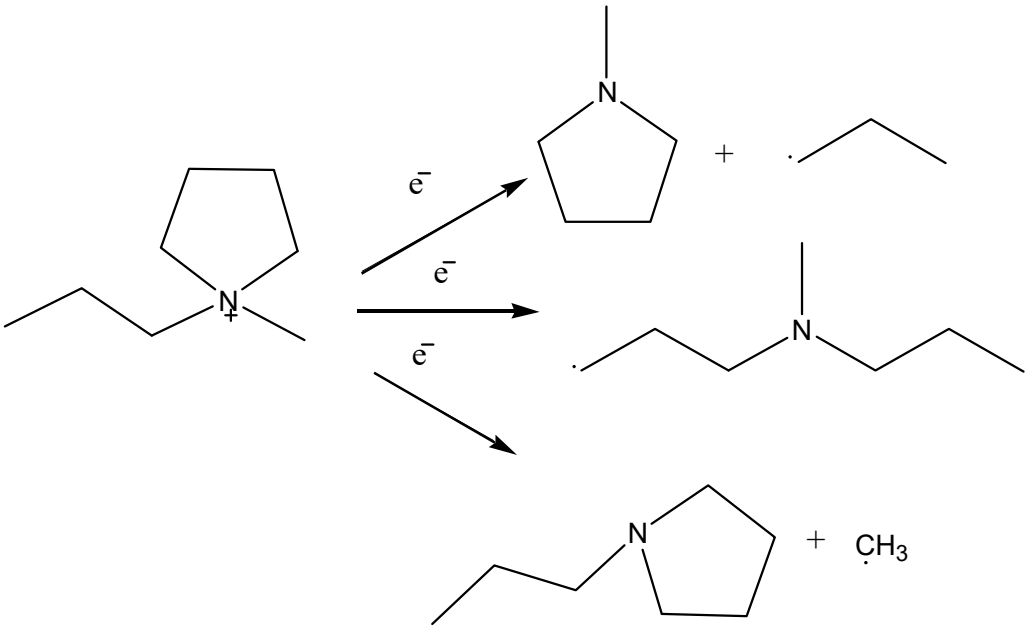

Figure 1.7. The decomposition mechanism of the pyrrolidinium cations into carbon radical**[56].**

Although the exact compounds in SEI layers from ionic liquid electrolytes cannot be precisely identified, the decomposition products can still be modified. Given the characteristics of anion-derived SEI layers, the SEI structure can be tailored through different anion selection strategies.[58] A similar approach has been applied in lithium-ion batteries, where LiFSI salts are added to Pyr_{14}TFSI ionic liquid to address the capacity failure issues of LiTFSI/Pyr_{14}TFSI electrolytes.[59] This strategy, known as "mixed-anion ionic liquid electrolytes," has proven effective in lithium-ion and sodium-ion batteries to achieve both the advantages of FSI and TFSI anions.[58, 60, 61] In this context, KFSI salts can also serve as stabilizers in Pyr_{13}TFSI, helping to enhance SEI stability and enable long-term cycling of graphite electrodes.

Understanding the SEI differences among the pure FSI ionic liquid, mixed-anion ionic liquid, and pure TFSI ionic liquid electrolytes in PIBs is essential for analyzing the complex anion-derived SEI layers formed by ionic liquid electrolytes. Due to the challenges in SEI analysis, analyzing the impact of mixed-anions on the surface chemistry of graphite electrodes remains a significant challenge. There is currently a gap in failure analysis regarding SEI layers formed by ionic liquids with different anions. Therefore, detailed surface analysis of graphite electrodes cycled with ionic liquid electrolytes containing various anions will be a central focus in addressing capacity failure in this thesis.

1.4.4. Electrolyte Additives for PIBs

Past research clearly indicates that conventional KFSI in carbonate electrolytes is unsuitable for graphite electrodes in PIBs. To address electrolyte design challenges, in addition to conventional salt regulation and ionic liquid modifications for enhancing SEI layers on graphite

electrodes, electrolyte additives are frequently used to adjust the inorganic composition within SEI layers. Electrolyte additives that preferentially decompose during the initial intercalation process of graphite electrodes can promote the formation of dense inorganic species within SEI layers.[62] In specific organic LIB electrolytes, fluorine-based and sulfur-based additives are commonly used to modify the SEI layers on graphite electrodes. However, the differences between potassium-ion and lithium-ion drive the different outcomes of additives against long cycling.

Fluoroethylene carbonate (FEC), a traditional cyclic electrolyte additive, is widely used commercially in lithium-ion batteries.[63-65] The commonly used fluorine-based additive FEC promotes the formation of carbon species, increasing the amount of stable Li_2CO_3 and LiF, which shifts the SEI layer composition towards more inorganic content and enhances its stability.[66] However, the capacity failure behavior of 5 wt% FEC in KFSI/ECPC electrolytes has been confirmed for graphite electrodes in PIBs[67, 68]. The findings indicate that differences in dielectric constants between KF, K_2CO_3 and LiF, Li_2CO_3 suggest that the effectiveness of FEC in lithium-ion batteries may not translate to PIBs.[69] The concentration of FEC must be carefully optimized to enhance SEI stability on graphite electrodes, as excess FEC decomposition can hinder the long-term cycling stability of these electrodes. The failure of FEC in KIBs highlights an important indication of the differing decomposition mechanisms of electrolyte additives in PIBs compared to LiBs.

In addition to fluorine-containing additives, researchers are exploring sulfur-containing electrolyte additives to improve graphite electrode performance in PIBs. Similar to FEC, the cyclic additives ethylene sulfite (ES) and 13,2-dioxathiolane 2,2-dioxide (DTD) are considered highly effective for graphite electrodes in lithium-ion batteries.[70-72] The main decomposition products of sulfur-containing additives can be the $LiSO_3$ and

LiS_x sulfides, which can both increase the chemical and mechanical stability of SEI layers. Due to their combined advantages, sulfur-containing electrolyte additives are being further explored in PIBs. DTD additives have been shown to effectively enhance the cycling stability of graphite at low concentrations of 0.2%.[44] This research further underscores the importance of optimizing electrolyte additive concentrations for SEI stability. While stable performance can be achieved at low concentrations, an overly low concentration of additives may lead to capacity failure under high-mass loading and extended cycling conditions.[62] In addition to DTD additives, 2% ES has been shown to be effective in KTFSI/Pyr_{14}TFSI ionic liquid electrolytes for enhancing the cycling stability of SEI layers on graphite electrodes.[54] However, the absence of surface analysis on SEI layers modified by ES additives prevents a clear understanding of the primary working mechanism of ES additives for graphite electrodes in PIBs. Additionally, the use of ES additives has so far been limited to organic electrolytes in PIBs. The lack of studies on ES in carbonate electrolytes highlights the need to investigate the modification effects of ES in specific carbonate-based electrolytes in this thesis.

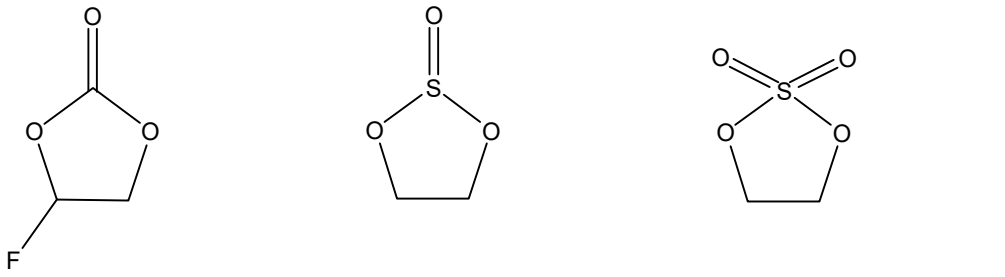

Figure 1.8. Common fluorine containing and sulfur containing cyclic additives in PIBs.

Although common electrolyte additives are widely used for graphite in PIBs, their concentrations should be carefully optimized to support long-term

cycling in full cells. Small amounts of additives may not sustain the long-term stability of the SEI on graphite electrodes, particularly with high mass loading during extended cycling. Conversely, an excess of additives can compromise SEI stability and pose safety risks to cathode materials due to high voltage and temperature decomposition. Measuring the decomposition products, particularly gases, of commercial electrolyte additives presents significant challenges in the industry. These issues have been well-documented and analyzed in lithium-ion batteries.[62, 73, 74] Therefore, for the highly reactive potassium dendrites, greater attention must be given to the drawbacks of common electrolyte additives. To solve with this issue, ionic liquids are considered promising alternatives to conventional electrolyte additives. As described above, ionic liquids offer advantages such as a wide voltage window, high thermal stability, low volatility, and the ability to form stable SEI layers. These properties have made KFSI/[Pyr_{13}]FSI a safe and stable electrolyte choice for PIBs.[15, 43, 53] The effectiveness of ionic liquids as additives has been demonstrated in LiBs.[75-78] The addition of Pyr_{13}FSI does not pose the same risks as common electrolyte additives, and the safe pyrrolidinium-based ionic liquid shows promise as an electrolyte additive that can support the long-term cycling of PIBs without introducing significant issues. Its high solubility in carbonate electrolytes allows for flexible design, including increased powder to enhance fire resistance. Although ionic liquids show significant potential as electrolyte additives, studies on their use in carbonate electrolytes for PIBs remain limited. The differences in SEI modification affecting cycling stability of graphite electrodes in PIBs between ionic liquid additives and conventional additives like FEC and ES are not yet fully understood.

To establish effective methods for electrolyte modification, capacity failure analysis must be conducted on the surface of graphite electrodes after

extended cycling. A comprehensive capacity failure analysis of carbon electrodes in PIBs, using a targeted electrolyte design method based on additives, is conducted to understand the benefits of additives on electrolytes.[44, 67, 68, 79] These efforts can effectively determine the suitability of specific electrolyte additive designs by focusing on the interfacial chemistry of the SEI layer, which significantly impacts the cycling stability of carbon materials. Based on previous research, capacity failure analysis is crucial for evaluating promising additive approaches, particularly those using ionic liquids in PIBs.

1.5. Capacity Failure Analysis of Electrolyte Designs for PIBs

In electrolyte design for PIBs, significant effort is focused on graphite electrodes due to the strong impact of electrolytes on their cycling stability.[6, 7, 9, 80] In general, the capacity failure reasons can be arisen by the interfacial evolution and the material deterioration. In long-term failure analysis of PIBs, significant capacity decline often results from the combined effects of prolonged polarization phenomenon. Activation polarization is the extra voltage loss at the electrode-electrolyte interface, caused by a limited electron transfer rate in the interfaces and slow reaction kinetics in the electrode materials. Activation polarization plays a crucial role in cycling performance, especially at higher cell currents and when rapid electrochemical behavior is required.[24, 81] Concentration polarization is the voltage loss that occurs when ion diffusion in the electrolyte fails to counteract the concentration gradient generated by electron reactions. Concentration polarization is primarily governed by the ion diffusion rate in the electrolyte, which can be compromised during high-rate operation and prolonged cycling due to the consumption of active species.[82] Thus,

Concentration polarization affects cell performance in rapid high-rate applications and degrades long-term cycling stability. [38] In addition, ohmic polarization refers to the voltage loss caused by the intrinsic resistance of the electrolyte, electrode, connecting components, and SEI. It is an unavoidable loss during cycling and becomes more pronounced as long-term use increases interface resistance, ultimately impacting capacity.[83]
In general, interfacial evolution and material degradation are the primary drivers behind variations in these polarization phenomena. For a comprehensive failure analysis, researchers consistently cycle potassium-ion battery cells at a fixed, low current to minimize variations in current diffusion. [6, 67, 80, 84] Effective capacity failure analysis involves identifying the primary drivers of interfacial degradation and conducting targeted material characterization to address the causes of capacity decay.[85] In an ideal scenario, the primary cause of degradation should be identified to inform effective electrolyte design.

1.5.1. Interfacial Analysis of SEI Layer on Graphite Electrodes for PIBs

Capacity decay in PIBs often results from interfacial failure. In most cases, increased interfacial failure is closely linked to improper SEI layer accumulation during cycling, which increases polarization and then reduces capacity. For cells with capacity failure outcome in graphite electrodes in PIBs, detailed interfacial analysis of SEI accumulation is performed to gain a deeper understanding of the decay reasons.[6, 67] Interfacial analysis is also conducted to understand how electrolyte optimization improves the interfaces on graphite electrodes.[7, 9, 22, 80, 84]
Although the primary formation of the SEI layer is thought to complete after

the initial cycles, the SEI layer continues to evolve with each cycle, particularly during extended cycling.

When the coin cells are undergoing long cycles, the nano-scale SEI layer will experience the partly dissolution/formation, the interface impedance will vary, increasing or decreasing based on changes in the SEI layers. Monitoring subtle changes in SEI layers is essential for addressing capacity failure due to interfacial decay.[86] Typically, the Galvanostatic Charge-Discharge (GCD) constant current test is used to assess gradual ohmic (mainly SEI) polarization, with a low, fixed current applied to minimize changed concentration and activation polarization. This constant current test is the most common method for evaluating electrolyte performance, as it allows clear observation of interfacial decay through capacity variation over cycles. By linking interfacial analysis to actual cycling tests, the study provides a more specific understanding of electrolyte behavior in long-term cycling.

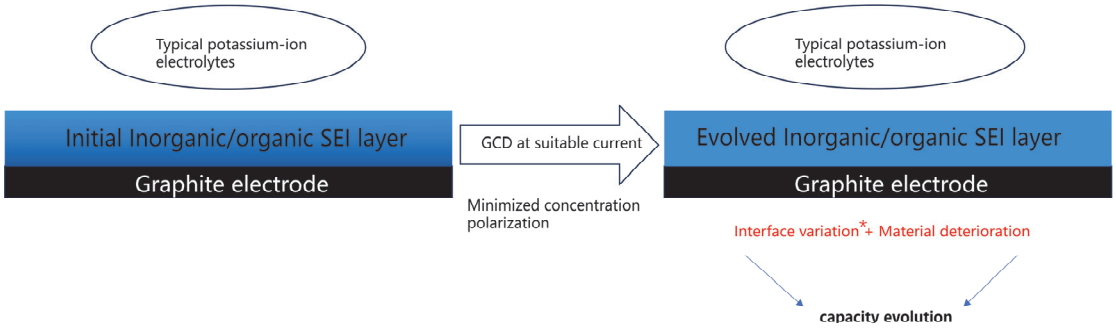

Figure 1.9. The evolution process of SEI layer during long-term cycling.

Interfacial analysis is essential for understanding capacity failure in graphite electrodes. To advance in this area, researchers are exploring suitable methods to detect changes in the decomposition products within the SEI layer. However, SEI layers are highly complex inorganic/organic nanoscale thin films, requiring a more accurate, surface-sensitive, and non-destructive technique to comprehensively characterize them. Previous

analyses of fluorinated electrolytes suggest that the SEI layer in potassium-ion batteries is a mixture of inorganic and organic species. The organic components, originating from both ionic liquids and carbonates, are believed to include K_2CO_3, $ROCO_2K$, ROK, as well as various organic oligomers (PEO, -$(CH_2CH_2O)_n$-) and polymers.[6, 7, 9, 87, 88] Due to the inherent complexity of the SEI layer, its precise composition remains elusive, and most research focuses on whether it preferentially forms specific compounds. For instance, ether-derived oligomers are considered to offer excellent mechanical stability, attributed to the elasticity of their O–K edge groups.[38, 87, 88] Thus, the SEI layer, preferred over ether derived oligomers, is considered to exhibit this property. Among bis(sulfonyl)imide (FSI^-, $TFSI^-$) anion-based electrolytes, sulfide and fluoride compounds are the primary inorganic species. Notably, SO_3^{2-} and K_2S—originating from the (S=O)–N bond—are recognized as stable decomposition products.[10, 89] In addition to sulfide species, KF plays a significant role in the SEI layer due to its lower dielectric constant (39% lower than LiF) and its relatively low ionic conductivity, which serves as a benchmark for the SEI's ionic conductivity.[69]
In summary, the SEI layer formed in PIBs using bis(sulfonyl)imide-based ionic liquids and organic electrolytes is composed of K_2CO_3, $ROCO_2K$, ROK organic oligomers, other organic polymers, K_2SO_3, K_2S, KF, and minor residual electrolyte species. The predominance of any specific compound critically influences the final properties of the SEI layer. Therefore, accurate qualitative and quantitative characterizations are essential for understanding these compositional preferences.
Such a technique should capture the full spectrum of decomposition product variations within the SEI layers. Common morphology analysis techniques, such as SEM and AFM, cannot provide elemental analysis of the SEI layer. Quantitative analysis with TEM is challenging due to difficulties in obtaining high-resolution images without causing minor

surface damage. Additionally, while ToF-SIMS can perform elemental analysis, it often induces surface damage and valence changes due to ion beam impact. Raman spectroscopy also struggles to detect inorganic-organic mixed SEI layers on graphite electrodes due to its low sensitivity to inorganic species.[90, 91]

Given these requirements, X-ray Photoelectron Spectroscopy (XPS) is the most suitable technique for analyzing nanoscale SEI layers under the inert atmosphere. XPS is a well-established and powerful surface analysis technique that provides detailed qualitative and quantitative chemical information about the SEI layer on the electrode surface. This characteristic makes XPS analysis highly effective for detecting comprehensive changes in the SEI layer, including any minor species accumulation. The investigation depth of XPS analysis is between 1 nm to 10 nm, especially suitable for the analysis of the nanoscale SEI layers.[92] To increase the detection depth, additional Ar- ion etching can be used to analyze deeper layers of the SEI, which is particularly important for SEI structures with an organic-rich outer layer and an inorganic-rich inner layer in PIBs. Furthermore, XPS analysis can preserve the surface information of the SEI layer using a specialized air-free transfer holder to the machine. This inert transfer and operational environment are especially crucial for analyzing the air-sensitive SEI layer, in order to achieve with conventional characterization methods.[93, 94]

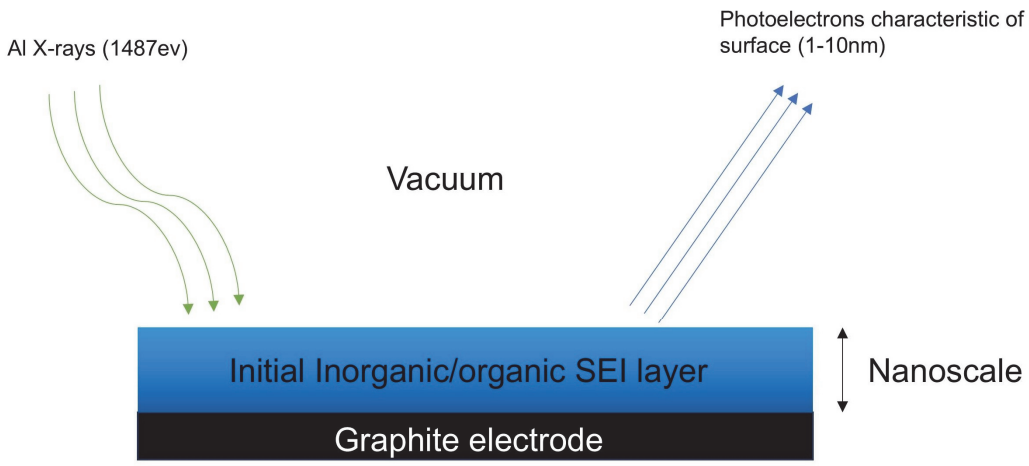

Figure 1.10. The working mechanism of XPS analysis for the nanoscale SEI layer on graphite electrodes.

Given the distinct advantages of XPS analysis, conducting precise XPS measurements is essential to identify the primary failure mechanisms of graphite electrodes in PIBs cycled with various electrolytes. The stable state after complete charge/discharge cycles, where the SEI has reached equilibrium, is chosen to avoid complex interfacial electrochemical changes during cycling. This interfacial XPS analysis strategy combined with additional surface characterization methods have been widely used in previous failure analyses of graphite electrodes in PIBs.[6, 9, 11, 43, 67, 68, 87, 95, 96] The same design concept is considered feasible for analyzing the CEI formed on organic electrodes.[97] Building on previous surface analysis work, we can apply a similar approach to the failure analysis of ionic liquid electrolytes and additives modified carbonate electrolytes. Accurate capacity failure analysis can serve as an effective guideline for optimizing coin cell electrolyte design, expanding material choices, and enhancing cycle life, performance, and safety over extended cycling.

1.5.2. Deterioration Analysis of Electrodes for PIBs

In PIBs, electrode material deterioration manifests as structural damage from prolonged expansion and shrinkage, irreversible phase transitions, and material shedding and dissolution over extended cycles. During long-term performance decay, these phenomena are typically accompanied by accumulated interfacial failure. The interfacial stability of PIBs largely determines whether safe and reversible intercalation/deintercalation can occur, thereby influencing the extent of electrode material degradation.

For cycling of graphite electrodes in PIBs, deterioration is evident when unsuitable organic electrolytes are used. The reduction in crystallinity is a key indicator of the decreased capacity of graphite electrodes to store potassium ions, as confirmed by SEM and XRD analysis. The combination of crystallization degradation and interfacial decay is considered a primary cause of graphite electrode deterioration, commonly observed in organic electrolytes.[80, 95, 96] Additionally, improper CEI formation accelerates the dissolution of high-voltage cathode materials, such as PTCDA electrodes, placing further strain on organic electrolytes during extended cycling.[23, 98]

To meet the demands for interfacial and material stability, modifications to organic electrolytes are essential. The performances of organic electrolytes rely on their ability into the stable long term SEI layers for long cycles. To verify the effects of electrolyte regulation methods, such as ionic liquids and electrolyte additives, failure analysis is conducted using a combination of interfacial and structural analysis. By conducting precise interfacial characterizations, we can gain a comprehensive understanding of failure behavior, which in turn supports the development of optimized electrolyte designs for promising PIBs.

1.6. Motivations and Innovation

Compared with the Lithium-ion batteries, the development of PIBs are facing much higher challenges. The high risks associated with PIBs necessitate a cautious selection of materials, separators, electrolytes, and overall coin cell design.[99] Due to the significant impact of electrolytes on interfacial stability, exploring electrolyte compositions is crucial for maintaining capacity stability.

In conventional graphite electrodes, the layered structure undergoes significant volume changes during cycling. These volume fluctuations generate increased mechanical stress, which transfers to interfacial stress when the expansion of the graphite electrode is constrained by the current collector, interface, and electrolyte. Compared to conventional lithium-ion batteries, PIBs require enhanced chemical and mechanical stability at the interface throughout cycling. Ensuring the long-term stability of the SEI layer on the graphite electrode is therefore essential for any electrolyte used in these systems.

To advance the use of safe ionic liquid electrolytes, this study explores anion selection and, for the first time, employs these ionic liquids as electrolyte additives to improve the cycling performance of ECPC electrolytes in PIBs, focusing primarily on graphite cycling stability. Additionally, traditional PTCDA electrodes are tested to evaluate the high-voltage feasibility of these electrolyte modifications.

Using detailed characterizations, primarily XPS analysis, we can track nanoscale interfacial changes in the SEI layer during cycling, providing insights into the capacity decay mechanisms. This enables us to assess the reliability of a specific electrolyte design and establish guidelines for electrolytes intended for long-term cycling.

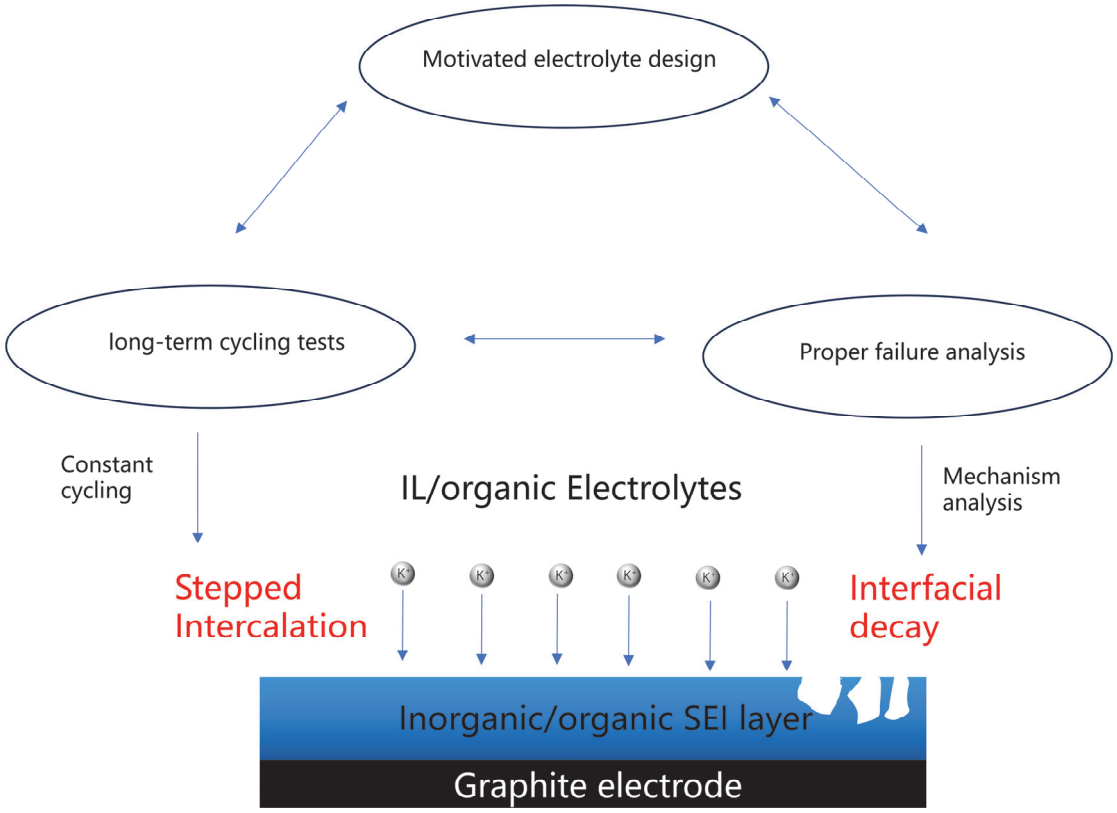

Figure 1.11. The overall design to evaluate the effectiveness of a specific electrolyte formulation for graphite electrodes in PIBs.

1.7. Aim

As one alternative to the lithium-ion batteries, it is very important to make sure that the whole cycling stability of PIBs is preserved. In this thesis, the aim is to explore the battery failure analysis of the ionic liquid electrolytes and organic electrolytes in the PIBs. The intention is to understand why in PIBs, different ionic liquid electrolytes and traditional carbonate electrolytes will show the capacity decay phenomena for common commercial electrodes along with the cycles. Since there are quite a few factors affect the capacity decay phenomenon, it is important to understand which factor should be the most important affecting the long-term cycling performance of different electrodes (graphite and PTCDA electrodes) in PIBs. Based on the detailed battery failure analysis, the electrolyte-regulation is designed

to help solve the problem of declining capacity of common carbonate electrolytes both with the replacement of the ionic liquid electrolyte and the electrolyte additives.

1.8. Overview

The thesis is divided into three parts, with the first and most important part focusing on a detailed failure analysis of fluorinated ionic liquid electrolytes and traditional KFSI/ECPC organic electrolytes. We involved the basic electrochemical tests to detect the constant cycling performances for different electrolytes, and found a few different cases arisen from the decomposition of SEI layers. We mainly analyze the long-term cycling performance (whole cycling life) of the graphite electrodes in different electrolytes to find the capacity failure problems happened in the ionic liquids with TFSI anions as the anions and for the traditional ECPC electrolytes. To understand this problem, several characterizations methods were carried out on the cycled the graphite electrodes, to understand the changes of the interfacial chemistry and the crystallization structure of the graphite electrode. The characterizations we selected are SEM, TEM, XRD, XPS of the electrodes, based on the detailed characterizations of the graphite electrodes, we found that the XPS analysis shows the most important interfacial data understanding the capacity decay problems in the PIBs, shows different interface chemistry information covered on the graphite electrodes, this direction we did detailed work on the battery failure analysis and the electrolyte optimization. To further explore battery failure similar analysis was applied to electrolyte additives in ECPC electrolytes, in order to detect whether suitable electrolyte additives can help us solving the capacity failure problems happening in traditional ECPC electrolytes. Common electrolyte additives

combined with ionic liquids are selected as the additives to solve the problem of the normal KFSI/ECPC electrolytes. In addition, the most important interfacial analysis XPS is used to understand the interfacial change of the graphite electrodes cycled with different additive modified ECPC electrolytes.

Finally, the applicability of electrolytes for full cell PIBs were studied. We selected the common PTCDA electrodes in PIBs as the cathodes to make one comparison with the FA analysis of graphite electrodes, in order to further understand the accumulated interface between the electrolytes and electrodes in ionic liquid and ECPC electrolytes.

Chapter 2 Experimental Methods

2.1. Preparation Methods of Coin Cells

2.1.1. Preparation Methods of Electrode Slices

For the electrode preparation methods of the electrodes for PIBs, the flake commercial graphite (3 μm, luoyang tongrun info technology co. ltd) and PTCDA (97%, sigma) powder was used. The graphite crystal powder (3 micrometer particle size) was stored in the dark before the use. The carbon black powder (99+%, super P conductive, sigma) as also used to increase the overall electrical conductivity of the materials, in order to increase the rate capability of the electrodes. In addition, the polyvinylidene fluoride (PVDF, 99%, sigma) was used to work as the binder. The whole graphite powder, super P carbon black additive, and PVDF binder were used to be mixed with the mass ratio of 8:1:1 in the agate mortar. The mixed powder was ground for about 1 hour carefully until the slurry was well mixed. Then the N-Methyl-2-pyrrolidone (NMP, 99.5%, sigma) solvent was added dropwise with grinding until the slurry is just dissolved. Then, the slurry was ground for 30 minutes, the final slurry behaved like black gloopy slurry which covered the agate mortar.

After the grinding procedure, the gloopy slurry was transferred to the Cu foil with one plastic tab. The large-scale graphite slurry was coated with the specific four-sided applicator, which have the thickness-controlled function. The 100-micrometer scale of the applicator was used to make sure the graphite electrode mass loading was close to 1.0 mg/cm^3. After the film coating, the electrodes were dried in the vacuum oven for 24 hours at 80 degrees, then the dried fresh electrodes were cut into small pieces of radius

of 12 mm with the specific cutting machine. The electrodes in small pieces were collected in the plastic boxes and dried for 2 additional hours in the vacuum oven. After the drying procedure, the electrodes were directly transferred to the glove box for preparation of coin cells.

Similar to the preparation of graphite electrodes, we tried the commercial PTCDA as the cathode electrodes. The whole PTCDA red powder, super P carbon black additive, and PVDF binder were used to be mixed with the mass ratio of 7:2:1 in the agate mortar. The mixed powder was grinded for about 1 hour and the same NMP solvent were used. After the NMP solvent was mixed with the slurry, the whole mixture was grinded for 30 minutes until all the slurry was completely mixed as one dark red slurry. Then the dark red slurry was flatly coated on the Aluminum-carbon collector. The specific four-sided applicator with the 200 sale was used to coat the large-scare PTCDA slurry set to close to 2.0 mg/cm^3, in order to match the capacity of the graphite electrodes. The dried electrodes were then cut into the smaller pieces of 12 mm with the same plastic cutting machine. The final pieces of electrodes were then put in the plastic boxes and dried for 2 additional hours in the oven for future use.

2.1.2. Preparation Methods of Electrolytes

In order to prevent all the possible impurities from the outside atmosphere, all the salts, the electrolytes (ionic liquids and organic electrolytes), and electrolyte additives Ethylene Sulfite (ES, 98%, sigma) and Fluoroethylene carbonate (FEC, 99%, sigma) were directly transferred to the glovebox after received. All the salts were taken from the glovebox and dried in the vacuum oven for 80 degrees overnight before the preparation of the solvent. All the preparation methods of electrolytes were done in the glovebox.

The commercial ionic liquids $Pyr_{13}FSI$ (99.9%, solvionic) and $Pyr_{13}TFSI$ (99.9%, solvionic), were weighted with one analytical balance and transferred with one syringe to the small glass vials. After the weighting procedure, the target salts of KFSI(99.9%, solvionic) and KTFSI (99.5%, solvionic) were transferred to the small vials of ionic liquids to make the KFSI/[Pyr_{13}]FSI, KFSI/[Pyr_{13}]TFSI and KTFSI/[Pyr_{13}]TFSI ionic liquids electrolytes with the same mole fraction (15%). The ionic liquid electrolytes were then stored tightly in the small vials in the glovebox for future use.

The organic ECPC electrolytes were made in the glovebox in the mass ratio of 1:1. All the additives are added based on the mass ratio. The target electrolyte additives were weighted and added dropwise to the ECPC electrolytes with the mass ratio of 0.5% and 10%. Then the KFSI salts were added to the ECPC electrolytes with different amounts of additives to make the 1 M KFSI/ECPC, 1 M KFSI/ (ECPC with 0.5%/10% ES), 1 M KFSI/ (ECPC with 0.5%/10% FEC) and 1M KFSI/ECPC with 10% $Pyr_{13}FSI$, 20% $Pyr_{13}FSI$ and 40% $Pyr_{13}FSI$ electrolytes. The 1 M KFSI/ECDEC electrolytes and saturated KFSI/ECPC were made with the same methods in the glovebox. All the electrolytes prepared will be the main analyzing target for capacity failure analysis in PIBs. All the materials came from the commercial supplies.

Although the preparation of the electrolytes was all done in the glovebox, the humidity of the electrolytes should be carefully controlled because of the active potassium metal. Thus, the humidity of the electrolytes was controlled with the specific drying method. Activated 3 Å Zeolite molecular sieve molecular sieves from sigma were added to the electrolytes. This kind of molecular sieve was widely used to absorb the unwanted water in the electrolytes, in order to lower the humidity, and prevent any water accumulation from the environment. Before the use, the molecular sieves were dried in the vacuum oven at 180 degrees for activation. Initially the

molecular sieves were put into the electrolytes, there were a few bubbles coming out from the electrolytes. The appearance of the bubbles arose from the release of the gas from the interspace, which can be also increased by the absorption of the water. After two days' drying, the finial electrolytes were prepared and stored for use in the glovebox.

2.1.3. Basic Coin Cell Preparation of PIBs

The basic coin cell design mainly followed the basic design of the lithium-ion battery. The 2032-coin cell design involved in this thesis contained the standard negative case, spring, stainless spacer, anode, spring and positive case. All the negative and positive cases, involving the spacer and spring were using the stainless metal, which can effectively prevent the corrosion of the electrolytes. The separator, we selected the Whatman GF/F separator with the enough ion diffusivity and mechanical strength. The anode materials, we used the excess potassium metal which was cut from the potassium chunk stored in the silicon foil. The potassium metal (98%, sigma) was carefully cut into the small pieces closer to the diameter of the spacer (15 mm) by the special abrasive tool. Then the silicon foil was removed by dried paper for further use. The cathode was selected to the be graphite or PTCDA electrode slices depends on the use, the electrode thin films were transferred to the potassium case with the current collector down attached to the case. The electrolytes were added to the separator (20 mm) with different volume (150 μL for graphite and 120 μL for PTCDA electrodes), less volume of electrolyte was used to decrease the dissolution behavior of PTCDA electrodes. After the separator was infiltrated and attached to the cathode electrode, potassium metal was attached to separator, the position of the potassium metal needed to cover

all the area of the cathode materials. The potassium metal was then rolled with the spacer evenly, the spring was put onto the spacer, with the cover of the negative case as one end. The loosely connected coin cells were packed by the hydraulic machine, the sealing gasket on the negative case can seal the whole coin cells, in order to provide the inert environment for cycling.

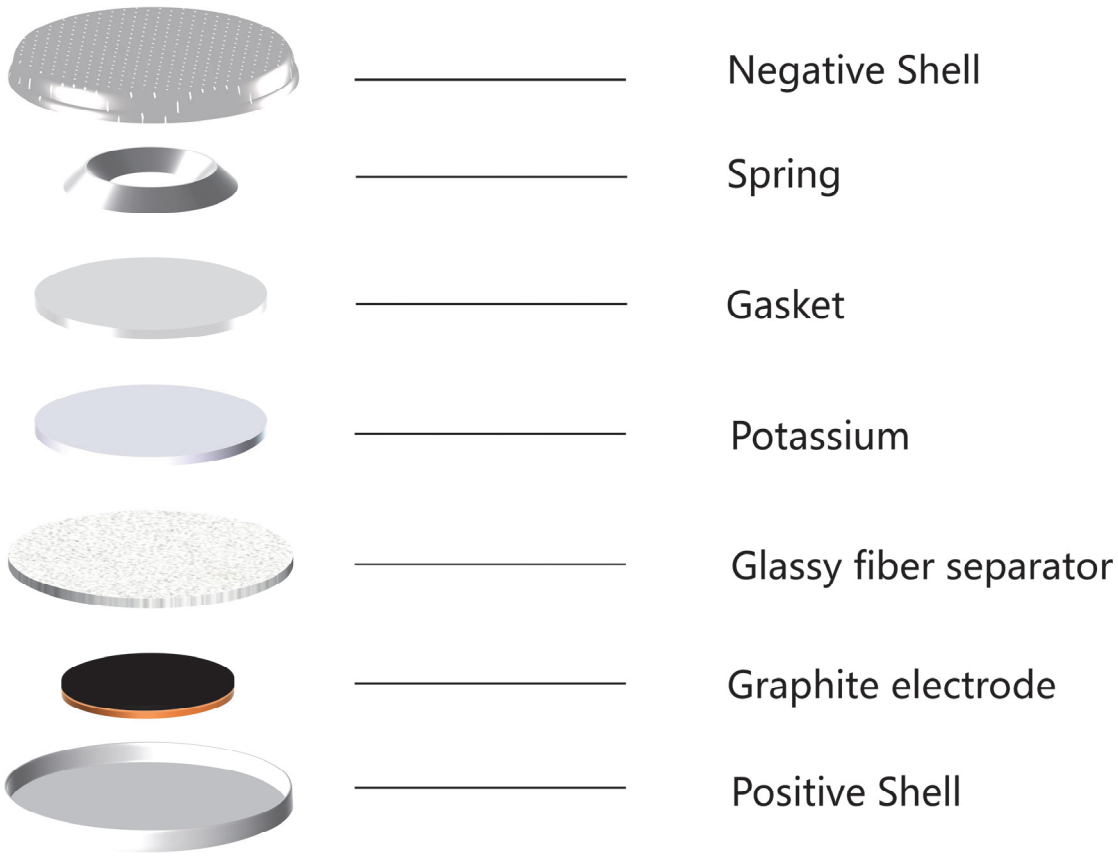

Figure 2.1. The cell configuration of graphite/potassium half cells.

2.2. Electrochemical Measurements of the Coin Cells

After the coin cells were well assembled, the coin cells were then taken and rested for at least 24 hours before the electrochemical test. The one-day rest can help the separator infiltrative by the electrolytes, which was important in PIBs. The coin cells were then cycled in separated channels

controlled by the Neware battery testing system. The long galvanostatic charge-discharge tests and rate capability were performed and controlled by the Neware system. The specific capacity was calculated based on the mass of the active material. The coin cells were cycled at the room temperature in one isolated room. For the other CV (cyclic voltammetry) and EIS analysis were performed with the Palmsens software and analyzed by the Zview software.

2.3. Sample Preparation of Thin Film Characterization

The characterizations of the graphite and PTCDA electrode thin films were performed with the ex-situ analysis. The cycling of the coin cells was stopped at OCV after the designed cycles were achieved. The target coin cells were then taken to the Ar-ion filling glovebox. To open the coin cells, two special ceramic pliers were used to open the coin cells in the glovebox. The ceramic pliers can effectively prevent the possible short circuit phenomenon arose from the metal pliers. After the coin cells were opened, the small ceramic tweezers were used to take the electrode film out, and put it in the PC solvent in the glass vial which was prepared in advance. The electrode film was rinsed slightly in the PC solvent for about 5 minutes, in order to help wash the IL or organic electrolyte out. After the 5 minutes' initial washing, the thin films were taken out to another PC-filled vials and washed for 10 minutes gently to help wash the residue of the electrolytes. The electrode thin films were then rested in the PC solvent for about 20 minutes for stabilization. To make all the samples involving the ionic liquid and organic electrolytes removed before the characterization, we applied the PC solvent with high polarity to dissolve the electrolytes and the salts. By using this way, in the SEI analysis, we found few solvents residue. While washing with PC solvent can partially dissolve the SEI layer on the graphite

electrode, it exerts an even greater effect on electrolyte removal due to enhanced co-dissolution. We propose that the partially dissolved SEI layer, which is in close proximity to the potassium salts in the electrolyte, coexists with a residual SEI component composed of undissolved organic and inorganic precipitates dispersed within the polar solvent. Although this residual fraction does not form a complete SEI, it nonetheless exhibits many of the long-term characteristics of a mature SEI due to its limited solubility in potassium-ion electrolytes. After the washing steps for each sample, the electrode thin films with few PC solvent was taken to the small chamber connected to the glovebox, the electrode was dried overnight under vacuum to completely remove the PC solvent. Thus, we obtained the dry graphite electrodes with thin SEI layer covered on it.

We applied the same washing method for PTCDA electrode slices, the PTCDA electrodes were also taken from the coin cells after the whole cycling tests at OCV. However, PTCDA electrodes were partly dissolved in the PC solvents with the shaking going. The different dissolution behavior was connected with the solubility difference of graphite and PTCDA electrodes in PC solvents, which will be discussed further in the discussion part.

2.4. Characterizations of Materials and Interfaces for Capacity Failure Analysis in PIBs

After the electrodes were washed and dried in the small chamber, the electrodes thin films can be then used for characterizations. We applied the ex-situ analysis to focus on the materials surface characteristics, in order to understand the surface changes of the electrode materials (mainly graphite) during the cycles. The SEM, TEM, and XRD analyses were conducted personally after complete training. For the XPS analysis, it was

done with the help of the Dr Mark Isaacs and Dr Arthur Graf in Harwell-XPS campus because of the high safety requirements. Thermal gravimetric analysis (TGA) were recorded on a TA instruments TGA 5500. The tests ran from RT to 450 °C at a heating rate of 10 °C per minute in a nitrogen atmosphere. The TGA measurements are done with help of Dr Tim Evans.

2.4.1. Scanning Electron Microscopy (SEM)

SEM analysis is widely used to detect the microstructure of the material with high-resolution. We applied the SEM analysis to detect the decay morphology of the graphite powder along with the cycles. The graphite electrode powder after washing was scraped off gently from the electrode thin film. The graphite powder was placed onto copper tape attached to an aluminum stub, with the copper tape effectively enhancing the sample's conductivity. The Al stub was then transferred to the sample holder and done with the specific gold coater procedure, in order to further increase the conductivity of the samples. The nano-scale gold on the graphite can help prevent the charging effect, provide the higher resolution images. After that, the samples were transferred to the SEM machine under vacuum for analysis. The SEM pressure was set (less than) $< 3 \times 10^{-4}$ Pa and the current of the electrons was set to close to 10.0 μA. After the sample area of the graphite electrodes was found, various images were obtained with the target magnification. In order to increase the image quality, the intensity of electron beams was carefully controlled and the focusing position and diameter of the electron beam were set to one specific area. After the careful adjustment of the settings, the images with good quality were obtained.

2.4.2. X-Ray Diffraction (XRD)

To characterize any change of crystalline change of the graphite during cycling, X-ray diffraction (XRD) was used. The graphite electrode, coated on the Cu foil, was put on the glass sheet and flattened by pressing with a second glass slide. XRD patterns were obtained by the Grazing incidence PXRD method, with an X-ray source of Cu Kα (λ = 0.154 nm) by using the scan parameters (2theta=10-60°, 0.05°/step, 2s/step). The X-ray spot was selected to the center of the electrode film for each sample. After 30 minutes scan, the XRD patterns of the graphite and copper can be clearly obtained.

2.4.3. Transmission Electron Microscopy (TEM)

The aim of the TEM was to detect the thickness of the SEI layer in a quantitative way. The fundamental imaging principle of TEM requires samples to be very thin to allow electron beams to pass through. Thus, the graphite electrodes were dissolved in the methanol separated with 30 minutes' centrifugal operation. The completely separated graphite particle was collected and transferred to the clean copper grid by one glass pipette. The graphite particles were dried for several minutes and transferred to the TEM machine under vacuum. The energy of the electron beams was 200 kv, the current was selected to 102±3 μA. After the target particle was found, the beams, condenser and sample height were carefully aligned to find the best positions for beams to go through the particle. Then the particle was carefully focused to find the images of the graphite. The whole alignment and the focus should be very precise to find the very clear image of the graphite particle. In addition, the large diameter made it much harder to let the beam current go across the graphite. Several hours were applied to

find the ultrathin region of the graphite crystal, providing both the images of the graphite and the SEI layer with the difference in crystalline state.

2.4.4. X-Ray Photoelectron Spectroscopy (XPS)

To analyze the detailed chemical information of the SEI layer, XPS analysis under inert environment was done with the surface of the target electrodes cycled in different electrolytes after long cycles. The coin cells were opened and washed in the glovebox in Harwell campus, the electrodes were dried overnight before the XPS analysis.

An air-free transfer technique was used to transfer samples from the glovebox to the XPS spectrometer without exposure to air. Samples were mounted in a stainless steel holder.

The electrode thin films were moiunted onto conductive carbon tape, and it was ensured the samples were flat with the help of ceramic tweezers.

After the thin films were mounted, the air-free holder was sealed and placed under vacuum inside the glove box. After 30 minutes of pumping down, the sealed air free holder was removed from the glovebox and taken to the XPS spectrometer (less than 1 minute travel time) and pumped down in the fast entry airlock until high vacuum was achieved. Samples were then transferred to the analysis chamber for XPS. All sample data was recorded at a pressure below 10^{-8} torr and a room temperature of 294 K. XPS Analysis was performed using a Thermo NEXSA XPS fitted with a monochromated Al kα X-ray source (1486.7 eV) , depth profiling was performed using monoatomic Argon ions at 0.5 kV over a 0.25x0.25 mm raster area. This XPS analysis with Ar-ion etching was done with the graphite electrodes cycled with the main ionic liquid electrolytes and 1M KFSI/ECPC electrolytes. For the graphite electrodes cycled with other electrolyte modified ECPC electrolytes, the basic XPS analysis without the

Ar-ion etching was done with the similar settings. XPS analysis was also carried out using inert transfer for the CEI analysis of PTCDA electrodes on AlC current collector. For other materials without the strict requirements for inert environment, standard sample loading was used. For example, the the surface analysis of the basic electrode materials for purity tests were analyzed with the basic XPS analysis, without inert transfer. All XPS data were processed using Casa XPS software, applying Shirley baseline correction, with calibration to the C 1s peak at 284.8 eV

Chapter 3 Capacity Failure Analysis of Ionic Liquid and Carbonate Electrolytes for Graphite Electrodes in PIBs

The ionic liquid electrolytes can be seen as one promising way to solve the problems of safety and capacity decay problems in traditional carbonate electrolytes in PIBs. The cycling performances of ionic liquid electrolytes are mainly affected by their anions because of the anion-derived SEI layers formed by ionic liquid electrolytes. The SEI chemistry evolution process will behave distinctly controlled by the selection of anions of ionic liquids, thus affecting the cycling stability with extended cycles. Our aim is to understand the underlying reasons why ionic liquid electrolytes with different anions exhibit significantly varied capacity performances in PIBs, through interface chemistry analysis. The detailed SEI evolution process of ionic liquid electrolytes will be analyzed to be corelated with the actual electrochemical performances of graphite/potassium half-cell tests. To enable comparison, a common carbonate electrolyte is included along with the SEI evolution analysis of ionic liquid electrolytes. Detailed failure analysis was carried out using XPS characterizations of the SEI on the cycled graphite electrode surface after long cycles of the galvanostatic cycling tests, supported by the materials characterization tools like SEM, TEM and XRD techniques. The traditional KFSI/ECPC carbonate electrolyte was also studied, so that ionic liquid could be compared with one mature widely used electrolyte. Thus, we can establish the relationship between SEI evolution and capacity decay for both ionic liquid electrolytes and common carbonate electrolytes.

3.1. Selections of Ionic Liquid Electrolytes with High Thermal Stability

To investigate the anion-derived SEI layer formed by ionic liquid electrolytes, the chosen ionic liquid electrolytes must be representative. The selected ionic liquid cation should enhance the influence of anions while providing both electrochemical stability and kinetic compatibility with potassium ions during cycling. The most common ionic liquid cations are mainly divided into aromatic (Imidazolium) and nonaromatic (pyrrolidinium) nitrogen heterocycles. The decomposition of imidazolium cations, however, cannot be stabilized without additional functional groups attached to the carbon chain.[51] To minimize the impact of cations, our approach aims to control their decomposition and shift SEI layer formation to be primarily anion-driven. In past research, the viscosity and the conductivity of ionic liquid electrolytes are highly related to the carbon length. The carbon chain length should be also decreased to increase the ionic conductivity of ionic liquid electrolytes, thus increasing the kinetics of the potassium ions during the cycling. Based on the facts, the cation is selected to N-Propyl-N-methylpyrrolidinium (Pyr_{13}), which is widely used as the safe ionic liquid electrolyte (KFSI/Py_{13}FSI) with high long-term performances.[15, 43]

The SEI layer formed by pyrrolidinium ionic liquid electrolytes is widely considered to be anion-driven[27, 53, 58], making these ionic liquids ideal for analyzing the impact of anions on SEI stability. The pyrrolidinium ionic liquid electrolytes based FSI anions have been proved effective for long cycling for graphite electrodes in PIBs. In addition, the capacity failure behavior become severe when the TFSI anions are selected for the pyrrolidinium ionic liquid electrolytes. The contrary performance further proves that the electrochemical performances of pyrrolidinium ionic liquid electrolytes are

controlled by their anions. To help understand and improve the decay performances of pure TFSI ionic liquids, we applied mixed-anion ionic liquid electrolytes with prat of FSI as anions the first time to understand the different SEI evolution process on graphite electrodes in PIBs between TFSI and FSI-based ionic liquid electrolytes. We applied different salts in different ionic liquid electrolytes, this method is seen effective feasible in lithium and sodium ion batteries.[58, 59, 61]

The used ionic liquids electrolytes in this thesis are then defined as:

Pure FSI ionic liquid electrolyte:

$$xKFSI+yPyr_{13}FSI \rightarrow K_x[Pyr_{13}]_yFSI$$

Pure TFSI ionic liquid electrolyte:

$$xKTFSI+yPyr_{13}TFSI \rightarrow K_x[Pyr_{13}]_yTFSI$$

Mixed-anion ionic liquid electrolyte:

$$xKFSI+yPyr_{13}TFSI \rightarrow K_x[Pyr_{13}]_yFSI_xTFSI_y$$

To make the effects limited by anions, the same mol% should be selected by the ionic liquids. 15 mol% are selected since it is close to the limited saturated KTFSI in $Pyr_{13}TFSI$ (~16mol%).[16] The high viscosity of $Pyr_{13}TFSI$ compared with $Pyr_{13}FSI$ cause that the potassium salts are weakly dissolved in $Pyr_{13}TFSI$ ionic liquids, make the whole selection of salts are controlled by the limited solubility of KTFSI in $Pyr_{13}TFSI$.[61] Based on the fixed mol%, the ionic liquid electrolyte used can be defined as $K_{0.15}Pyr_{0.85}FSI$, $K_{0.15}Pyr_{0.85}FSI_{0.15}TFSI_{0.85}$ and $K_{0.15}Pyr_{0.85}TFSI$. To simplify the terminology, we will refer to the ionic liquid electrolytes with 15 mol% salts in the thesis as **pure FSI ionic liquid electrolyte** (KFSI/[Pyr_{13}]FSI), **pure TFSI ionic liquid electrolyte** (KTFSI/[Pyr_{13}]TFSI), and **mixed-anion ionic liquid electrolyte** (KFSI/[Pyr_{13}]TFSI).

The basic physical properties are variable when the anions are changed. According to previous research, the viscosity order of ionic liquid

electrolytes at the same molar concentration is as follows: pure FSI ionic liquids electrolyte< mixed-anion ionic liquids electrolyte < pure TFSI ionic liquids electrolyte.[61] This difference is attributed to variations in intermolecular forces between the ions. Higher intermolecular forces, in turn, result in higher TGA (Thermogravimetric Analysis) temperatures of ionic liquid electrolytes.[100] In electrolyte design, a higher TGA temperature indicates that the ionic liquid can meet stringent safety requirements, significantly reducing the risk of fire.[101] To evaluate this crucial physical property, we conducted TGA measurements on the designed ionic liquid electrolytes.

As is seen in figure 3.1, the decomposition temperatures are increased a lot when $K_{0.15}Pyr_{0.85}FSI$ are replaced with $K_{0.15}Pyr_{0.85}FSI_{0.15}TFSI_{0.85}$ and $K_{0.15}Pyr_{0.85}TFSI$. Specifically, the decomposition onset temperature of pure $K_{0.15}Pyr_{0.85}TFSI$ and $K_{0.15}Pyr_{0.85}FSI_{0.15}TFSI_{0.85}$ increases to nearly 400°C. At this temperature, most of the pure $K_{0.15}Pyr_{0.85}FSI$ species have decomposed, reducing the weight percentage to approximately 20%. The excellent thermal stability of $K_{0.15}Pyr_{0.85}TFSI$ and $K_{0.15}Pyr_{0.85}FSI$ demonstrates their suitability as high-safety electrolytes, particularly when compared to organic KFSI/ECPC, which easily lose all their weight at temperatures as low as 200°C.

Based on the results, exploring mixed-anion pyrrolidinium ionic liquid electrolytes can help tailor viscosity and TGA temperature to meet the needs of various battery applications, enabling the development of ionic liquid electrolytes with both strong electrochemical performance and enhanced safety. For the designed ionic liquid electrolytes, our focus is on the primary thermal endurance of different ionic liquids and common carbonate electrolytes. This allows us to confirm that these electrolytes can maintain the safety of PIBs, addressing the critical safety concerns associated with developing new electrolytes for PIBs with high safety

standards.

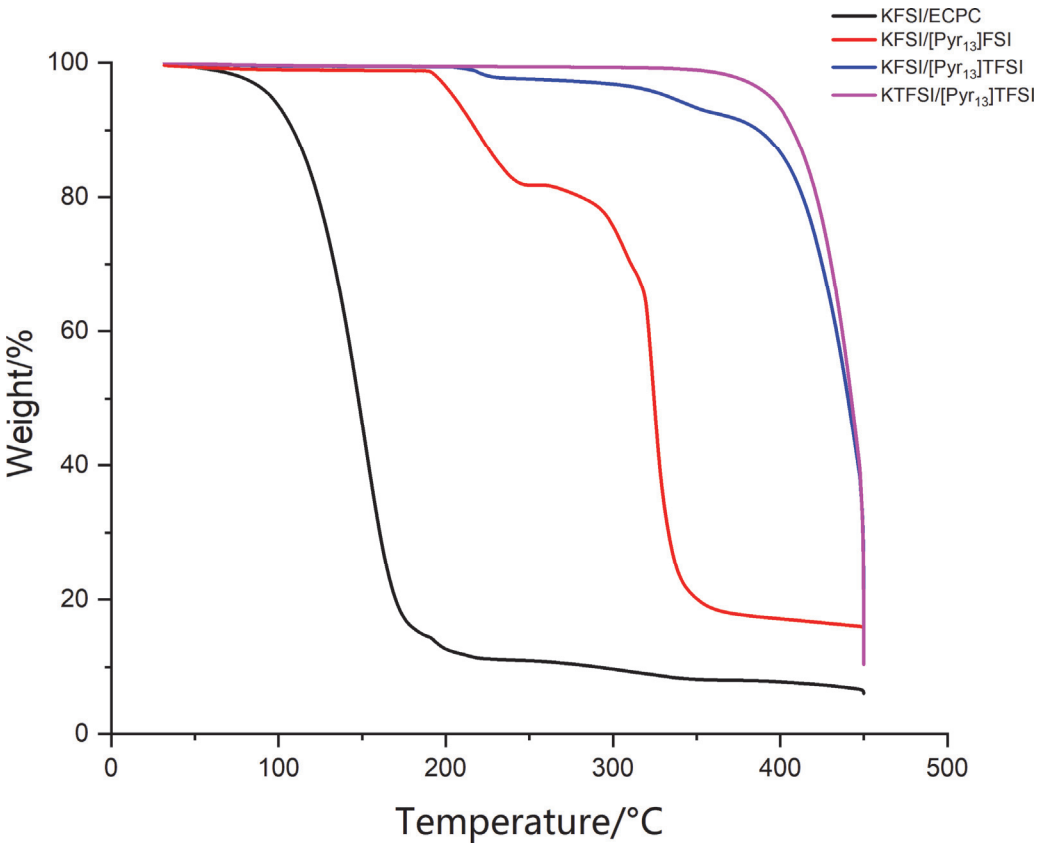

Figure 3.1. TGA measurements of the $K_{0.15}Pyr_{0.85}FSI$, $K_{0.15}Pyr_{0.85}TFSI$, $K_{0.15}Pyr_{0.85}FSI_{0.15}TFSI_{0.85}$ and KFSI/ECPC electrolytes.

3.2. Electrochemical Characterization of Ionic Liquid and Carbonate Electrolytes for Graphite Electrodes in PIBs

Once the safety of the designed electrolytes is confirmed, we can shift our focus to evaluating the long-term cycling performance of various anion-derived ionic liquid electrolytes. The goal of these electrochemical tests is to assess capacity retention for different ionic liquid and carbonate electrolytes under a constant current. Through extended cycling, we can determine whether the designed ionic liquid electrolyte supports durable cycling for graphite electrodes. Additionally, we will analyze polarization

changes caused by interfacial decay, as these impact capacity retention. The cycling tests will provide insights into the stability and effectiveness of SEI layers over prolonged use, offering a foundation for further interfacial failure analysis.

3.2.1. Cyclic Voltammetry

The initial formation of the SEI layer is known to play a crucial role in determining the long-term cycling performance of a given electrolyte on graphite electrodes. To start the electrochemical analysis, Cyclic Voltammetry (CV) tests were conducted to examine the role of SEI formation cycles in ionic liquid and organic electrolytes. A low scan rate of 0.05 mV/s was selected to observe the initial SEI formation on graphite electrodes. The coin cells used had consistent configurations across all long cycling tests. The response current was calculated using the electrode area of graphite electrodes with a 12 mm diameter and a mass loading of approximately 1.0 mg/cm². To begin with, incorporating TFSI into the ionic liquid electrolytes results in a reduction in current under the same scan rate. The notably weaker cycling performance of KTFSI/[Pyr13]TFSI suggests that pure TFSI ionic liquids facilitate the formation of an unstable SEI, which in turn leads to higher interfacial resistance and slower surface kinetics. On the contrary, pure FSI ionic liquids facilitate the formation of stable SEI layers, which in turn enhance the response current. In comparison to 15 mol% ionic liquid electrolytes (<0.72M at RT)[16, 49], the 1.0 M KFSI/ECPC system exhibits improved ion diffusion. This enhanced ion mobility, when combined with high initial interfacial resistance and rapid surface kinetics, ultimately leads to a fast response current. Nonetheless, a high initial response current alone does not fully reflect all the advantages of a specific

electrolyte system. The results from the initial SEI formation cycles reveal that potassium ion decomposition varies across different electrolyte environments. For KFSI/[Pyr_{13}]FSI and KFSI/[Pyr_{13}]TFSI mixed-anion ionic liquids, SEI formation appears as two distinct peaks from 1.5 to 0.5 V, prior to potassium intercalation, which occurs between 0.4 and 0.01 V. In contrast, SEI formation in pure TFSI ionic liquids is much broader, with a large, unexpected peak near the potassium intercalation voltage at 0.4 V. This broad peak likely results from unstable potassium intercalation and partial solvent intercalation of pure TFSI ionic liquid electrolytes into the graphite layers[54, 102], the minor cathodic peak at 1.5 V may indicate solvent de-intercalation. The CV cycles highlight different cycling behaviors of ionic liquids with different anions as electrolytes for graphite electrodes. Additionally, the CV tests of the KFSI/ECPC carbonate electrolyte reveal minor polarization in the shifts of the intercalation/de-intercalation stages. The stepped intercalation behavior of potassium ions into the graphite layer emphasizes the need to further examine the long-term electrochemical performance of ionic liquid electrolytes and ECPC electrolytes for graphite electrodes in PIBs.

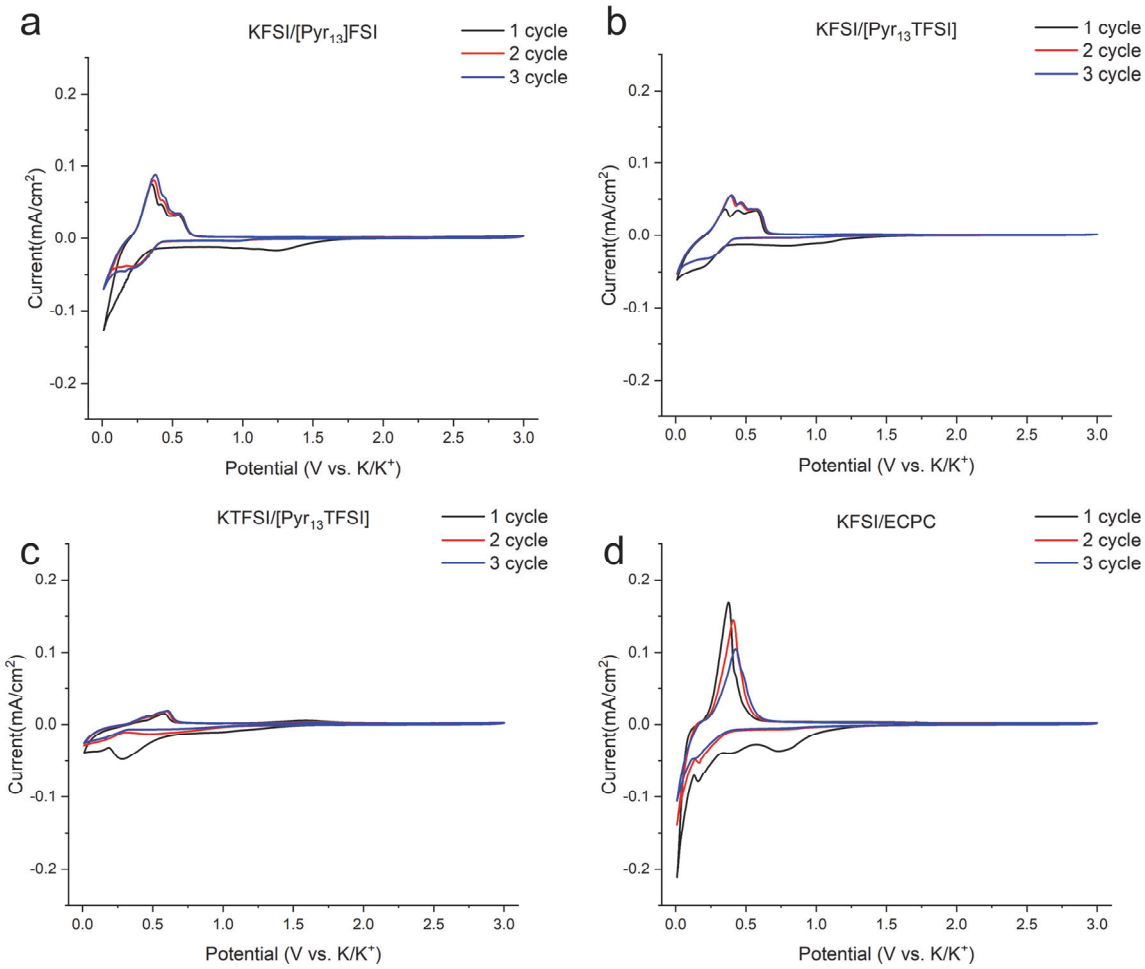

Figure 3.2. Initial CV cycles of K/Graphite cells in (a) KFSI/[Pyr_{13}]FSI, (b) KFSI/[Pyr_{13}]TFSI, (c)KTFSI/[Pyr_{13}]TFSI, (d) KFSI/ECPC electrolytes at 0.05 mV/s.

3.2.2. Galvanostatic Charge-Discharge Cycling

To analyze the effects of various anions on ionic liquid electrolytes in terms of capacity failure, long-term cycling tests were conducted at different currents for both ionic liquid and organic electrolytes. To minimize rapid polarization effects, currents were limited to no more than 100 mA/g to accurately assess cycling retention. The mass loading of the coin cells was set near 1.0 mg/cm² to increase active sites for electrolyte infiltration. The activated mass of the graphite electrodes is determined by subtracting the

mass of the copper foil. Due to minor variations in copper foil mass and differences in electrolyte infiltration across coin cells, slight capacity fluctuations may occur.[24] To minimize differences in infiltration, compaction density, and mass variation, capacity retention is used as the primary indicator of electrolyte stability over cycling, emphasizing its importance for electrochemical performance. All coin cells are assembled with the same method, electrolyte volume, separator, and an excess of potassium metal to ensure stability of the counter/reference electrodes. This approach enables us to use long-term cycling retention as a detection of electrolyte degradation, which is the main focus of analysis in this thesis.

To start the constant cycling tests, capacity retention at a low current of 25 mA/g was analyzed to evaluate the capacity preservation of common ionic liquid electrolytes. The capacity of the coin cells fluctuates with changes in ohmic polarization resulting from SEI layer evolution. For FSI ionic liquids and mixed-anion ionic liquid electrolytes, cycling stability is well-maintained at 25 mA/g.

For FSI-modified mixed-anion ionic liquid electrolytes, there is a slight capacity increase from the first to the tenth cycle (figure 3.3 a, b). This fluctuating performance stabilizes by around 70 cycles, followed by consistent cycling for the remaining cycles. Notably, overall cycling performance improves from the first 5 cycles to the 100th cycle, with a 2% capacity increase. In contrast, pure TFSI ionic liquids and ECPC electrolytes exhibit higher entire polarization, as shown in figure 3.3 (c, d). Capacity retention is challenging to maintain in TFSI and ECPC electrolytes, with pure TFSI showing a significant capacity decline, highlighting its extreme instability. For pure ECPC electrolytes, a gradual decrease is observed, leaving only 90% of the initial capacity after 100 cycles at a low current.

Figure 3.3 illustrates that, despite a significant variation in capacity

retention, the Coulombic Efficiency remains close to 100% throughout the cycles. The incremental interfacial changes during each discharge cycle are minimal, resulting in a nearly constant CE. This complex process is difficult to detect based solely on the apparent battery performance. In addition, the consistently high Coulombic Efficiency suggests that capacity loss may be linked to electrode material deterioration, such as loss of crystallinity and material pulverization and deactivation. Therefore, analyzing electrode material degradation is crucial along with the interfacial failure analysis.

The cycling performance results indicate that pure FSI and mixed-anion ionic liquid electrolytes exhibit stable cycling, effectively preventing electrolyte decomposition. The increasing capacity in the mixed-anion ionic liquids suggests "activation cycles," where stable cycling performance after these activation cycles indicates enhanced interface stability from the highly flexible electrolyte system. The relationship between SEI evolution and capacity variation has been a classic area of research in alkali-ion batteries.[13, 103, 104] In PIBs with a slow SEI formation process, the activation cycles appear as initial cycles of one specific current with increasing coulombic efficiency and specific capacity.[5, 9, 11, 14] In contrast, the declining cycling performance in pure TFSI ionic liquids and traditional 1M ECPC likely results from interfacial instability, with a tendency for electrolyte accumulation on graphite electrodes, ultimately impairing cycling stability.

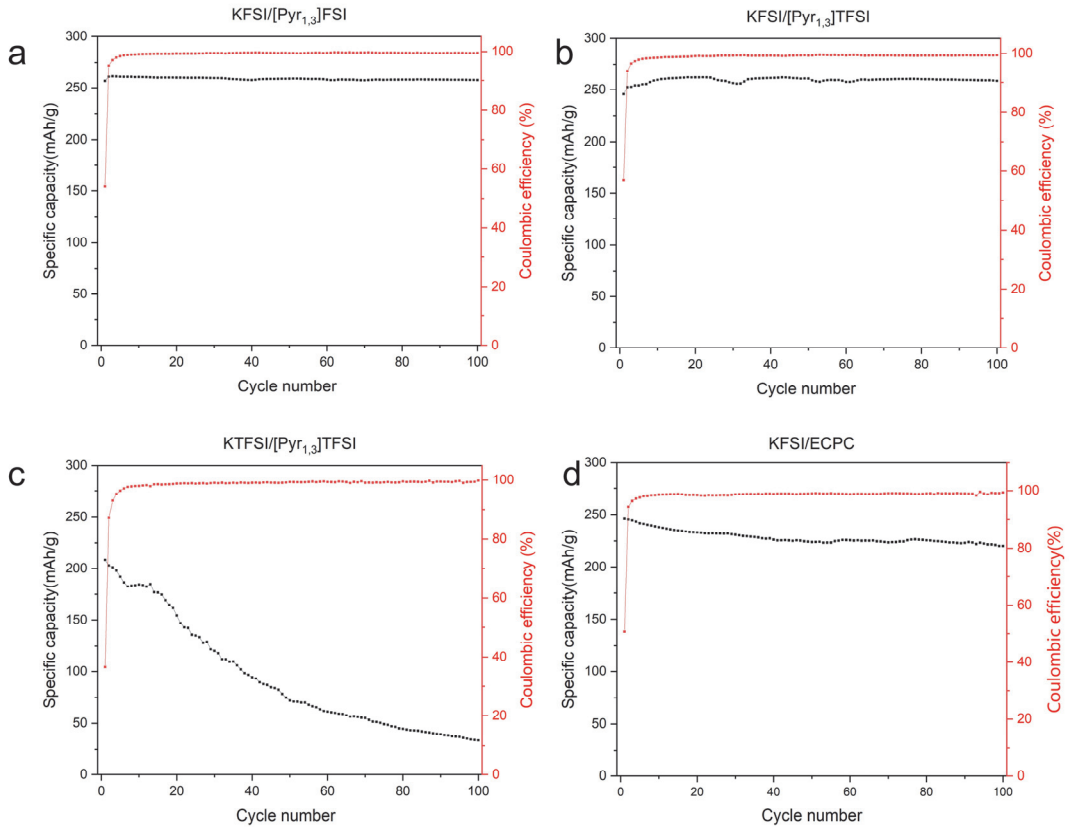

Figure 3.3. Long-term galvanostatic cycling tests of K/Graphite cells in (a) KFSI/[Pyr_{13}]FSI (b) KFSI/[Pyr_{13}]TFSI (c) KTFSI/[Pyr_{13}]TFSI,(d) KFSI/ECPC electrolytes at 25 mA/g for 100 cycles.

To further investigate polarization changes during extended cycling, GLD tests were conducted at a higher current for various ionic liquid electrolytes and 1 M KFSI/ECPC organic electrolytes. At a higher current of 100 mA/g, the pure FSI ionic liquid electrolyte demonstrated similarly stable cycling capacity retention as observed at the lower current of 25 mA/g. The capacity failure phenomenon is strengthened for the pure TFSI ionic liquid electrolytes, the capacity come to one end rapidly close to the end of 100 cycles (figure 3.4 c). The interfacial failure process is exacerbated during constant current cycling at higher currents.

However, unusual capacity fluctuations are observed during the initial cycles of mixed-anion ionic liquids. For this electrolyte, extended activation

cycles are more pronounced under higher current in the coin cell. The rapid capacity changes suggest a preference for FSI anions in mixed-anion ionic liquids to form a stable SEI layer over repeated cycles. The observed capacity recovery is likely attributed to gradual interfacial changes in the SEI layer during cycling, which subsequently affect resistance of interfaces.[13] For mixed-anion ionic liquid electrolytes, an equilibrium state is reached after the initial ~100 cycles, maintaining stability over the subsequent 400 cycles (figure 3.4b). Notably, after these activation cycles, mixed-anion ionic liquids exhibit cycling stability comparable to the pure FSI ionic liquid electrolyte, in stark contrast to the performance failures observed with pure TFSI ionic liquids. Incorporating FSI effectively mitigates capacity failure, even in TFSI-dominated systems such as $K_{0.15}Pyr_{0.85}FSI_{0.15}TFSI_{0.85}$.

For traditional carbonate electrolytes, anticipated capacity decay issues is achieved over the initial 500 cycles. Although cycling with 1M KFSI/ECPC electrolytes does not involve activation cycles, a decreasing trend of capacity failure remains irreversible, regardless of whether 25 mA/g or 100 mA/g current is applied (figure 3.3 d, figure 3.4 d). Compared to $K_{0.15}Pyr_{0.85}FSI$ and $K_{0.15}Pyr_{0.85}FSI_{0.15}TFSI_{0.85}$, which offer improved interfacial stability, the conventional 1.0M ECPC electrolytes demonstrate poorer cycling stability. This performance highlights the different importance of different interfacial evolution process of ionic liquid and carbonate electrolytes.

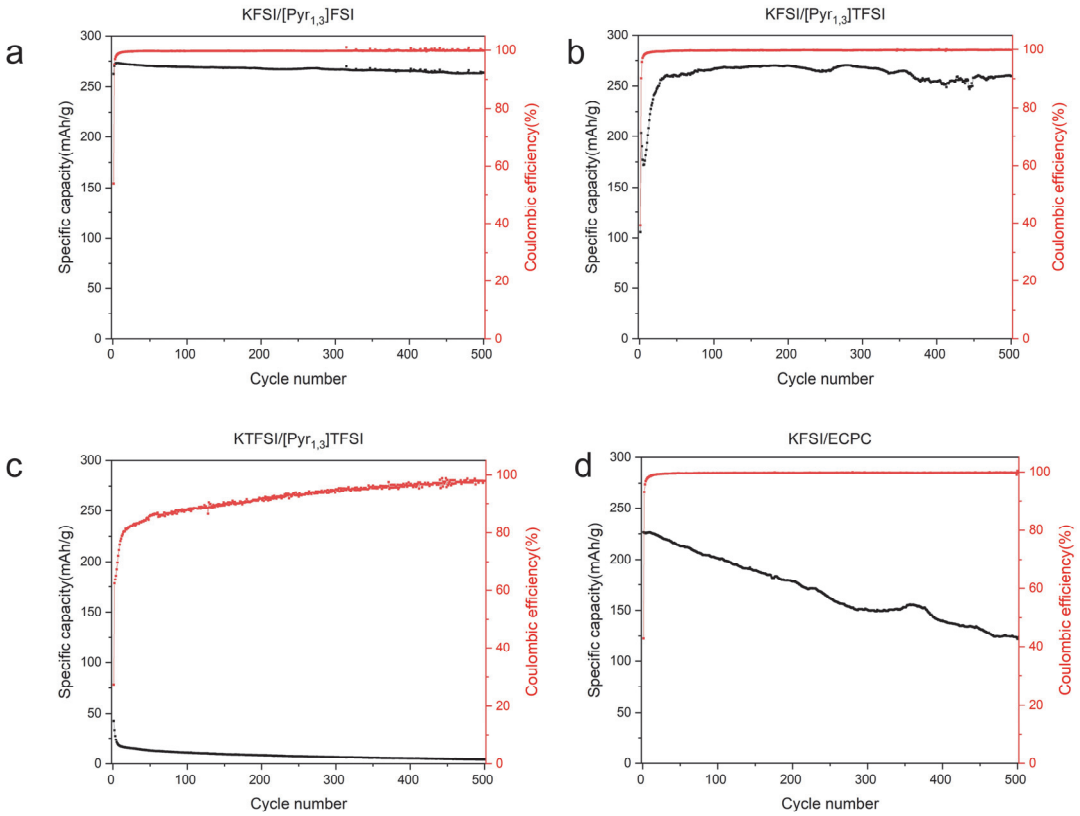

Figure 3.4. Long-term galvanostatic cycling tests of K/Graphite cells in (a) KFSI/[Pyr_{13}]FSI (b) KFSI/[Pyr_{13}]TFSI (c)KTFSI/[Pyr_{13}]TFSI, (d) KFSI/ECPC electrolytes at 100 mA/g for 500 cycles.

To further examine the failure phenomenon, a current of 25 mA/g was selected for SEI layer 5 formation cycles and to evaluate the capacity retention of various ionic liquid and organic electrolytes after extended cycling at a standard current of 100 mA/g. This approach, which involves using a low current to establish an initial stable SEI layer prior to prolonged cycling, is a widely adopted strategy in the cycling design of lithium-ion and PIBs.[9, 14, 43] The capacity stabilizes after 5 cycles at 25 mA/g, with the coulombic efficiency increasing to nearly 99%. Therefore, the capacity at the 5th cycle at 25 mA/g is used as a baseline to analyze retention changes at 100 mA/g, which is widely used in lithium-ion battery.[24, 25] Capacity retention of one specific x cycle at 100 mA/g is calculated as **Capacityx/Capacity5×100%**, and the results will be included in the

subsequent discussion.

The graphite/potassium coin cells were initially cycled at a low current of 25 mA/g for the first 5 cycles to facilitate stable SEI layer formation. Each electrolyte system showed markedly different performance over cycles, as shown in figures 3.5: To begin with, in the initial cycle, the Coulombic efficiency (CE) of graphite electrodes cycled with pure FSI ionic liquid and mixed-anion ionic liquids was 52.3% and 58.1%, respectively. In contrast, the CE for pure TFSI ionic liquid and ECPC electrolyte was considerably lower, at 39.2% and 45.3%, respectively. Although the CE for all four electrolytes increased to above 97% after five cycles at a current density of 25 mA/g, the reduced initial CE can be attributed to the formation of thicker and non-uniform solid electrolyte interphase (SEI) layers. These inferior initial SEI layers result in a significantly lower pristine capacity, even in the absence of noticeable capacity decline trends.The initial specific capacity at 5 cycle of the half cells with KFSI/[Pyr_{13}]FSI (~274 mAh/g) was higher than those with KTFSI/[Pyr_{13}]TFSI (~220 mAh/g) and KFSI/ECPC electrolyte (~254 mAh/g).

As shown in figure 3.5 c, upon repeated cycling, rapid failure is observed for KTFSI/[Pyr_{13}]TFSI, with the capacity decreasing significantly with every cycle, falling close to zero after long cycles. In contrast, the capacity of the of the pure FSI ionic liquid electrolyte is very stable up to 105 cycles, and has a retention rate of 88.7% after 1000 cycles (figure 3.5 a). The poor performance of the pure TFSI half-cells further confirms the complete capacity failure of pure TFSI ionic liquid electrolytes. In contrast, the mixed-anion system demonstrates superior performance, with a high capacity of approximately 273 mAh/g during the 25 mA/g SEI formation cycles. Notably, the capacity increases rapidly after 100 activation cycles at 100 mA/g. After 1000 cycles, the mixed-anion electrolyte cells retain 87.2% of the capacity compared to the 5th cycle (figure 3.5 b). The capacity recovery observed

during the initial 100 cycles in the mixed-anion system indicates evolving interfacial chemistry, consistent with observations at both 25 mA/g and 100 mA/g.

Nadherna et al. demonstrated that controlling mixed-anions in ionic liquid electrolytes effectively enhances SEI stability, leading to improved capacity retention in LiFSI/Pyr_{14}TFSI systems.[59] It can be deduced that the SEI layer evolution in KFSI/[Pyr_{13}]TFSI transitions from unstable interfaces during the initial cycles at a low current of 25 mA/g to more stable interfaces at 100 mA/g under extended cycles. Additionally, graphite in KFSI/ECPC electrolytes exhibited predictable capacity decay at 100 mA/g, even when the SEI layer was initially stabilized at 25 mA/g (figure 3.5 d). Overall, the significant capacity variations caused by extended cycling and current changes are linked with distinct ohmic polarization evolution behaviors across different electrolytes., emphasizing the importance of understanding ohmic polarization related to the SEI interfacial changes during the potassium intercalation process within graphite layers.

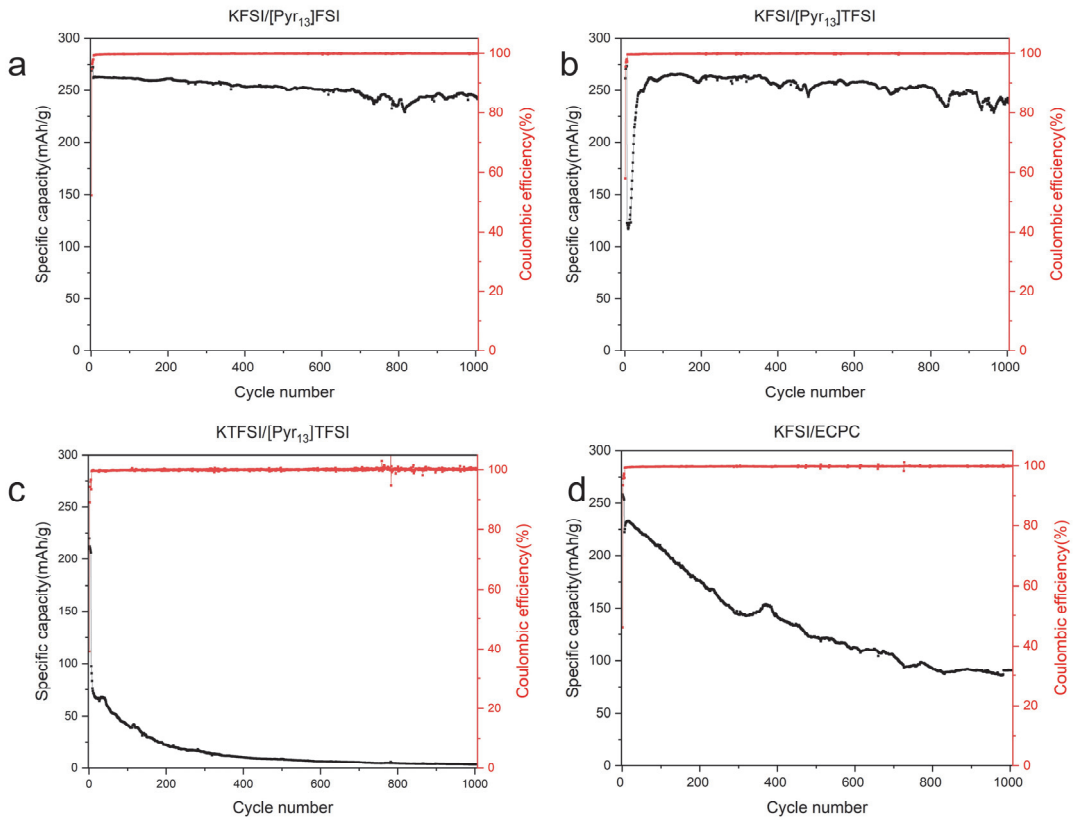

Figure 3.5. Long-term galvanostatic cycling tests of K/Graphite cells in (a) KFSI/[Pyr_{13}]FSI, (b) KFSI/[Pyr_{13}]TFSI, (c) KTFSI/[Pyr_{13}]TFSI, (d) KFSI/ECPC electrolytes at 25 mA/g for 5 cycles with additional 1000 cycles at 100 mA/g.

To examine polarization changes resulting from interface failure over extended cycling, the charge/discharge behavior was analyzed across all 1005 cycles, including the initial SEI formation cycle. To begin with, for the KFSI/[Pyr_{13}]FSI pure ionic liquid electrolyte and KFSI/[Pyr_{13}]TFSI mixed-ionic liquid electrolytes, the whole potassium intercalation process is protected (figure 3.6 a,b). Based on the past research of intercalation process of potassium into graphite layers, we can divide the whole potassium intercalation process into two stages (C-KC_{36}-KC_{24}, 0.4 V – 0.2 V) as the initial stage and (KC_{24}-KC_8 0.2V -0.01V) as the secondary stage.[1, 2] There is minimal to no decay observed in the first intercalation stage,

transitioning from pure graphite to initial (KC_{36}) and then partially intercalated graphite (KC_{24}).

However, stepped polarization behavior is observed during the transition from partially intercalated KC_{24} to the KC_8 structure, attributed to long-term structural damage and SEI accumulation. Although there is the slight polarization of the voltages in KFSI/[Pyr_{13}]FSI electrolytes and KFSI/[Pyr_{13}]TFSI mixed-anion ionic liquid electrolytes, the deterioration of materials cannot be completely stopped by applying the best design of electrolytes. However, when we focus on the intercalation process of pure TFSI ionic liquids, we can find the polarization phenomenon are strengthened when the long cycles are applied (figure 3.6 c). Additionally, in traditional 1M KFSI/ECPC electrolytes, the observed stepped decrease in capacity over long cycles is likely influenced by both material degradation and SEI layer instability, as reported in previous studies (figure 3.6 d). The significantly poorer cycling performance of KFSI/ECPC electrolytes compared to FSI-based ionic liquid electrolytes demonstrates that FSI-modified ionic liquid electrolytes can provide a more stable long-term intercalation environment for potassium ions within the graphite layered structure, compared with the traditional organic electrolytes.

From the cycling performance, it is evident that capacity failure primarily arises from stepped polarization, leading to incomplete KC_8 potassiation over cycles, as observed in KTFSI/[Pyr_{13}]TFSI ionic liquid electrolytes and KFSI/ECPC electrolytes. Conversely, the recovery trend in KFSI/[Pyr_{13}]TFSI mixed-anion ionic liquid electrolytes at 100 mA/g suggests a reverse surface evolution trend, which reduces surface resistance and improves cycling capacity. To investigate this complex surface transformation, the first 100 cycles at 100 mA/g across all ionic liquid electrolytes and KFSI/ECPC are selected as the focus for surface analysis. Detailed surface characterization will provide insights into how

anion-derived SEI layers formed by ionic liquid electrolytes stabilize during the initial cycles, offering a comparison with traditional ECPC electrolytes.

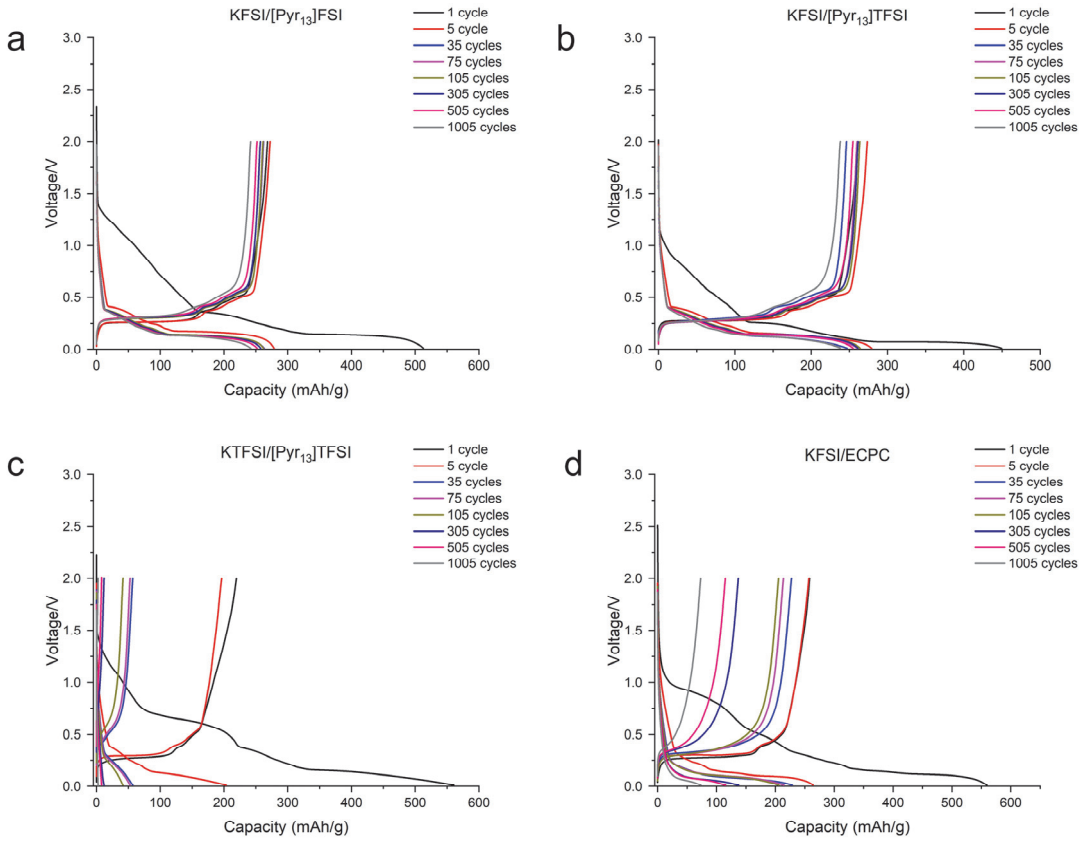

Figure 3.6. Galvanostatic discharge/charge profiles of K/Graphite cells in (a) KFSI/[Pyr_{13}]FSI (b) KFSI/[Pyr_{13}]TFSI (c) KTFSI/[Pyr_{13}]TFSI,(d) KFSI/ECPC electrolytes at 25 mA/g for 5 cycles with additional 1000 cycles at 100 mA/g.

3.2.3. Rate Capability

Based on long cycling tests with a low current of 25 mA/g for SEI formation cycles and 100 mA/g for extended cycling, we observe that capacity behavior varies significantly depending on the selected current.

When the current increases, both activation (kinetic) and concentration polarization intensify, leading to a reduction in capacity. [38] To further

investigate the polarization effects caused by current variation in ionic liquid and organic electrolytes, rate capability tests were conducted using currents ranging from 25 to 50, 100, 200, 300, 400, 25 mA/g to assess capacity under increasing current conditions (figure 3.7). For the pure FSI ionic liquid and mixed-anion ionic liquid electrolytes, similar capacity retention is observed between 25 mA/g and 100 mA/g, with capacity recovery evident in mixed-anion ionic liquids. However, a noticeable decline occurs at higher currents (≥200 mA/g). This performance drop at high currents indicates that concentration and activation polarization limits the effectiveness of ionic liquid electrolytes, primarily due to the requirement of rapid interfacial diffusion and efficient electrode reactions..[105, 106] Significant high concentration and activation polarization means the capacity failure phenomenon cannot be attributed to gradual interfacial decay and material degradation, thus making the whole analysis even harder. Thus, a low current of 100 mA/g is intentionally selected to reduce concentration and activation polarization, simplifying the decay process and enabling a clearer correlation between SEI chemistry and capacity failure, without complications from polarization effects.

The capability test for pure TFSI ionic liquids reveals that capacity failure occurs irrespective of the applied current. The decay process cannot be mitigated by reducing rapid polarization, indicating that improper interfacial accumulation plays a dominant role in the failure of pure TFSI ionic liquids. In addition, ECPC electrolytes exhibit capacity failure that worsens with higher currents, linking the poor electrochemical performance to the declining cycling stability of carbonate electrolytes under these conditions. This highlights the persistent decay behavior in conventional carbonate electrolytes, which requires further investigation for better understanding.

Although concentration polarization occurs in all ionic liquid and carbonate

electrolytes cycled at high current, it can be mitigated by applying a low current (<=100mA/g), allowing for more efficient ion diffusion. Notably, unlike the recovery cycles at 25 mA/g after the rate capability tests observed in $K_{0.15}Pyr_{0.85}FSI$, $K_{0.15}Pyr_{0.85}FSI_{0.15}TFSI_{0.85}$, and 1M KFSI/ECPC carbonate electrolytes, the graphite electrodes cycled with $K_{0.15}Pyr_{0.85}TFSI$ at 25 mA/g after rate tests exhibit unrecoverable performance. This indicates significant irreversible interfacial and material damage caused by pure TFSI ionic liquid electrolytes.

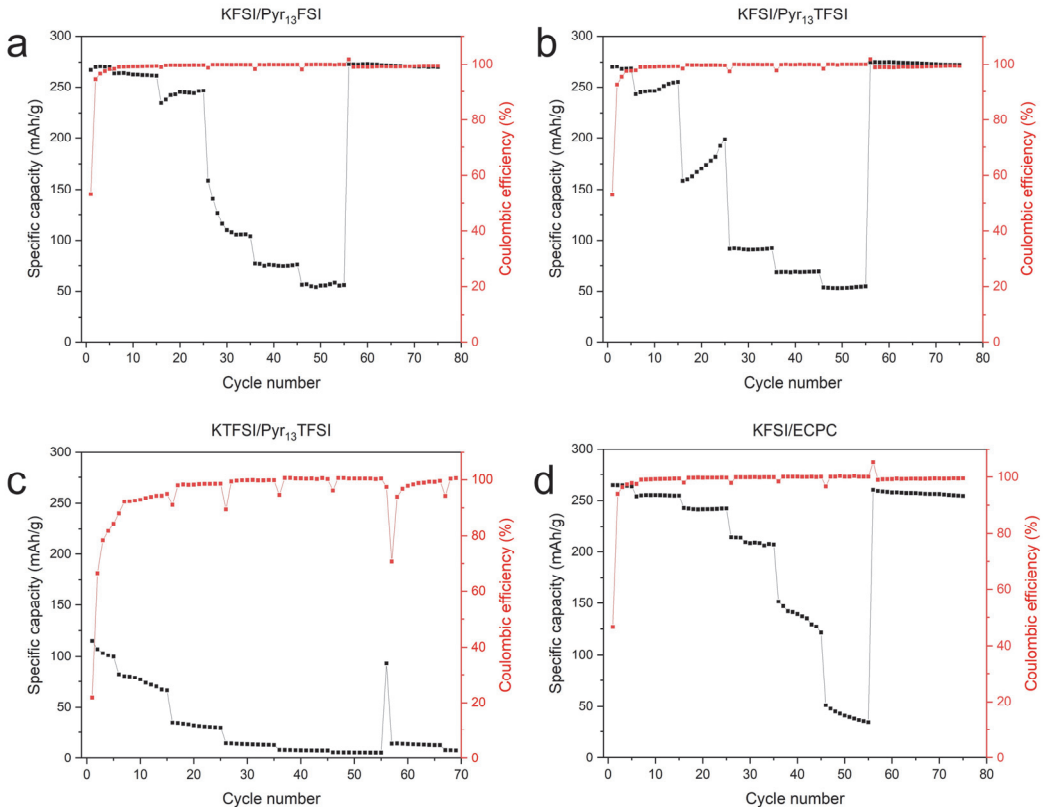

Figure 3.7. The rate capability of K/Graphite cells in (a) KFSI/[Pyr_{13}]FSI (b) KFSI/[Pyr_{13}]TFSI (c)KTFSI/[Pyr_{13}]TFSI,(d) KFSI/ECPC electrolytes.

In general, due to the complete failure of half cells containing pure TFSI anion ionic liquids, the design of $K_{0.15}Pyr_{13}FSI_{0.15}TFSI_{0.85}$ mixed-anion ionic liquids is predicted to have greater practical value. The long activation cycles observed in $K_{0.15}Pyr_{13}FSI_{0.15}TFSI_{0.85}$ at low the current of 25 mA/g,

50 mA/g, and 100 mA/g (Figure 3.7.b) indicate significant stepped interfacial changes during cycling. The unique recovery phenomenon in KFSI/[Pyr_{13}]TFSI ionic liquids further suggests that SEI interfacial chemistry evolves differently between the initial and prolonged cycling stages in ionic liquid electrolytes when the current is fixed.

To explore these interfacial changes, detailed impedance, interfacial, and material characterizations are essential for all ionic liquid electrolytes and the organic KFSI/ECPC system. The focus is on long cycling tests involving 25 mA/g for 5 SEI formation cycles, followed by 100 mA/g for the subsequent 100 cycles (figure 3.5). During these extended cycles, a notable contrast is observed: $K_{0.15}Pyr_{0.85}FSI_{0.15}TFSI_{0.85}$ exhibits significant capacity recovery, while $K_{0.15}Pyr_{0.85}TFSI$ shows marked capacity failure. By employing appropriate characterizations, we aim to establish a clear correlation between capacity variations and interfacial evolution in both ionic liquid and KFSI/ECPC electrolytes.

3.2.4. Electrochemical Impedance Spectroscopy

To investigate interfacial changes, electrochemical impedance spectroscopy (EIS) tests, as shown in Figure 3.9 (a-d), are utilized to analyze the variations in interface impedance across each of the studied systems. To stabilize interfacial reactions and eliminate transient effects after cycling, we selected OCV conditions with a 2-hour rest period. The resting period at OCV has been found to correlate with interfacial resistance[107-109]. To counteract the effects of aging on interfaces during cycling, we applied a consistent rest period of 2h.

To analyze impedance changes with extended cycles, modified Randles Model was employed, a widely used framework for impedance analysis of interface for alkali metal-ion batteries[4, 5, 55, 84, 110]. This model is based on

the classical Randles model[111], includes the electrolyte resistance in the high-frequency region, SEI resistance in the high-to-medium frequency region, charge transfer resistance in the medium frequency region, and diffusion impedance in the low-frequency region.

Figure 3.8. EIS equivalent circuit

Analysis of the impedance across different electrolytes revealed significant overall impedance variations between ionic liquid electrolytes and organic electrolytes. Although the Modified Randles Model was applied to analyze impedance changes, a clear overlap was observed between the two semicircles representing SEI resistance and charge transfer resistance. This overlap can be simplified as $R_{interface}$= R_{SEI}+R_{ct}, representing a combined interfacial resistance in a simplified model.[24] Thus, we can perform the suitable fitting of the modified Randles model to understand the variation of the impedance. To begin with, the pure FSI electrolyte system in contrast shows decreasing $R_{interface}$ with ongoing cycling, falling from 518 Ω after 5 cycles to 250 Ω after 105 cycles. The mixed-electrolyte system shows a $R_{interface}$ value of 710 Ω after 5 cycles, falling sharply to 187 Ω after 105 cycles, lower than the value for the pure FSI electrolyte system. However, in the pure TFSI system, the semicircle increases rapidly in diameter with successive cycles up to 105. The modelled charge transfer and SEI resistance (R_{SEI+CT}) of the pure TFSI electrolyte system increased from close to 1 kΩ in cycle 5 to over 10 kΩ by cycle 105. This large increase in the interface resistance correlates with the observed rapid capacity decrease on cycling. The contrary resistance evolution process of FSI-modified ionic liquid electrolytes and pure TFSI ionic liquid electrolytes can

help reveal why the capacity evolution of cycling tests exhibit significant differences depending on the choice of anion. In order to further understand and contextualize the variation of the interfaces of ionic liquids, the carbonate electrolyte is also run with the ex-situ EIS test. The decrease on in the resistance between 5 cycle and 35 cycle shows the initial stabilization of interfaces by the higher current. The following increasing trend of the resistance from 35 cycles to 105 cycles can tell the gradual decaying process of interface, which is can be closely linked with the gradual decrease on the capacity of KFSI/ECPC electrolytes.

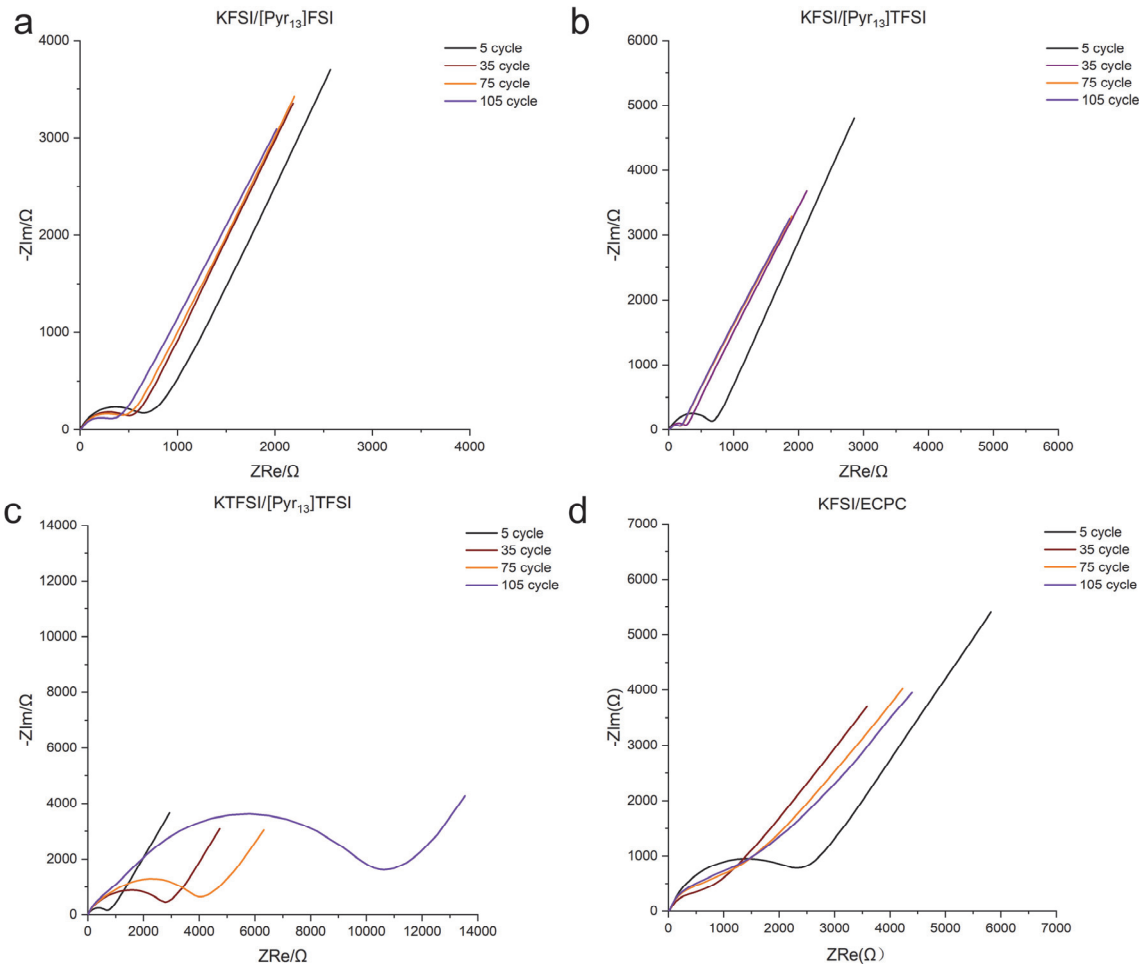

Figure 3.9. Impedance variation of K/Graphite cells cycled in (a) KFSI/[Pyr_{13}]FSI (b) KFSI/[Pyr_{13}]TFSI (c)KTFSI/[Pyr_{13}]TFSI,(d) KFSI/ECPC electrolytes at 25 mA/g for 5 cycles with additional 100 cycles at 100 mA/g.

In general, we are mainly focusing on the varying trend of impedance of graphite half cells cycled with different electrolytes. It can be understood that for the KFSI/[Pyr_{13}]FSI ionic liquid electrolytes, one decrease on the impedance is observed, this trend proves that the SEI layer is transferred to one state with high ion conductivity. One special case is, the increase of the interface resistance seen with TFSI anions is reversed when part of the anion is replaced with FSI in the electrolyte $K_{0.15}Pyr_{0.85}$TFSI. The reverse trend proves the influence of FSI anions in ionic liquid electrolytes on stabilizing the interfacial behavior. The stabilization trend of the SEI layer is absent in common carbonate electrolytes with interface impedance increasing after 35 cycles. This decrease in impedance is associated with the interface activation process over cycling in PIBs.[20]In addition, the variation of the Warburg resistance (closer to concentration resistance)[112] is minor along with the cycles, which proves the dominating role of interfacial changes in determining the impedance. This provides a foundational understanding of capacity failure behavior and emphasizes the importance of interfacial analysis on graphite electrodes during extended cycling, setting the stage for future research.

3.3. Characterization of Cycled Graphite Electrodes for Capacity Failure Analysis

The detailed electrochemical analysis above clearly demonstrates that variations in capacity failure are predominantly influenced by the composition of different ionic liquid electrolytes and carbonate electrolytes. To investigate the distinct failure processes in PIBs, graphite electrodes cycled in different electrolytes were selected as the primary analysis targets. These include electrodes after the initial cycles (25 mA/g for 5 cycles) and extended cycles (25 mA/g for 5 cycles followed by 100 mA/g for long

cycling). We focus on the structural damage by using the SEM and XRD techniques, and the interfacial analysis using XPS and TEM techniques. Through comprehensive failure analysis, we can identify the most critical tools and extract key failure information occurring during cycling.

3.3.1. SEM Characterization of Morphology of Cycled Graphite Electrodes

To examine structural damage in graphite electrodes during extended cycling in PIBs, SEM is commonly employed to study the morphological changes in graphite crystals over time. The initial SEM images of the graphite electrodes clearly reveal a flake-like structure, regardless of the microscope's orientation relative to the electrode. We can see from the original images of graphite electrodes, the graphite flakes are stacked together (figure 3.10). In addition, a few agglomerates are observed attached to the graphite flakes. These agglomerates likely result from the aggregation of tiny conductive carbon black particles, which, due to its high specific surface area, tends to cluster for aggregation.[113] This agglomeration behavior of carbon black is commonly observed in SEM analysis of graphite electrodes in PIBs.[87, 95, 96] The overall image reveals the flake graphite with smooth surfaces and sharp edges. Additionally, the graphite electrodes exhibit stacking properties, partly attributed to the effective role of the PVDF binder in connecting the graphite flake crystals. During cycling, the flake surfaces of the graphite electrodes generally become rougher. Closer examination reveals distinct surface differences on graphite electrodes cycled with different electrolytes. When the cycles are given to 5 cycles, one important trend is that the entire graphite structures are preserved well in KFSI/[Pyr_{13}]FSI (figure 3.11 a,b) and KFSI/[Pyr_{13}]TFSI](figure 3.11 c,d). However, fractures in the graphite

crystal become apparent when the graphite electrode is cycled in KTFSI/[Pyr_{13}]TFSI electrolytes (figure 3.11 e,f). In addition, noticeable cracking is observed in graphite electrodes cycled in KFSI/ECPC electrolytes (figure 3.11 g,h), indicating higher stress accumulation under these conditions. The deterioration of graphite crystals is a common observation in PIB graphite analysis and is more pronounced in electrolytes exhibiting capacity failure behavior.[87, 95, 96] This indicates that graphite crystals are better preserved when cycled with FSI-based ionic liquid electrolytes.

As shown in figure 3.12, prolonged cycling leads to an overall crystal rounding behavior in all samples. The edges of flake graphite crystals transition from sharp (after 5 cycles) to smooth (after 5+100 cycles). This trend highlights the long-term mechanical and physical effects of the potassium intercalation process. The primary difference between electrolytes lies in the extent of graphite electrode deterioration. Significant deterioration is observed in electrodes cycled with pure TFSI ionic liquids (Figures 3.12 e, f) and pure ECPC electrolytes (figures 3.12 g, h). In contrast, the surfaces of stacked graphite crystals cycled in the pure FSI ionic liquid and the mixed-anion ionic liquid electrolytes appear smoother.

In general, we selected two resolution ratios to capture subtle structural changes during cycling. For flake graphite powder with a particle size of approximately 3 micrometers, these resolutions are well-suited for analyzing individual graphite particles. However, for larger graphite particles, imaging isolated particles may not yield representative results due to the inherent limitations of SEM, particularly its constrained sampling area.[114] While enlarging the scanned area can include more graphite particles, it also complicates the detection of minor surface alterations. These limitations underscore the importance of incorporating complementary characterization techniques to fully elucidate the

electrode's structural evolution.

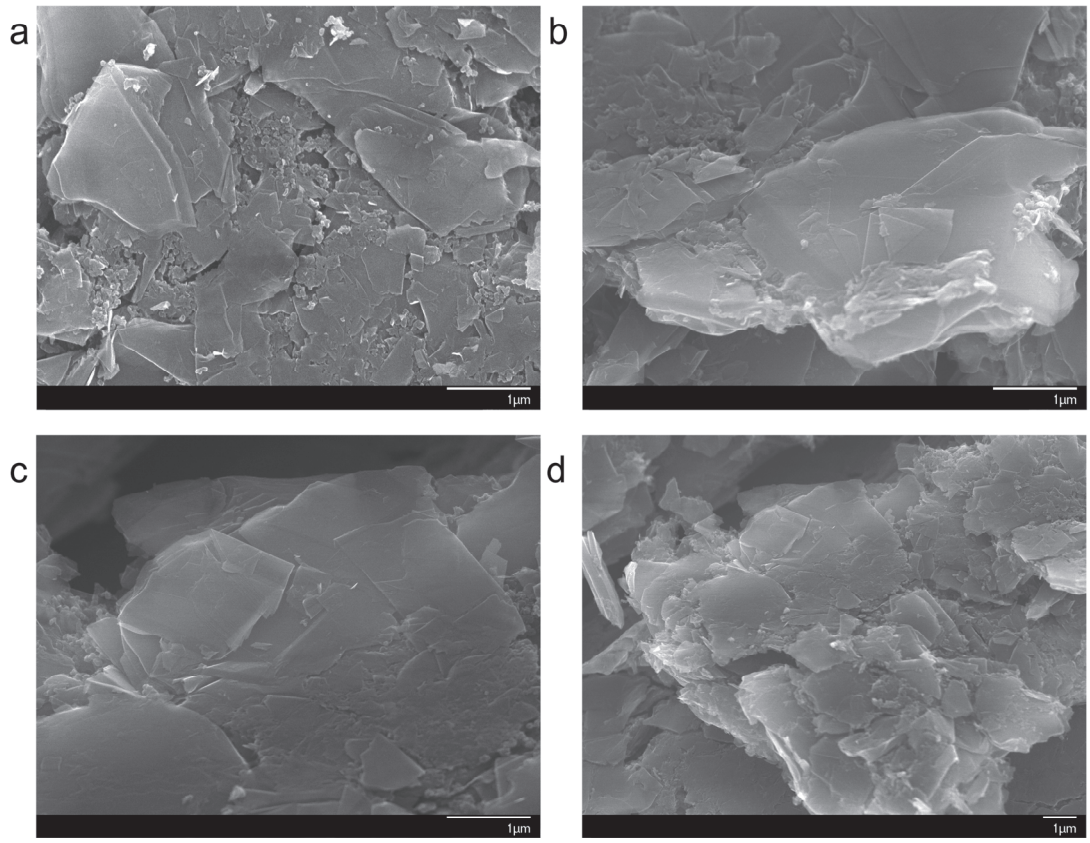

Figure 3.10. SEM images (a-d) of initial graphite flake structure.

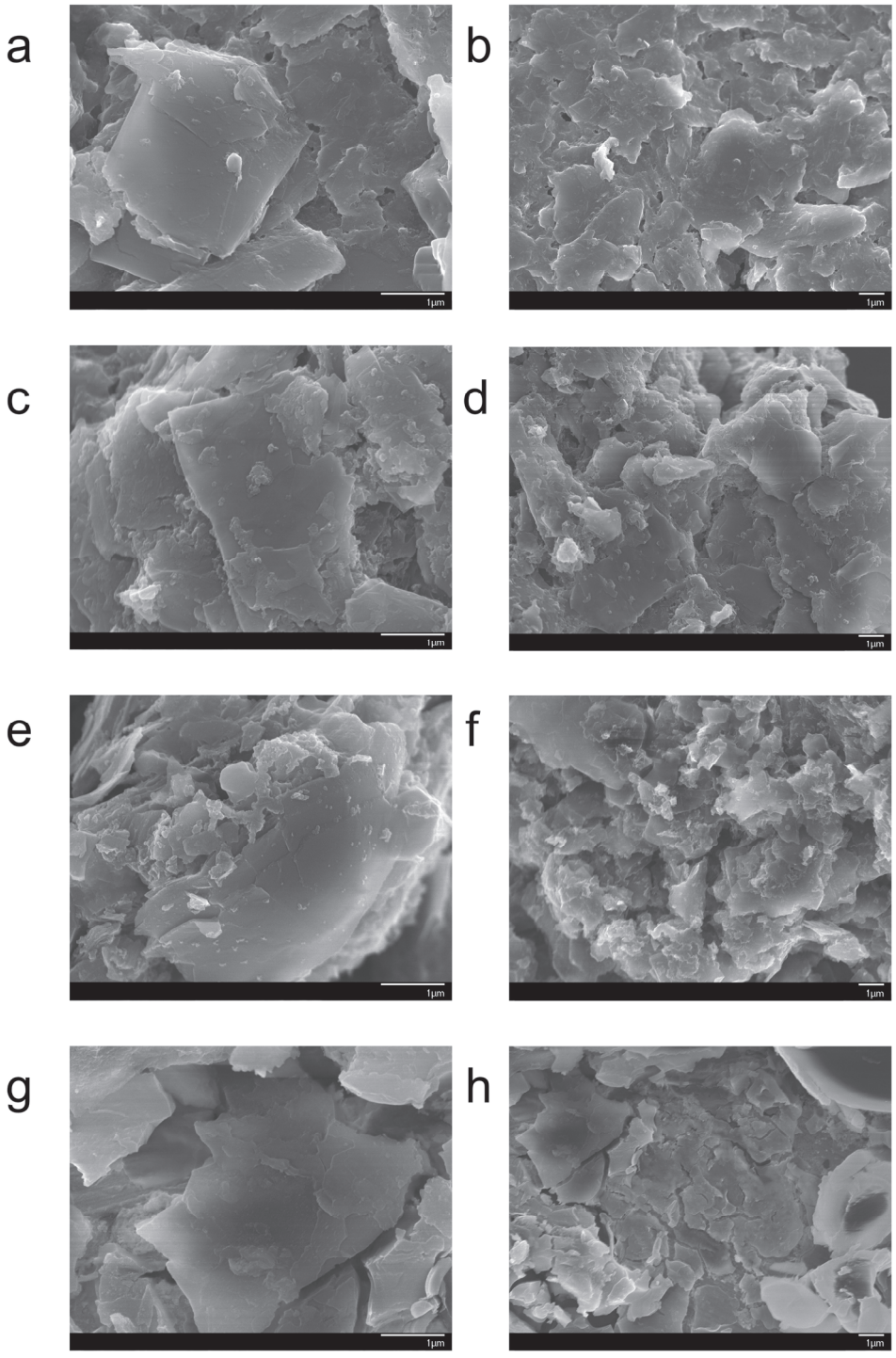

Figure 3.11. SEM images of the graphite electrodes cycled in (a,b) KFSI/[Pyr_{13}]FSI(c,d)KFSI/[Pyr_{13}]TFSI(e,f)KTFSI/[Pyr_{13}]TFSI,(g,h)KFSI/EC PC electrolytes at 25 mA/g for 5 cycles.

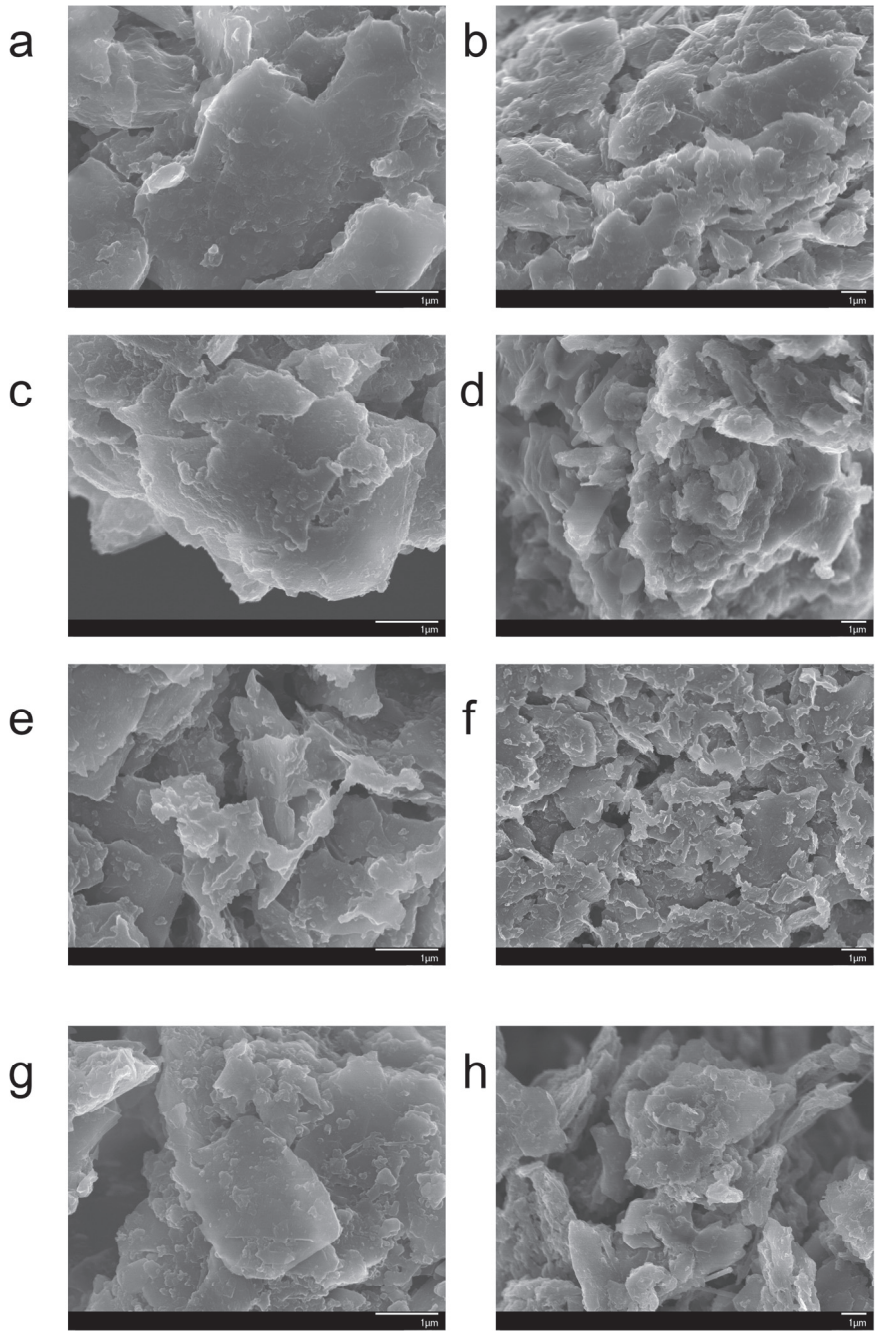

Figure 3.12. SEM images of the graphite electrodes cycled in (a,b) KFSI/[Pyr_{13}]FSI(c,d)KFSI/[Pyr_{13}]TFSI(e,f)KTFSI/[Pyr_{13}]TFSI,(g,h)KFSI/EC PC at 25 mA/g for 5 cycles with additional 100 cycles at 100 mA/g.

Based on SEM analysis of cycled graphite electrode crystals, it is evident that long-term cycling is linked to variations in the crystal structure. The degradation of graphite electrode materials may contribute to differences in capacity retention among electrolytes after extended cycling. However, capturing clear images of graphite crystal morphology (~3 micrometers) requires a high-resolution ratio, limiting the ability to observe the full extent of crystal changes. To provide a more comprehensive understanding of crystalline changes in graphite electrodes, alternative methods of crystal analysis are being considered.

3.3.2. XRD Characterization of Structural Degradation in Cycled Graphite Electrodes

Based on the SEM analysis of the cycled electrodes, it is clear that the crystal of the graphite electrodes can be degraded after extended cycles.
To further validate our findings on graphite crystal variation, we employed standard ex-situ X-ray diffraction (XRD) to gain deeper insights into crystallinity changes. This method is widely used for analyzing graphite electrodes in alkali metal-ion batteries. For graphite crystals with a layered structure, the intense [002] peak is regarded as the most critical feature.
As illustrated in Figure 3.13, a noticeable difference in peak intensity is observed when the graphite thin films, direct comparisons of graphite intensity are challenging when the actual mass loading is hard to be preserved. To emphasize subtle variations in the graphite pattern, the full-width at half-maximum (FWHM) is used as an independent measure to assess structural degradation. The full-width at FWHMof the [002] peak is a key metric for assessing the crystallinity variation of graphite in PIBs, independent of peak intensity.[6, 80, 89] Larger FWHM indicates lower crystal quality. However, the accuracy of FWHM measurements is highly sensitive

to the selection of the [002] peak region.[115] To ensure consistent analysis across all cycled graphite electrode crystals, we employed standard ex-situ XRD analysis over the angle range of [10° to 60°], with a particular focus on the crystalline changes of the [002] peak.

To begin with, the crystalline state is preserved at the initial cycles and after 100 additional cycles when the KFSI/[Pyr_{13}]FSI and KFSI/[Pyr_{13}]TFSI are used (figure 3.13 b-e). The crystalline state closely resembles that of the pristine graphite electrode, indicating minor structural damage to the graphite electrodes.However, a significant decline in the crystalline state is observed in graphite crystals cycled with pure TFSI electrolytes (0.41° at 105 cycles, figure 3.13g) and pure KFSI/ECPC electrolytes (0.54° at 105 cycles, figure 3.13 i), consistent with the stepped structural damage identified through SEM analysis. .

To compare the primary graphite patterns of cycled electrodes exhibiting structural degradation, the XRD patterns of graphite cycled in different electrolytes for 105 cycles were normalized for FWHM analysis (Figure 3.14a).The crystalline state of graphite is better preserved in PIBs even after 100 additional cycles when suitable ionic liquid electrolytes are used. This indicates a more reversible and safe intercalation process, resulting in less graphite crystal degradation in the pure FSI ionic liquid and mixed-anion ionic liquid electrolytes, as evidenced by crystallinity analysis. For graphite crystals cycled in pure TFSI and ECPC electrolytes, a pronounced loss of crystallinity is observed. The reduction in the intensity of the pristine graphite peaks, coupled with peak broadening, gives rise to numerous small, convoluted peaks upon normalization. These minor features indicate that, in addition to the overall broadening of the central graphite 002 peak, there is an extra polycrystalline state characterized by a layer with reduced d-spacing. The broadening of the peak near the [002] reflection indicates that highly ordered graphite has transformed into a more disordered state,

as reported in previous studies.[1, 80, 116] This outcome tells that the solvent co-intercalation process, stress accumulation and uneven SEI distribution can happen and ultimately affect the crystal structures when unsuitable electrolyte systems are used.

To assess the influence of graphite microstructures on capacity failure, the distorted cycled graphite was refreshed by removing the SEI and electrolyte. This refreshed graphite restored an initial capacity comparable to that of the graphite in identical graphite/K half-cell configurations. The performance proved that the microstructure damage of graphite electrode as the SEI evolution in potassium-ion batteries.[80] Based on previous research, we consider the accumulated crystalline loss to be a minor factor affecting capacity. Additionally, in two Graphite/Potassium system cycled in KTFSI/[Pyr13TFSI] and KFSI/ECPC electrolytes, the disordered graphite structure is even restrained after 100 additional cycles (figure 3.14 b) with the decrease of FWHM (Table 1). Despite the highly ordered structure of graphite, severe capacity failure is observed after 100 additional cycles at 100 mA/g. With the exception of the extreme cases of KTFSI/[Pyr_{13}]TFSI and KFSI/ECPC electrolytes, only a slight increase in FWHM is noted for KFSI/[Pyr_{13}]FSI and KFSI/[Pyr_{13}]TFSI electrolytes, indicating that the graphite experiences minimal structural damage over these 100 cycles. Based on the XRD patterns, we conclude that the crystalline failure observed cannot solely account for the complex capacity failure problems, suggesting that the evolution of the SEI layer is the dominant factor in the failure analysis.

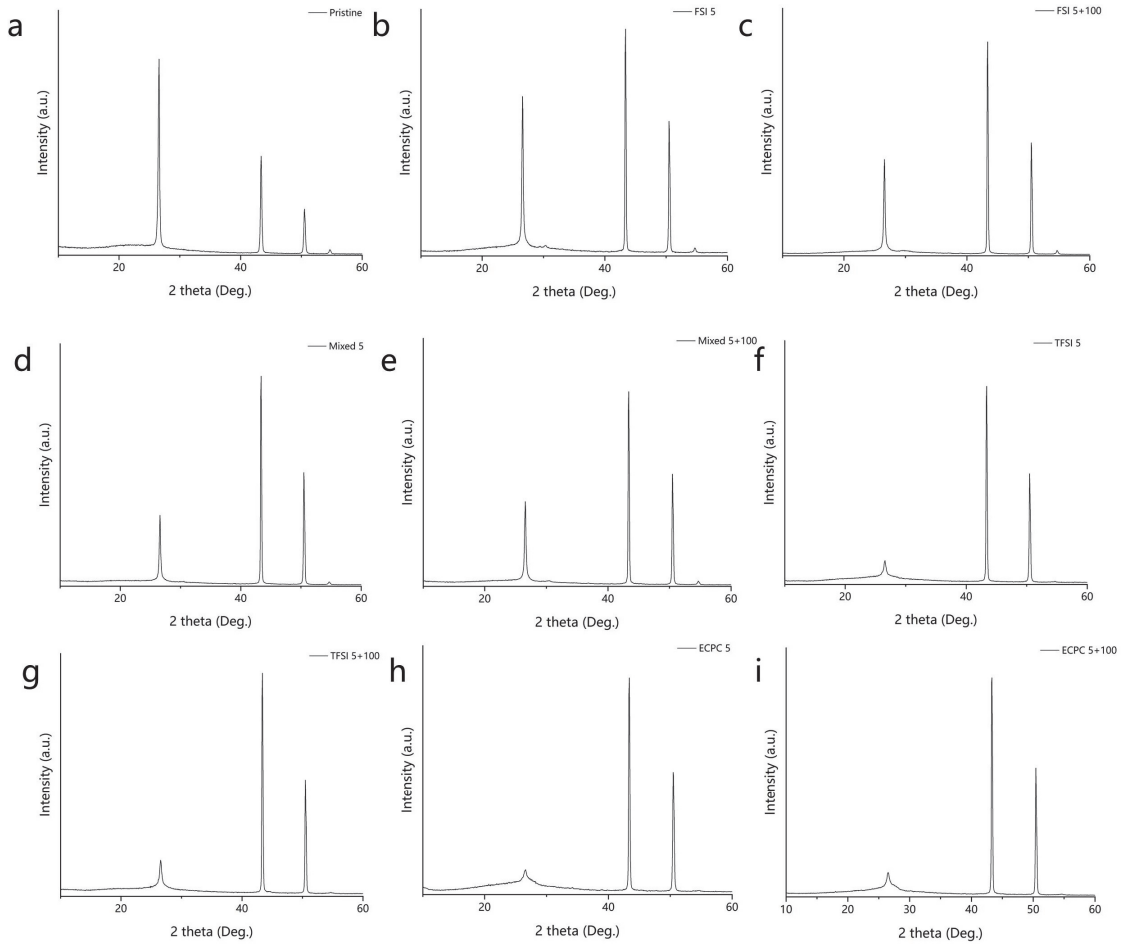

Figure 3.13. Overall XRD patterns of (a) fresh graphite and (b-i) cycled graphite electrodes in (b,c) KFSI/[Pyr_{13}] FSI (d,e) KFSI/[Pyr_{13}]TFSI (f,g) KTFSI/[Pyr_{13}]TFSI (h,i) KFSI/ECPC electrolytes at 25 mA/g for 5 cycles without and with additional 100 cycles at 100 mA/g.

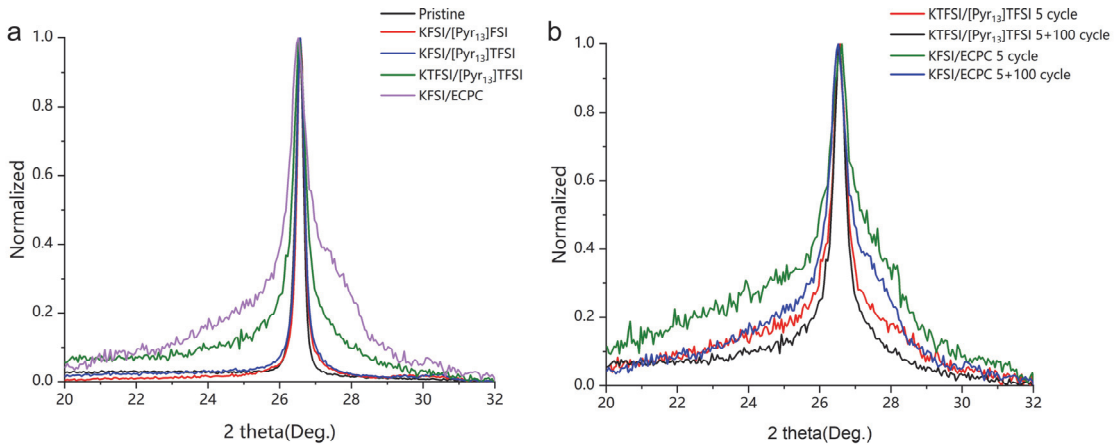

Figure 3.14. (a) The XRD pattern after normalized of the cycled graphite electrodes in ionic liquid and KFSI/ECPC electrolytes at 25 mA/g for 5 cycles with additional 100 cycles at 100 mA/g (b) The XRD pattern after normalized of the cycled graphite electrodes in KTFSI/[Pyr_{13}]TFSI and KFSI/ECPC electrolytes at 25 mA/g for 5 cycles with and without 100 additional 100 cycles at 100 mA/g

Table 1. Full width at half maximum of [002] peak with the baseline range of 1.5° of the graphite electrodes cycled by different electrolytes

Cycle number	KFSI/[Pyr_{13}]FSI	KFSI/[Pyr_{13}]TFSI	KTFSI/[Pyr_{13}]TFSI	KFSI/ECPC	Prinstine
5th	0.24°	0.26°	0.43°	0.56°	0.25°
105th	0.25°	0.27°	0.41°	0.54°	

3.3.3. Interfacial analysis of the Cycled Graphite Electrodes using TEM

Given the morphological features from SEI analysis and the crystalline state insights from XRD, it can be concluded that the graphite electrode crystals are well-preserved when cycled with KFSI/[Pyr_{13}]FSI and KFSI/[Pyr_{13}]TFSI ionic liquid electrolytes, providing a foundation for long-term stable cycling. However, the evolution of SEI layers in both ionic liquid electrolytes and KFSI/ECPC electrolytes remains poorly understood, the detailed variation of the thin SEI layer with cycles on graphite electrodes remains challenging to analyze comprehensively. Thus, the techniques with higher resolution ratio of the thin SEI layers are required.

TEM analysis of the SEI layer is widely used to examine the surface of graphite electrodes and determine the thickness of SEI layers. The nanoscale structure of the SEI on graphite electrodes has become a focal point in potassium-ion battery research.[6, 7, 9, 87, 95]

To quantitatively measure the SEI layer thickness, we performed TEM analysis on separated graphite particles. In most cases, the TEM images primarily display stacked graphite electrode crystals, as shown in Figure 3.15 (a, c). The stacked layered structure of graphite is a prevalent feature in electron transmission analysis and has been extensively investigated in previous in situ and cryo-TEM studies focusing on the solid electrolyte interphase (SEI).[117-119] In previous SEI analyses of graphite in PIBs using conventional ex-situ TEM, researchers focused on targeting the edges of thin graphite layers to enhance electron transmission, aiming to obtain clear images that reveal both the graphene layered structure and the SEI.[6, 7, 9, 87, 95]. We attempted to focus on the edges of the graphite, but the stacked graphite structure makes it challenging to find the suitable region that encompasses both the interfaces and the graphite electrodes

simultaneously. Only in the specific ultra-thin regions (Figure 3.15 b, d) can the difference between the SEI layer and the graphite electrodes be distinctly observed. The [002] structure of the graphite, with its outline parallel to the edge, is clearly visible in (Figure 3.15 b).

Although it is challenging to clearly delineate the SEI layer on graphite electrodes using TEM, one conclusion can be given: the SEI layer is an ultrathin coating (~5 nm) covering the graphite electrodes with nanoscale depth. TEM analysis of the graphite electrode provides valuable quantitative support for XPS measurements, aiding in determining the estimated thickness of the SEI layer. Furthermore, the ultrathin nature of the SEI layer observed in the TEM images explains why it is not visible in SEM images. The SEI layer's thickness is significantly smaller than the resolution limit of SEM, making it difficult to detect through SEM analysis.

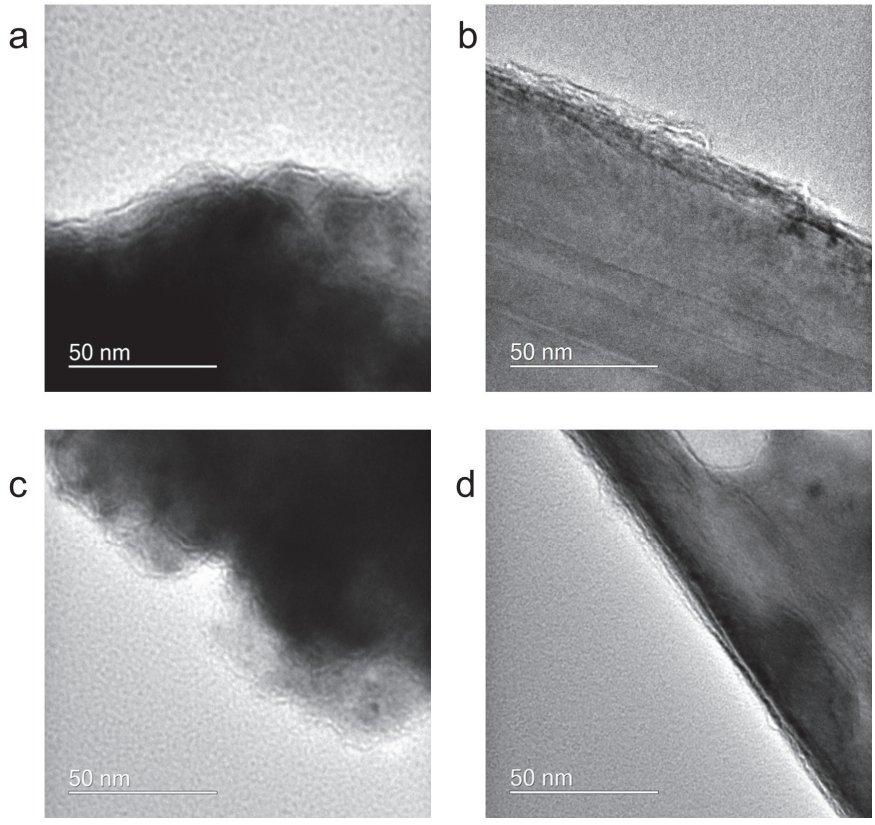

Figure 3.15. The surface structure of graphite particle cycled in KFSI/Py_{13}TFSI ionic liquid cycled at 25 mA/g for 5 cycles (a,b) without and (c,d) with additional 100 cycles at 100 mA/g.

3.3.4. Characterization of Graphite Electrodes Using XPS

Due to the limitations of TEM in accurately analyzing interfacial evolution, more detailed nanoscale surface characterization methods are needed. XPS analysis is particularly suitable because of its high surface sensitivity and ability to detect both inorganic and organic species, providing detailed chemical information about the interface. To investigate the causes of graphite electrode degradation, it is essential to obtain accurate interfacial information through XPS analysis. This will enable a deeper understanding of the interfacial changes driving the capacity failure phenomenon.

3.3.4.1. Surface XPS Characterization of Materials Used in Potassium/Graphite cells

To gain a better understanding of the surface transformation of the SEI, XPS analysis was performed on the graphite electrode and ionic liquid electrolyte. This analysis provides an initial understanding of the primary signals from both the electrode and the ionic liquid electrolyte, enabling the identification and separation of potential electrolyte residues and electrode during SEI surface XPS analysis. Additionally, analyzing the surface of the commercial glassy fiber separator allows us to assess whether its purity is maintained, which is critically important for nanoscale XPS surface analysis. To begin with, it can be observed that the graphite powder exhibits binding energy and peak shapes (Figure 3.16 a, b) that are quite similar, which is attributed to their comparable C-C environments.[120] When XPS analysis is performed on the graphite electrode thin film, the similarity in binding energy makes it difficult to distinguish the signals from graphite and carbon black. However, a distinct CF_2 peak, located near 291 eV, is clearly

separable from the main C-C group in C1s spectra. The presence of the CF_2 signal in both the C 1s and F 1s spectra serves as a key indicator of the PVDF binder in the graphite electrode. Contrary to the high binding energy of CF_3 (>292 ev) from $Pyr_{13}TFSI$ which can be overlapped with potassium species. The XPS signal of the PVDF binder can be used as a criterion to determine whether the graphite electrode is involved in the surface XPS analysis.

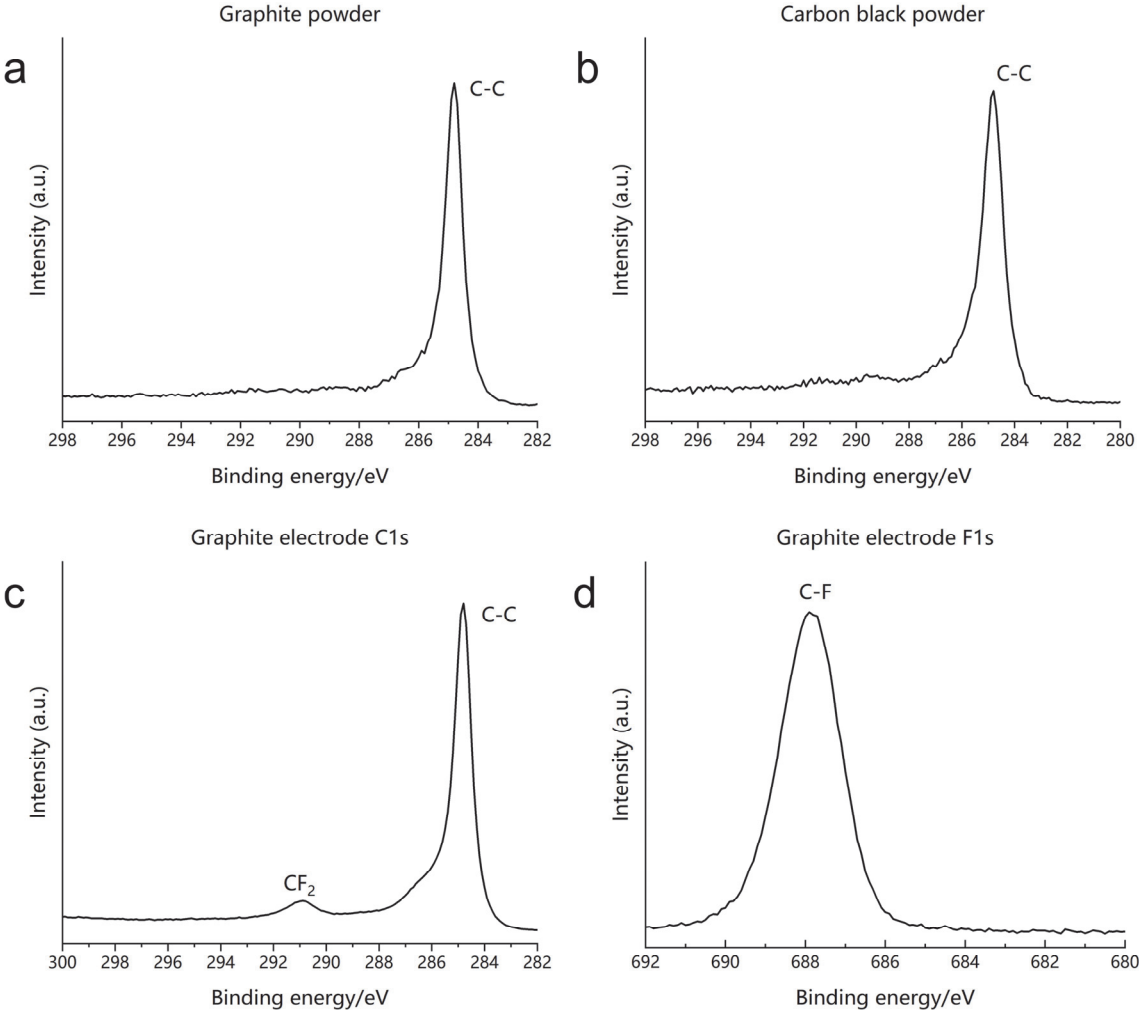

Figure 3.16. (a-d) C1s and F1s high resolution spectra from pure graphite electrodes.

In addition to analyzing the basic graphite electrodes, we also performed XPS analysis on the glassy fiber separator used in the study. As the glassy fiber separator is a critical material in PIBs and has potential industrial

applications, it is essential to evaluate its purity before conducting surface analysis of the SEI layer on the graphite electrode.

XPS analysis of the glassy fiber surface revealed significant findings: even in fresh commercial glassy fiber separators, clear impurities of Na and K were detected (figure 3.17 a,b). These impurities suggest that the use of glassy fiber could introduce trace amounts of sodium and potassium species during battery cycles. Specifically, the ratio of sodium to silicon peaks is approximately 1:9, the peak area analysis indicates that sodium species cannot be ignored. This observation is particularly important, as glassy fiber separators are widely employed in PIBs to mitigate the accumulation of potassium dendrites on the separator surface throughout cycling. For the even more active potassium metal compared with the lithium metal, the glassy fiber is one very important and safe separator used for electrochemical analysis.[121] Based on the surface analysis of the glassy fiber, the detected impurities of Na and K in the separator highlight that the role of glassy fiber should not be overlooked in the capacity failure of PIBs. In reality, the presence of trace transition metal impurities is common due to the industrial manufacturing processes involved in producing glassy fiber.[122] However, in previous studies analyzing the SEI layer on graphite electrodes using glassy fiber as the separator, the glassy fiber has often been assumed to be a pure and clean medium, incapable of contributing impurities.[6, 9-11]

In most cases, minor transition metals are not expected to accumulate in the SEI layer during cycling. However, a notable exception is sodium, which shares very similar reducibility and redox potential with potassium. This high similarity may allow common sodium salts in the SEI layer, such as Na_2O, Na_2CO_3[123], to incorporate into the SEI layer of PIBs, even in scenarios where sodium species are not anticipated. To address this previously overlooked aspect, we introduce, for the first time, a detailed SEI

analysis of minor sodium species—an area that has been a blind spot in prior investigations.

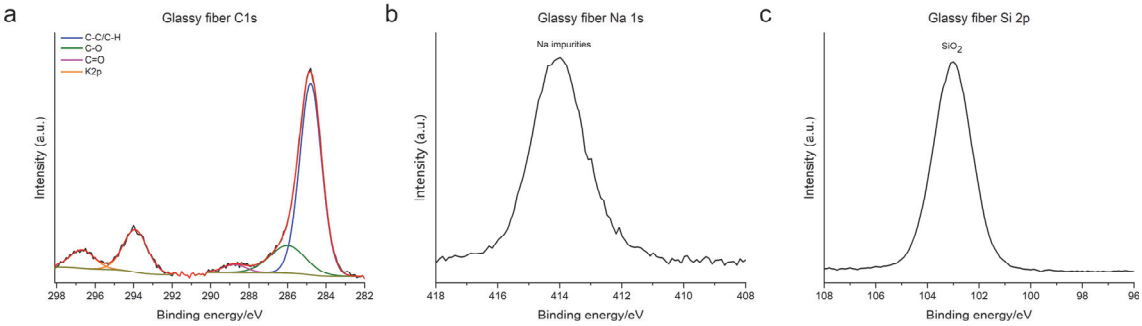

Figure 3.17. (a-c) XPS analysis of the fresh commercial glassy fiber without any surface treatment.

Compared to well-studied carbonate electrolytes, the XPS surface analysis of SEI layers formed by ionic liquid electrolytes is significantly more complex due to the uncertainty surrounding the degradation mechanisms of ionic liquids. The high vacuum stability of ionic liquid electrolytes allows them to be preserved under such conditions. This means that it is possible to measure XPS spectra from the ionic liquids themselves. XPS was measured on $Pyr_{13}FSI$ and $Pyr_{13}TFSI$ ionic liquids to investigate the XPS binding energies of their key functional groups, providing a foundation for understanding the decomposition processes of ionic liquids during SEI layer formation (figure 3.18).

For the C 1s spectra, peaks corresponding to carbon in different chemical environments can be easily identified. To begin with, a distinct CF_3 peak is observed at 292.5 eV, which overlaps within the binding energy range of potassium ions (K 2p peak). This creates a significant challenge in fitting the CF_3 peak and the K2p peak when TFSI anions are present in the electrolytes. In contrast, the CF_2 peak from the graphite electrode, located at 291 eV, exhibits a substantial binding energy difference from the potassium peak, making it easier to distinguish. Additionally, the C-N peak

(286.5 eV) and C-C peak (284.8 eV) are clearly observed in the C1s spectra (Figure 3.18 a, b). Although the C-C and C-N bonds from the Pyr_{13} cation should exhibit the same peak area ratio in $Pyr_{13}FSI$ and $Pyr_{13}TFSI$ ionic liquids, our experiment reveals differences in the overall peak shapes. The differences in mobility and surface charge distribution arisen from anions contribute to the variations in intensity observed for these two main peaks.[124, 125]

In the N 1s region, two distinct peaks corresponding to N_{cation} (402 ev) and N_{anion} (399ev) are observed with similar intensity areas, reflecting the stoichiometric equivalence of the two nitrogen species. The range between 404–396 eV provides valuable reference data for subsequent XPS analysis of the SEI layer, particularly when nitrogen is present in trace amounts. For the O 1s spectra of the two ionic liquid electrolytes, a peak assigned as S=O at 532.2 eV is present in both liquids. The fitting of oxygen spectra is challenging due to the overlap and similarities among most oxygen peaks. Therefore, accurate analysis relies primarily on the peak area, provided the selected region (536–528 eV) minimizes background noise. Additionally, the sulfur spectra exhibit two distinct peaks, S $2p_{1/2}$ and S $2p_{3/2}$, which clearly indicate the presence of (S=O)-N groups from the anions. In the fluorine spectra, clear differences are observed between the S-F peak at 687.4 eV and the C-F peak at 688.4 eV. These binding energies provide valuable reference points for identifying and fitting the C-F and S-F components in subsequent spectral analyses.

In addition to providing qualitative analysis of elemental valence changes, XPS enables valuable quantitative insights into the composition of surface species. During the initial analysis of ionic liquids, the atomic ratios of elements were collected and compared with the theoretical atomic percentages derived from the chemical formula. To enhance the accuracy of atomic ratio calculations, an appropriate fitting range and a Shirley

baseline were employed to accurately determine the integrated area of target elements, even at low resolution. This approach ensures minimal error in atomic ratio calculations for the bulk system After calculating the atomic ratios, it is evident that the mol% values for the individual elements closely align with those of the actual chemical formula. For example, the calculated atomic ratios of N (9.32%) and F (9.19%) are close to the theoretical ratio of 11.11%. While the atomic ratios derived from XPS analysis may not perfectly match the true atomic ratios of the ionic liquid electrolytes, the quantitative results still effectively reflect the relative proportions of the elements. This similarity highlights an important feature of XPS quantitative analysis: it can reliably provide the relative ratios of elements, even when their surface distributions vary due to the mobility of the liquid.

Table 2. The experimental and theoretical atomic ratio of the $Pyr_{13}FSI$ and $Pyr_{13}TFSI$ ionic liquid

	C	N	O	S	F
$Pyr_{13}FSI$ (Experiment)	48.15%	9.32%	20.9%	12.43%	9.19%
$Pyr_{13}FSI$ (Theoretical)	44.44%	11.11%	22.22%	11.11%	11.11%
$Pyr_{13}TFSI$ (Experiment)	42.18%	7.26%	16.08%	9.65%	24.8%
$Pyr_{13}TFSI$ (Theoretical)	41.67%	8.33%	16.67%	8.33%	25%

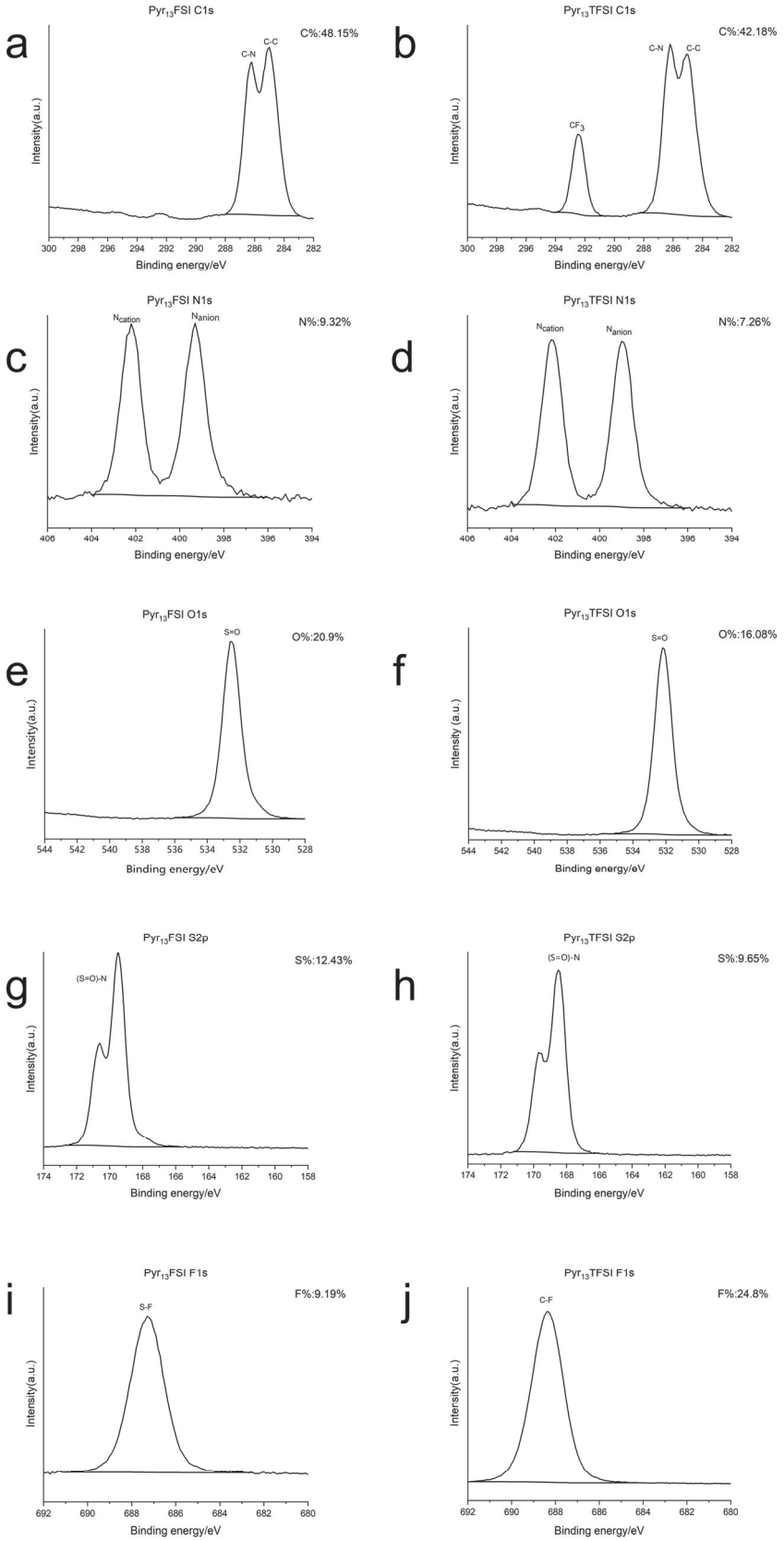

Figure 3.18. (a-j) XPS analysis of the fresh $Pyr_{13}FSI$ ($C_8H_{18}F_2N_2O_4S_2$) and $Pyr_{13}TFSI$ ionic liquid ($C_{10}H_{18}F_6N_2O_4S_2$).

3.3.4.2. XPS characterization of the Surface of Unwashed Graphite Electrodes after Cycling

After examining the surface characteristics of the IL and glassy fibrer materials, we can devise an effective approach for analyzing the SEI layer on graphite electrodes. Understanding the chemical composition of the SEI layer requires identifying a precise method to separate the electrolytes from the SEI at the interfaces. However, this analysis is particularly challenging due to the persistent difficulty of completely removing residual electrolytes from the interfaces.

In order to understand the residual quantity of the electrolytes on the graphite electrodes, we took unwashed graphite electrode from the coin cell after 5 cycles in KTFSI/[Pyr_{13}]TFSI ionic liquid electrolytes as the target for surface XPS analysis. However, the surface XPS information of cycled graphite electrodes (figure 3.19) exhibits significant similarities to that of pure TFSI ionic liquids (figure 3.18). For example, the carbon spectrum is characterized by distinct peaks corresponding to CF_3, C-N, and C-C groups (figure 3.19a). Although there is overlap between the potassium peak and the CF_3 signal, the presence of potassium species is difficult to discern due to the dominance of the large carbon peak at 292 eV. Additionally, the N1s spectrum reveals two prominent C-N peaks, likely originating from the cations and anions. The distinct separation of these peaks, along with a significant atomic percentage of 7.3%, suggests the unreacted presence of the both cation and anion functional groups. Furthermore, an unexpected observation is the minimal change in peak positions for O=S in the O1s spectrum and S=O in the S2p spectrum. The atomic ratio of surfur main peaks at 1:2 confirms that the sulfide backbone of the anions remains largely intact and undecomposed.The strong similarity in XPS data between the unwashed graphite surface and ionic liquid electrolytes

suggests the possibility that the graphite surface is coated with electrolytes, at a thickness beyond the detection depth of XPS (around 5 nm). To confirm this hypothesis, Ar ion etching was applied to the ionic liquid electrolytes to evaluate the effects of Argon etching on revealing deeper layers of the unwashed surface. To assess whether the ethcing has removed the IL overlayer, the presence of the SEI layer was detected using the F1s spectrum, specifically to detect the presence of KF, a key component of the SEI layer formed by fluorine-containing electrolytes in PIBs.[6, 10, 11, 41, 89, 96] However, when etching methods were applied to pure TFSI ionic liquids, the main signal remained unchanged, and no XPS evidence of SEI layer components, such as KF, was observed (Figure 3.19f). The absence of KF suggests that the SEI layer may be obscured by a thick layer of ionic liquid electrolytes, which cannot be removed simply through Ar ion etching. Furthermore, atomic ratio calculations from Figure 3.19f reveal a high similarity in the atomic percentage of fluorine (F), confirming the inability of etching to access the surface information of the SEI layer beneath the ionic liquid electrolytes.

In summary, the XPS analysis of the unwashed graphite electrode surface reveals that, based on the atomic percentages and specific peak positions of individual elements, the surface is predominantly covered by a significant amount of electrolyte, resembling pure ionic liquids. Attempts to etch with Ar-ion failed to remove this layer andto access the SEI. Therefore specialized alternative treatment methods are necessary for effective SEI analysis using XPS.

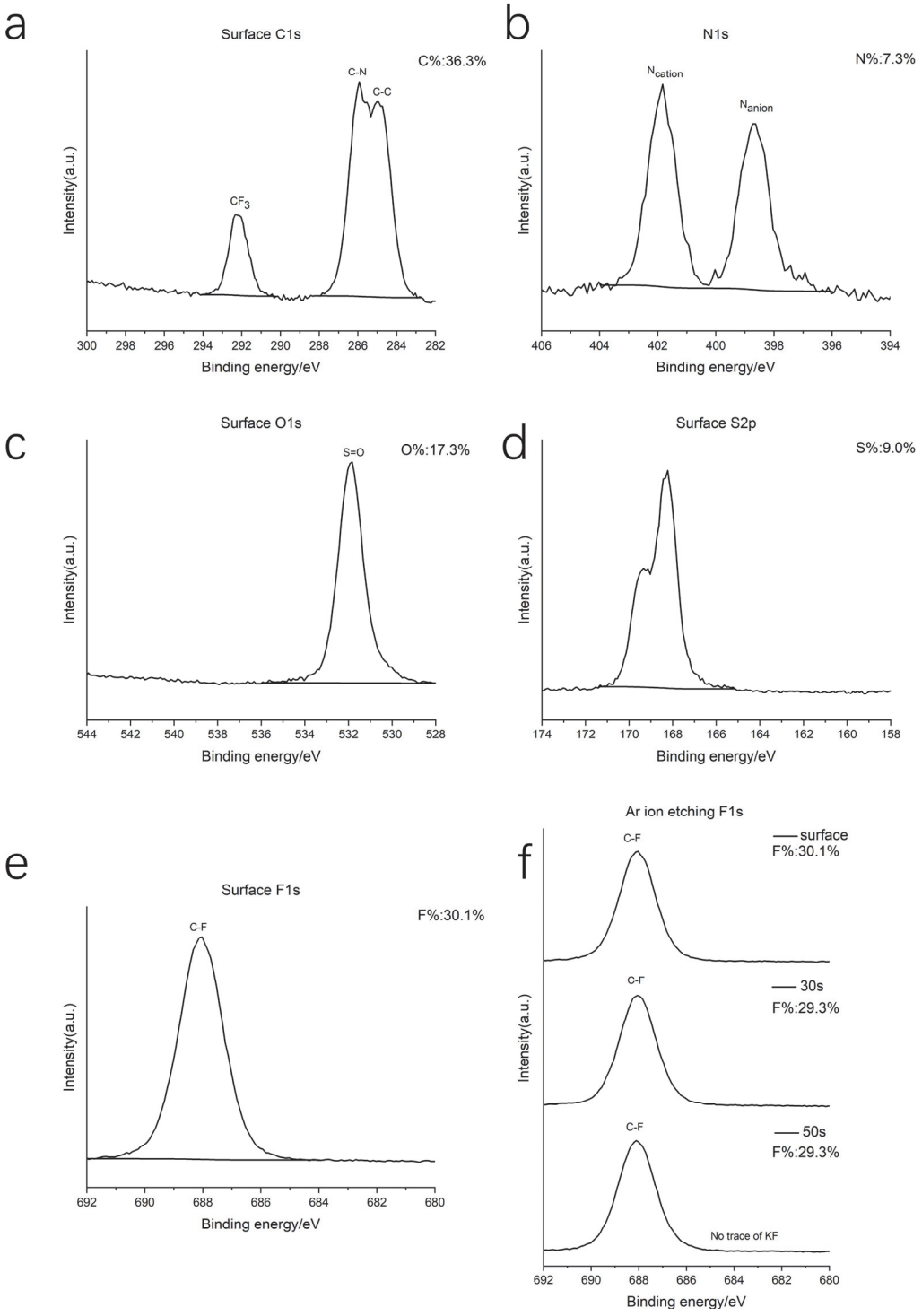

Figure 3.19. XPS spectra of (a-e) the surface of graphite electrode, and (f) the fluorine spectra of graphite electrode with Ar ion etching in in KTFSI/[Pyr_{13}]TFSI ionic liquids at 25 mA/g for 5 cycles.

3.3.4.3. Interfacial Characterization of Cycled Graphite Electrodes Using XPS with Ar-Ion Etching

The inability of Ar-ion etching to remove electrolytes from the surface demonstrates its ineffectiveness in eliminating ionic liquids from graphite electrodes. Therefore, additional methods are required to address the broad signals caused by electrolyte coverage. Drawing on previous XPS analyses, researchers have employed solvent washing to tackle the issue of electrolyte residue. To ensure complete removal of electrolyte signals during XPS surface analysis, a suitable washing method is essential.

To address this, PC (propylene carbonate) solvent, known for its high polarity, was used to selectively dissolve electrolyte residues from graphite electrodes. Previous studies have demonstrated that carbonate electrolytes highly effective in removing organic solvent residues, making them the excellent washing solvents for preparing a well-defined SEI layer.[6, 9, 10] Furthermore, carbonate is highly compatible with ionic liquid electrolytes, further enhancing its suitability for applications involving SEI layer formation with ionic liquid electrolytes.[27, 43, 126] Based on this evidence, PC solvent washing was adopted as an effective method to eliminate electrolyte residues, enabling a clear analysis of the true SEI layer beneath the ionic liquid electrolytes. The study focused on the XPS data of cycled ionic liquid and carbonate electrolytes after 5 cycles at 25 mA/g, as well as after 5 cycles at 25 mA/g followed by 100 cycles at 100 mA/g, to investigate capacity failure mechanisms. Detailed XPS analysis was correlated with the capacity decay and recovery phenomena observed in galvanostatic charge-discharge tests.

The SEI layer, known for its layered structure with an organic outer layer and an inorganic inner layer, was further analyzed to verify its reliability on

the surface. To complement the surface XPS analysis, an Ar-ion etching procedure was performed under an inert atmosphere. A gentle Ar-ion etching process was applied to minimize mechanical damage and preserve the chemical states of the surface. Ultimately, the detailed surface XPS analysis, supplemented with Ar-ion etching information, provided valuable insights into the interface evolution during the prolonged cycling process over 100 cycles. For all quantitative analyses of the elements (C, N, O, S, F, K, Na), their concentrations are calculated using the RSF-corrected peak areas of C1s, N1s, O1s, S2p, F1s, K2p, and Na1s.

In the XPS analysis of the SEI layer on graphite electrodes on PIBs, the fine spectrum analysis of K2p and C1s spectra is one huge difficulty. The fitting of specific K2p peaks is inherently challenging due to the close binding energy gap of approximately 2.8 eV between the $K2p_{1/2}$ and $K2p_{3/2}$ peaks. This complexity makes it particularly difficult to accurately fit potassium salts. As a result, the fitting of potassium species is often omitted in XPS analysis of SEI layers in PIBs. The researchers are mainly analyzing the adjacent carbon spectra to investigate the variations in organic decomposition within the SEI layers.[11, 43, 67, 88, 95, 96] Here, no attempt is made to fit different K 2p environments, instread, the K 2p peak is fitted with a single doublet. This allows the K2p peaks to be used as a quantitative reference for peak areas associated with other SEI components.

The qualitative analysis of organic species based on the XPS anlaysis of carbon spectra is always a difficulity. One primary challenge has already been highlighted: the peak overlap between K2p species and carbon species in more electron-deficient environments, such as C-F. In the C1s spectrum of specific SEI layers, potential CF_3 groups (~292 eV) from ionic liquid anions may overlap with K2p peaks (292–294 eV). To address this, C1s spectral analysis is often combined with F1s surface analysis to

distinguish the overlapping CF_3 peaks. After minimizing peak overlap, detailed peak fitting can be conducted to analyze other decomposition species in less electron-deficient environments.

Based on the binding energy difference, we can then separated the organic main peaks into C-C/C-H, C-O, C=O and CO_3^{2-} (Figure 3.20). The fitting of organic species is based on a series of XPS analyses of organic components in SEI layers of PIBs.[6, 11, 67, 87, 95]

In all cases, the C1s spectrum features a prominent narrow peak at low binding energy near 285 eV, corresponding to the most intense C-C signal. This peak combines contributions from sp^2 and sp^3 carbon species, whose similar binding energies make the C-C partial peak a useful reference for defining the length of aliphatic carbon chains and the presence of polymer species. Additionally, three higher binding energy (BE) components represent specific oxidized functional groups. The component at 286.0–286.5 eV is attributed to C-O environments, while the peak at 288.0–288.5 eV likely corresponds to C=O environments, including contributions from CO_2 and OCO_2 groups. The component above 290 eV is typically associated with carbonate species. These C-O environments are attributed to SEI components such as PEO oligomers (-$(CH_2CH_2O)_n$-) and potassium alkoxides (RO-K). The ether-based oligomers can be regarded as active frameworks for potassium ion diffusion due to their high mechanical flexibility.[38, 87, 88] The C=O species may originate from potassium ethanoate (RCO_2K) and semi-carbonate decomposition products of carbonate electrolytes.[87] Carbonates, likely originating from K_2CO_3, can enhance the viscoelastic properties of the SEI layer, contributing to its structural integrity and performance.[127]

Due to the chemical and mechanical stability of these oxidized organic species, it can be assumed that the overall stability of the organic components is significantly influenced by the oxidized organic species.

Based on the fitting of carbon spectra, we can reliably distinguish the graphitic/aliphatic carbon peaks from those representing more oxidized carbon environments. In the pure FSI electrolyte (figure 3.20 a), approximately 56% of the carbon on the graphite electrode surface is in oxidized environments (BE > 285 eV), with the remaining 44% being aliphatic carbon (BE ≈ 285 eV), which contributes to polymer species formation. With prolonged cycling up to 105 cycles, the proportion of oxidized carbon increases to 65% of the total carbon. In contrast, the pure TFSI system (figure 3.20 c) initially exhibits a higher proportion of oxidized carbon species, with 63% of the total carbon in oxidized environments after 5 cycles. However, this proportion decreases over cycling, reaching 50% of the total carbon by the 105^{th} cycle.

Based on the ratio of oxidized carbon environments, we can better understand the decreasing trend in C-C peaks. The C-C aliphatic/polymer peaks are considered a key component of the organic polymer species within the SEI layers. We hypothesize that C-C species originate from unstable organic decomposition products, contributing to the high proportion of polymer species among the organic components. Drawing on previous elastic tests of ether-based oligomers and the high mechanical stability of potassium carbonate salts, the decreasing C-C ratio leads to an increased proportion of oxidized carbon species. This shift, particularly favoring elastic properties, is observed in KFSI/[Pyr_{13}]FSI and KFSI/[Pyr_{13}]TFSI ionic liquid electrolytes with cycles. The reduction in organic species drives the SEI layer to evolve toward a more inorganic composition while retaining its elastic properties after 100 additional cycles. This specific evolution of the SEI layer offers initial insights into the distinct capacity retention behaviors observed during long-term cycling. For the stable capacity trends in KFSI/[Pyr_{13}]FSI and KFSI/[Pyr_{13}]TFSI systems, the organic species transition toward oxidized organic components with

preserved elasticity (Figure 3.20 a,b). In contrast, this trend is absent in electrolytes exhibiting capacity decay (Figure 3.20 c,d). Based on this observation, an initial hypothesis is that capacity decay may be connected with the accumulation of organic species in the SEI layers.

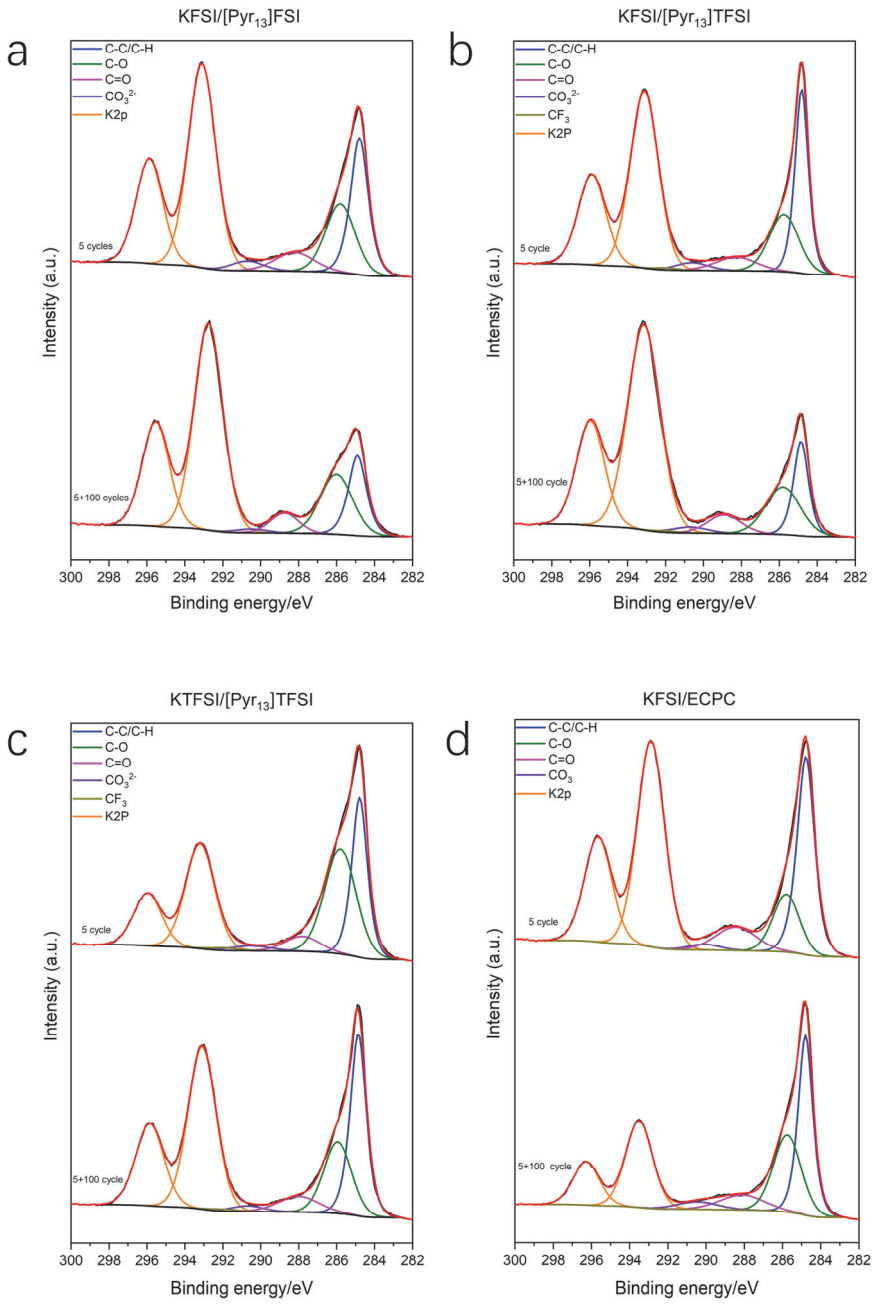

Figure 3.20. K2p and C1s spectra of surface of graphite electrodes cycled in (a) KFSI/[Pyr_{13}]FSI (b) KFSI/[Pyr_{13}]TFSI (c) KTFSI/[Pyr_{13}]TFSI (d) KFSI/ECPC electrolytes at 25 mA/g for 5 cycles without and with additional 100 cycles at 100 mA/g.

Although we conducted surface analysis of the organic species in the SEI layer, a comprehensive understanding of the SEI cannot be confined to surface-level observations. A stable SEI layer on the graphite electrode typically consists of an organic outer layer combined with an inorganic inner layer. To assess the gradient evolution from the outer to the inner regions, analyzing the atomic ratio of the SEI layer at both the surface and deeper layers after a specific etching duration with atomic radio analysis is crucial. Therefore, we focus on the variations in the atomic ratios of specific elements to address this question. To ensure effective quantitative analysis, we used the areas of specifically fitted carbon species for each sample (figure 3.21). The fitting strategy for the carbon species after 50s of etching was consistent with that applied at the surface. Additionally, the regional areas of other elements (N, O, S, F, K, Na) were collected for each sample, enabling the calculation of carbon% to evaluate the organic content across different samples. The selection procedures for non-overlapping regions will be discussed in detail in the following paragraphs. Finally, the atomic% at the surface and after 50s of etching (the longest etching time) was primarily analyzed as a representative analysis to evaluate the effects of Ar ion etching on surface characterization.

As is seen in figure 3.21 a, without considering etching, the atomic% for the pure FSI ionic liquid electrolyte decreases significantly from 46.64% to 37.72%, indicating a substantial reduction in organic species with cycling. Similarly, a decreasing trend is observed for mixed-anion ionic liquids and

pure TFSI ionic liquids, with atomic% declining from 47% to 33.76% (figure 3.21 b) and 57.25% to 44.88% (figure 3.21 c), respectively. This trend suggests that the SEI layer formed in ionic liquid electrolytes transitions toward a more inorganic composition during cycling.

When etching is applied, a noticeable decrease in the carbon concentration is observed, which becomes more pronounced with longer etching. A notable observation is that for the pure FSI ionic liquid electrolyte, the SEI layers show little to no change and even a slight increasing trend in carbon concentration after 5 cycles. However, after 100 cycles, the SEI layer evolves into a distinct organic (outer)–inorganic (inner) gradient structure, with the atomic% decreasing from 37.72% at the surface to 28.40% after etching (figure 3.21 a,b). Similarly, the SEI layer transitions to an outer (33.76%)–inner (30.21%) structure for mixed-ionic liquids (figure 3.21 c,d) and an outer (44.88%)–inner (35.44%) structure for pure TFSI ionic liquid electrolytes (figure 3.21 e,f). These similarities indicate that the characteristic organic/inorganic stratified SEI layer becomes more pronounced in ionic liquid electrolytes with cycling. When etching is applied to organic electrolytes, only minor changes in the organic species are observed across all etching layers, from the surface to the 50s etching layer (figure 3.21 g,h). The SEI layer in KFSI/ECPC electrolytes transitions into a more homogeneous organic composition with cycling, a characteristic associated with poor cycling stability.

To examine the surface transformation across etching layers, all etching layers are normalized to analyze the intensity of individually fitted peaks at the surface (figure 3.22). From the stepped etching procedure, it is evident that there is nearly no binding energy shift in the separated carbon species. The intensity changes from the surface to the deepest etching layer proceed steadily, controlled by the etching time. Through detailed analysis of the surface and the deepest etching layer (50s), we can determine the

monolithic structure of the SEI layer from the inner to the outer layer.

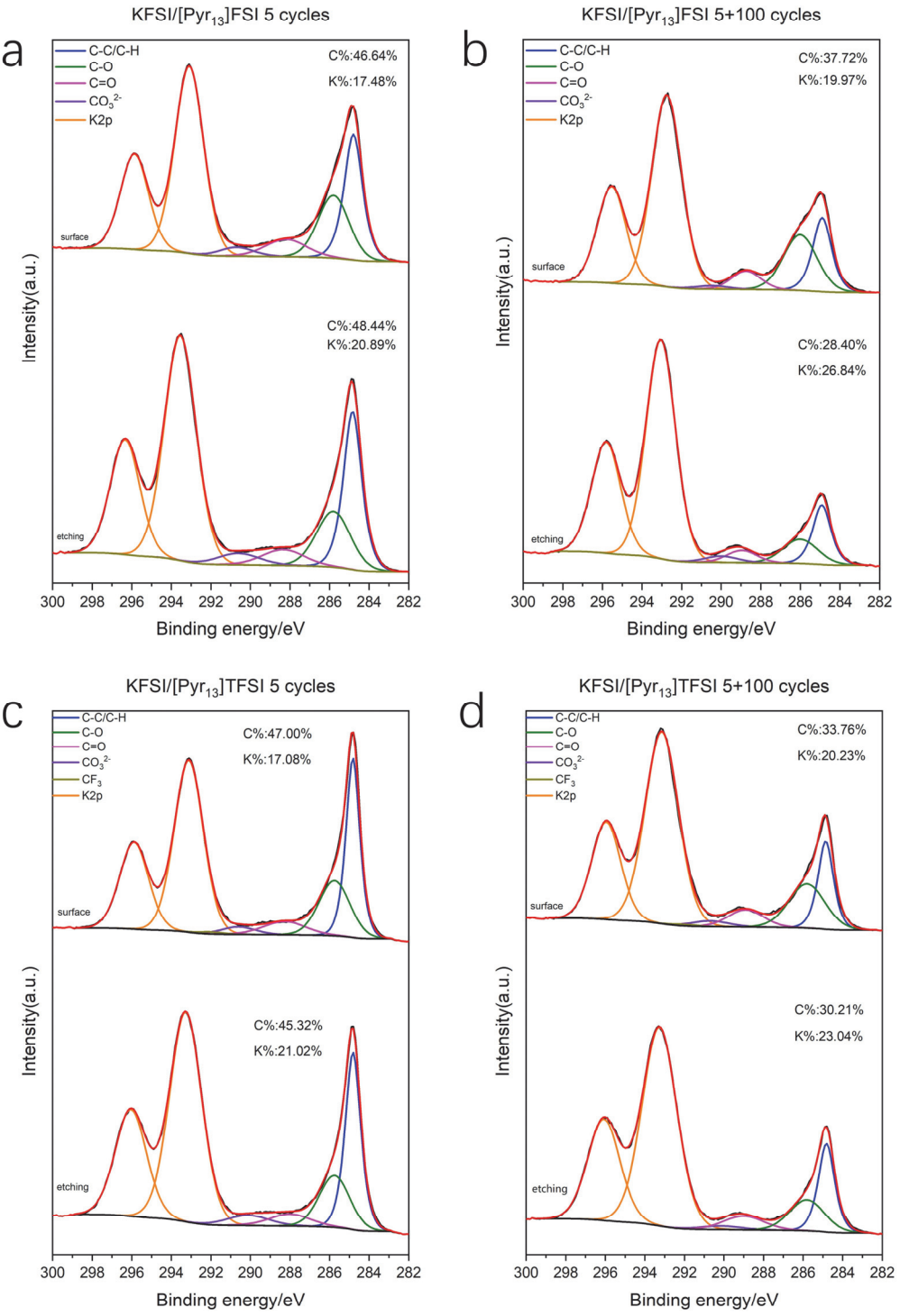

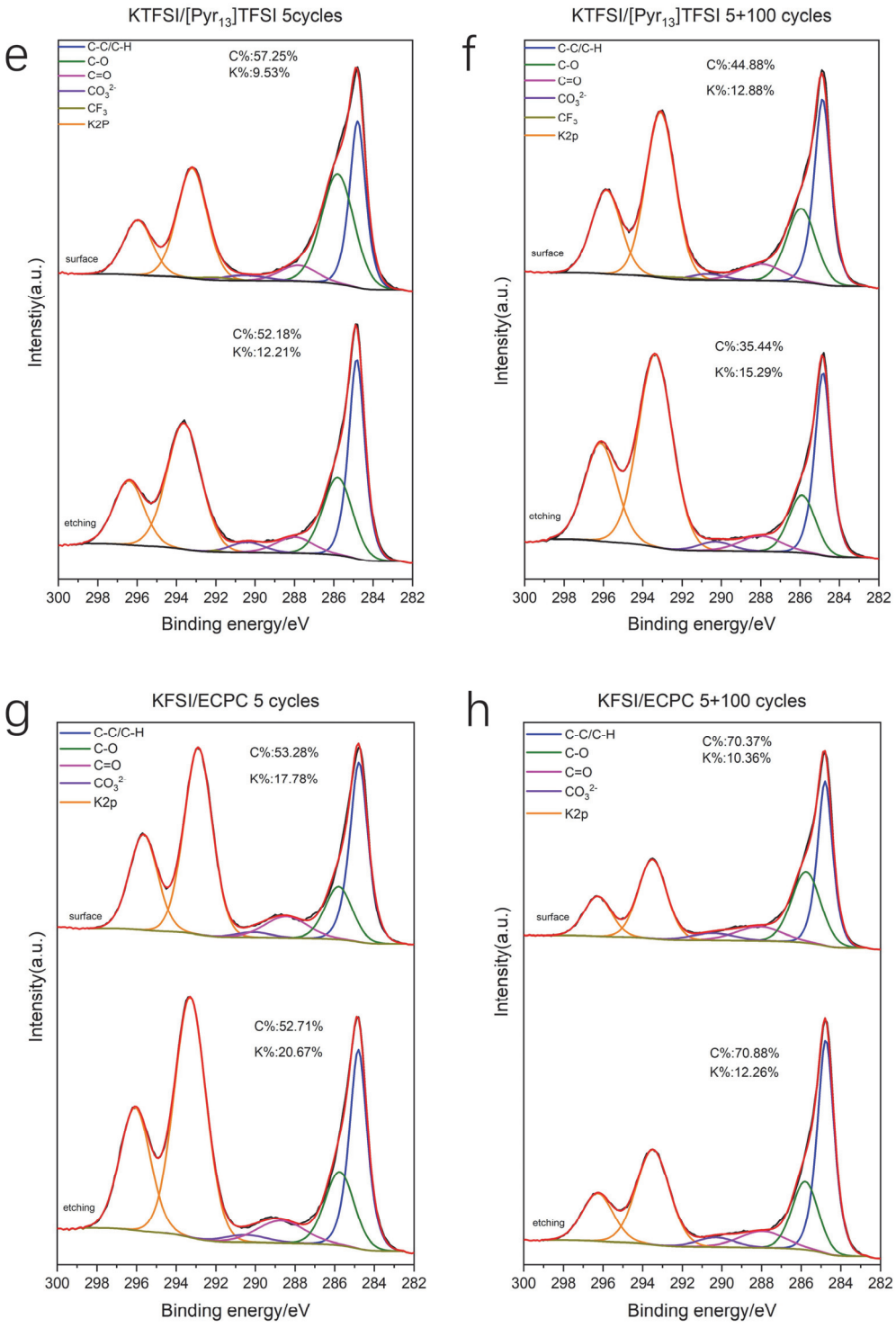

Figure 3.21. K2p and C1s spectra of surface and etching layer (50s) of graphite electrode cycled in (a) KFSI/[Pyr_{13}]FSI (b) KFSI/[Pyr_{13}]TFSI (c) KTFSI/[Pyr_{13}]TFSI (d) KFSI/ECPC electrolytes at 25 mA/g for 5 cycles without and with additional 100 cycles at 100 mA/g.

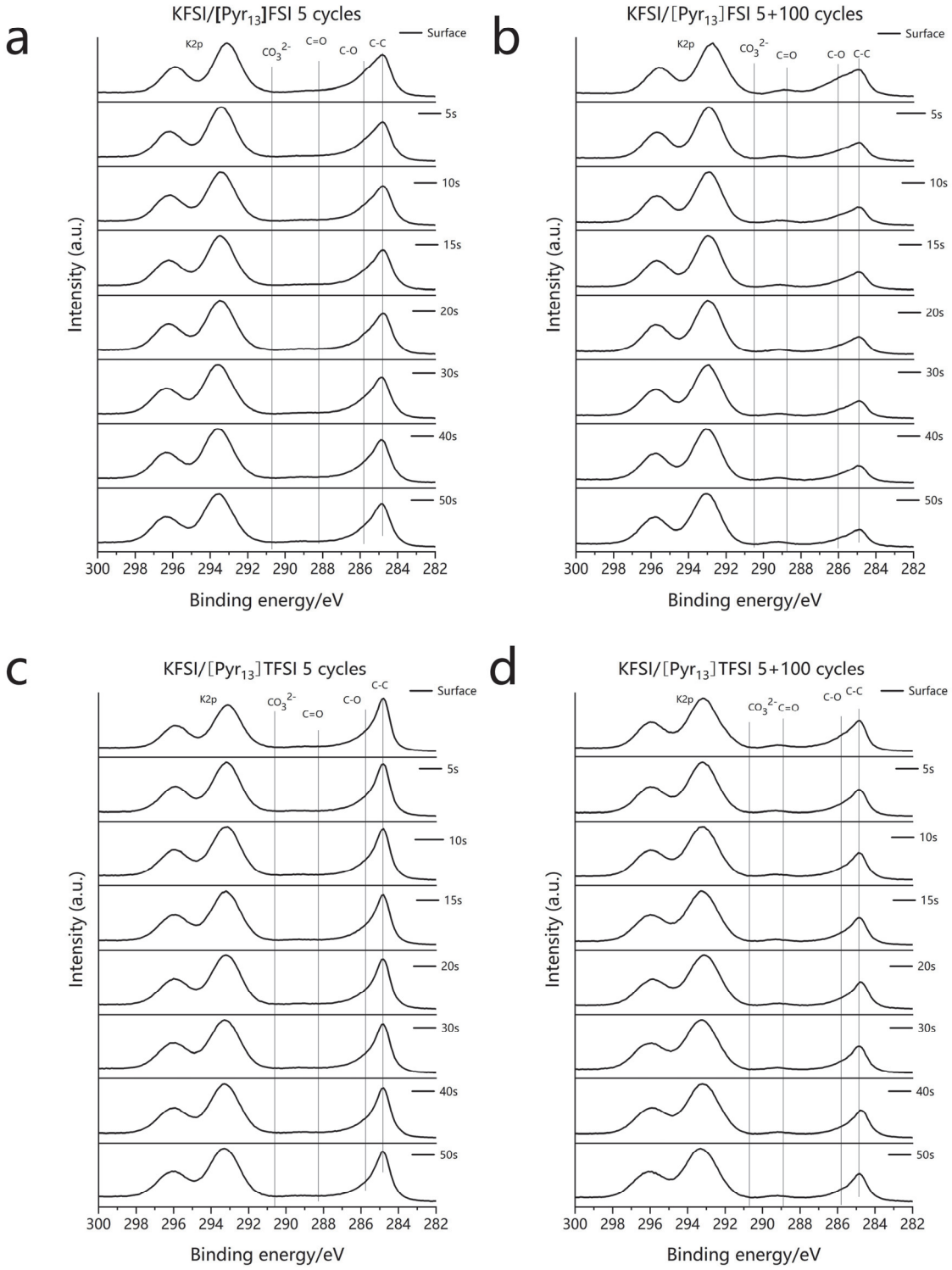
a
KFSI/[Pyr13]FSI 5 cycles
K2p
CO3 2-
C=O
C-O
C-C
Surface
5s
10s
15s
20s
30s
40s
50s
Intensity (a.u.)
300 298 296 294 292 290 288 286 284 282
Binding energy/eV
b
KFSI/[Pyr13]FSI 5+100 cycles
K2p
CO3 2-
C=O
C-O
C-C
Surface
5s
10s
15s
20s
30s
40s
50s
Intensity (a.u.)
300 298 296 294 292 290 288 286 284 282
Binding energy/eV
c
KFSI/[Pyr13]TFSI 5 cycles
K2p
CO3 2-
C=O
C-O
C-C
Surface
5s
10s
15s
20s
30s
40s
50s
Intensity (a.u.)
300 298 296 294 292 290 288 286 284 282
Binding energy/eV
d
KFSI/[Pyr13]TFSI 5+100 cycles
K2p
CO3 2-
C=O
C-O
C-C
Surface
5s
10s
15s
20s
30s
40s
50s
Intensity (a.u.)
300 298 296 294 292 290 288 286 284 282
Binding energy/eV

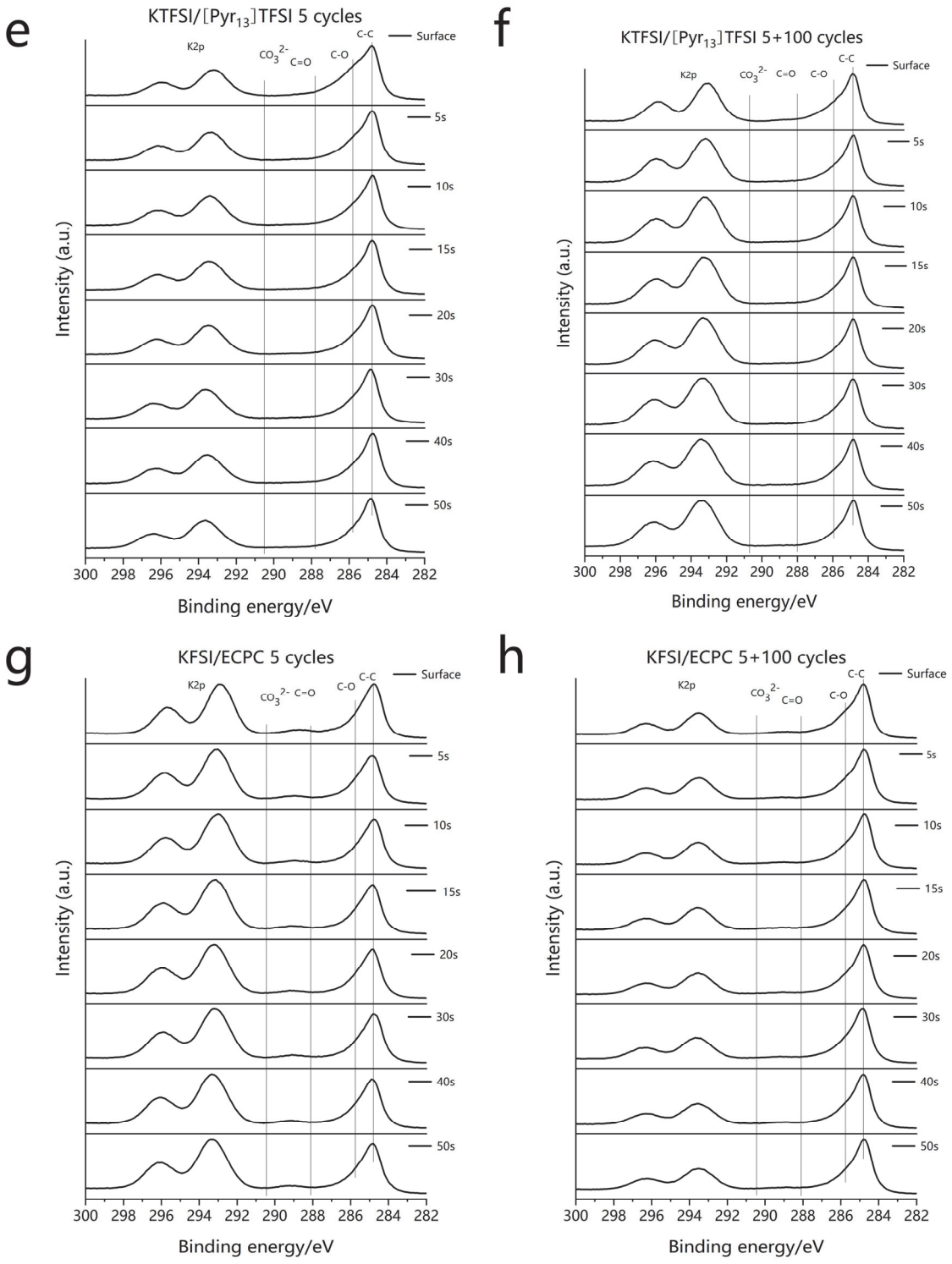

Figure 3.22. K2p and C1s spectra of surface and different etching layer of graphite electrode cycled in (a,b) KFSI/[Pyr_{13}]FSI (c,d) KFSI/[Pyr_{13}]TFSI (e,f) KTFSI/[Pyr_{13}]TFSI (g,h) KFSI/ECPC electrolytes at 25 mA/g for 5 cycles without and with additional 100 cycles at 100 mA/g.

Based on the surface analysis of the unwashed graphite electrode cycled for 5 cycles in Pyr_{13}TFSI ionic liquid electrolytes, nitrogen species, with an atomic ratio of 7.3%, play a significant role in the electrolyte residues (Figure 3.23). However, after washing with PC solvent, the presence of nitrogen species in the SEI layers is significantly reduced (Figure 3.23). The decrease in the nitrogen cation peak indicates the near-complete decomposition of azacyclo-compounds, leaving only a partial contribution from anions in the nitrogen spectra.

This diminished concentration of nitrogen components leads to noisy N1s spectra,making detailed peak fitting unsuitable for analysis. Instead, by calculating atomic ratios based on peak areas within the same spectra region (404–396 eV), we observe that nitrogen species play a minimal role. Even in the SEI layer with the highest surface nitrogen content formed in the pure FSI ionic liquid electrolyte after 5+100 cycles, the nitrogen ratio drops to approximately 1% after 50s of etching (Table 4).

This observation supports the assumption that nitrogen species primarily originate from electrolyte residues. Their weak resistance to Ar-ion etching further indicates that nitrogen species do not play a significant role in the main properties of the SEI layers.

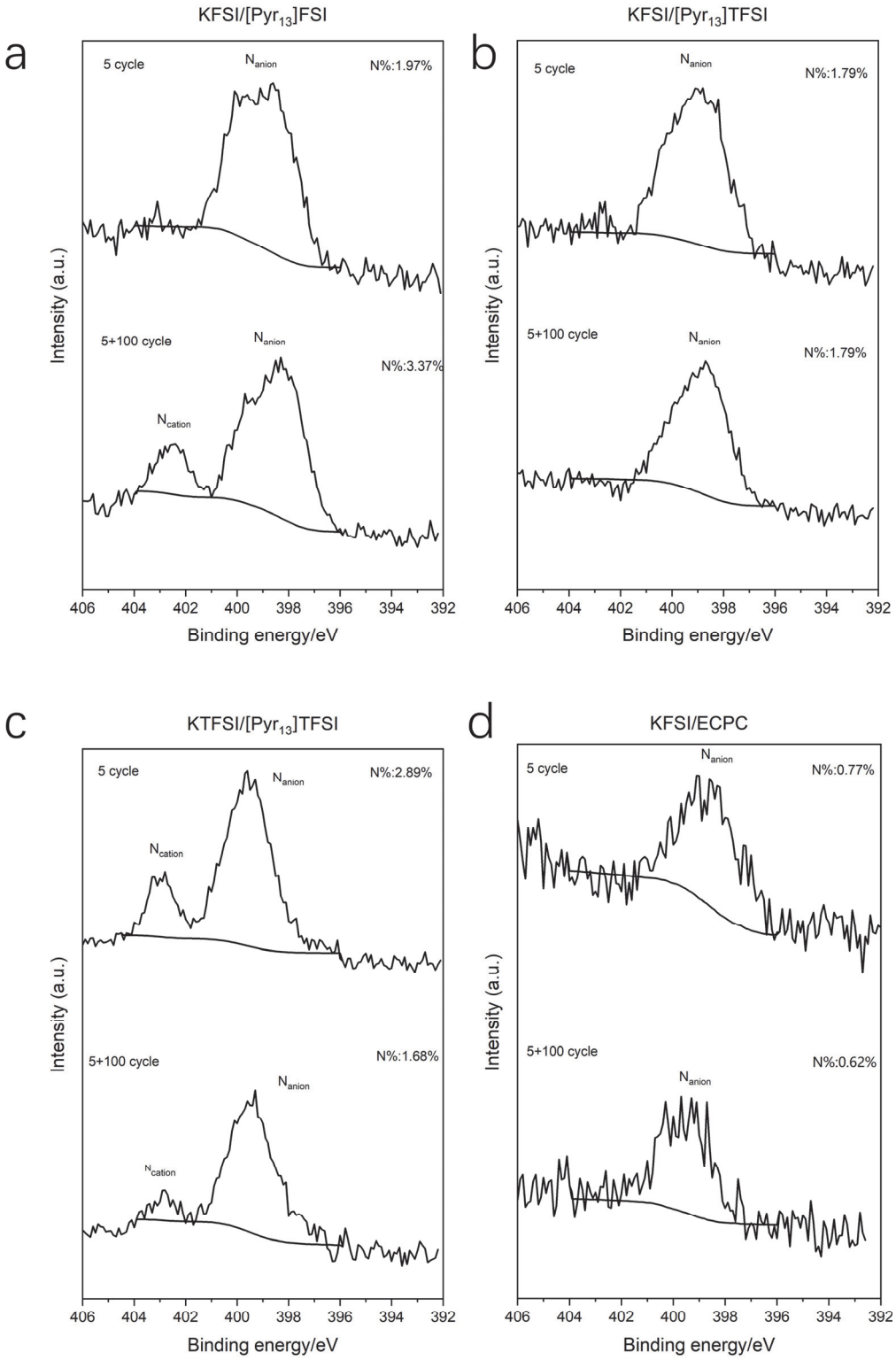

Figure 3.23. N1s spectra of surface of graphite electrode cycled in (a) KFSI/[Pyr_{13}]FSI (b) KFSI/[Pyr_{13}]TFSI (c) KTFSI/[Pyr_{13}]TFSI (d) KFSI/ECPC electrolytes at 25 mA/g for 5 cycles without and with additional 100 cycles at 100 mA/g.

Detailed analysis of the carbon spectra indicates that oxidized organic salts play a vital role in stabilizing the SEI layer. However, fitting the oxygen spectra remains a significant challenge. The fitting range for oxygen in various chemical environments is broad and often flexible, tailored to meet different researchers' requirements. Notably, the oxygen peaks from SEI layers formed by different electrolytes exhibit similar binding positions and peak widths, leading to the possibility of producing vastly different fitting results for the same spectra. As with the broad K2p peaks discussed earlier, applying inappropriate fitting methods risks yielding inaccurate interpretations of the XPS spectra. Nevertheless, valuable insights can still be extracted from the oxygen spectra. By focusing on the atomic percentage (O%) within an appropriate spectral region, a clear increasing trend is observed for FSI-modified ionic liquids. This trend supports the notion of a progressively oxidized SEI layer composition during cycling. Thus, monitoring the atomic ratio of the oxygen element offers additional evidence to support analysis based on other elements. In particular, the analysis oxygen atmic% reveals a significant increase in the oxygen concentration for SEI layer of the pure FSI ionic liquid electrolyte, rising from 20.18% after 5 cycles to 29.41% after 105 cycles (figure 3.24 a). In contrast, the oxygen concentration in the SEI formed in pure TFSI ionic liquid electrolytes remains consistently low, around 11%, throughout the cycling process.In addition, the oxygen concentration in pure ECPC electrolytes decreases from 21.36% after 5 cycles to 14.56% after 105 cycles (figure 3.24 d). This shift in atomic percentages provides quantitative evidence for the tendency of the SEI layer in the pure FSI ionic liquid to evolve into a composition enriched with the classical stable inorganic K_2O[32, 128], elastic oxidized ether organic species, and sulfide inorganic compounds over cycling.

When analyzing the oxygen peak, a significant observation was made

regarding sodium contamination. As shown in figure 3.24 b,c, a distinct Na Auger peak with a binding energy similar to that of oxygen is observed in the oxygen spectrum, a feature observed in SEI XPS studies formed by KFSI/[Pyr_{13}]FSI ionic liquid electrolytes in sodium-ion batteries.[27] Determining the origins of sodium contamination is a complex issue. Two potential contributors are commercial glassy fiber and potassium metal (98% purity, Sigma-Aldrich. In previous study, trace sodium impurities were detected in commercial potassium metals, potentially contributing to sodium contamination within the electrolyte system. [129] Although we cannot confirm that the potassium metal we used is encountering the same issues observed in previous research. Based on our XPS analysis of the glass fiber separator, the minor Na impurities likely originate from the glass fiber material. This leads to the assumption that the Na Auger peak is caused by sodium accumulation in the SEI layer, originating from the glass fiber separator (proved by experiments) and potassium metal—a phenomenon not previously reported in potassium-ion battery research since the design of commercial potassium metal and glassy separator were used and considered pure without any Na impurity It is challenging to define which source plays the more significant role in sodium provision. We can ensure that cells with different electrolytes are cycled under identical sodium impurity conditions.Notably, for pure TFSI ionic liquid electrolytes, prominent Na Auger peaks are observed near the main oxygen peaks. The pronounced presence of sodium Auger peaks (figure 3.25) highlights the effectiveness of XPS in detecting impurities within SEI layers, providing robust quantification and valuable insights into SEI composition. To further investigate this trend, Ar ion etching was applied to the SEI layer, revealing an increasing sodium ratio with etching, particularly in pure TFSI based ionic liquid electrolytes (Figure 3.25 c-d). Although peak fitting for oxygen spectra cannot reliably identify specific components from different oxidized

compounds, the atomic% of oxygen provides a clear understanding of the overall variation in oxygen species during cycling. In addition, the sodium Auger peaks, located near the oxygen peaks, indicate the presence of sodium species in the SEI layer. It can be deduced that these sodium species, primarily originating from the GFF glass fiber separator, accumulate more significantly when TFSI anions are used in ionic liquid electrolytes. This issue is most pronounced in KTFSI/[Pyr_{13}]TFSI ionic liquids and worsens with extended cycling. Furthermore, sodium Auger peaks grow larger with prolonged cycling and increased Ar ion etching on the SEI layer surface. The rising trend in sodium Auger peaks reveals two critical characteristics of sodium species in TFSI-containing electrolytes:

- Sodium species accumulate progressively with extended cycling.
- Sodium species tend to concentrate further in the inner SEI layers

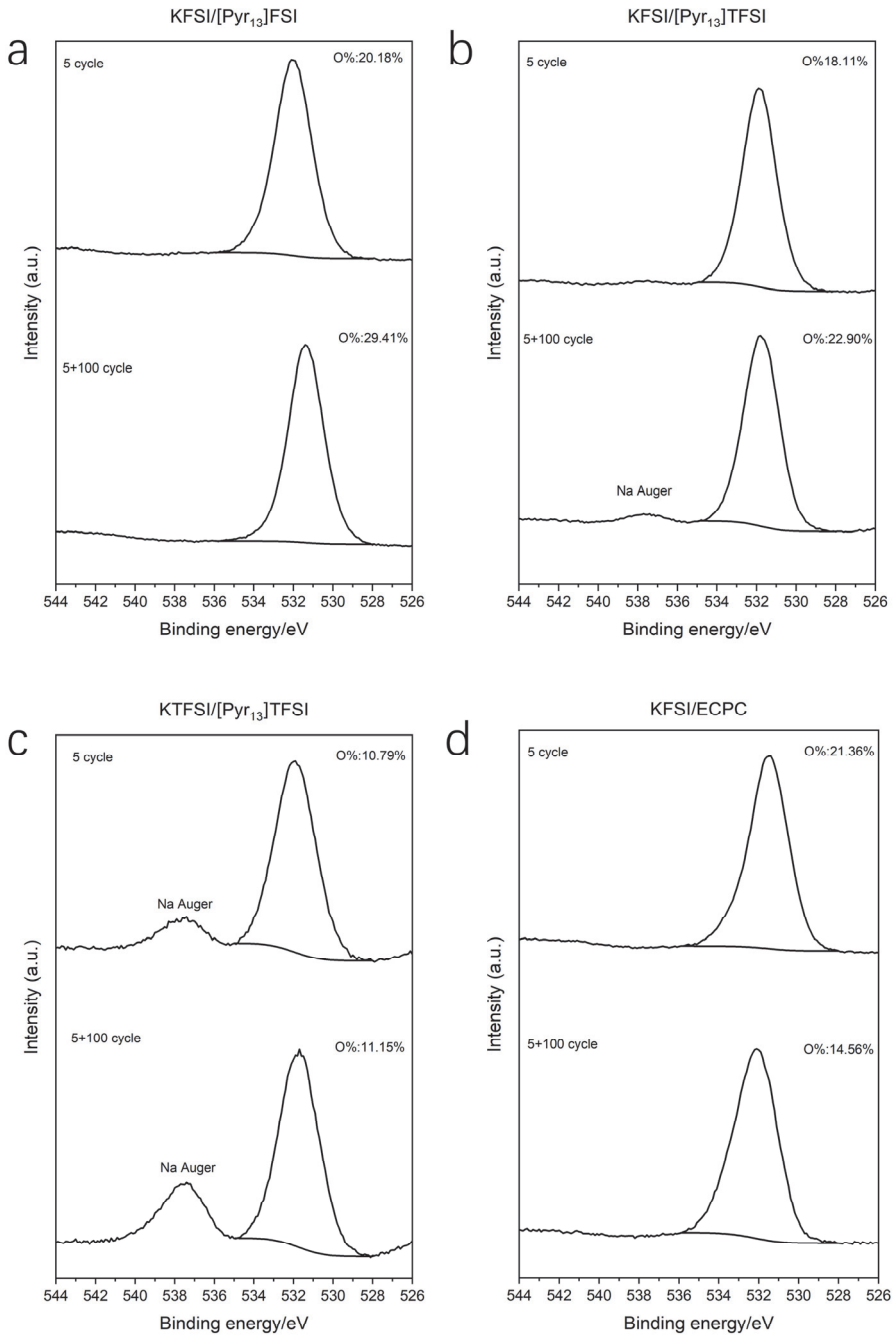

Figure 3.24. O1s spectra of surface of graphite electrodes cycled in (a) KFSI/[Pyr_{13}]FSI (b) KFSI/[Pyr_{13}]TFSI (c) KTFSI/[Pyr_{13}]TFSI (d) KFSI/ECPC electrolytes at 25 mA/g for 5 cycles without and with additional 100 cycles at 100 mA/g.

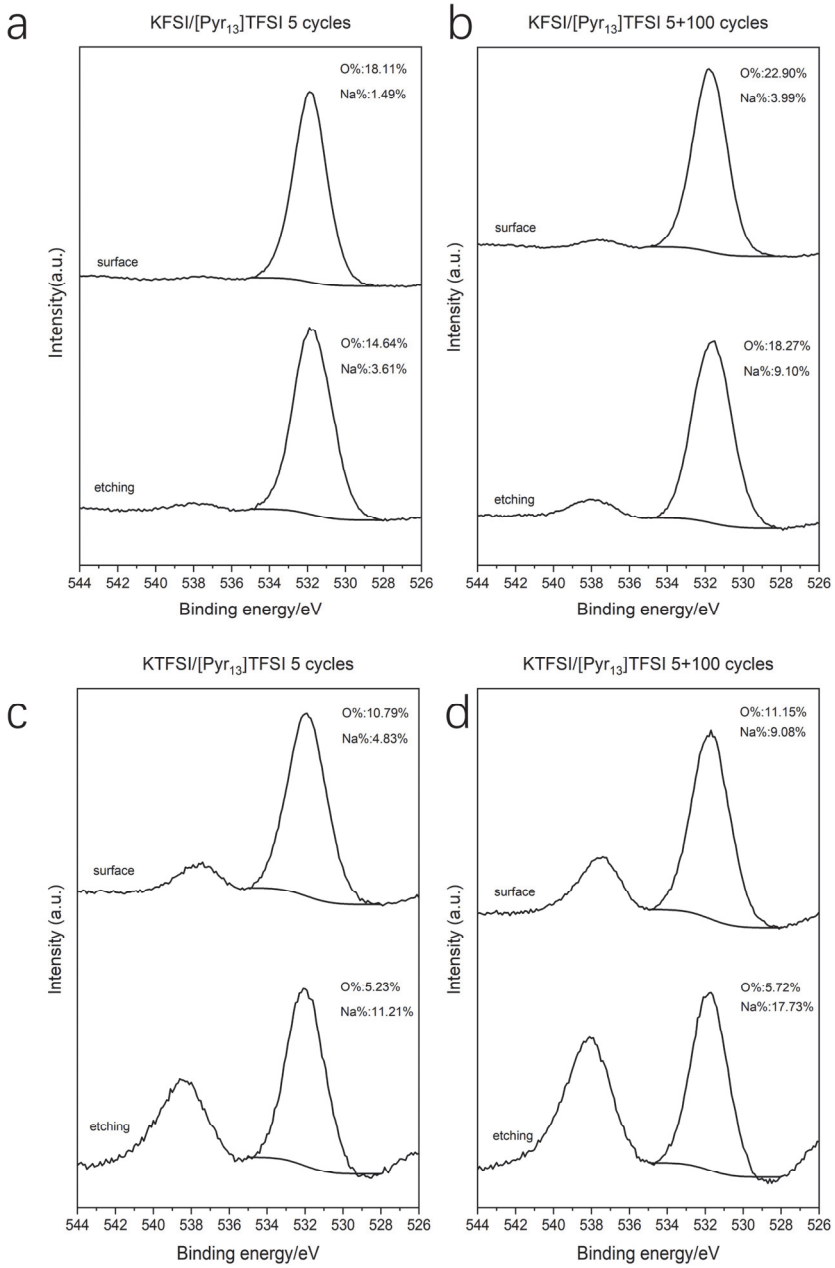

Figure 3.25. O1s spectra of surface and etching layer (50s) of graphite electrodes cycled in (a,b) KFSI/[Pyr_{13}]TFSI (c,d) KTFSI/[Pyr_{13}]TFSI ionic liquid electrolytes with sodium impurities at 25 mA/g for 5 cycles without and with additional 100 cycles at 100 mA/g.

The analysis of inorganic species in the SEI layer is crucial, complementing the organic species analysis derived from the C1s spectra. To monitor the variations in inorganic components, the F1s and S2p spectra are particularly important due to their strong association with the decomposition of anions. Focusing on fluorine analysis provides a strong starting point, as it is a key research target for SEI surface characterization in PIBs using fluorine-containing electrolytes. Potassium fluride (KF) is always thought as one representative of SEI species, distinguished from the anions peaks. Many XPS analyses use a broad fitting range of 683 eV to 685 eV for KF and even attempt to separate the KF peak into two distinct peaks. These studies often employ a graphite/potassium half-cell configuration with glass fiber as the separator.[7, 9, 96] However, this approach to fitting may be flawed, as it overlooks potential changes in the chemical environment of metal fluoride species, which warrants greater attention.

Thus, we can make one assumuption that the large broad 'KF'peaks can be one mixture of KF and NaF in sodium containing SEI layers. Based on the electronegativity difference between K and Na, the fluorine in NaF is expected to experience a more electron-deficient environment.[130] As a result, the NaF peak is predicted to appear as a distinct peak with a larger binding energy, close to 685 eV. As shown in Figure 3.26 a, the KF peak from the pure FSI ionic liquid serves as a crucial source of XPS data. The KF peak, located at approximately 683.5 eV, provides valuable information about KF and serves as a reference for fitting the binding energy of KF within the broad metal-fluorine peak observed in all samples containing sodium impurities. To analyze these broad metal-fluoride peaks, we selected the range of 684–683.3 eV for KF as a fitting baseline. This approach helps to address the specific issues arising in the broad metal-fluoride peaks. Our findings suggest that, after separating the KF peaks, the broader fluorine peaks can primarily be attributed to the presence of

sodium. This effect is particularly notable in KTFSI/Py_{13}TFSI ionic liquids, where significant sodium impurities are observed after 5 and 5+100 cycles (Figure 3.26 c).

The primary goal of the fitting process is to determine the actual peak ranges of C–F, S–F, and metal fluorides. The FWHM (full width at half-maximum) for metal fluorides is set to the same value for NaF and KF due to their similar chemical environments. A detailed surface analysis reveals that, in the case of the pure FSI ionic liquid, fluorine species predominantly transition into KF as the main component within the SEI layer. Notably, the fluorine atomic percentage decreases significantly from 6.84% to 2.15% after 100 additional cycles, indicating a suppression of fluorine species within the SEI layer (figure 3.26a). However, when TFSI is used as the anion in KTFSI/[Pyr_{13}]TFSI ionic liquids, an increasing trend in fluorine atomic percentage is observed, rising from 11.41% at 5 cycles to 17.04% after 105 cycles (figure 3.26c). This increase is potentially linked to the accumulation of sodium species after extended cycles. In KFSI/[Pyr_{13}]TFSI ionic liquids, an intermediate fluorine species is observed, between the characteristics of the pure FSI and TFSI ionic liquid electrolytes. This phenomenon suggests that excess fluorine species, which can lead to capacity failure, can be mitigated through anion modification in ionic liquid electrolytes. For fluorine species in organic components, we hypothesize the presence of an intermediate compound peak near KF. However, this peak is difficult to define precisely. Notably, this peak is not associated with NaF, as sodium species are not detected in the XPS survey.

When etching is applied to the surface of graphite electrodes, the fluorine species exhibit varying trends (Figure 3.27). To simplify the comparison, the fitting binding energies of the separated peaks are used, and the intensities are normalized to analyze the effects of etching on the individual peaks. Particularly, it is evident that the separated peaks for C–F and S–F

weaken under etching, as fluorine species shift closer to metal fluoride species with longer etching durations. For metal fluorides, a significant trend is observed: the binding energy of metal fluorides increases with extended etching. This shift is likely due to the accumulation of sodium species during the etching process, leading to a higher proportion of NaF within the SEI layer.

Due to the similar F 1s binding energies of NaF and KF, determining the optimal fitting approach for the complex mixed metal-fluoride peaks is challenging. However, by utilizing the well-defined KF peaks (683.4–684 eV) obtained from the pure FSI ionic liquid electrolyte and considering the electronegativity differences between potassium and sodium, we can separate the complex mixed metal-fluoride peaks. This allows us to extract key information from the fluorine spectra, particularly highlighting the impact of sodium accumulation on metal fluorides, which is neglected in past research.

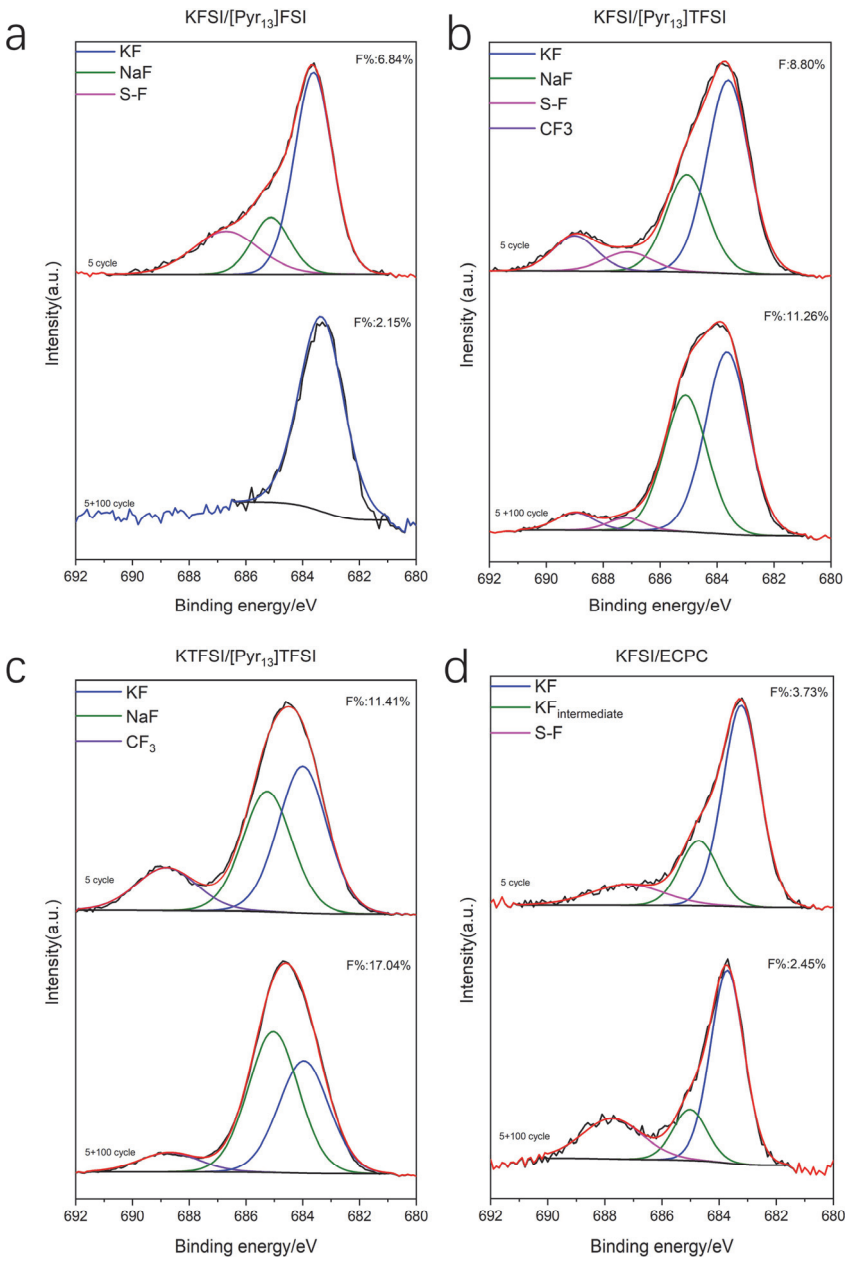

Figure 3.26. F1s spectra of surface of graphite electrode cycled in (a) KFSI/[Pyr_{13}]FSI (b) KFSI/[Pyr_{13}]TFSI (c) KTFSI/[Pyr_{13}]TFSI (d) KFSI/ECPC electrolytes at 25 mA/g for 5 cycles without and with additional 100 cycles at 100 mA/g.

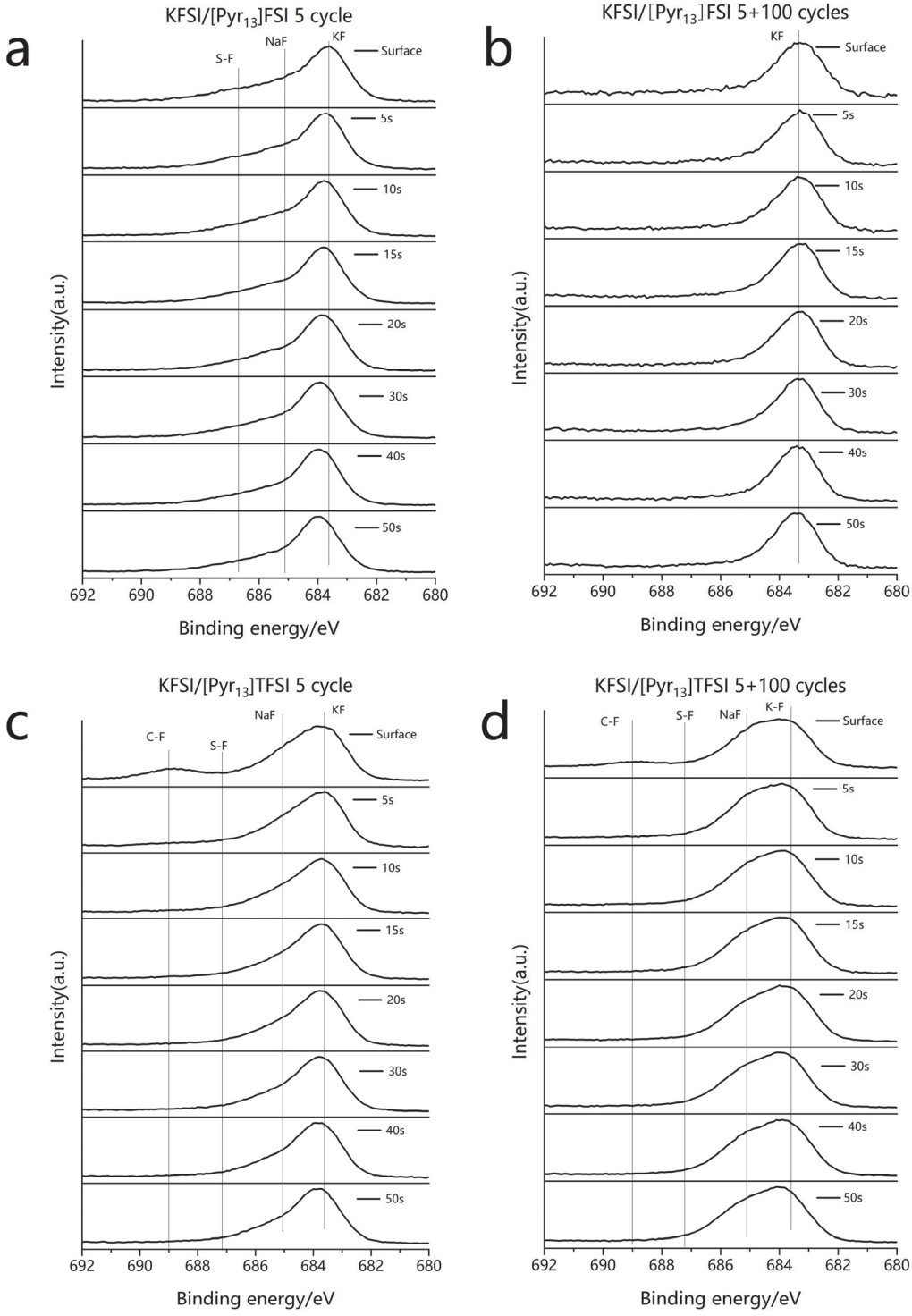
a
KFSI/[Pyr13]FSI 5 cycle
S-F
NaF
KF
Surface
5s
10s
15s
20s
30s
40s
50s
Intensity(a.u.)
692
690
688
686
684
682
680
Binding energy/eV
b
KFSI/[Pyr13]FSI 5+100 cycles
KF
Surface
5s
10s
15s
20s
30s
40s
50s
Intensity(a.u.)
692
690
688
686
684
682
680
Binding energy/eV
c
KFSI/[Pyr13]TFSI 5 cycle
C-F
S-F
NaF
KF
Surface
5s
10s
15s
20s
30s
40s
50s
Intensity(a.u.)
692
690
688
686
684
682
680
Binding energy/eV
d
KFSI/[Pyr13]TFSI 5+100 cycles
C-F
S-F
NaF
K-F
Surface
5s
10s
15s
20s
30s
40s
50s
Intensity(a.u.)
692
690
688
686
684
682
680
Binding energy/eV

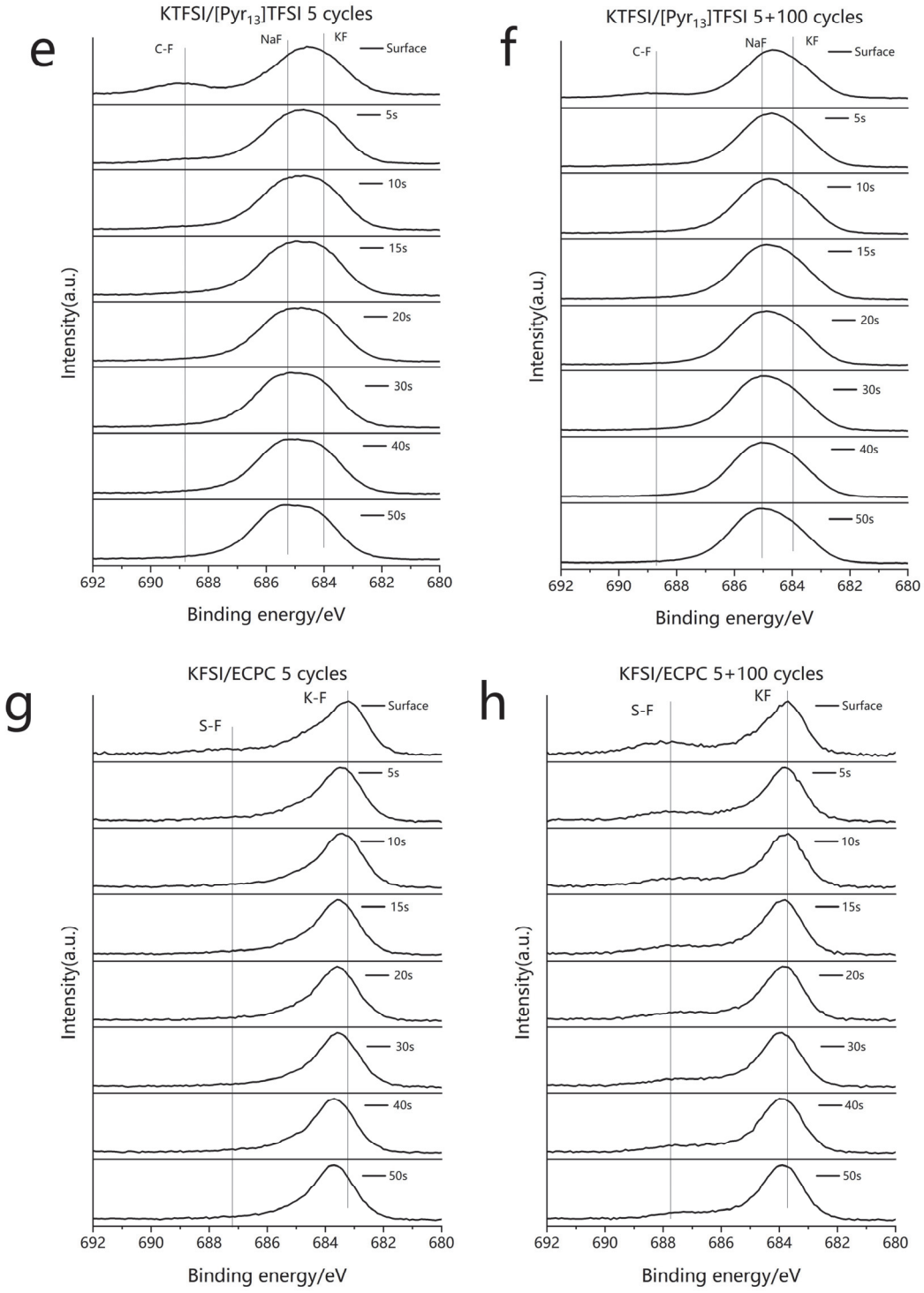

Figure 3.27. F1s spectra of graphite electrode after different etching time cycled in (a,b) KFSI/[Pyr_{13}]FSI (c,d) KFSI/[Pyr_{13}]TFSI (e,f) KTFSI/[Pyr_{13}]TFSI (g,h) KFSI/ECPC electrolytes at 25 mA/g for 5 cycles without and with additional 100 cycles at 100 mA/g.

Unlike the fitting of single KF peaks in the metal fluoride spectra, fitting the S2p spectra is significantly more complex. The S2p spectra consist of two distinct peaks, $S2p_{3/2}$ and $S2p_{1/2}$, with a theoretical area ratio of 2:1 and a binding energy difference of 1.18 eV.[131, 132] Since the sulfur peaks are a mixture of $S2p_{3/2}$ and $S2p_{1/2}$ components, separating them becomes considerably more challenging, especially when accounting for the binding energy differences between sodium and potassium species.

To simplify the analysis, we combine the sodium and potassium species into a single category labeled as "metal species" and examine the changes in three sulfide compounds under different environments. These sulfide compounds include (S=O)-N, originating from the original anions; SO_3^{2-}, formed as a decomposition product of (S=O)-N; and MxSy, a mixture of Na_2S and K_2S, representing a stable decomposition product, the fitting of the compounds is based on a combination of surface XPS analysis from potassium-ion and sodium-ion batteries.[10, 27, 89, 133]As shown in figure 3.28, the sulfur species at the surface of the SEI layer exhibit similar overall peak shapes across all electrolytes. However, the primary difference lies in the atomic percentages of the sulfide species. For KFSI/$[Pyr_{13}]$FSI (7.38 at% at 105 cycles) and KFSI/$[Pyr_{13}]$TFSI (6.07 at% at 105 cycles) ionic liquids, a higher concentration of sulfur species is observed compared to KTFSI/$[Pyr_{13}]$TFSI ionic liquid (3.30 at% at 105 cycles) and KFSI/ECPC electrolyte (1.64 at% at 105 cycles).

When the etching procedure is applied to the graphite electrode, a significant transformation of the SEI layer is observed across all electrolytes (figure 3.29). Notably, for sulfur species, there is a substantial increase in SO_3^{2-} and metal sulfides as etching progresses. This trend is consistent across both ionic liquid and organic electrolytes. The transformation is likely due to the further decomposition of sulfur species within the inner layers of the SEI. In contrast, the sulfur species are closer

to the decomposition of (S=O)-N, indicating a limited extent of decomposition. The increase in SO_3^{2-} species and metal sulfides with progressive etching has been recently observed in a similar Ar-ion etching XPS analysis of the SEI layer on carbon electrodes formed by NaFSI/[Pyr_{13}]FSI and carbonate electrolytes.[27] This phenomenon is attributed to the thicker SEI layers formed by ionic liquid electrolytes compared to carbonate electrolytes, which exhibit a higher inorganic composition.

Based on this information, it is evident that the evolution of sulfide compounds follows a similar trend during etching and cycling, regardless of whether ionic liquid or carbonate electrolytes are used. The primary distinction lies in the quantitative analysis of the sulfide compound content. Although there are differences in sodium impurity contamination in the SEI layer between the pure FSI and TFSI ionic liquid electrolytes, the similarity in sulfide compound behavior suggests that sodium accumulation is primarily associated with fluorine species, particularly in the form of NaF inorganic species within the SEI layer.

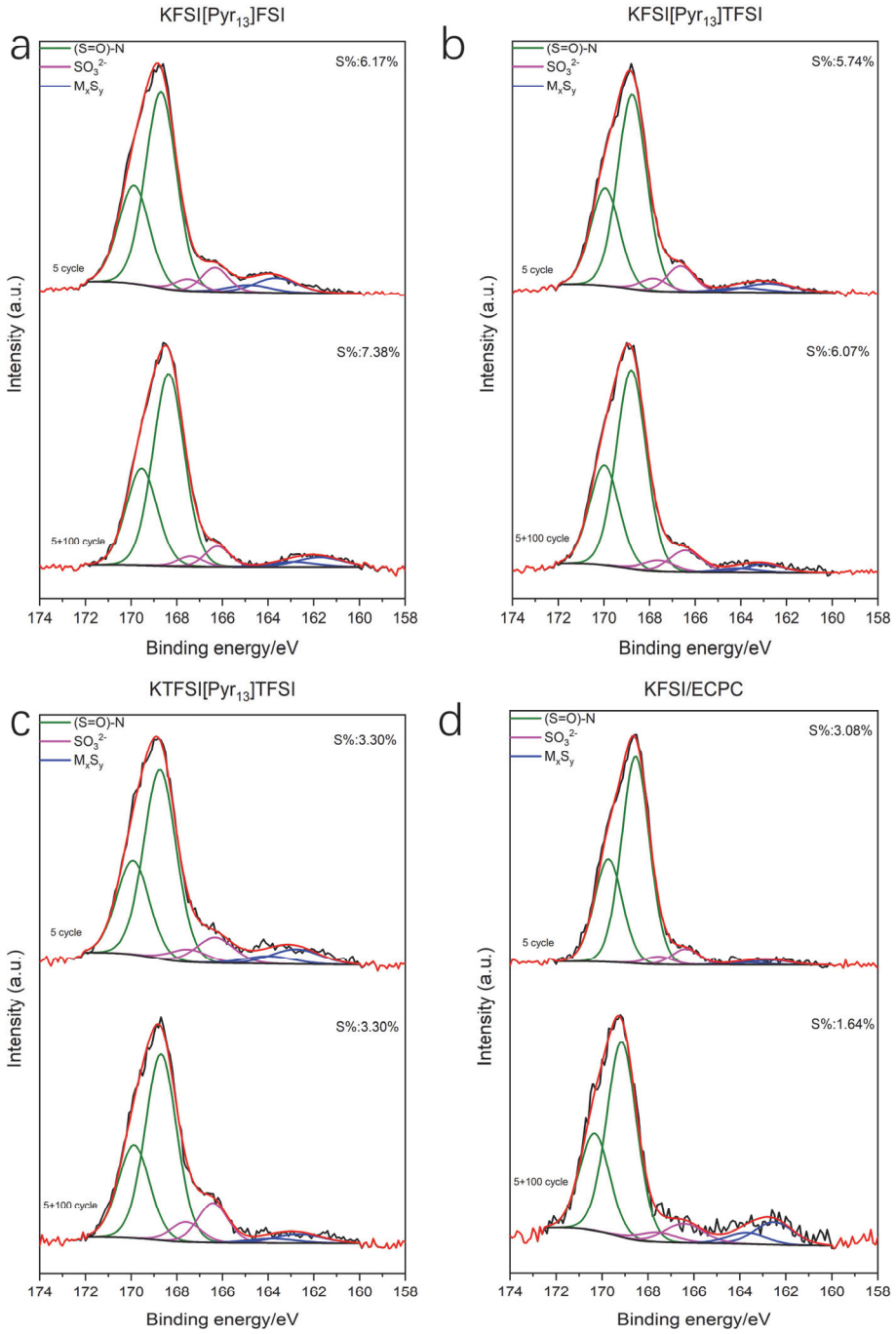

Figure 3.28. S2p spectra of surface of graphite electrode cycled in (a) KFSI/[Pyr_{13}]FSI (b) KFSI/[Pyr_{13}]TFSI (c) KTFSI/[Pyr_{13}]TFSI (d) KFSI/ECPC electrolytes at 25 mA/g for 5 cycles without and with additional 100 cycles at 100 mA/g.

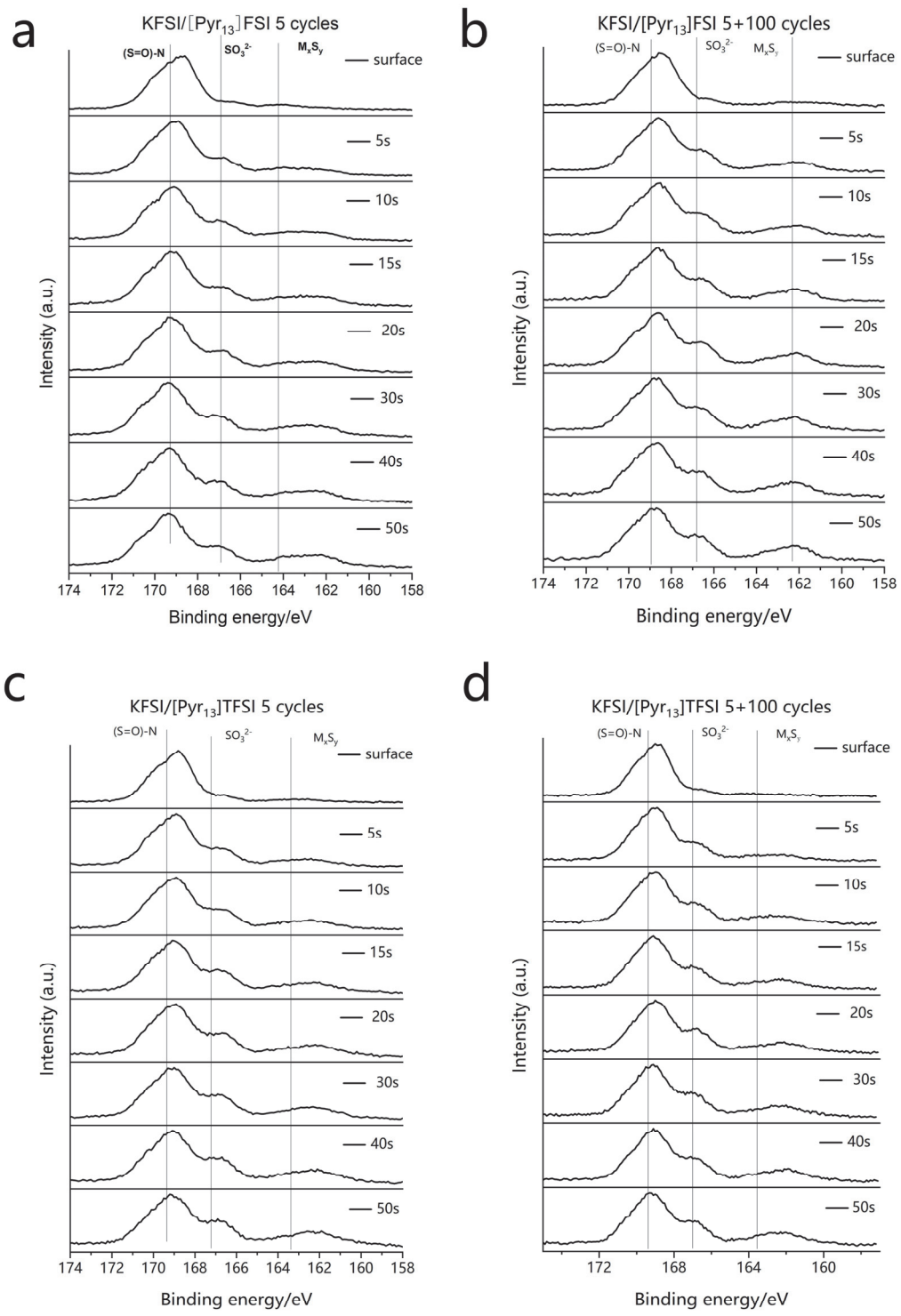
a
KFSI/[Pyr13]FSI 5 cycles
(S=O)-N
SO3 2-
MxSy
surface
5s
10s
15s
20s
30s
40s
50s
Intensity (a.u.)
174 172 170 168 166 164 162 160 158
Binding energy/eV
b
KFSI/[Pyr13]FSI 5+100 cycles
(S=O)-N
SO3 2-
MxSy
surface
5s
10s
15s
20s
30s
40s
50s
Intensity (a.u.)
174 172 170 168 166 164 162 160 158
Binding energy/eV
c
KFSI/[Pyr13]TFSI 5 cycles
(S=O)-N
SO3 2-
MxSy
surface
5s
10s
15s
20s
30s
40s
50s
Intensity (a.u.)
174 172 170 168 166 164 162 160 158
Binding energy/eV
d
KFSI/[Pyr13]TFSI 5+100 cycles
(S=O)-N
SO3 2-
MxSy
surface
5s
10s
15s
20s
30s
40s
50s
Intensity (a.u.)
172 168 164 160
Binding energy/eV

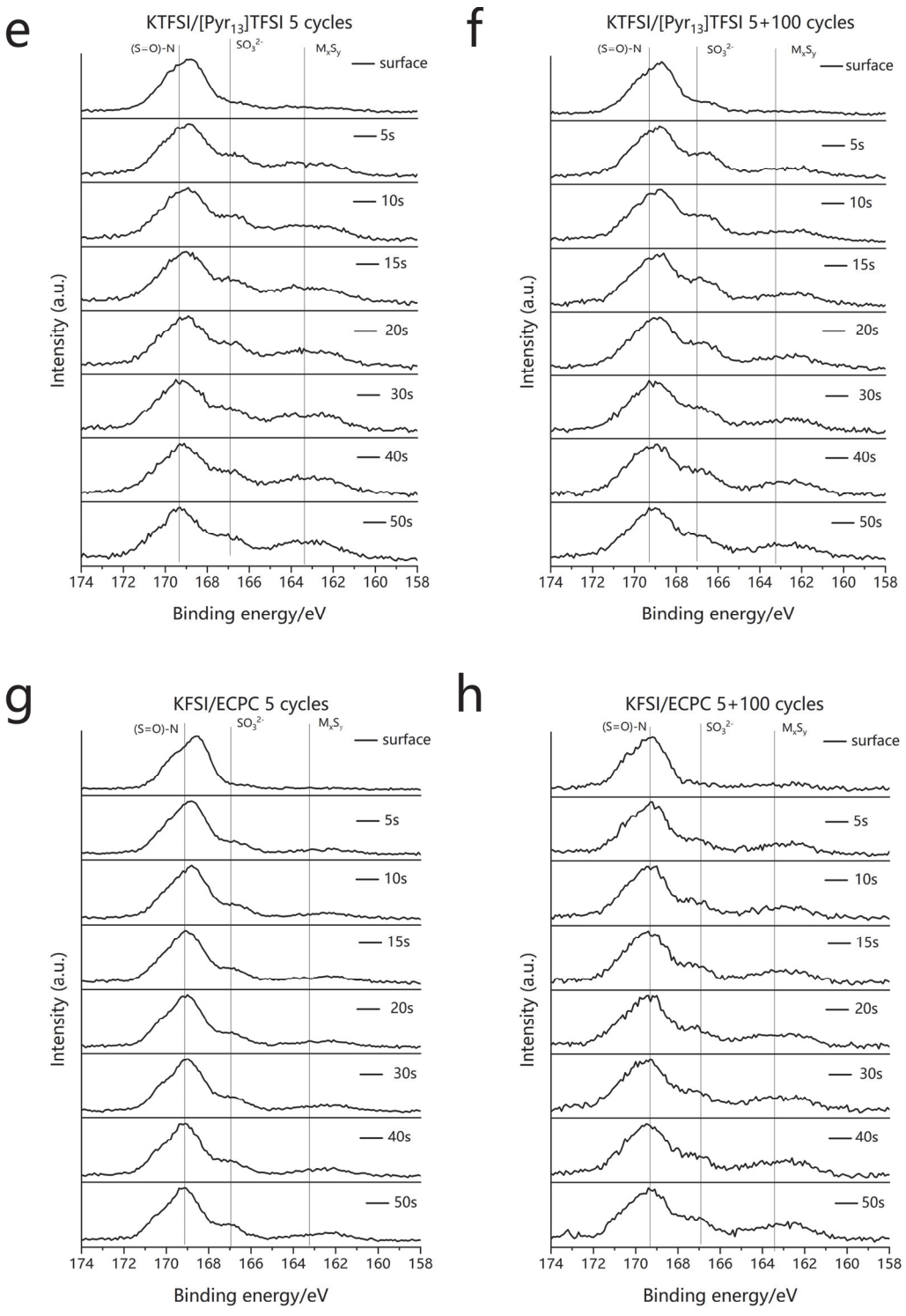

Figure 3.29. S2p spectra of surface and different etching layer of graphite electrode cycled in (a,b) KFSI/[Pyr_{13}]FSI (c,d) KFSI/[Pyr_{13}]TFSI (e,f) KTFSI/[Pyr_{13}]TFSI (g,h) KFSI/ECPC electrolytes at 25 mA/g for 5 cycles without and with additional 100 cycles at 100 mA/g.

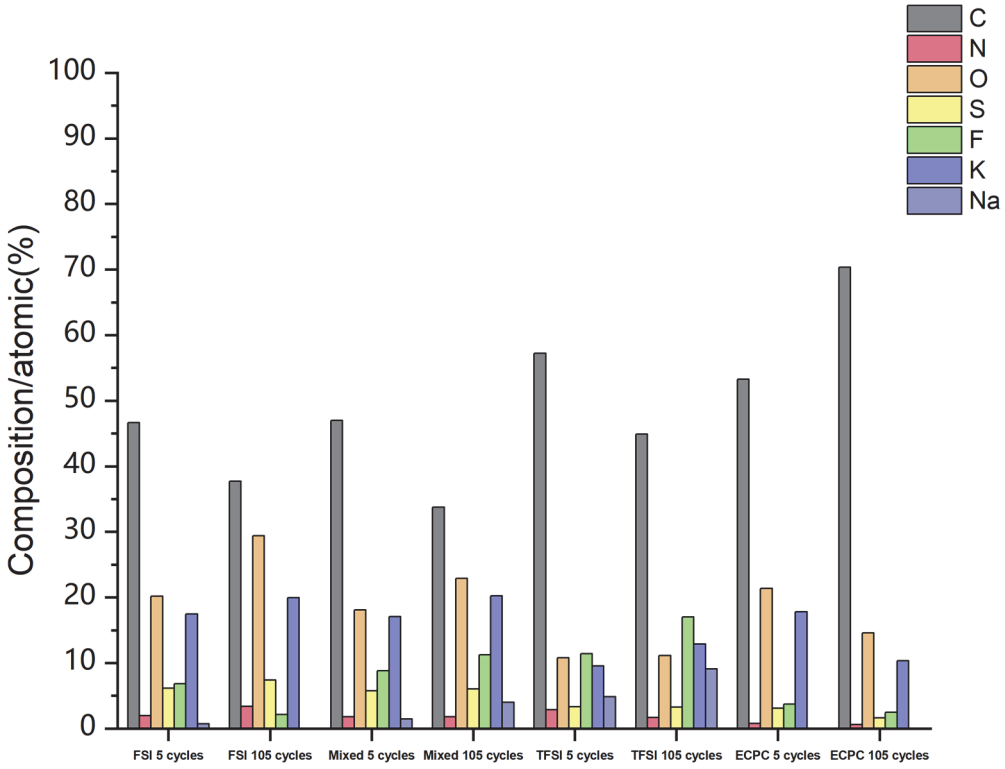

Figure 3.30. The atomic ratio of the elements of the surface SEI layer formed by ionic liquid electrolytes and organic electrolytes

Table 3. The atomic ratio of the elements of the surface SEI layer

	C	N	O	S	F	K	Na
FSI 5 cycles	46.64%	1.97%	20.18%	6.17%	6.84%	17.48%	0.73%
FSI 105 cycles	37.72%	3.37%	29.41%	7.38%	2.15%	19.97%	
Mixed 5 cycles	47.00%	1.79%	18.11%	5.74%	8.80%	17.08%	1.49%
Mixed 105 cycles	33.76%	1.79%	22.90%	6.07%	11.26%	20.23%	3.99%
TFSI 5 cycles	57.25%	2.89%	10.79%	3.30%	11.41%	9.53%	4.83%
TFSI 105 cycles	44.88%	1.68%	11.15%	3.30%	17.04%	12.89%	9.08%
ECPC 5 cycles	53.28%	0.77%	21.36%	3.08%	3.73%	17.78%	
ECPC 105 cycles	70.37%	0.62%	14.56%	1.64%	2.45%	10.36%	

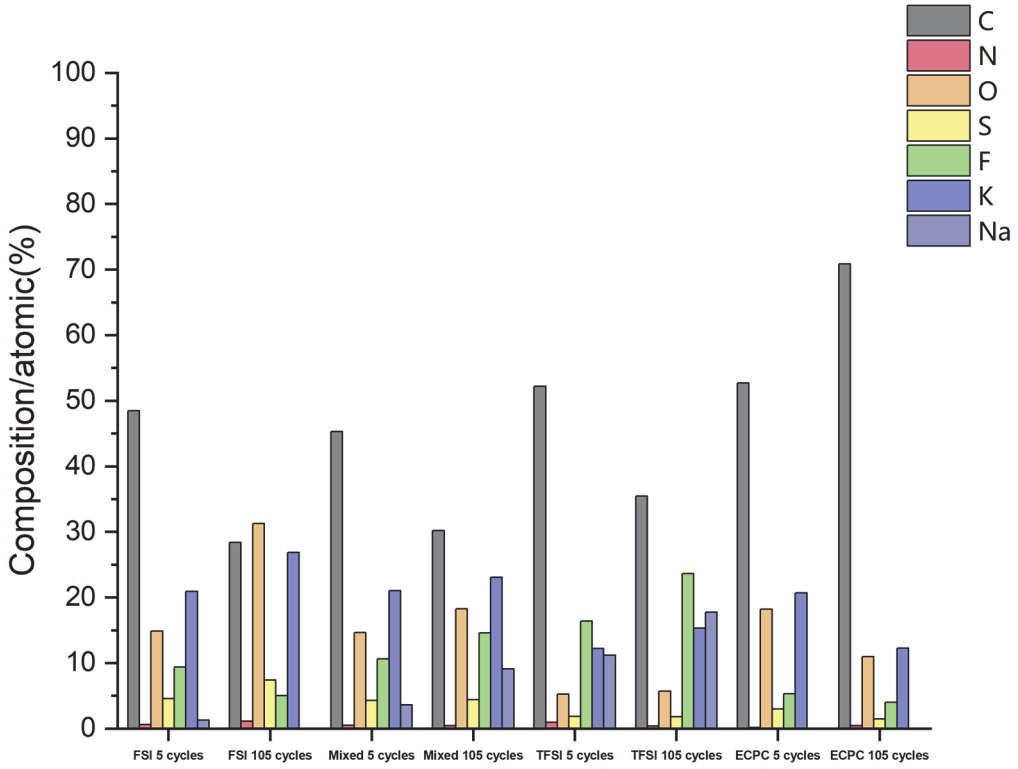

Figure 3.31. The atomic ratio of the elements of the SEI layer after 50s' etching formed by ionic liquid electrolytes and organic electrolytes

Table 4. The atomic ratio of the elements of the SEI layer after 50s' etching

	C	N	O	S	F	K	Na
FSI 5 cycles	48.44%	0.61%	14.84%	4.56%	9.38%	20.89%	1.30%
FSI 105 cycles	28.40%	1.14%	31.24%	7.38%	5.00%	26.84%	
Mixed 5 cycles	45.32%	0.50%	14.64%	4.31%	10.61%	21.02%	3.61%
Mixed 105 cycles	30.21%	0.44%	18.27%	4.38%	14.57%	23.04%	9.10%
TFSI 5 cycles	52.18%	0.95%	5.23%	1.88%	16.37%	12.19%	11.21%
TFSI 105 cycles	35.44%	0.41%	5.72%	1.80%	23.6%	15.29%	17.73%
ECPC 5 cycles	52.71%	0.15%	18.19%	3.00%	5.28%	20.67%	
ECPC 105 cycles	70.88%	0.46%	10.93%	1.46%	4.01%	12.26%	

3.3.4.4. Failure Phenomena of SEI Layer on Graphite Electrodes Revealed by Ar-Ion Etching XPS Characterization

Detailed surface analysis offers a fundamental understanding of the capacity failure phenomenon in pure TFSI ionic liquid and ECPC electrolytes. Through XPS analysis, we gain comprehensive insights into interfacial transformations, both quantitatively and qualitatively. Overall, the SEI layer formed by ionic liquid electrolytes exhibits a greater shift toward inorganic species compared to that formed by ECPC electrolytes, this trend becomes more pronounced with longer etching durations.

This shift can be attributed to potassium ions being surrounded by a salt-rich environment in ionic liquid electrolytes. After an additional 100 cycles at 100 mA/g, the SEI layers formed by ionic liquid electrolytes further evolve toward an inorganic-rich composition on the graphite electrodes. While inorganic-rich SEI layers are considered a key feature of stable SEI,[13, 21, 31, 134-136] The low dielectric constants of excess KF and NaF hinder potassium ion migration across the SEI layers formed by pure TFSI ionic liquid electrolytes.[67, 69] Therefore, an ideal SEI layer should be rich in inorganic components with minimal accumulation of KF and NaF.

Detailed XPS analysis reveals that the SEI layer formed by the pure FSI ionic liquid electrolyte is stabilized by its inorganic-rich composition (37.72%) and a higher preference for oxidized species (29.41%). These characteristics contribute to enhanced mechanical and chemical stability, likely due to the presence of K_2O, sulfide compounds, and elastic organic components. While it is challenging to quantify these compounds directly, the overall elemental analysis provides insights into the general evolution trends of SEI layers.A notable example is the mixed-anion electrolytes, which demonstrate significantly improved cycling performance compared to pure TFSI ionic liquid electrolytes on graphite electrodes. The SEI layer

formed in mixed-anion systems evolves similarly to that of the pure FSI ionic liquid electrolyte, which may explain the substantial recovery cycles observed during the initial 100 cycles. Furthermore, these electrolytes effectively limit the formation of fluorine species, a key factor contributing to the failure of pure TFSI ionic liquid electrolytes on graphite electrodes.

Unlike ionic liquid electrolytes, the SEI accumulation process in carbonate electrolytes shifts predominantly toward organic species during cycling. The deficiency of inorganic species is likely a primary cause of capacity failure in carbonate electrolytes. Furthermore, Ar-ion etching reveals that SEI layers formed by conventional organic electrolytes are entirely organic across both outer and inner regions. In contrast, SEI layers formed by ionic liquids typically exhibit an organic outer layer and an inorganic inner layer, a critical feature for ensuring SEI layer stability.[31] [13] Therefore, it is evident that carbonate-based electrolytes require supplementary strategies to enhance the inorganic content within SEI layers.

3.4. Conclusions on Capacity Failure in Ionic Liquid and Carbonate Electrolytes for Graphite Electrodes in PIBs

We can now summarize the key findings of this study. The performances of PIB half-cells of various IL electrolyte systems and KFSI/ECPC electrolytes were thoroughly examined. Long-term cycling tests were conducted, with the first 5 cycles at 25 mA/g designated as the SEI formation phase, followed by 1000 cycles at 100 mA/g to analyze capacity failure. Two specific points, after 5 cycles and after an additional 100 cycles, were selected to investigate the interfacial transformations within the SEI layers.

Detailed surface analysis reveals that XPS is a powerful tool for examining surface transformations and providing insights into capacity failure

mechanisms. The KFSI/[Pyr_{13}]FSI electrolyte system demonstrates an initial capacity of 273 mAh/g and retains 88.7% of its capacity after 1000 cycles. The SEI layer formed in this system evolves toward a composition rich in inorganic species, stabilized by oxidized compounds, while limiting fluorine accumulation during cycling. The transformation of the SEI layer corresponds to a reduction in R_{SEI+CT} resistance. Additionally, the crystallinity of the graphite electrode remains nearly unchanged from its pristine state.

In contrast, the KTFSI/[Pyr_{13}]TFSI electrolyte system saw a rapid decrease in capacity from an initial value of 220 mAh/g, retaining close to zero capacity after 1000 cycles. XPS showed that the sodium species and major metal fluoride are accumulated in the SEI layers on graphite electrodes cycled by pure TFSI ionic liquids. The amount of metal fluoride in the SEI increased as cycling continued, and this correlated with a dramatic increase in the R_{SEI+CT} resistance to over 10 kW. The graphite electrode was degraded upon extended cycling as shown by loss of crystallinity and breaking up of the graphite flakes.

We surmise that the FSI anion has several important properties that lead to stable cycling performances for graphite electrodes. Firstly, it aids formation of a stable SEI with the more oxidized organic component and appropriate sulphur-fluorine mixed inorganic species. This SEI has a lower resistance and is able to protect the graphite electrode from degradation.

Pure TFSI does not form a stable SEI layer, but can give rise to the greater thermal stability compared with FSI based ones . The resulting SEI is metal fluoride rich and highly resistive. As shown in figure 3.32, the predicted different SEI layers formed by KFSI/[Pyr_{13}]FSI and KTFSI/[Pyr_{13}]TFSI result in distinct cycling performance after extended cycles.The poor electrochemical performance of pure TFSI samples can be explained by the excess accumulation procedure of fluorine species with low dielectric

constants in the interface. TFSI ionic liquids is also capable of transferring Na impurities from the glass fiber, which prove the minor transition metal species with similar characteristic with potassium metal can be accumulated in the SEI layer. It may be that Na can enhance the degradation of the crystallinity of the graphite electrode, as it is known that Na cannot intercalate stably into graphite.

The Na-rich surface may impede the transport of K^+ across the interface with cycling, both KF and NaF both have the low dielectric constants, which are connected with the high activation barriers of ion diffusion. By using a mixed-anion IL system, with only 15% of the ions as FSI, we can see that the ability of FSI to form a stable SEI is retained even when used in the presence of TFSI. The mixed-anion systems give SEIs that have sufficient organic component to retain low resistivity. Indeed, by controlling the TFSI:FSI ratio, we suggest that the inorganic:organic ratio of the SEI can be controlled. In this case, we find the 15% FSI formulation gives a similar capacity retention and lower RSEI+CT resistance like the pure FSI electrolyte. Even though minor accumulation of Na is observed, this does not lead to breakdown of the crystalline structure of the graphite, nor to capacity loss. This shows that the formation of the stable SEI with the correct inorganic:organic composition sufficient to protect the electrode from damage due to the presence of Na.

In general, the SEI layers are tansferred to closer to the inorganic species during the cycles in ionic liquid electrolytes, the ratio of the metal fluoride should be one key role in stabilization the inorganic species of the SEI layers. On the contrary, the SEI layer formed by 1 M KFSI/ECPC is dominated by the organic species with cycles. Considering the decreasing trend of the cycling performances, the enhanced organic species combined with the weaker crystalline state should be the main casues of the capacity failure. For the KFSI/[Pyr_{13}]FSI and KFSI/[Pyr_{13}]TFSI ionic liquid

electrolytes, the SEI layer is transferred to the specific inorganic SEI layer with low resistance with cyces, the crystalline state is also preserved all over the cycles. For the pure TFSI ionic liquid electrolytes, the existance of fluroine species and soidum species can be the main cause of the highest capacity failure among the electrolytes, which can provide the guideline for the commercial failure analysis.

Based on the previous analysis, the variable process of SEI layer is the main cause of the capacity retention of PIBs with different electrolytes. The crystallinity of graphite and the spearator are also nonnegligible in the capacity failure analysis. Based the detailed analysis, the FA model can be developed to analyze the decaying trend of capacity of PIBs. We can understand the electrochemical performaces of graphite electrodes with one interface chemistry method.

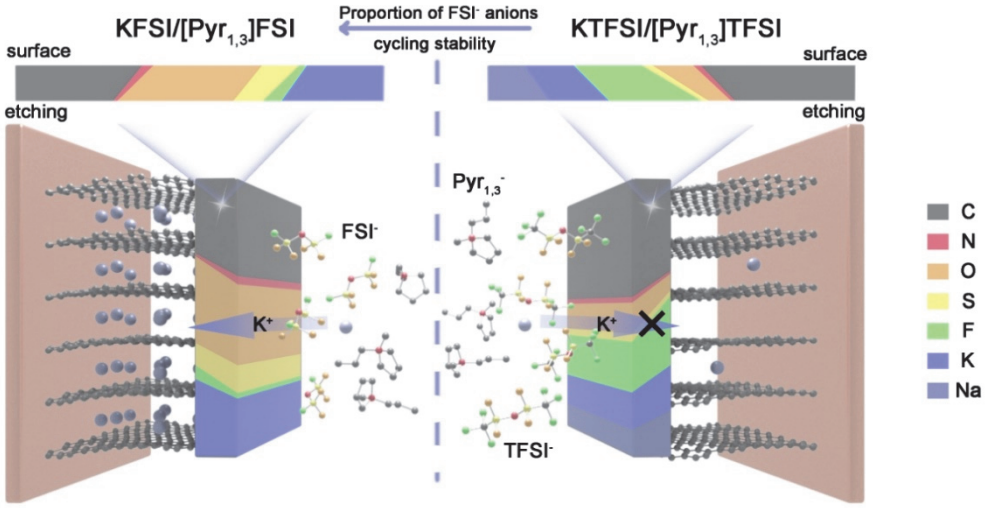

Figure 3.32. Predicted SEI structure on the graphite electrod cycled in the typical KFSI/[Pyr_{13}]FSI and KTFSI/[Pyr_{13}]TFSI ionic liquids covered at 25 mA/g for 5 cycles with additional 100 cycles at 100 mA/g.

Chapter 4 Exploring the Role of Electrolyte Additives in Carbonate Electrolytes for Graphite Electrodes in PIBs

4.1. Limitations of Carbonate Electrolytes for PIBs

A comparison between ionic liquid electrolytes and ECPC organic electrolytes indicates significant capacity degradation of graphite electrodes with standard ECPC electrolytes. Preliminary findings suggest that this capacity loss in KFSI/ECPC electrolytes is primarily due to the accumulation of unsuitable organic species in the SEI layers during repeated cycling. The absence of inorganic species differentiates the SEI layer from the classic inorganic-organic mixed SEI structure.[31] To mitigate this issue, a more effective approach would focus on enhancing the proportion of inorganic species in the SEI layers.

To address these issues, long-cycle tests were conducted using DEC as an alternative to PC solvent and saturated KFSI in ECPC electrolytes. This strategy aimed to regulate the inorganic species in the SEI layer by adjusting the electrolyte composition and salt concentration. However, similar to the performance decline observed with ECPC, a stepped decrease in capacity was noted when the PC cyclic ester was replaced with the DEC linear ester (Figure 4.1a). This substitution resulted in capacity failure outcomes comparable to previous potassium-ion battery studies of carbonate electrolyte regulation for graphite electrodes.[5] Additionally, the use of high-concentration saturated KFSI in ECPC electrolytes demonstrated that excessive salt levels could lead to unstable interfacial accumulation reactions, producing thicker SEI layers after extended cycles (>150 cycles, figure 4.1b). Although previous research has shown that high-concentration electrolytes can benefit the long-term cycling of graphite

electrodes[11], the observed capacity failure highlights the limited effectiveness of carbonate electrolytes at unsuitable high concentrations. This limitation is particularly critical when considering the practical application of high-concentration electrolytes in commercial settings.

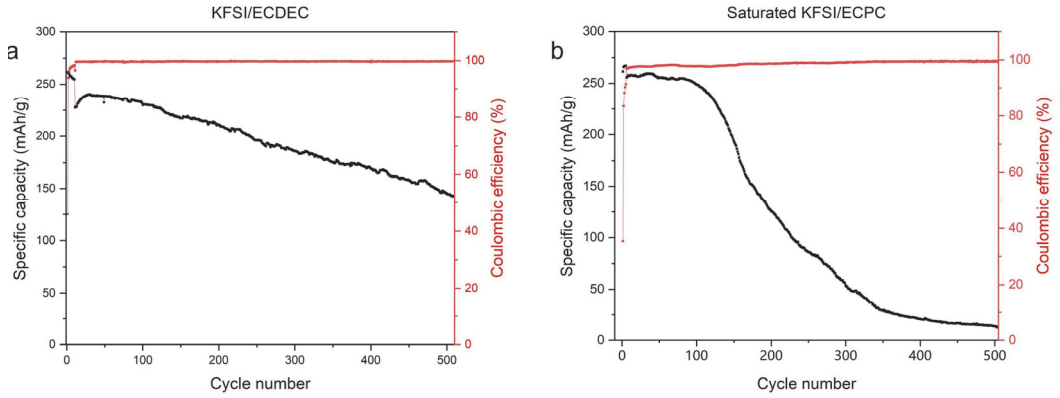

Figure 4.1. Long-term galvanostatic cycling tests of K/Graphite cells in (a) KFSI/ECDEC (b)Saturated KFSI/ECPC electrolytes at 25 mA/g for the initial cycles with additional 500 cycles at 100 mA/g.

Given the limitations of solvent regulation and high-concentration electrolytes, solvent additives are crucial for developing commercially viable electrolytes with long-term cycling stability. XPS analysis of KFSI/ECPC electrolytes indicates that the SEI layer suffers from unsuitable accumulation of ECPC components. To address this issue, classic fluorine-containing FEC additives and sulfur-containing ES additives are employed as potential solutions. Long-term cycling tests will be conducted to evaluate whether these additives can mitigate capacity failure. Additionally, interfacial analyses similar to those in Chapter 3 will be performed on additive-modified electrolytes. By establishing a correlation between interface chemistry and cycling stability, we aim to gain deeper insights into the unique characteristics of stable SEI layers for graphite electrodes in PIBs.

Based on the conclusion that the pure FSI ionic liquid electrolyte demonstrates significantly more stable cycling performance compared to

KFSI/ECPC organic electrolytes, the potential of ionic liquids as effective electrolyte additives in PIBs is evident. Furthermore, despite their common use as electrolytes, the role of ionic liquids as additives has not been thoroughly analyzed.To address the performance decline of ECPC electrolytes, the approach of using ionic liquids as additives will be explored. This will provide a comprehensive understanding of additive-modified SEI layers, encompassing both conventional additives and novel ionic liquid additives.

4.2. Thermal stability of the Ionic liquid modified carbonate electrolytes

To establish the thermal stability of the new electrolyte, we conducted thermogravimetric analysis (TGA) on ionic liquid (IL)-modified electrolytes, specifically 1M KFSI/ECPC with 10wt%, 20wt%, and 40wt% IL $Pyr_{13}FSI$ (figure 4.2). The TGA results demonstrate a significant improvement in the thermal stability of ECPC-based organic electrolytes with the addition of ionic liquids. Notably, the inclusion of ILs enhances thermal stability up to 200°C compared to conventional organic electrolytes. At 200°C, the weight retention increases with higher IL content, reaching nearly 40%. This enhanced stability is primarily attributed to the high thermal stability of the $Pyr_{13}FSI$ ionic liquid. However, further weight loss observed between 200°C and 350°C corresponds to the decomposition of $Py_{13}FSI$, indicating that the fire resistance provided by IL additives diminishes above 350°C. Overall, the TGA results confirm that incorporating ionic liquids into ECPC electrolytes effectively enhances their thermal stability, making them suitable as fire retardant components in such systems. This establishes the initial advantage of IL-modified ECPC electrolytes as being safer than

commercially available additive-modified electrolytes.

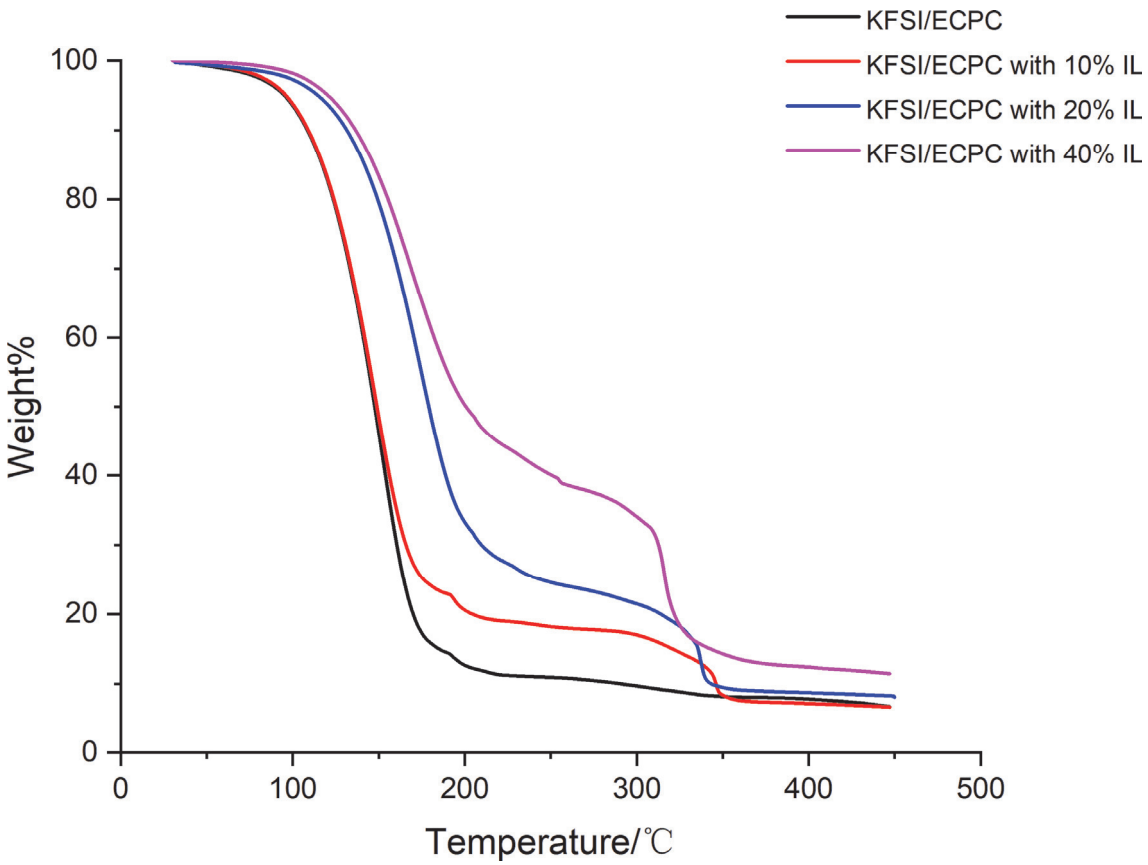

Figure 4.2. TGA tests of 1 M KFSI/ECPC electrolytes, 1M KFSI/ECPC with 10% $Pyr_{13}FSI$, 1 M KFSI/ECPC 20% $Pyr_{13}FSI$ and 1 M KFSI/ECPC with 40%IL.

4.3. Electrochemical Characterization of Carbonate Electrolytes with Various Additives for Graphite Electrodes in PIBs

To further investigate the effects of IL as additives in carbonate-based electrolytes, we examined three groups of IL-modified carbonates: 1M KFSI/ECPC with 10%, 20%, and 40% IL. These were compared against carbonate electrolytes with conventional additives: 1M KFSI with 0.5% and 10% ES, and 1M KFSI with 0.5% and 10% FEC. By applying the capacity failure analysis strategy discussed earlier, we aim to determine whether

$Pyr_{13}FSI$ is a promising IL for enhancing the cycling stability of graphite electrodes. Additionally, we evaluate how the concentration of additives impacts interfacial chemistry, both for ILs and traditional electrolyte additives. To further analyze the role of additives in promoting an inorganic-rich SEI layer, we included saturated concentrated IL as a reference group, which is known to form SEI layers predominantly composed of inorganic species.[11, 29]

4.3.1. Cyclic Voltammetry

To begin with, it is essential to understand the formation process of the SEI layer in KFSI/ECPC electrolytes modified with additives. The response current was calculated using the electrode area of graphite electrodes with a 12 mm diameter and a mass loading of approximately 1.0 mg/cm².

During the initial SEI formation cycle, the inclusion of electrolyte additives extends the SEI formation stage, facilitating the development of the SEI layer prior to the standard SEI formation phase observed in unmodified electrolytes. When FEC and ES additives are introduced into the electrolytes, their decomposition occurs at a higher voltage range of 1.0 V to 1.5 V agansit SHE of potassium [67, 68], preceding the typical SEI layer formation voltage range of 1.0 V to 0.4 V. Increasing the concentration of these additives enhances the decomposition peak, resulting in a significantly thicker SEI layer that uniformly covers the graphite electrodes (figure 4.3 b,d). The addition of ILs and salts to the ECPC electrolytes does not influence the decomposition of organic species but increases the decomposition peaks of FSI anions (from 0.8 V to 1.0 V). This enhanced FSI decomposition contributes to a higher proportion of inorganic species in the SEI layer, which helps improve the stability of the SEI layer (as shown in Figure 4.3 e-g). However, a different trend is observed in saturated

KFSI/ECPC electrolytes (figure 4.3 h). When excessive salts are added, the decomposition of FSI anions continues even after the formation of the SEI layer, potentially leading to further capacity degradation. Apart from the SEI decomposition process, the incorporation of both FEC and ES additives results in a significant decrease in the response current at the same scan rate. This reduction can be attributed to the formation of an unstable SEI layer, which increases both ohmic and kinetic resistance, ultimately leading to poorer cycling performance. Furthermore, the addition of an ionic liquid does not impose an extra barrier to electron diffusion, thus enabling high current densities comparable to those observed in KFSI/ECPC (figure 3.2) and saturated KFSI/ECPC electrolytes. The CV tests reveal that although the primary SEI layer formation occurs during the initial cycles, the SEI layer continues to accumulate, resulting in varying capacity retention across different electrolytes. The CV curves indicate that incorporating IL as an additive in ECPC electrolytes promotes the formation of a stable SEI layer, as evidenced by accelerated SEI stabilization cycles and improved ion diffusion processes.

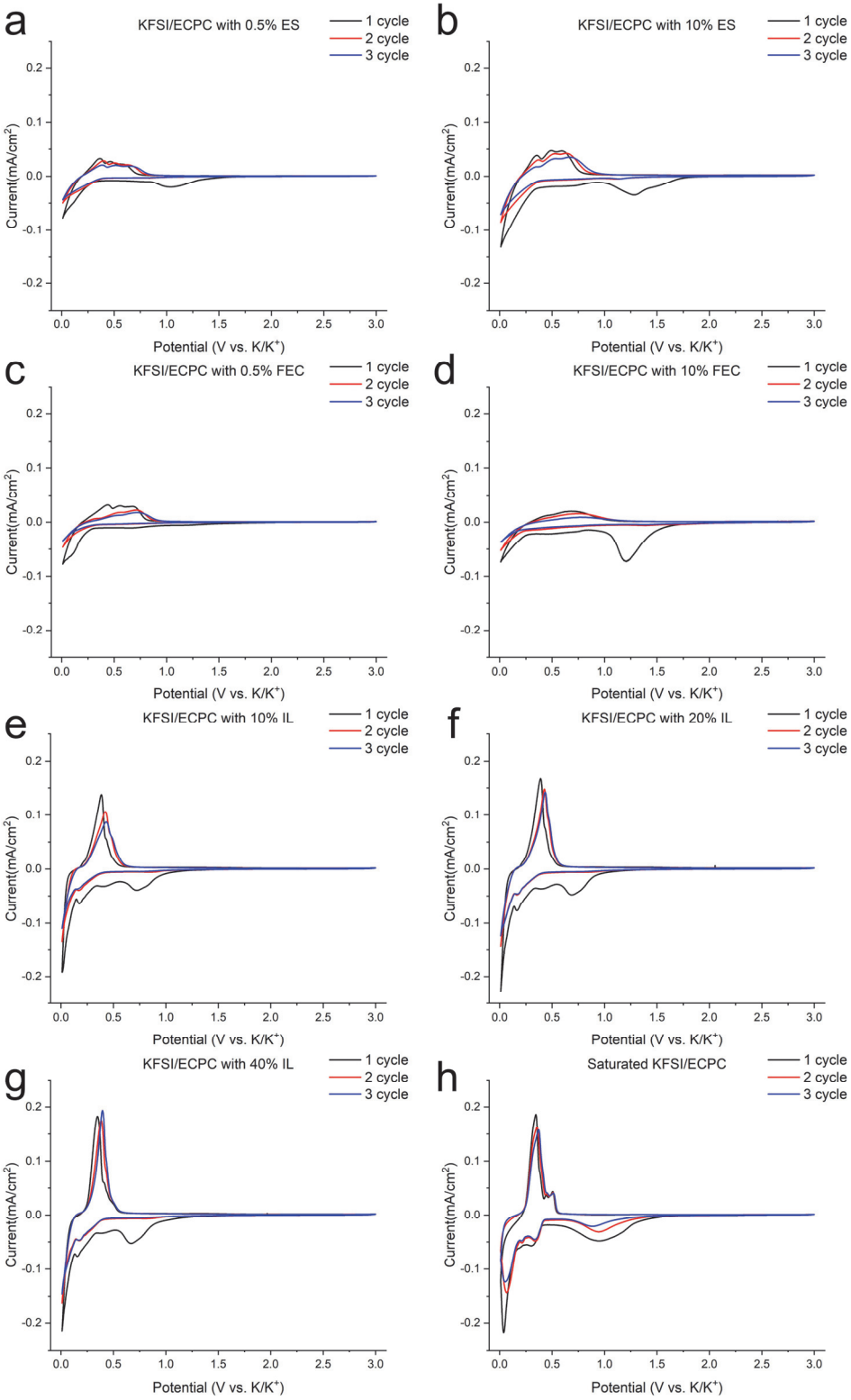

Figure 4.3. Cyclic voltammetry of K/Graphite cells in KFSI/ECPC with (a) 0.5%ES (b)10%ES (c) 0.5% FEC (d) 10% FEC (e) 10% IL (f) 20% IL (g) 40% IL, (h) saturated KFSI/ECPC.

4.3.2. Galvanostatic Charge-Discharge Cycling

To analyze capacity failure in various electrolytes for graphite electrodes, SEI formation cycles were performed at a low current density of 25 mA/g using electrolytes with different additives. Clear decreasing trends in capacity were observed for electrolytes with excessive additives (figure 4.4 b, d). In the case of 10% ES-modified electrolytes, partial capacity retention was observed at low current, although with some fluctuations. Conversely, excessive FEC-modified electrolytes exhibited rapid capacity failure, with performance collapsing even at the low current of 25 mA/g. This capacity degradation is attributed to the unsuitable working mechanisms of these additives under high currents, which lead to improper SEI layer formation and accumulation arisen from excess additives in PIBs.[67, 68]

For ECPC electrolytes with limited additive concentrations, capacity failure was partially mitigated, indicating that additive concentration plays a crucial role in interfacial stability (figure 4.4 a,c). This conclusion is further supported by the performance of IL-modified carbonate electrolytes (figure 4.4 e-g), which show improved capacity retention, increasing from 94.2% to 97.1% as additive concentration increases, compared to 91.1% capacity retention for conventional 1M KFSI/ECPC electrolytes (Figure 4.4 i). Excluding the saturated and FEC conditions, the high Coulombic Efficiency (CE) observed throughout the cycles indicates that most samples experience only minimal SEI evolution. However, in these two specific cases, excessive SEI formation significantly undermines capacity. For samples that exhibit a decline in capacity despite maintaining a 100% CE during the cycles, additional electrode failure analysis is necessary for accuracy.

Overall, cycling performance can be significantly improved through appropriate additive modifications. However, a notable exception is

saturated KFSI/ECPC electrolytes, where uneven SEI layer accumulation leads to pronounced capacity decay over cycling. This further highlights the limitations of using highly concentrated carbonates in PIBs.

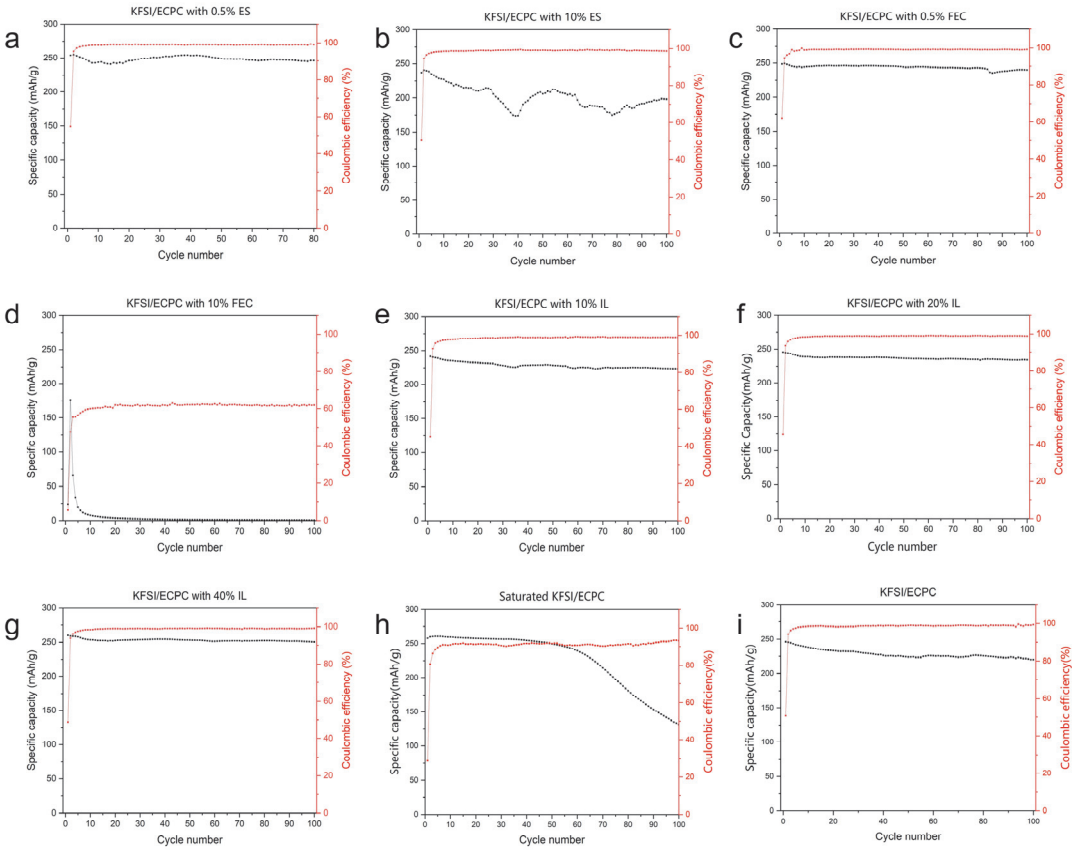

Figure 4.4. Long-term galvanostatic cycling tests of K/Graphite cells in KFSI/ECPC with (a) 0.5%ES (b)10%ES (c) 0.5% FEC (d) 10% FEC (e) 10% IL (f) 20% IL (g) 40% IL, saturated KFSI/ECPC and KFSI/ECPC electrolytes at 25 mA/g

When a higher current is applied to coin cells cycled with additives, the capacity variation due to surface modifications becomes more pronounced. For KFSI/ECPC electrolytes with conventional additives figure 4.5A (a-d), capacity retention worsens compared to standard KFSI/ECPC electrolytes. Specifically, when ES and FEC are used as additives, the results show that ES is unsuitable regardless of its concentration. Even the best-performing 0.5% FEC in ECPC electrolytes exhibits capacity variations figure 4.5A (c),

leading to prolonged activation cycles similar to those observed in KFSI/[Pyr_{13}]TFSI electrolytes. This indicates that the formation of a modified SEI layer is slow and remains unsatisfactory. The drastic capacity fluctuations confirm that the SEI layer modified by additives in ECPC electrolytes is not significantly improved. Moreover, the poor cycling performance suggests that the decomposition of additives becomes uncontrolled over cycles. This trend is commonly observed in PIBs, where the use of unsuitable FEC additives in organic electrolytes leads to inferior cycling performance.[7, 67]

Based on the cycling performance of commonly used additive modification techniques, the application of ionic liquids as electrolyte additives eliminates the issue of excess active additive measurement in organic electrolytes figure 4.5A (e-g). Pyr_{13}FSI ionic liquid has been proved as an effective electrolyte for PIBs. Its integration into ECPC electrolytes enhances cycling performance of close to 200 mAh/g at the end of 500 cycles, regardless of the quantity added. This results in improved capacity retention and shorter activation cycles compared to standard 1M KFSI/ECPC electrolytes without additives figure 4.5A (i) and the saturated KFSI/ECPC with failure trend after extended cycles after 150 cycles figure 4.5A (h).

It is well established that effective additives promote the formation of a stable, dense SEI layer at the expense of only a minimal decrease in Coulombic efficiency (CE). In comparison to the ECPC electrolyte's low initial CE (45.3%), the addition of commercial additives unexpectedly increased the initial CE—0.5% ES yielded 51.3%, 10% ES resulted in 50.5%, and 0.5% FEC reached 57.6%—suggesting that these additives did not adequately thicken the SEI layer. In contrast, only an excessive amount of FEC reduced the CE to a significantly unsatisfactory 25.4%. Conversely, the incorporation of ionic liquid (IL) additives consistently lowered the CE,

regardless of concentration: 10% IL gave 44.6%, 20% IL produced 44.2%, and 40% IL resulted in 44.7%. These values, which are comparable to the saturated ECPC electrolyte CE of 35.4%, confirm that IL additives function as intended by forming a robust SEI layer with minimal CE loss. The long addition of ES and FEC increased the SEI formation starting voltage close to 1.5 V figure 4.5B (a-d). This additional SEI preformation can accelerate the SEI formation cycle, resulting in higher Coulombic efficiency when an appropriate amount of additive is employed. However, the extended SEI formation cycle observed in ECPC with 10% FEC additives suggests that excessive additive usage can compromise SEI formation and lead to capacity failure. The resulting low Coulombic efficiency, similar as that of saturated ECPC electrolytes, arises from the formation of an overly thick SEI layer, which can hinder long-term cycling. In contrast, even with excessive IL additives, the resulting SEI layer is not excessively thick, as indicated by the SEI formation cycles in Figure 4.5B (e-g). These cycles closely resemble those of the base ECPC electrolytes without additives Figure 5B (i). This similarity indicates that the initial SEI layer formed by IL-containing electrolytes is comparable to that in bare electrolytes, suggesting that the primary function of IL as an additive may become more significant during extended cycling.

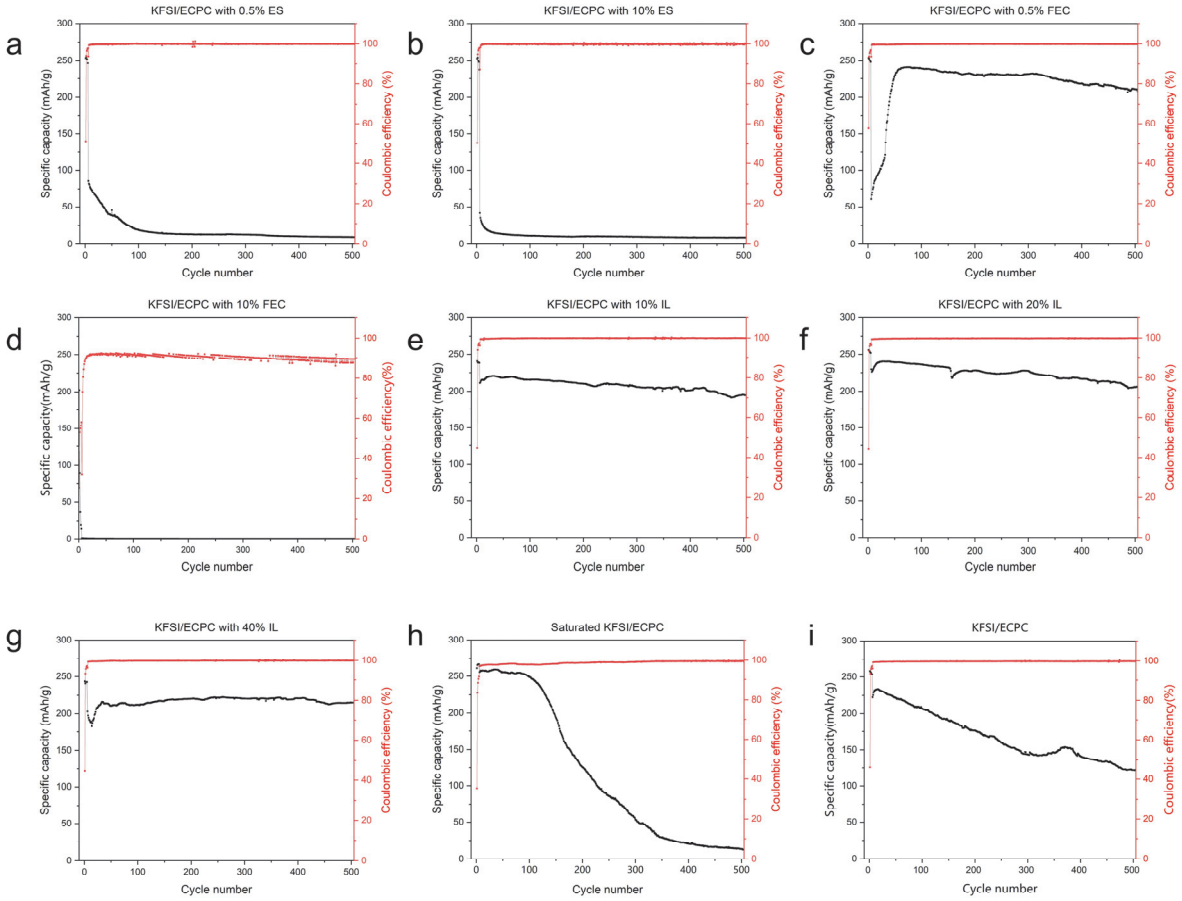

Figure 4.5A. Long-term galvanostatic cycling tests of K/Graphite cells cycled in KFSI/ECPC with (a) 0.5%ES (b)10%ES (c) 0.5% FEC (d) 10% FEC (e)10% IL (f) 20% IL (g) 40% IL, saturated KFSI/ECPC and KFSI/ECPC electrolytes at 25 mA/g for 5 cycles with 500 cycles at 100 mA/g.

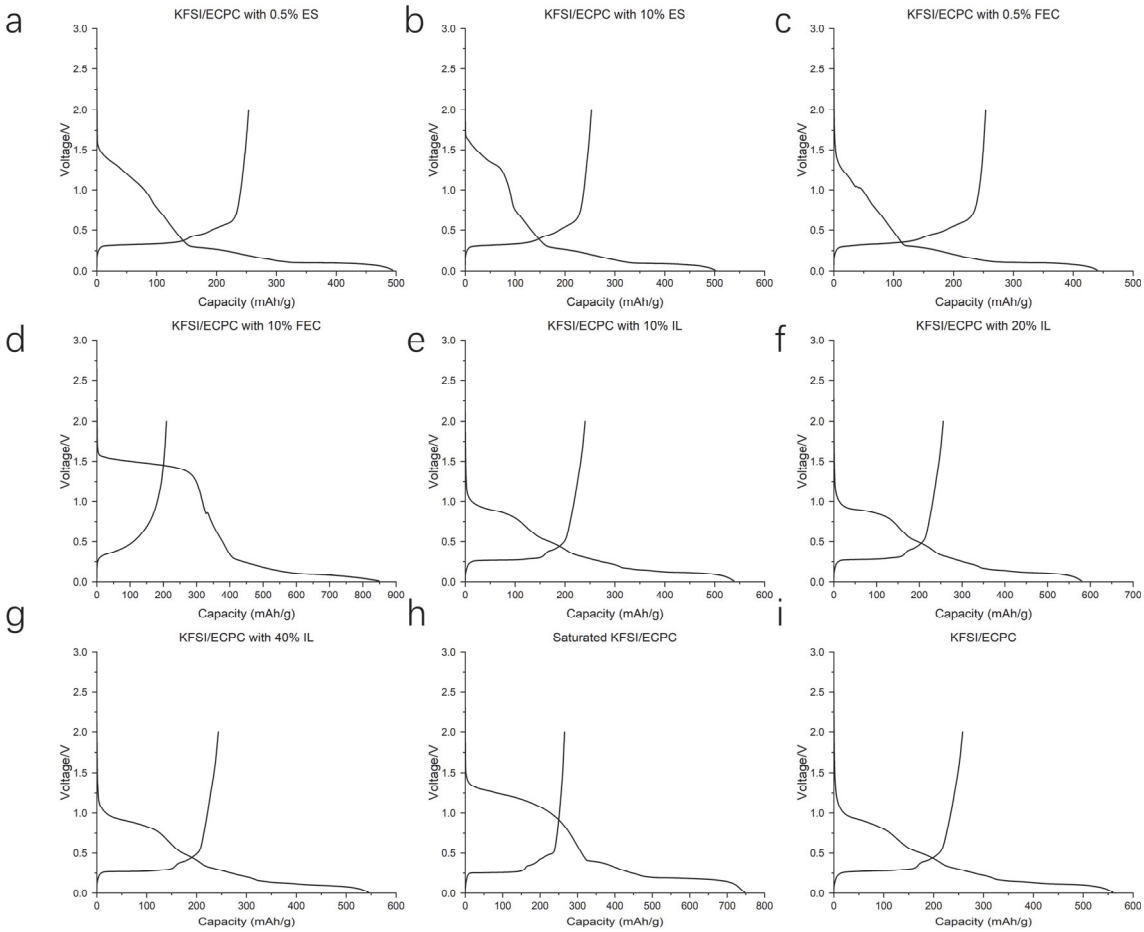

Figure 4.5B. First SEI formation cycle of long-term galvanostatic cycling tests of K/Graphite cells cycled in KFSI/ECPC with (a) 0.5%ES (b)10%ES (c) 0.5% FEC (d) 10% FEC (e)10% IL (f) 20% IL (g) 40% IL, saturated KFSI/ECPC and KFSI/ECPC electrolytes at 25 mA/g for 5 cycles with 500 cycles at 100 mA/g.

4.3.3. Rate Capability

It is evident that stable cycling performance can be achieved with ionic liquid-modified ECPC electrolytes. The improvement in cycling performance becomes more pronounced as the current increases from 25 mA/g to 100 mA/g, suggesting that current plays a significant role in cycling stability. To explore this further, we conducted rate capability tests ranging from 25 to 50, 100, 200, 300, 400, 25 mA/g to assess capacity under increasing current conditions for the electrolyte additives-modified electrolytes.

For ECPC electrolytes modified with common additives such as ES and FEC, cycling performance shows a fluctuating decline across varying current densities. At higher currents, particularly at 300 mA/g (~1C), these electrolytes exhibit rapid performance degradation, ultimately leading to dead cycling. This weaker cycling performance is attributed to the fragile SEI layer formed on the graphite electrode, which is insufficient to mitigate large concentration and activation polarization, even when potassium ion concentration remains unchanged.

A significant observation is the decreasing capacity trend at 25 mA/g following the rate capability tests. This indicates that excessive electrolyte additives have a detrimental effect on the electrode interface, compromising its stability and safety. Once damaged, the interface cannot recover, even under low current conditions (figure 4.6 b, d). The poor rate capability further demonstrates that the damage to the SEI layer caused by FEC and ES additives accumulates over time and becomes irreversible.

Compared to conventional electrolyte additives, ionic liquid-modified organic electrolytes (figure 4.6 e-g) also experience capacity decline at higher currents. However, the decrease is significantly mitigated, particularly when compared to KFSI/ECPC electrolytes with 0.5% FEC

(figure 4.6 c), making ionic liquid-modified ECPC a promising candidate for PIBs. The improved capacity retention demonstrates that ionic liquid-modified ECPC electrolytes can achieve stable cycling performance with minimal impact on rate capability (figure 4.6 e-g). Since concentration is a key factor solving polarization issues in PIBs[11], excess concentrated KFSI in ECPC electrolytes was investigated (4.6 h). Although an increase in capacity is observed at higher currents, the lower Coulombic efficiency (CE) at low currents indicates an unstable SEI accumulation process in saturated ECPC electrolytes. This instability likely results from excessive SEI formation on the electrode surface, which compromises overall performance.

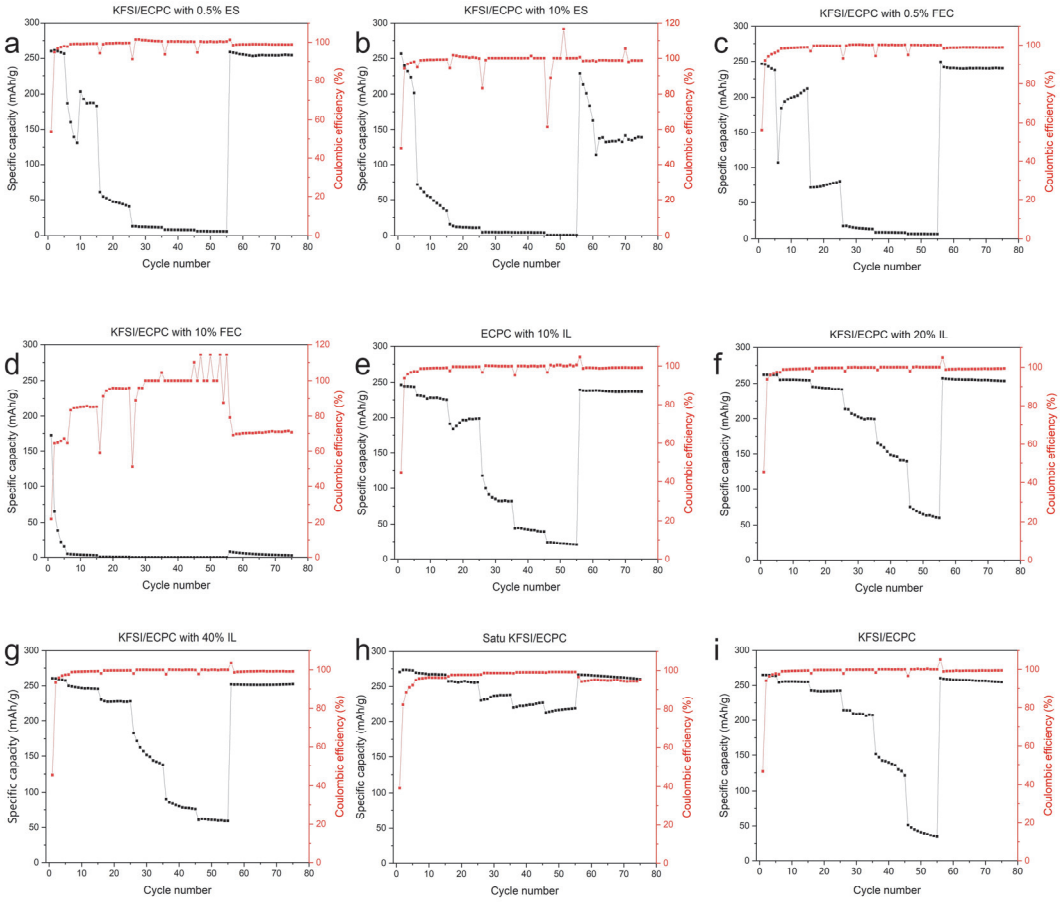

Figure 4.6. The rate capability of K/Graphite cells cycled in KFSI/ECPC with (a) 0.5%ES (b)10%ES (c) 0.5% FEC (d) 10% FEC (e)10% IL (f) 20% IL (g) 40% IL, saturated KFSI/ECPC and KFSI/ECPC electrolytes.

4.3.4. Electrochemical Impedance Spectroscopy

EIS analysis of additive-modified electrolytes was conducted to examine interface changes in different electrolytes during cycling (figure 4.7). Due to the high similarity in performance among EP 10% IL, EP 20% IL, and EP 40% IL during long cycling tests at 100 mA/g, EP 10% IL was selected as a representative ionic liquid-modified ECPC electrolyte for comparison with other graphite electrodes cycled in various additive-modified electrolytes. There are dramatic increasing trends on the impedance when the excess 10% FEC and ES are added to the carbonate electrolytes, the results show a general increasing trend in impedance to answer the severe capacity failure issues of carbonate electrolytes with excess commercial additives. This dramatic increase of impedance, are also existed for the ECPC with 0.5% ES electrolytes, connected closely with the poor cycling performances. Comparing ECPC 0.5% FEC with ECPC 10% IL electrolyte, the lower impedance until 105 cycles for ECPC 10% IL demonstrates that a more stable surface transformation is achieved, even with only 10% IL added to the ECPC electrolyte. Apart from the additives modified carbonate electrolytes, a notable exception is the saturated KFSI/ECPC electrolyte. When an excessively high concentration of KFSI is applied, the impedance does not undergo a stable transformation similar to that seen with FSI-modified ionic liquids. Instead, a stepped increase in impedance is observed, indicating that while a stable SEI layer can form initially on the electrode surface, excessive KFSI salts hinder long-term SEI stability, becoming a barrier to sustained performance.

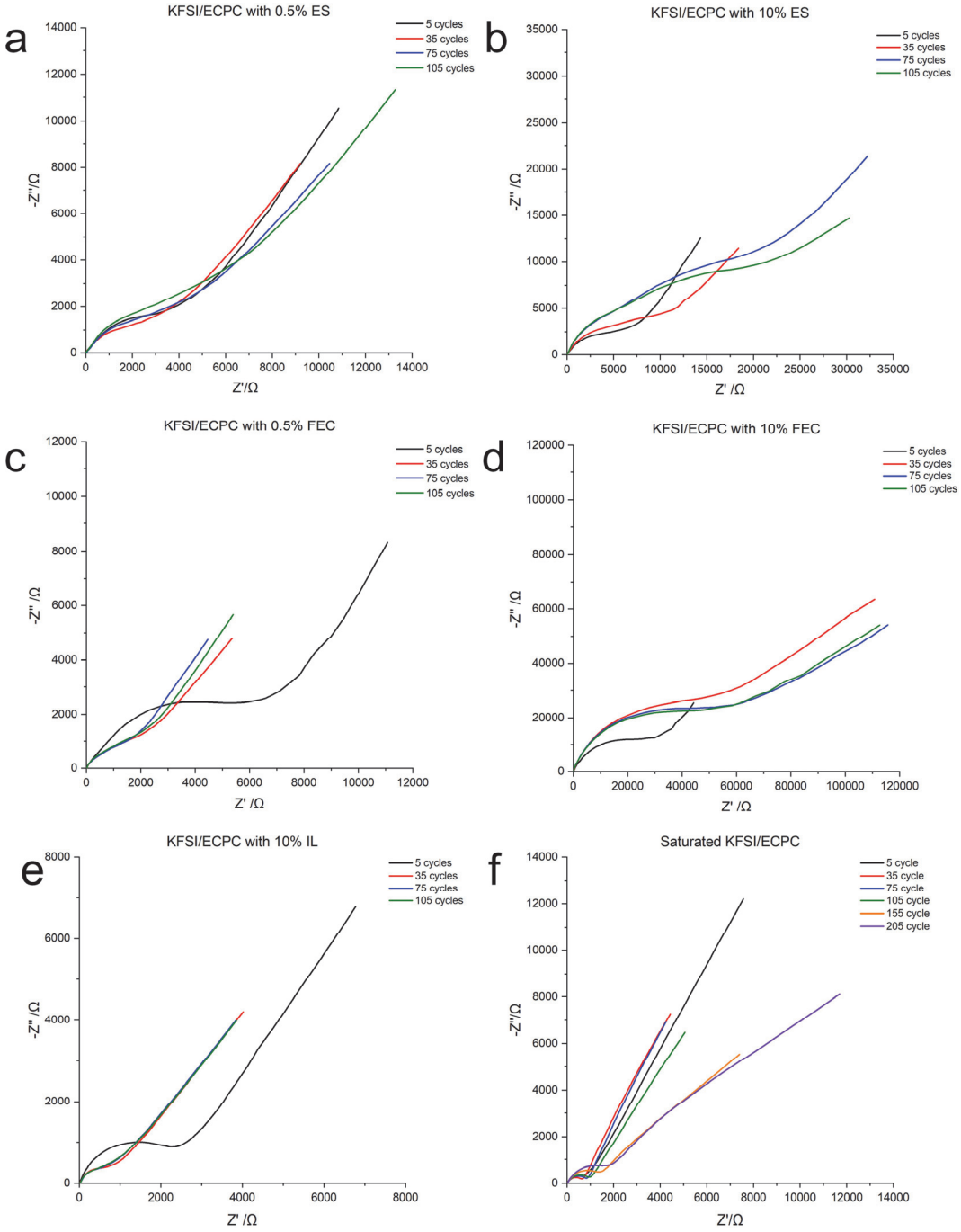

Figure 4.7. EIS analysis of K/graphite cells cycled in KFSI/ECPC with (a) 0.5%ES (b)10%ES (c) 0.5% FEC (d) 10% FEC (e)10% IL and saturated KFSI/ECPC electrolytes at 25 mA/g for 5 cycles with 100 cycles at 100 mA/g.

4.4. Characterization of Cycled Graphite Electrodes for Capacity Failure Analysis

4.4.1. XRD Characterization of Structural Degradation in Cycled Graphite electrodes

Before conducting a detailed surface analysis of the SEI degradation mechanism in different electrolytes, it is crucial to first analyze the degradation of graphite crystalline structures with cycles. Due to the limitations of SEM in detecting crystalline state changes within a localized area[114], it is not an effective method for studying overall graphite crystal degradation. To address this, XRD patterns were used again to investigate the effects of long cycles on the graphite crystals in electrolytes modified with different additives (figure 4.8). The results show that the addition of electrolyte additives, such as ES and FEC, does not significantly degrade the graphite crystals (FWHM) remain close to 0.25°) over extended cycles. Only minor degradation was observed in the excess FEC-modified electrolytes, as detailed in the corresponding figure 4.8 d. The high degree of graphite preservation indicates that degradation in common electrolyte additives is primarily driven by the further accumulation of the SEI layer on the graphite electrodes, which can be analyzed in greater detail using XPS. For ionic liquid-modified electrolytes, ECPC with 10% IL was selected as a representative and compared with standard KFSI/ECPC electrolytes. The XRD patterns reveal high similarity between the two, indicating that the potassium insertion process in the 10% IL-modified ECPC is comparable to that in KFSI/ECPC electrolytes (figure 4.8 e,f). This finding underscores the critical role of SEI accumulation in determining cycling stability during prolonged cycling.

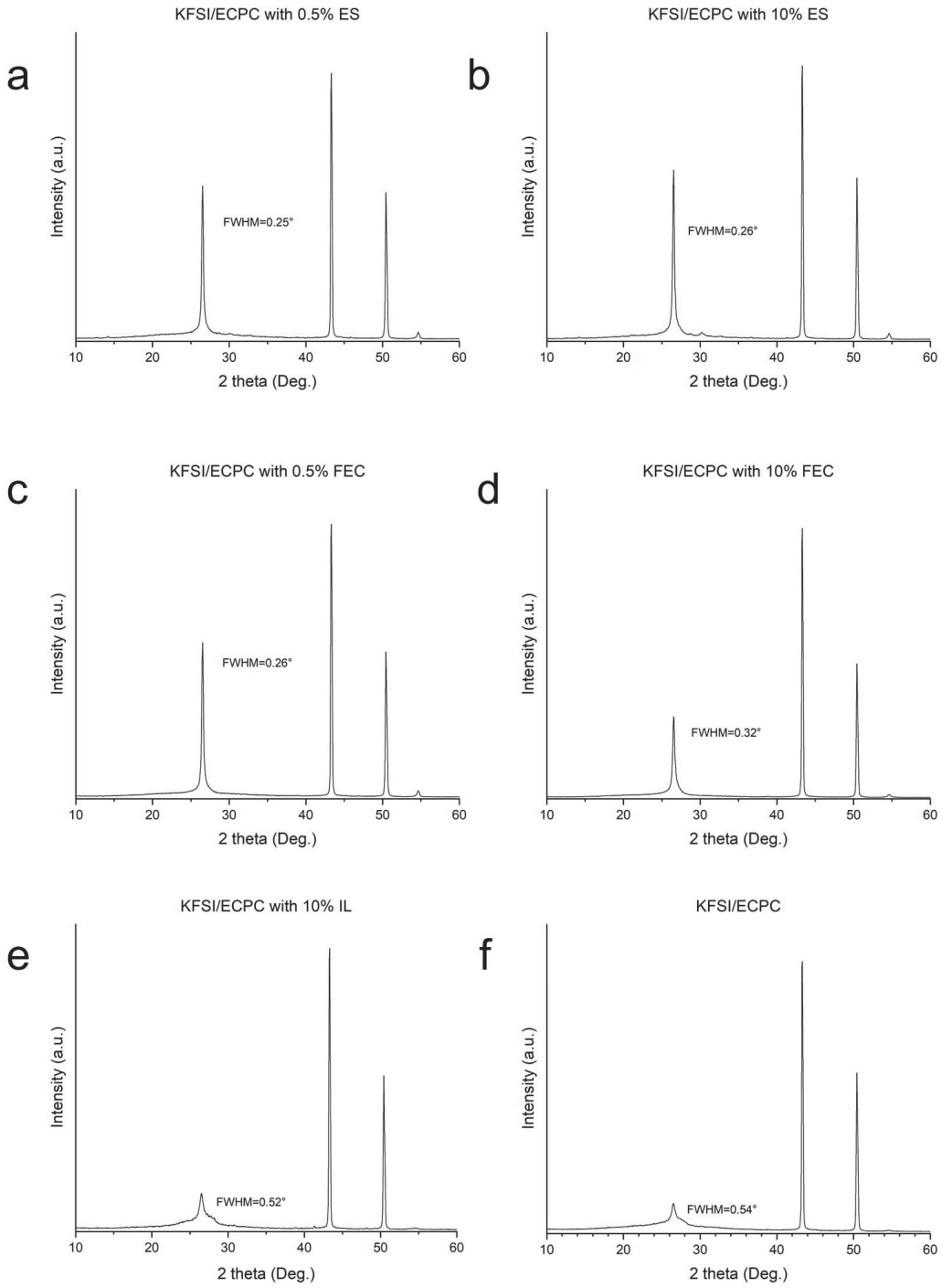

Figure 4.8. XRD pattern of the graphite electrodes cycled in KFSI/ECPC with (a) 0.5%ES (b)10%ES (c) 0.5% FEC (d) 10% FEC (e)10% IL and KFSI/ECPC electrolytes at 25 mA/g for 5 cycles with additional 100 cycles at 100 mA/g.

4.4.2. Interfacial Characterization of Cycled Graphite Electrodes Using XPS

Given the high reliability of surface XPS in analyzing ionic liquid electrolytes, the capacity failure behavior of graphite electrodes cycled with different additive-modified ECPC electrolytes was then investigated. Like the previous surface analysis, the cells were cycled under 5 SEI formation cycles at 25mA/g+100 long cycling tests at 100mA/ cycles and subjected to the same surface treatment to study the SEI accumulation process over cycling. Based on the SEI surface analysis of KFSI/ECPC electrolytes after 5+100 cycles (Figure 4.9), we propose that the primary cause of capacity failure in KFSI/ECPC electrolytes is the limited deposition of inorganic potassium salts on the graphite electrodes, combined with the accumulation of organic species on the graphite surface. This phenomenon is confirmed by the atomic ratio of the surface SEI layer after 105 cycles formed by KFSI/ECPC (C: 70.37%, N: 0.62%, O: 14.56%, S: 1.64%, F: 2.45%, K: 10.36%). These atomic ratios provide valuable guideline for surface XPS analysis of additives-modified carbonate electrolytes.

To evaluate the extent of inorganic species in the SEI layers, the SEI layer formed in saturated ECPC electrolytes characterized by an inorganic-rich SEI [7, 11, 137] was analyzed for comparison with all additive-modified ECPC electrolytes. In saturated ECPC electrolytes, the SEI layer is designed to favour inorganic species due to the FSI-dominant solvent environment surrounding the potassium ions. By analyzing the graphite electrodes cycled in saturated ECPC electrolytes, XPS provides valuable insights into the formation of a stable, inorganic-preferred SEI layer. This analysis highlights the potential of additive modification in KFSI/ECPC electrolytes to achieve such stable layers, offering critical support for evaluating the safety and performance of different additive-modified ECPC electrolytes.

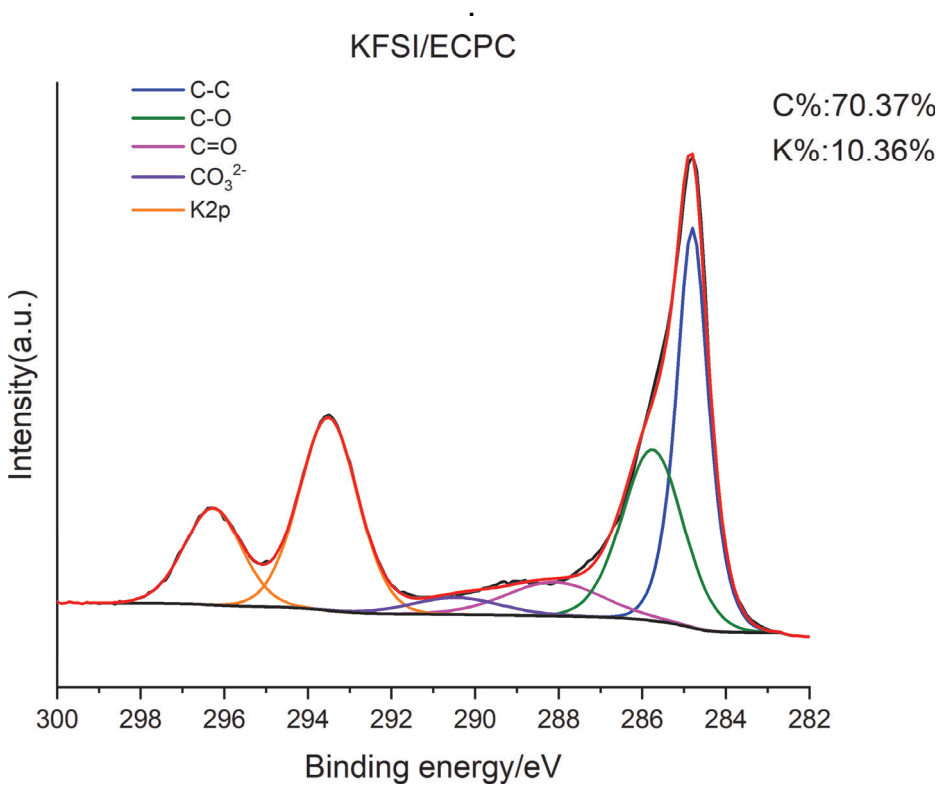

Figure 4.9. C1s and K 2p spectra of surface of cycled graphite electrodes in KFSI/ECPC electrolytes at 25mA/g for 5 cycles with additional 100 cycles at 100 mA/g

To investigate the effects of additives on the SEI layer structure, we selected a specific XPS spot for both quantitative and qualitative analyses (Figures 4.10–4.15). Additionally, an extra XPS detection spot was employed to further refine the quantitative measurements, thereby enhancing the reliability of our surface XPS analysis (Figure 4.16).To analyze the accumulation of organic species, the C1s spectra were fitted using the same method applied to ionic liquid and organic electrolytes, categorizing the organic species into four main groups: C-C/C-H, C-O, C=O, and CO_3^{2-}. As shown in Figure 4.10, for all electrolyte additives except 10% FEC, a notable increase in potassium content was observed. Since potassium species represent the total accumulation of both inorganic and organic potassium salts, this increase indicates enhanced salt deposition

facilitated by the additives. However, this trend contrasts with the performance failure observed in excess FEC for carbonate electrolytes, highlighting the distinct effects of additive concentration on salt accumulation and SEI formation. Apart from the potassium species, there are large difference on the C1s separated spectra for all of the electrolytes. For the excess 10% ES and FEC modified electrolytes (figure 4.10 b,d), there are obviously one over accumulation of the organic species (the organic ratio is close to 58%) compared with the normal ECPC with the few electrolyte additives with the organic ratio lower than 50%. For the graphite electrodes cycled with excess FEC modified electrolytes. There is one obvious increasing trend on the C-C peak, accompanied by the increase of one broad of C-O and C=O peaks along with long cycles, which can be answered by the excess decomposition of FEC along with long cycles. Based on the failure analysis we did for the ionic liquid electrolytes, the increase of C-C is one bad characteristic of the polymer organic decomposition species, which can be seen as the characteristics of fragile SEI layers cycled in the coin cells with the rapid decomposition trend. This trend is also obvious in coin cells undergoing the most significant capacity failure in the KFSI/ECPC with excess 10% ES and 10% FEC.

In general, the SEI layers formed by common additive-modified ECPC electrolytes with controlled concentration (figure 4.10 a,c) and ionic liquid-modified ECPC electrolytes (figure 4.10 e-g) exhibit very similar content of organic species. The organic species covering the graphite electrodes do not achieve exactly the same characteristics as those in FSI-modified KFSI/[Pyr_{13}]FSI and KFSI/[Pyr_{13}]TFSI ionic liquid electrolytes particularly in terms of polymer species control. The difference provide further evidence of a partially modified SEI interface on the graphite surface both by ionic liquid and minor commercial additives modified carbonate electrolytes. For saturated KFSI/ECPC electrolytes, as previously predicted, the excess

KFSI salts effectively suppress the accumulation of organic species, thereby increasing the contribution of inorganic species in the SEI layer.[7, 11] This trend is evident in the figure 4.10 h, where the proportion of organic species is significantly reduced to approximately 27.5%, as indicated by the smaller organic peaks relative to the K2p-separated peaks.

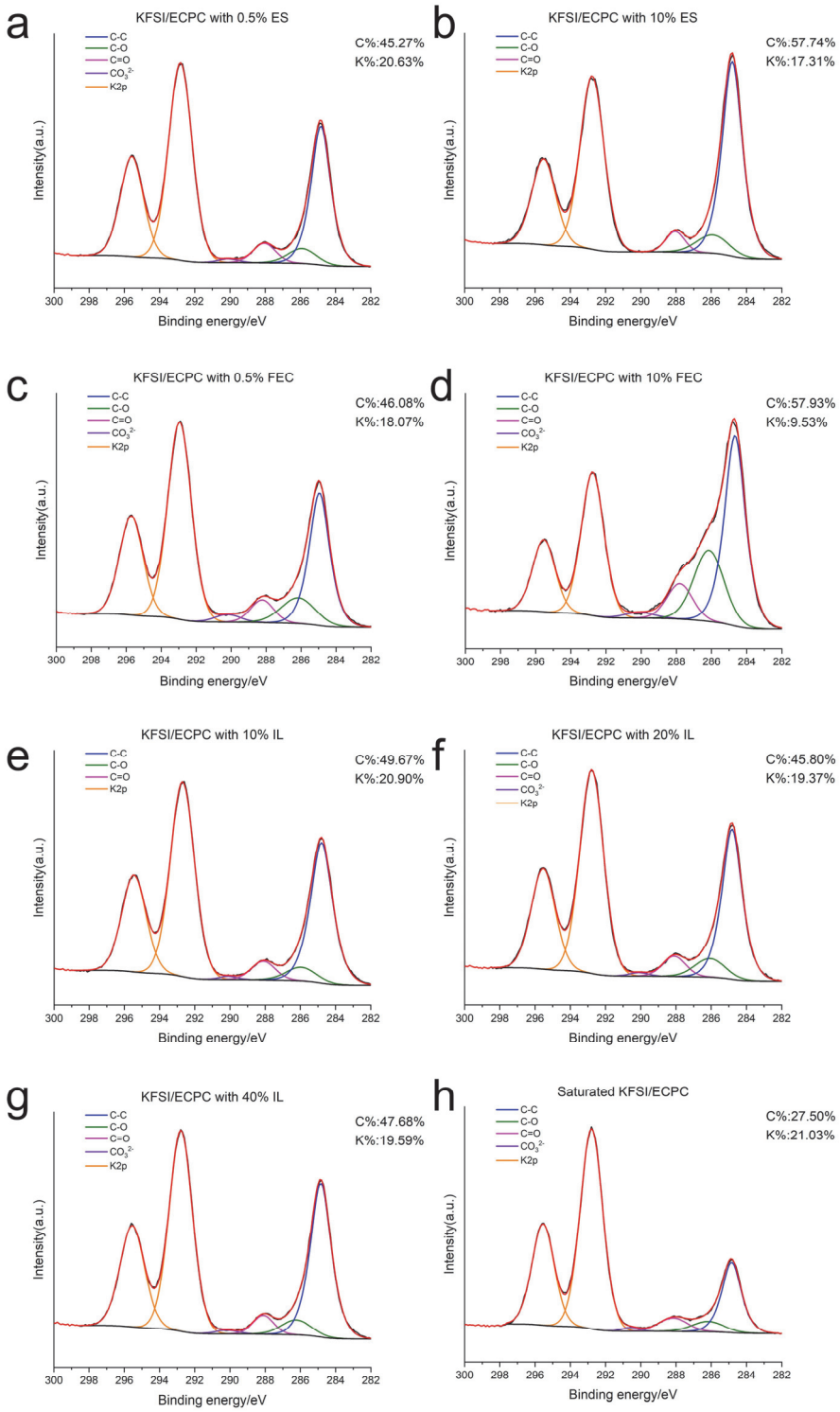

Figure 4.10. C1s and K2p spectra of the surface of graphite electrodes cycled in KFSI/ECPC with (a) 0.5%ES (b)10%ES (c) 0.5% FEC (d) 10% FEC (e)10% IL (f) 20% IL (g) 40% IL, (h) saturated KFSI/ECPC at 25mA/g for 5 cycles with additional 100 cycles at 100 mA/g.

When analyzing nitrogen in the SEI layer, only low intensity, noisy N 1s signals were observed. This made peak fitting challenging. However, based on prior analysis of the nitrogen spectrum in pure ionic liquids, we know that nitrogen anions exhibit binding energies within the range of 401–396 eV. This range was selected for defining regions and calculating separated anions peak areas for quantitative analysis.

Based on the surface analysis of traditional KFSI/ECPC electrolytes, we can understand that the nitrogen species are controlled with the low atomic% of 0.62%. In all electrolyte additive-modified ECPC electrolytes except saturated KFSI/ECPC, nitrogen species constitute less than 2 atomic%, indicating minimal residual nitrogen compounds in the SEI layer (figure 4.11 a-g). This low composition demonstrates the effectiveness of the solvent in removing electrolyte residues from the electrode surface. A notable exception is the saturated KFSI/ECPC electrolyte, where the atomic ratio of nitrogen peaks reaches 4.48%, significantly higher than that observed in additive-modified ECPC electrolytes (figure 4.11 h). This elevated nitrogen content suggests that residues of imide anions remain in the SEI layer of saturated KFSI/ECPC electrolytes, contributing to further SEI accumulation and ultimately leading to capacity failure.

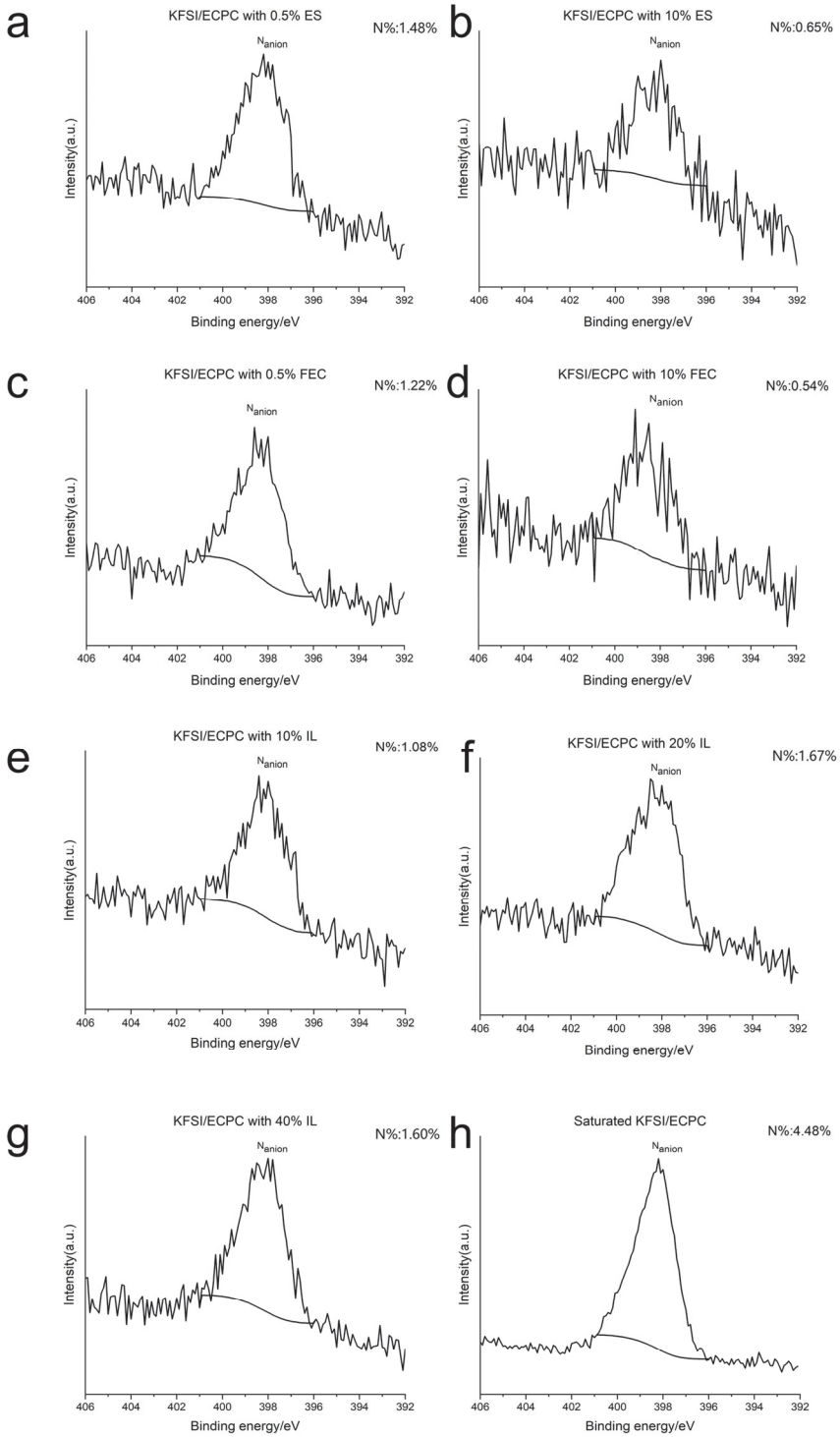

Figure 4.11. N1s spectra of the surface of graphite electrodes cycled in KFSI/ECPC with (a) 0.5%ES (b)10%ES (c) 0.5% FEC (d) 10% FEC (e)10% IL (f) 20% IL (g) 40% IL, (h) saturated KFSI/ECPC at 25mA/g for 5 cycles with additional 100 cycles at 100 mA/g

When considering the O1s spectra of additives-modified ECPC electrolytes, a key preliminary conclusion is that no obvious sodium Auger peaks are observed in any of the samples (figure 4.12). This trend correlates with the low sodium content (<2%) in most samples. Additionally, the shape and binding energy position of the main oxygen peak are consistent across all electrolytes, except for one special case: KFSI/ECPC with 10% FEC.

In the XPS analysis of carbon spectra (Figure 4.12 d), a prominent C-O peak is observed for KFSI/ECPC with 10% FEC, significantly higher than in other electrolytes. This increase is further corroborated by the appearance of a distinct oxygen peak at a higher binding energy, potentially attributed to the rise in C-O bonds observed in the O1s spectra.

Another distinct case is the saturated KFSI/ECPC electrolyte, which shows the highest oxygen content (27.19%, figure 4.12g). This elevated oxygen content is attributed to a high proportion of sulfate species (SO_3^{2-} and SO_4^{2-}), with sulfur content S% reaching 9.22%, along with more stable K_2O inorganic species. These findings indicate that the predominantly inorganic SEI layer in saturated KFSI/ECPC electrolytes after 5+100 cycles consists mainly of oxidized inorganic species.

In general, like the O1s analysis conducted for ionic liquid electrolytes and standard KFSI/ECPC electrolytes in previous analysis, the highly overlapping O1s environments make accurate fitting challenging. To avoid misinterpretation, we focus instead on comparing the overall oxygen ratios across different samples rather than fitting specific O 1s environments. Through quantitative analysis, we can determine whether the SEI layer is stabilized by the presence of sulfates, carbonate salts, and K_2O inorganic salts.

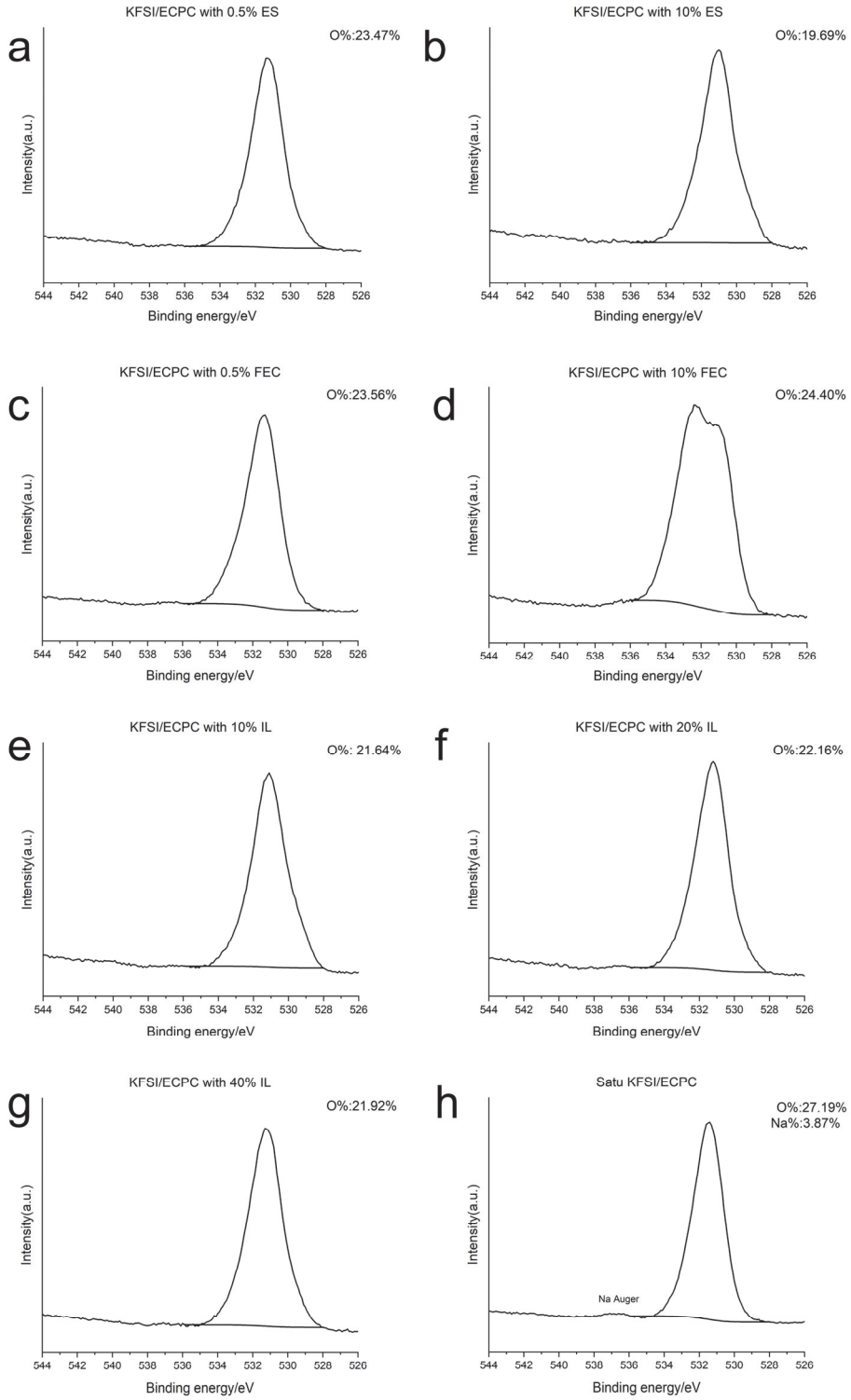

Figure 4.12. O1s spectra of the surface of graphite electrodes cycled in KFSI/ECPC with (a) 0.5%ES (b)10%ES (c) 0.5% FEC (d) 10% FEC (e)10% IL (f) 20% IL (g) 40% IL, (h) saturated KFSI/ECPC at 25mA/g for 5 cycles with additional 100 cycles at 100 mA/g

Based on the previous sodium species, we already know the introduction of Na species can be possible when unsuitable salts are used. Different from the TFSI-based electrolytes, the existence of sodium species is minor, which can be observed for all the KFSI/ECPC electrolytes with the electrolyte additives (figure 4.13 a-g), only a bit strengthened in the concentrated KFSI in ECPC electrolytes (figure 4.13 h). Based on the fluorine analysis of the samples cycled with the pure FSI ionic liquid electrolyte, it is supposed that the NaF and KF have similar FWHM, then the fluorine peaks can be separated and analyzed. When we focus on the F1s of the SEI layers formed by FEC-modified electrolytes, one special case is found. Based on the decomposition reactions of FEC, it is known that the metal fluoride should become the main decomposition products among the SEI layer.[67, 68] However, there are significant residual of FSI anions in the SEI layers. We can predict that the FEC additives do not work properly in KFSI/ECPC electrolytes, which will compete with the decomposition of FSI anions and leave large active residue of FSI anions peaks among the SEI layers (figure 4.13 c,d).

For all the SEI layers analyzed, fluorine species are present in minimal amounts. This suggests that when KFSI salts are used in ECPC electrolytes, the decomposition of S-F bonds is effectively limited, resulting in KF salt formation being controlled to levels below 5% in most cases. Even in saturated ECPC electrolytes, the FSI-dominated environment does not significantly influence the overall fluorine ratio. This indicates that KF formation is determined not by electrolyte concentration or additive variety, but solely by the nature of the salt anions.

The low atomic ratio of S (1.64%) in common KFSI/ECPC electrolytes is an important indicator of inorganic deficiency. This characteristic can be used to determine whether a more inorganic SEI layer has formed in additives-modified carbonate electrolytes. When analyzing the S 2p

spectra, the same fitting strategy previously discussed is applied for consistency. (figure 4.14). In general, similar sulfur species were observed on the surface, with differences primarily in their quantitative distribution. A notable exception is the ES-modified ionic liquid electrolytes, where the SEI layer does not transition to a sulfur-dominated environment despite the excess additive. Even for the 10% ES is added to the electrolytes, the overall sulfur content is only 2.19%, even lower than that in KFSI/ECPC with 0.5% ES (4.94%) in figure 4.14 (a,b). This unexpected result indicates that excess ES additives fail to promote a SO_3^{2-} and SO_4^{2-} environment as usual[72], leaving the additive as an active SEI disruptor within the electrolyte. In contrast to the poor performance of ES in ECPC electrolytes, there is a significant increase in sulfur content in SEI layers formed by ionic liquid-modified electrolytes controlled by the concentration of IL (figure 4.14 e-g). The similar S% indicates some similarity between IL-modified and 0.5% ES-modified ECPC electrolytes at 105 cycles. However, excess IL in the electrolyte can effectively supply sulfur species for extended longer cycles since the formation of an inorganic-preferred SEI layer with S% of 7.38% can be achieved by the KFSI/[Pyr_{13}]FSI. Similarly, the SEI layer in saturated KFSI/ECPC electrolytes exhibits a high sulfur content of 9.22%, comparable to the sulfur-rich SEI in KFSI/[Pyr_{13}]FSI (figure 4.14h). These observations confirm that only electrolytes based on an FSI-dominated environment and can reliably form sulfur-rich SEI layers, which are essential for stability and performance. The SEI layer can be possibly protected by this feature by applying excess IL to the carbonate electrolytes for long cycles.

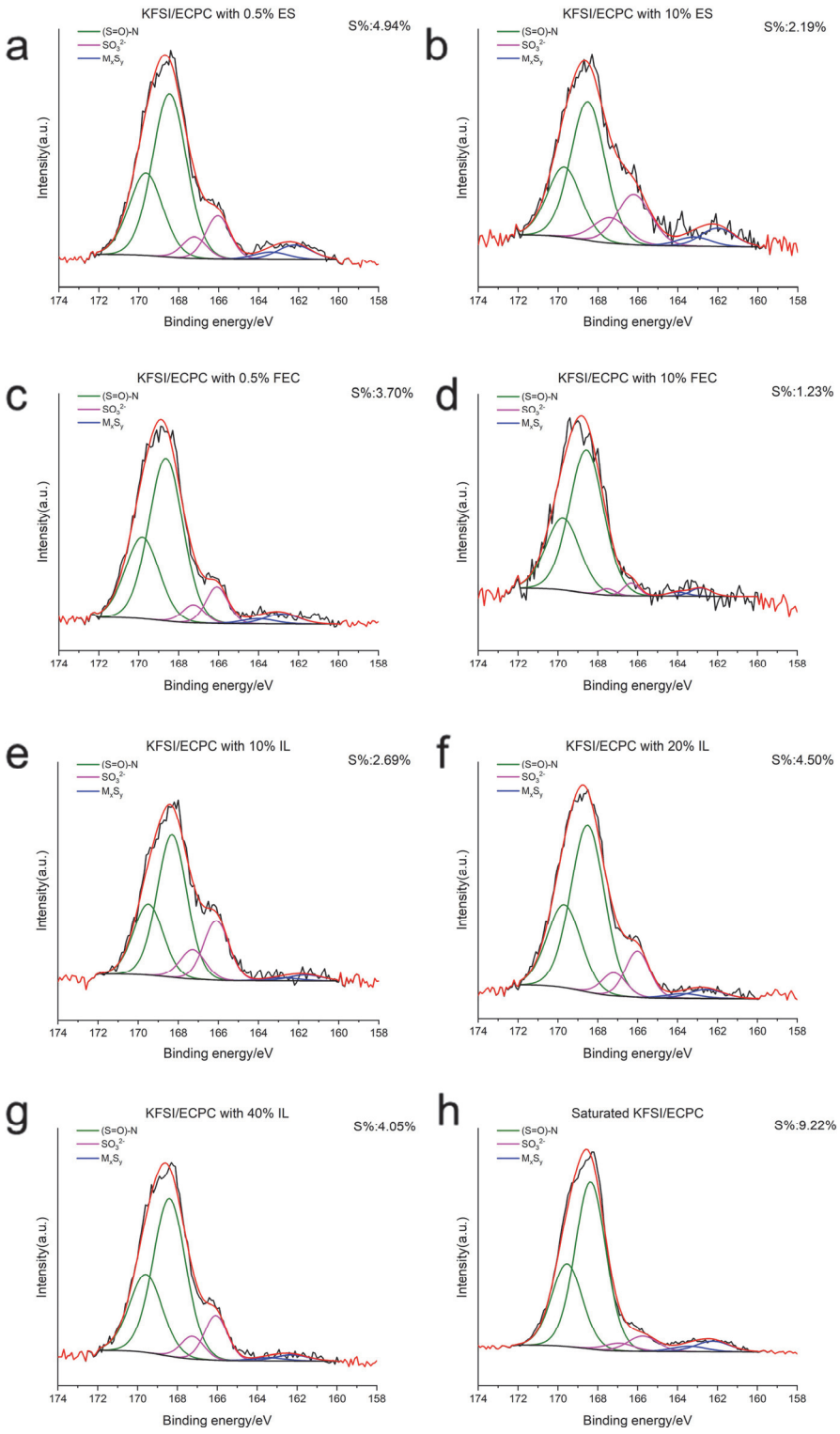

Figure 4.14. S2p spectra of the surface of graphite electrodes cycled in KFSI/ECPC with (a) 0.5%ES (b)10%ES (c) 0.5% FEC (d) 10% FEC (e)10% IL (f) 20% IL (g) 40% IL, (h) saturated KFSI/ECPC at 25mA/g for 5 cycles with additional 100 cycles at 100 mA/g

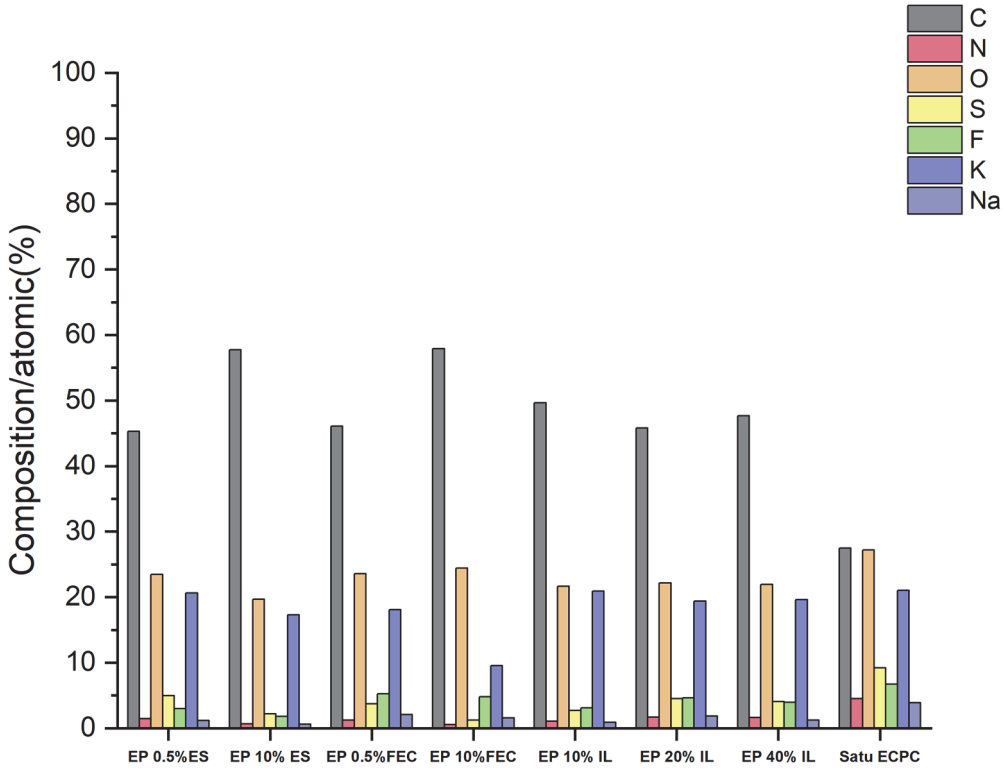

Figure 4.15. The atomic ratio of the elements of the surface SEI layer of one specific measurement spot formed by carbonate electrolytes modified by $Pyr_{13}FSI$ ionic liquid, FEC and ES additives

Table 5. The atomic ratio of the elements of the surface SEI layer

	C	N	O	S	F	K	Na
EP 0.5% ES	45.27%	1.48%	23.47%	4.94%	3.01%	20.63%	1.20%
EP 10% ES	57.74%	0.65%	19.69%	2.19%	1.79%	17.31%	0.63%
EP 0.5% FEC	46.08%	1.22%	23.56%	3.70%	5.27%	18.07%	2.10%
EP 10% FEC	57.93%	0.54%	24.40%	1.23%	4.80%	9.53%	1.58%
EP 10% IL	49.67%	1.08%	21.64%	2.69%	3.11%	20.90%	0.91%
EP 20% IL	45.80%	1.67%	22.16%	4.50%	4.65%	19.37%	1.84%
EP 40% IL	47.68%	1.60%	21.92%	4.05%	3.95%	19.59%	1.21%
Saturated ECPC	27.50%	4.48%	27.19%	9.22%	6.71%	21.03%	3.87%

As illustrated in Figure 4.15, the composition of the SEI layer formed in the electrolytes remains remarkably consistent regardless of the proportion of ionic liquid additives. To address potential experimental errors and clarify the evolution trend of the SEI layer with the addition of ionic liquid and other additives, an extra measurement spot was incorporated. The average atomic ratio from these two spots was then employed to enhance the accuracy of the quantitative analysis (as shown in figure 4.16 and Table 6). Notably, variations in measurement location exerted minimal influence on the SEI composition, confirming that the quantitative results from a single spot (as shown in Table 5) are representative of the overall SEI layer (as shown in Table 6). Although XPS analysis was performed only twice, the consistent atomic ratios between the primary analysis spot and the overall average provide confidence in the uniformity of the SEI layer on the graphite electrodes.

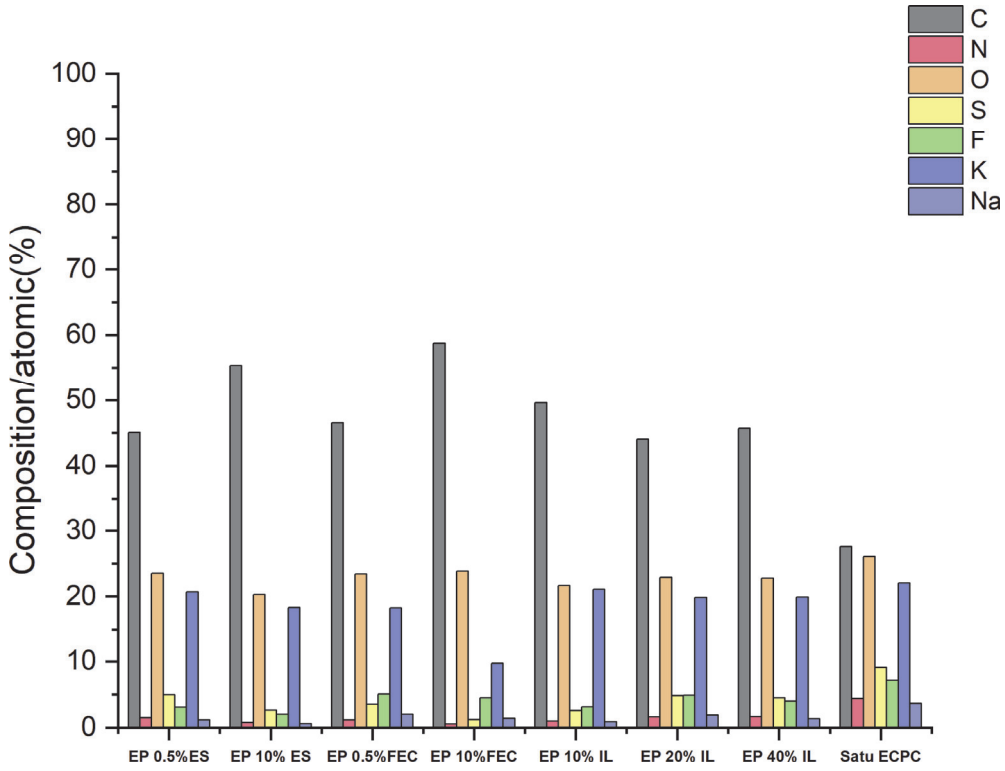

Figure 4.16. The average atomic ratio of the elements of the surface SEI layer of two measurements spots formed by carbonate electrolytes modified by $Pyr_{13}FSI$ ionic liquid, FEC and ES additives

Table 6. The average atomic ratio of the elements of the surface SEI layer of two measurement spots

	C	N	O	S	F	K	Na
EP 0.5% ES	45.05%	1.53%	23.49%	4.97%	3.09%	20.70%	1.18%
EP 10% ES	55.34%	0.79%	20.29%	2.63%	2.01%	18.33%	0.61%
EP 0.5% FEC	46.56%	1.18%	23.38%	3.53%	5.05%	18.28%	2.02%
EP 10% FEC	58.73%	0.57%	23.86%	1.21%	4.49%	9.74%	1.41%
EP 10% IL	49.62%	1.01%	21.64%	2.59%	3.15%	21.08%	0.92%
EP 20% IL	44.03%	1.61%	22.87%	4.86%	4.91%	19.82%	1.90%
EP 40% IL	45.71%	1.69%	22.79%	4.53%	4.01%	19.91%	1.36%
Saturated ECPC	27.58%	4.42%	26.05%	9.07%	7.18%	22.03%	3.66%

4.5. Evaluation of the Effectiveness of Ionic Liquids as Additives in Carbonate Electrolytes

To evaluate the effects of electrolyte additives on improving the cycling performance of carbonate electrolytes, a detailed capacity failure analysis is essential to understand how interfacial decay contributes to variations during cycling tests. The failure analysis in this chapter builds on the surface XPS analysis of ionic liquid electrolytes and common KFSI/ECPC electrolytes presented in Chapter 3, identifying XPS as the most effective method for surface-level failure analysis.

In summary, all additive-modified ECPC electrolytes exhibit increased salt deposition on the electrode surface. The safety of the additives is closely associated with the proportion of inorganic species in the SEI layers. This relationship is first evidenced by the SEI layer formed in ECPC electrolytes with poor cycling performance, which contains the highest organic content at approximately 58%. From the XPS analysis of promising SEI layers, it can be concluded that ECPC electrolytes with 0.5% FEC, 0.5% ES, and ionic liquid modifications form SEI layers with similar surface species.

However, the capacity failure trends in Figure 4.5 (a-d) and the increasing impedance in figure 4.7 (a-d) reveal that the decomposition of FEC and ES additives fails to form a sufficiently stable SEI layer for prolonged cycling. SEI layers in 0.5% FEC and ES modified electrolytes are rich in organic species (carbon ratio >45%), in contrast to the more stable inorganic-rich SEI layer (organic species ratio ~37%) formed in the pure FSI ionic liquid electrolyte with a more oxidized environment.

Conversely, the stable decomposition behavior of ionic liquid electrolytes helps minimize further decomposition of the additives themselves. Even in interfaces with similar species to those in common additive-modified ECPC electrolytes, the prolonged cycling stability of IL-modified electrolytes in

PIBs is maintained, demonstrating their superior ability to support long-term cycling performance. This cycling stability is primarily attributed to the excess $Pyr_{13}FSI$ in the electrolyte environment of IL-modified carbonate electrolytes, which continuously promotes the formation of an inorganic SEI layer throughout cycling.

For saturated KFSI/ECPC electrolytes with excess KFSI salts promoting the formation of inorganic species, the reduction in organic content to 27% further underscores the development of a more inorganic-rich SEI layer. This layer, characterized by the highest sulfur and fluorine species, enhances the stability of graphite electrodes in PIBs, maintaining cycling stability for nearly 150 cycles. The FSI-dominated environments in KFSI/$Py_{13}FSI$ and saturated KFSI/ECPC electrolytes effectively suppress the decomposition of organic species, leading to the formation of SEI layers with higher inorganic content. The similarities between the pure FSI ionic liquid electrolyte and saturated ECPC electrolytes in FSI-dominated environments demonstrate their ability to produce an elastic, inorganic-favored SEI layer. This trend is supported by detailed XPS analysis, combining peak differentiation and atomic ratio measurements to verify the composition and structure of the SEI layer.

Chapter 5 Exploring the Role of Ionic Liquid Electrolytes in Mitigating Capacity Decay of Organic PTCDA Electrodes in PIBs

Based on electrochemical and interfacial analyses of surface stability, it has been established that $Pyr_{13}FSI$ ionic liquid contributes to stable cycling performance for graphite electrodes, both as a standard electrolyte and as an additive in carbonate-based electrolytes. However, the compatibility of FSI-based ionic liquid electrolytes and ionic liquid-modified organic electrolytes with common PTCDA electrodes for PIBs remains uncertain.
To evaluate the feasibility of these electrolytes for PIBs, long-term cycling tests and detailed surface analysis using XPS are conducted. The goal is to determine whether the pure FSI ionic liquid, mixed-anion ionic liquid electrolyte and ionic liquid-modified organic electrolytes can achieve comparable cycling stability with PTCDA electrodes. Additionally, these analyses aim to identify the key factors contributing to capacity failure in the target electrolytes when paired with PTCDA electrodes.

5.1. Electrochemical Characterization of Ionic liquid electrolytes and Carbonate Electrolytes with Various Additives for PTCDA Electrodes in PIBs

Based on the failure analysis of graphite electrodes, it is clear that constant current cycling plays a crucial role in ensuring the safety of PIBs. Interfacial XPS analysis indicates that the stability of the SEI layer is enhanced by the presence of more inorganic species during cycling. To further investigate this, we conducted long-term cycling tests on K/PTCDA coin cells to determine whether a similar correlation between capacity failure phenomena and interfacial chemistry can be established for the widely

studied PTCDA electrode in PIBs. Thus, we can obtain the suitable solvent to achieve the similar solvent design of improving PTCDA electrode cycling performances[20, 23, 138, 139]

For ionic liquid electrolytes, we selected KFSI/[Pyr_{13}]FSI, KFSI/[Pyr_{13}]TFSI, KTFSI/[Pyr_{13}]TFSI, and 1M KFSI/ECPC to investigate the effects of anions on cycling stability and surface chemistry in unique ionic liquid systems. To identify effective additives for carbonate-based electrolytes, we included 1M KFSI/ECPC with 0.5% ES and 10% ES, as well as 1M KFSI/ECPC with 0.5% FEC and 10% FEC, for comparison with carbonate electrolytes containing 10% and 40% ionic liquid, respectively.

These tests aim to evaluate electrochemical performance and conduct interfacial analyses to determine which specific electrolytes contribute to improved cycling stability and CEI stability for PTCDA electrodes.

5.1.1. Galvanostatic Charge-Discharge Cycling

Similar to the constant cycling tests conducted with graphite electrodes, long-term cycling tests were performed using 25 mA/g for SEI formation cycles and 100 mA/g for subsequent cycling to evaluate the stability of different electrolytes over extended cycles. To ensure that capacity variations can be attributed to interfacial decay, the electrode mass loading was standardized at approximately 2.0 mg/cm², maintaining consistent cycling conditions across all tests.

As shown in Figure 5.1, common ionic liquid electrolytes, along with ES- and FEC-modified ECPC electrolytes, were compared against ionic liquid-modified ECPC electrolytes. When analyzing the evolution of Coulombic Efficiency (CE) in relation to CEI formation during cycling, we observed that for all electrolytes the CE remains stable even from the first cycle. This indicates a comparatively gentle initial CEI formation process, as opposed

to the typically lower CE observed during the initial SEI formation. Moreover, the minor fluctuations in CE allow it to approach nearly 100% after a few recovery cycles (Figure 5.1 a,b). Notably, in PTCDA/K half cells cycled with KTFSI/[$Pyr_{1,3}$]TFSI and in KFSI/ECPC with 10% FEC electrolytes, a pronounced fluctuation in CE was observed during prolonged cycling, coinciding with a sharp capacity decline. This phenomenon underscores that a stable CE is a key prerequisite for long-term cycling stability. However, no clear correlation exists between high Coulombic Efficiency (CE) and capacity retention, as is the case with graphite electrodes, and further analysis is needed to determine whether PTCDA electrodes experience failure during cycling.

From the long-term cycling tests on PTCDA electrodes, capacity retention improved significantly when similar ionic liquid and additive design strategies were applied, as previously demonstrated with graphite electrodes.For FSI-modified ionic liquid electrolytes, particularly KFSI/[Pyr_{13}]FSI, the highest capacity retention of approximately 78% was achieved for PTCDA electrodes after 300 cycles. However, when a portion of the FSI anions was replaced with TFSI anions, the cycling stability of the PTCDA electrodes decreased, resulting in reduced capacity retention. This trend may be attributed to the limited effectiveness of pure TFSI electrolytes, an issue that can be mitigated through mixed-anion designs incorporating FSI anions, as evidenced by the improved performance of graphite electrodes in PIBs. Additionally, a notable case arises with pure ECPC electrolyte, where severe capacity degradation is observed, resulting in only 41% capacity retention. This failure is likely attributed to a combination of electrode dissolution and an unstable interfacial layer, underscoring the limitations of unmodified carbonate electrolytes in sustaining long-term cycling stability for PTCDA electrodes.

To address these issues, electrolyte additives were introduced. As

concluded previously, only ECPC electrolytes with 0.5% FEC, 10% IL, and 40% IL demonstrated an increasing trend in capacity retention. This improvement likely results from a combination of reduced electrode dissolution and enhanced interfacial stability.

Among poorly performing electrolytes, ECPC with an excess of FEC additive stands out, as severe decomposition of the additives was observed during cycling, likely due to their high susceptibility to oxidation.[140] This excessive decomposition not only accelerates electrolyte breakdown but also may consume the active PTCDA material, resulting in a more unstable interface on the PTCDA electrodes. Based on the poor cycling performance of KFSI/ECPC with 10% FEC (figure 5.1 h), it can be predicted that even for KFSI/ECPC with 0.5% FEC, hidden risks may emerge under unsuitable current conditions, posing potential threats to cycling stability.

However, for ionic liquid electrolytes used as additives, the issue of decomposition can be effectively prevented based on the ability of pure ionic liquid KFSI/[Pyr_{13}]FSI to maintain the stable cycling performance (figure 5.1 a , i , j). By incorporating a higher ratio of ionic liquid into ECPC, it is possible to design an electrolyte that balances both interfacial stability and electrode dissolution control, particularly for electrochemically active PTCDA electrodes.

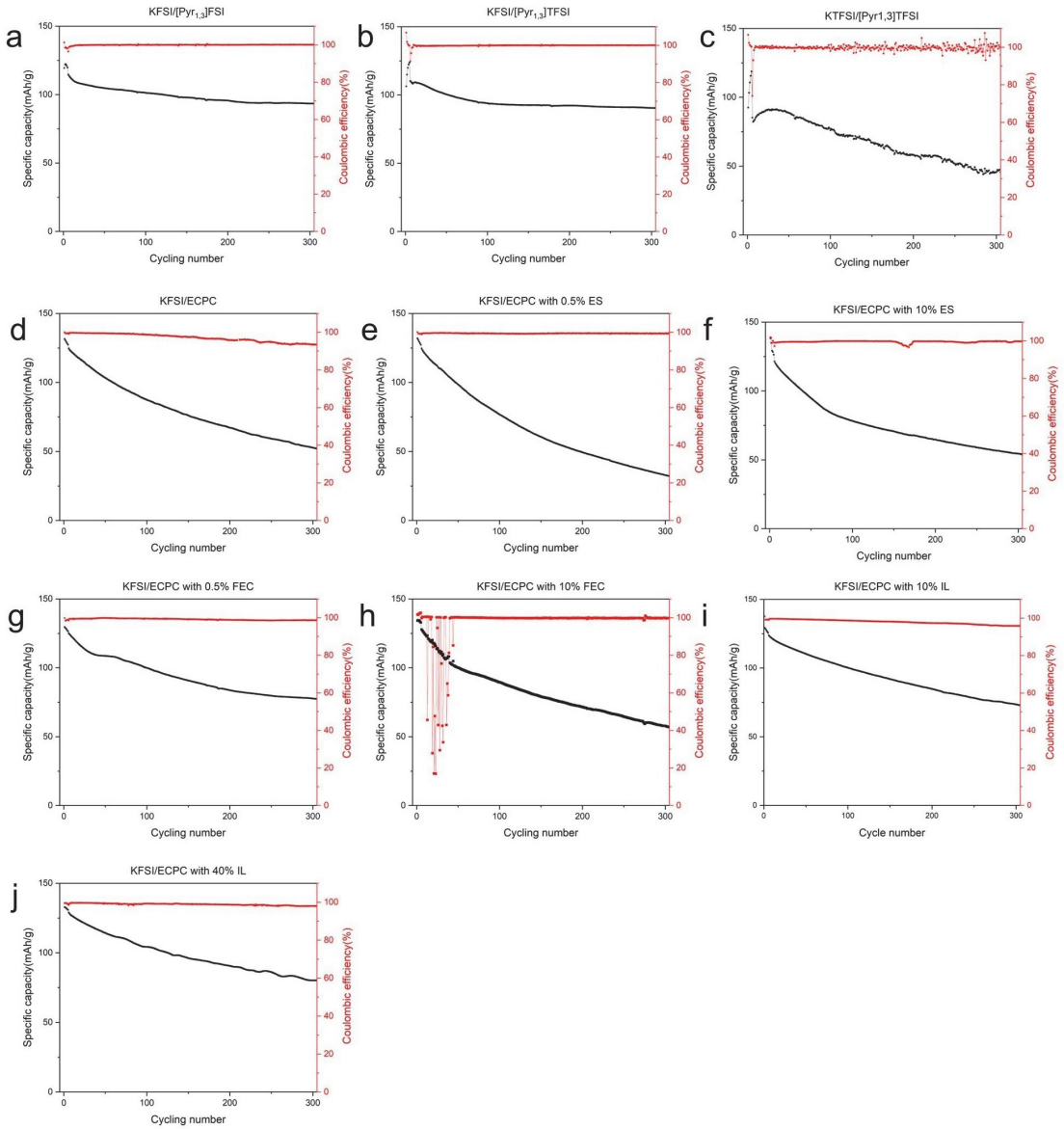

Figure 5.1. Long-term galvanostatic cycling tests of K/PTCDA cells in (a) KFSI/[Pyr_{13}]FSI (b) KFSI/[Pyr_{13}]TFSI (c) KTFSI/[Pyr_{13}]TFSI, (d)KFSI/ECPC and KFSI/ECPC with (e) 0.5% ES (f) 10% ES (g) 0.5% FEC (h) 10% FEC (i) 10% IL and (j) 40% IL electrolytes at 25mA/g for 5 cycles with additional 300 cycles at 100 mA/g

To further validate the role of Pyr_{13}FSI ionic liquid in preventing failure, four representative electrolytes were selected for polarization analysis, as shown in the figure 5.2. The results demonstrate that capacity decay is notably restrained when KFSI/[Pyr_{13}]FSI ionic liquid electrolytes are used.

The smooth conversion of PTCDA to K_2PTCDA is maintained up to approximately 305 cycles (figure 5.2a). In contrast, when traditional organic electrolytes (KFSI/ECPC) are used, polarization phenomenon between the charge and discharge stages increases, resulting in overall capacity decline (figure 5.2b). Adding a small amount of ionic liquid (IL) to carbonate electrolytes effectively controls polarization, leading to a stable capacity of around 70 mAh/g at the end of cycling (figure 5.2c). However, adding 10% FEC to carbonates causes a prolonged fluctuating charge cycle (from 3.0 to 3.3 V), indicating FEC decomposition, which poses a risk and eventually results in capacity failure (figure 5.2d).

Similar to graphite electrodes, interfacial degradation significantly influences the capacity decay rate of PTCDA electrodes.[20] Our analysis of long-term cycling reveals that KFSI/[Pyr_{13}]FSI ionic liquid electrolytes can effectively mitigate polarization growth during extended cycling. Therefore, it is predicted that a more stable CEI layer can be formed with ionic liquid electrolytes, maintaining stability throughout prolonged cycles. This benefit can also be partially transferred by incorporating Pyr_{13}FSI ionic liquid into carbonate electrolytes, resulting in better performance compared to those using common electrolyte additives.

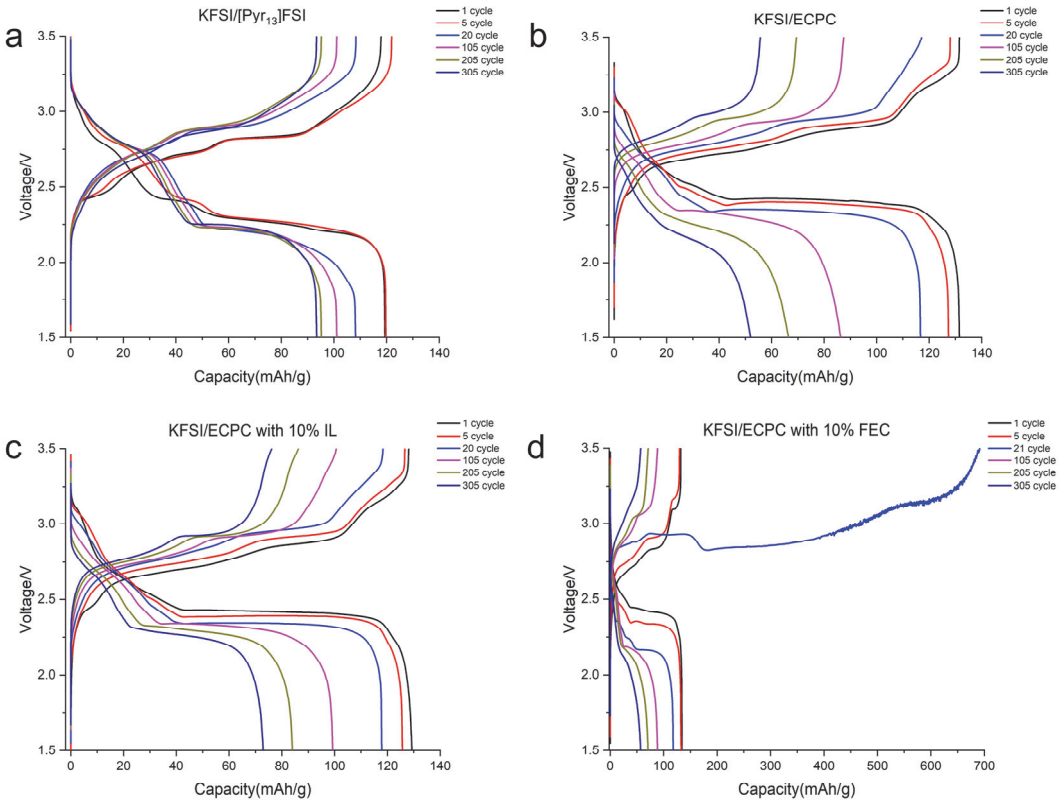

Figure 5.2. Galvanostatic discharge/charge profiles of K/PTCDA cells in (a) KFSI/[Pyr_{13}]FSI (b) KFSI/ECPC (c) KFSI/ECPC with 10% IL (d) 10% FEC electrolytes at 25mA/g for 5 cycles with additional 300 cycles at 100 mA/g

5.1.2. Rate capability

To further evaluate CEI stability during cycling, PTCDA/K batteries with selected electrolytes were tested at higher currents to enhance rapid polarization. Given the high-rate capabilities of PTCDA electrodes, rate capability tests were conducted with increasing current densities of 25, 50, 100, 200, 300, 400, 500, 1000 and 25 mA/g to predict the performance limits of PTCDA electrodes.

Consistent with the conclusions from the Galvanostatic Charge-Discharge Cycling of electrolytes, the pure FSI ionic liquid and mixed-anion ionic liquids demonstrated superior performance compared to ECPC

electrolytes (Figure 5.3 a,b,d). This improved capability is predicted to be arisen by the preference of ionic liquids for forming stable CEI layers, which benefit organic electrodes.

In contrast, when ECPC electrolytes with poor performance were modified using common additives such as FEC and ES, an unexpected trend emerged: the cycling performance of these additive-modified electrolytes was even worse (figure 5.3 e-h). This decline in performance is likely due to the weaker CEI layers formed by these additives, a limitation that becomes more pronounced at higher currents.

In contrast, the ionic liquid-modified ECPC electrolytes demonstrated the highest rate capability, particularly with ECPC electrolytes containing 10% IL as an additive (figure 5.3 i). This suggests that the incorporation of IL can enhance the formation of a stable CEI, even when used as an additive. Furthermore, the reduced solubility of PTCDA in ILs also contributes to improved performance when ILs are used as additives. These combined factors explain the significantly better rate capability of IL-modified ECPC electrolytes compared to both standard carbonate ECPC electrolytes and additive-modified ECPC electrolytes. This superior performance further motivates a detailed failure analysis of the cells to uncover the key mechanisms behind the suppression of polarization under both high current and long cycling conditions.

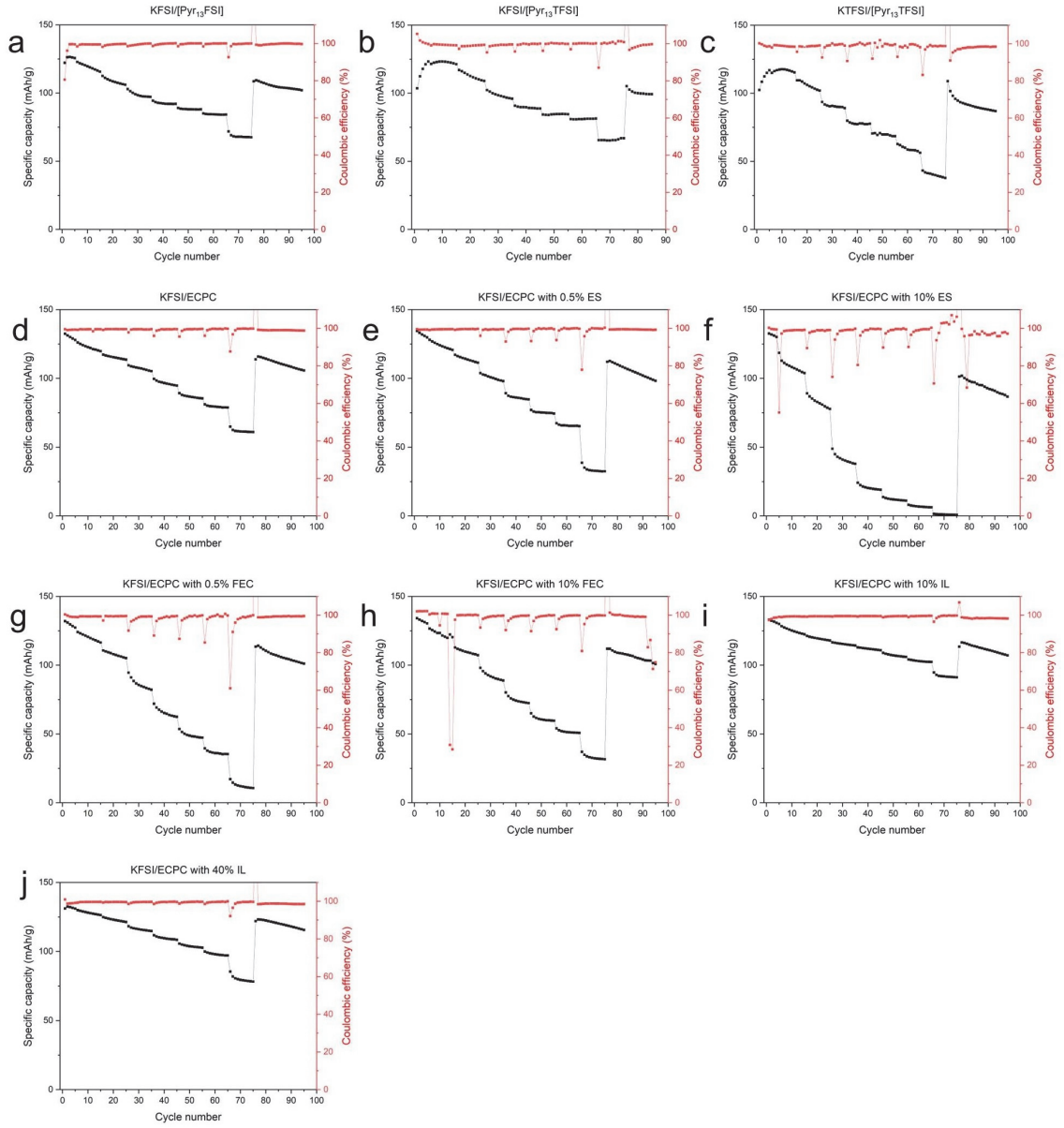

Figure 5.3. Rate capabilities of K/PTCDA cells in (a) KFSI/[Pyr_{13}]FSI (b) KFSI/[Pyr_{13}]TFSI (c) KTFSI/[Pyr_{13}]TFSI, (d)KFSI/ECPC and KFSI/ECPC with (e) 0.5% ES (f) 10% ES (g) 0.5% FEC (h) 10% FEC (i) 10% IL and (j) 40% IL electrolytes

5.2. Characterization of Cycled PTCDA Electrodes for Capacity Failure Analysis

To analyze the potential CEI formation on PTCDA electrodes, it is important to address a critical factor: as an organic electrode, PTCDA is highly susceptible to dissolution in organic electrolytes.[23] Notably, in traditional ECPC electrolytes, PTCDA electrodes tend to dissolve progressively during cycling. This dissolution is a primary contributor to capacity decay over extended cycles. Thus, we need to first understand the effects of dissolution behavior on cathode materials.

5.2.1. Dissolution phenomenon of the PTCDA electrodes

In general, the dissolution of PTCDA in ECPC electrolytes exacerbates the negative effects of commercial glass fiber separators. Over cycling, the dissolved PTCDA compounds are attached to the glass fiber, creating challenges for interfacial analysis. This process can result in a situation called the "puncture phenomenon," where dissolved PTCDA attaches to the glass fiber separator, leading to a gradual reduction in the active mass of the electrodes over successive cycles.[141]

To better understand the "puncture phenomenon," four typical cells were analyzed after 100 cycles in PTCDA/K and Graphite/K half-cells cycled at 100 mA/g with $Py_{13}FSI$ ionic liquid and ECPC organic electrolytes. Notably, for Graphite/Potassium cells cycled with both ionic liquid and ECPC electrolytes, there was minimal dissolution of graphite electrodes into the electrolytes. Upon opening the coin cells, only a negligible amount of graphite was found attached to the glass fiber separator (figure 5.4. a,c) . This minimal graphite loss indicates that, in Graphite half-cells, most of the

capacity loss is attributed to SEI accumulation during cycling rather than electrode dissolution. This distinction highlights the contrasting dissolution preferences between graphite and PTCDA electrodes under similar conditions.

However, the situation is markedly different for PTCDA electrodes. Significant amounts of PTCDA are found attached to the glass fiber separator after opening the coin cells, indicating severe electrode dissolution. This substantial mass loss onto the glass fiber demonstrates the instability of PTCDA electrodes in ECPC electrolytes. Moreover, the attached PTCDA is strongly bound to the glass fiber, making it difficult to remove even with tweezers (Figure 5.4 d). The observed mass loss of PTCDA onto the separator occurs in all ECPC electrolytes with additives, further confirming the dissolution issue associated with ECPC electrolytes. Interestingly, when $Py_{13}FSI$ ionic liquid is used, only minimal PTCDA attachment to the glass fiber is observed (Figure 5.4 b). This finding aligns with expectations, highlighting the lower solubility of PTCDA electrodes in ionic liquids. This phenomenon provides valuable insight into the decay mechanism. For ionic liquid and ionic liquid-modified ECPC electrolytes, the improved capacity retention may be partially

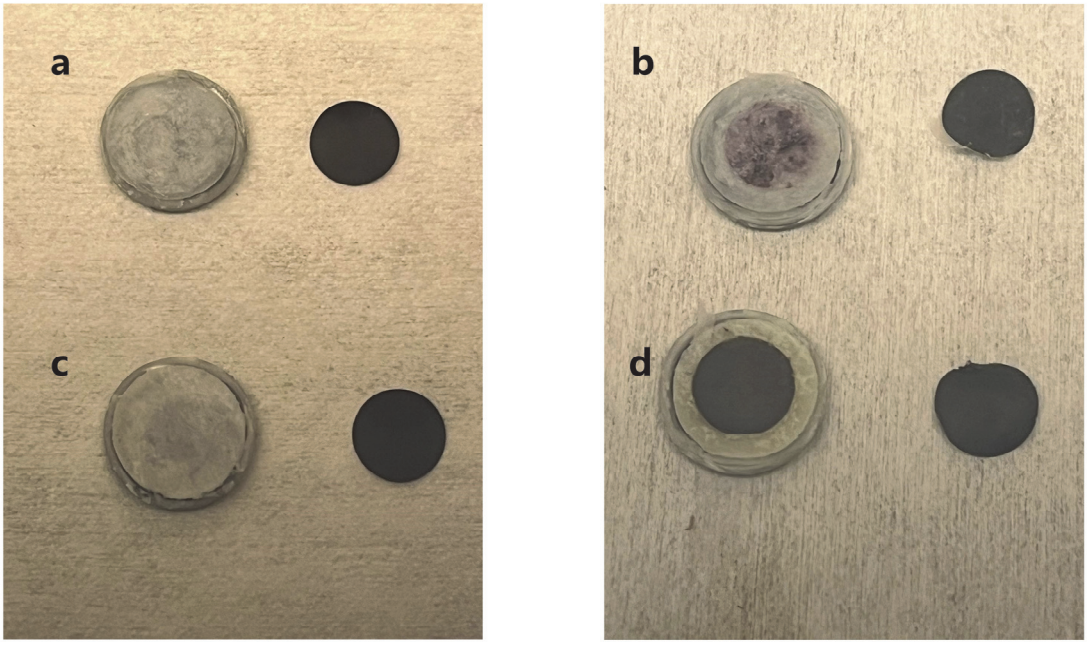

Figure 5.4. Figures of graphite electrodes and glassy fibers cycled in (a) KFSI/[Pyr_{13}]FSI and (c) KFSI/ECPC electrolytes; and PTCDA electrodes with glassy fibers in (b) KFSI/[Pyr_{13}]FSI and (d) KFSI/ECPC electrolytes at 25mA/g for 5 cycles with additional 100 cycles at 100 mA/g

5.2.2. Interfacial Characterization of Cycled PTCDA Electrodes Using XPS

To further investigate the capacity failure analysis, we have initiated surface XPS analysis of uncycled PTCDA electrodes to understand how the composition of the CEI varies at the electrode surface with extended cycling. Based on the initial analysis, the PTCDA electrodes exhibit complex carbon species signals due to their composition. These electrodes, formulated in a 7:2:1 ratio of PTCDA: Super P: PVDF binder, produce signals from all three components.

The most prominent signals include the C=C peak, primarily arising from the PTCDA, and the C-C peak, largely attributed to the carbon black.

Additionally, a strong CF_2 signal near 290.6 eV is observed, originating from the PVDF binder, reflecting its contribution to the PTCDA electrode composition. These findings indicate that the surface signals of the PTCDA electrodes are significantly influenced by their organic components, particularly the characteristic C=C peaks. This organic specificity implies that surface CEI layer analysis may involve partial separation or differentiation of the PTCDA electrode components.

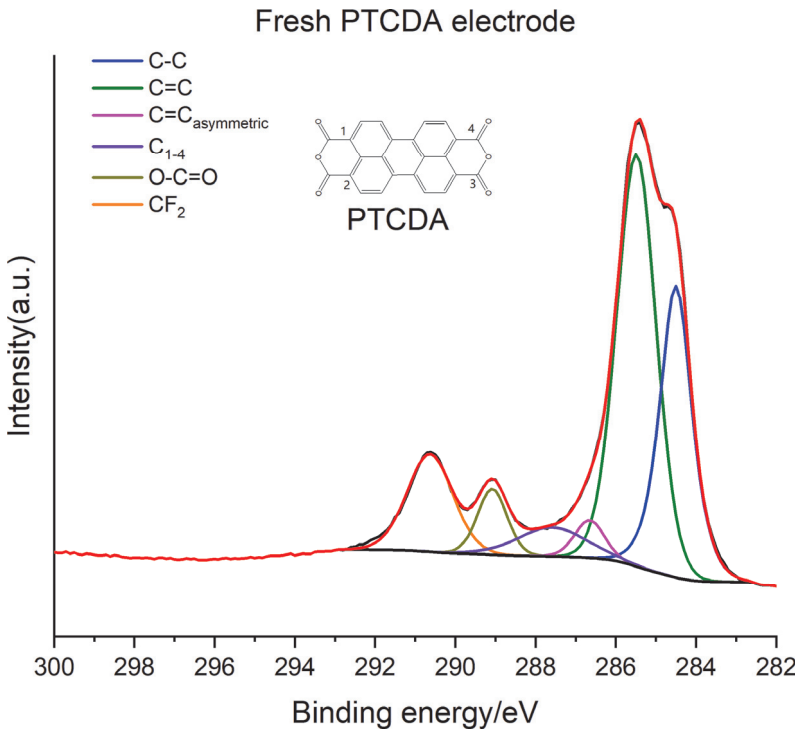

Figure 5.5. The C1s spectrum of the fresh PTCDA electrodes

Previous analyses have shown that surface analysis of the CEI formed on PTCDA electrodes is challenging due to the "puncture" phenomenon that occurs during extended cycling. As a result, it is difficult to directly correlate capacity failure issues with interfacial changes in the CEI layers covering PTCDA electrodes during cycling.

Unlike pure graphite electrodes, where the atomic ratio of the SEI layer can be clearly detected, the surface of cycled PTCDA electrodes is significantly

influenced by the presence of glass fiber. This glass fiber is known to have a substantial impact on the SEI layer of graphite electrodes as well. Therefore, before conducting surface analysis of the SEI on PTCDA electrodes, it is critical to first determine whether the glass fiber signal contributes to the overall signal.

To address this issue, we conducted an specific XPS survey of cycled graphite electrodes and PTCDA electrode surfaces cycled in KFSI/[Pyr_{13}]FSI ionic liquid electrolytes. For the cycled graphite electrodes in KFSI/[Pyr_{13}]FSI (figure 5.6a), the surface XPS analysis revealed signals corresponding to basic elements such as C, N, O, S, F, and K, along with the copper collector peak. Notably, the absence of a Si signal indicates minimal dissolution of graphite into the electrolyte, preventing any significant contribution from attached glass fibers. This trend was consistently observed across all electrolytes analyzed in Chapters 3 and 4. In contrast, as shown in figure 5.6 b, the XPS survey of PTCDA electrodes clearly displays a Si 2p peak. This peak, likely arising from SiO_2, strongly indicates the detection of glass fiber, contributing a significant Si signal. While PTCDA electrodes generally exhibit less dissolution in ionic liquids, those with severe dissolution behavior show more pronounced Si signals.

Overall, the XPS survey supports our earlier prediction for PTCDA electrodes: substantial "puncture" of the glass fiber occurs during cycling, significantly affecting surface CEI analysis. This incorporation of Si species could interfere with detailed fine-spectrum analysis of CEI.

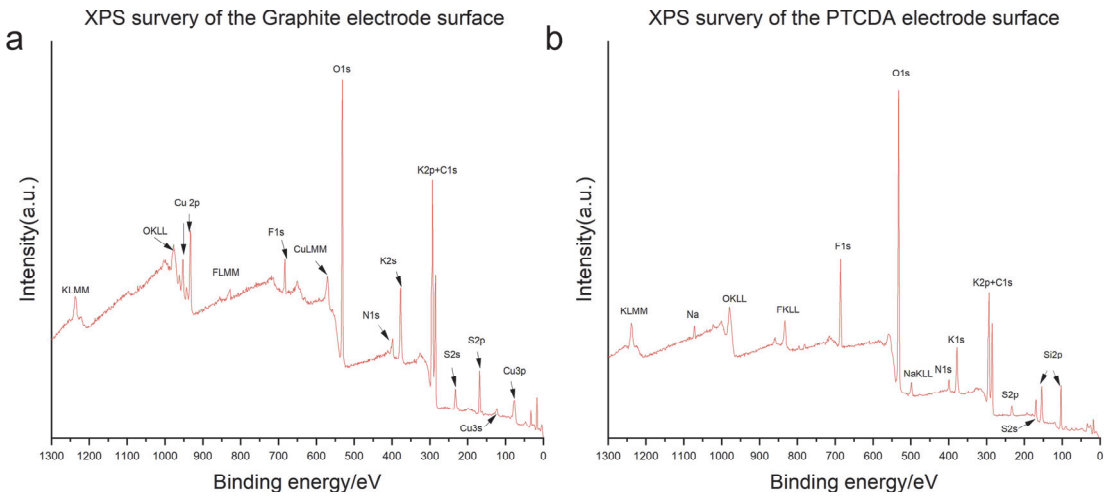

Figure 5.6. The XPS survey of (a) SEI layer covered on the graphite electrodes (b) CEI layer covered on the glassy fiber electrodes cycled in pure KFSI/[Pyr_{13}]FSI ionic liquid at 25mA/g for 5 cycles with additional 100 cycles at 100 mA/g

The capacity failure described above appears to stem from a combination of electrode dissolution and interfacial decay. In some cases, electrode dissolution is exacerbated by an unstable CEI layer, further emphasizing the importance of analyzing surface failure mechanisms. In lithium-ion batteries, SEI layer analysis on graphite electrodes has proven effective for studying CEI stability. [104] These studies often focus on the electrode surface after full cycling at OCV, using XPS analysis to evaluate CEI stability. However, the surface analysis of the CEI layer, particularly for PTCDA electrodes, remains limited. To address this complex issue of capacity failure in PTCDA electrodes, we employed a similar XPS-based interfacial analysis as used in previous research. Our goal was to identify the key features of a stable CEI layer that contribute to long-term cycling stability.

To investigate the specific capacity failure problems mentioned above, we focused on the point where capacity failure begins to manifest—after 5 cycles at 25 mA/g followed by 100 cycles at 100 mA/g. Three ionic liquid

electrolytes, KFSI/[Pyr_{13}]FSI, KFSI/[Pyr_{13}]TFSI, and KTFSI/[Pyr_{13}]TFSI, were selected to assess the role of anions in CEI accumulation. Additionally, carbonate electrolytes containing 0.5% and 10% ES, as well as 0.5% and 10% FEC, combined with a specific ionic liquid-modified carbonate, were used to evaluate whether additive modifications significantly influence the CEI chemistry in conventional 1 M KFSI ECPC electrolytes.

XPS analysis of the CEI on PTCDA electrodes presents several challenges. For CEI layer analysis, atomic ratio measurements are often unreliable due to potential variations in the amount of glass fiber across different areas, complicating oxygen analysis. Additionally, it is recognized that SiO2 can get corroded by fluorides at certain conditions[142], the difficulty in analyzing inorganic species may stem from the corrosion of the SiO_2 separator by FSI^- anions during cycling. This makes the analysis of inorganic species both difficult and less meaningful. Despite some challenges, glass fiber remains the best choice for a PTCDA electrode with a potential dissolution trend. Using a common polymer separator could lead to dissolution, compromising the separator's integrity and increasing the risk of short circuits, which must be avoided to ensure system safety.

Due to the interference from silicon impurities, we have simplified the CEI analysis by focusing on potassium and organic species, which are more closely related to the actual CEI composition. Thus, we calculated the area of potassium species to determine the amount of potassium salts formed on the surface of PTCDA electrodes. Additionally, we analyzed the area of carbon species after fitting to quantify the organic species formed. Using these data, we performed a quantitative analysis by calculating the ratio of potassium area divided by carbon area after R.S.F. adjustment. We primarily use the K/C ratio as a substitute for atomic ratios to determine whether potassium salts contribute to an inorganic-preferred CEI, favoring high interfacial stability. We conducted a quantitative analysis focusing on

a specific XPS spot for different electrolytes (see Figures 5.7–5.8). To further validate our findings, the K/C ratios from two XPS spots were calculated and compared, as summarized in Table 7.To simplify this analysis, we divided the electrolytes into two categories: ionic liquid electrolytes and organic electrolytes, to better understand CEI layer accumulation. To identify key organic species in the CEI, we applied a fitting strategy similar to that used for graphite electrodes. This involved combining most of the sp^3 carbon and sp^2 carbon signals into a single C-C peak, while separating the C-O, C=O, and CO_3^{2-} peaks.

Using this fitting approach, we assumed a similar CEI formation process occurs on the surface of PTCDA electrodes. This process overlays the primary peaks from the PTCDA material, resulting in specific organic-inorganic species on the electrode surface, like those observed on graphite electrodes.

To begin with, for ionic liquids, if we consider the K/C ratio as an indicator of the amount of inorganic species in the CEI. It is evident that the CEI of KFSI/[Pyr_{13}FSI] exhibits a higher inorganic content, with a K/C ratio of 40% during cycling. This higher concentration of inorganic species is associated with the enhanced chemical stability of the anion-driven CEI, which likely contributes to the excellent capacity retention observed during cycling.[18, 19, 21, 143] Furthermore, the inorganic-to-organic ratio in the CEI can be adjusted by modifying the anions. For KFSI/[Pyr_{13}FSI] ionic liquids, the CEI composition lies between that of the pure FSI and pure TFSI ionic liquid electrolytes, closely aligning with the trends observed in SEI analysis of ionic liquid electrolytes on graphite electrodes.

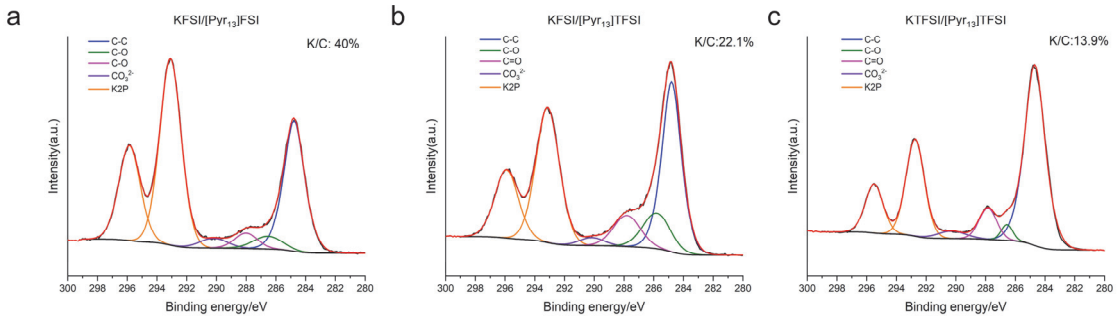

Figure 5.7. The K2p and C1s spectrum of the surface of PTCDA electrodes in (a) KFSI/[Pyr_{13}]FSI, (b) KFSI/[Pyr_{13}]TFSI and (c) KTFSI/[Pyr_{13}]TFSI ionic liquid electrolytes after galvanostatic cycling tests at 25mA/g for 5 cycles with additional 100 cycles at 100 mA/g

When the analysis shifts to organic electrolytes, the CEI layer formed on PTCDA electrodes shows a higher proportion of organic species when KFSI/ECPC electrolytes are used (figure 5.8 a). Additives are shown to significantly alter the inorganic ratio within the CEI. For ionic liquid-modified ECPC electrolytes, the characteristics of SEI of the pure FSI ionic liquid electrolyte are transferred to the CEI layer when KFSI/ECPC with 10% ionic liquid is used. The strong similarities in K/C ratios (approximately 40%) demonstrate that even a small addition of 10% IL can substantially influence the interfacial properties of the CEI on PTCDA electrodes (figure 5.8 b), which likely contributes to the improved cycling performance.

In contrast, the effects of conventional additives such as ES and FEC are less pronounced compared to IL additives. A notable exception is observed in carbonate electrolytes with excess FEC additives (figure 5.8f). In this case, the CEI layer consists predominantly of organic species, likely due to the excessive decomposition of FEC during cycling. This results in a polymer-like interface forming on the PTCDA electrodes. To further enhance the reliability of the quantitative data for the CEI layer, we conducted an analysis on a second spot (Spot 2) using a similar peak-fitting

method. As shown in Table 7, the K/C ratio yielded consistent results with low experimental error across all samples. Additionally, the average ratio further supports the magnitude relationship observed at the primary spot, reinforcing our confidence in the uniformity of the CEI layer on the graphite electrode. The error tests we did above, as performed in Chapter 4, demonstrate the homogeneity of the SEI analysis via XPS. Although the current measurements were limited to only two spots, our analysis indicates that selecting more detection spots in the future would yield more accurate and representative average quantitative XPS data.

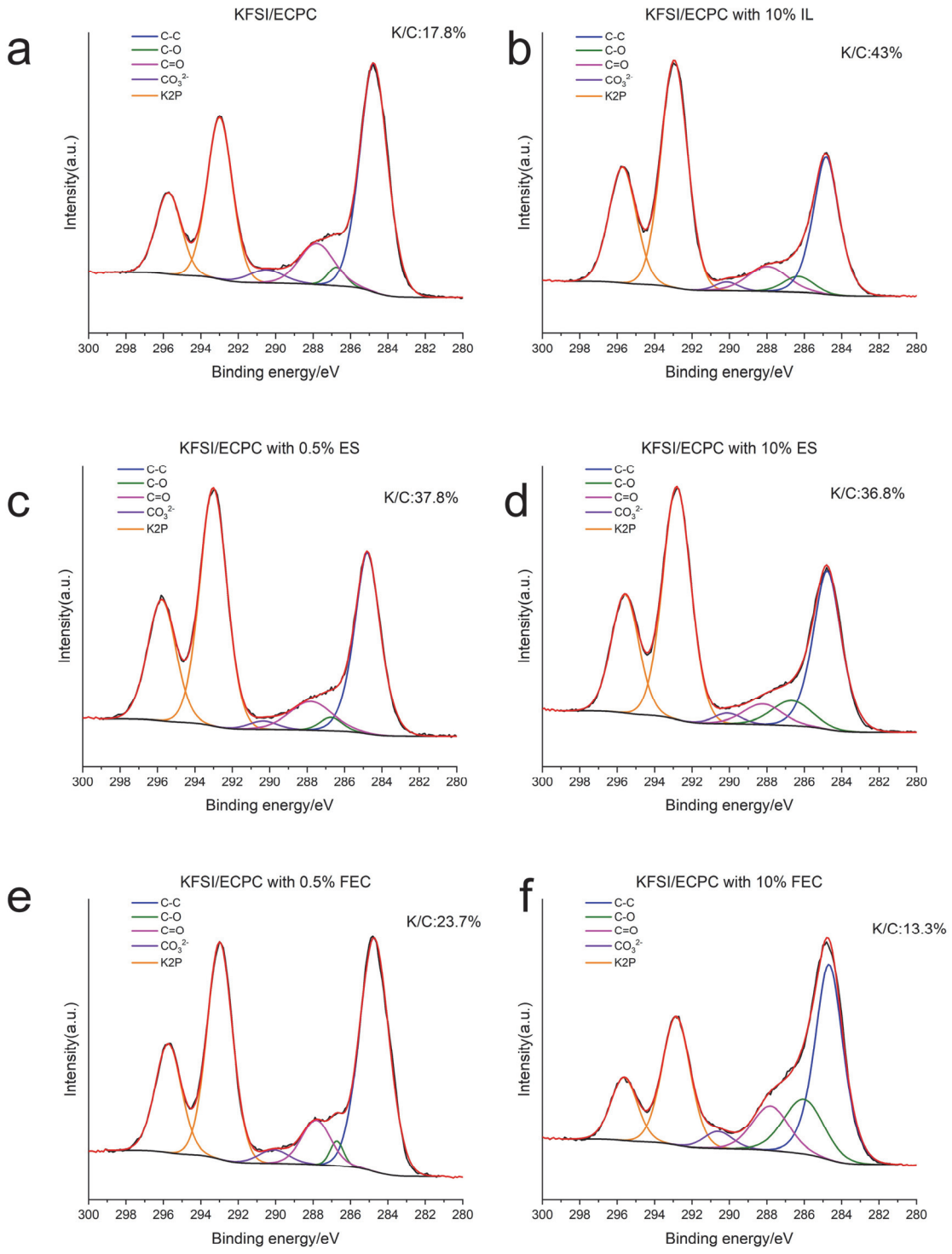

Figure 5.8. The K2p and C1s spectrum of the PTCDA electrodes cycled in ECPC electrolytes with (a) no additives, (b) 10% IL (c) 0.5% ES (d)10% ES (e) 0.5% FEC and (f) 10% FEC after galvanostatic cycling tests at 25mA/g for 5 cycles with additional 100 cycles at 100 mA/g

Table 7 The atomic radio of K/C in the surface CEI layer of two XPS measurement spots

	Main spot	Additional spot	Average
KFSI/[Pyr_{13}]FSI	40%	42.49%	41.24%
KFSI/[Pyr_{13}]TFSI	22.1%	21.80%	21.95%
KTFSI/[Pyr_{13}]TFSI	13.9%	14.70%	14.30%
KFSI/ECPC	17.8%	15.90%	16.85%
KFSI/ECPC with 10% IL	43%	42.80%	42.90%
KFSI/ECPC with 0.5% ES	37.8%	40.90%	39.35%
KFSI/ECPC with 10% ES	36.8%	32.20%	34.50%
KFSI/ECPC with 0.5% FEC	23.7%	25.80%	24.75%
KFSI/ECPC with 10% FEC	13.3%	14.56%	13.93%

In summary, the failure analysis of PTCDA electrodes highlights several key challenges and findings. The dissolution of PTCDA electrodes in electrolytes makes surface analysis particularly difficult. Conventional characterization techniques cannot fully exclude the effects of glass fiber intrusion during cycling. However, with the use of surface-sensitive XPS techniques, several important conclusions can still be drawn:

1. **Glassy Fiber Intrusion:** The intrusion of glass fibers is clearly observed in XPS surveys, identifying a potential failure mechanism in battery systems caused by separator degradation.
2. **Regulating the CEI Composition:** While the precise composition of the CEI on PTCDA electrodes remains unclear, the inorganic-to-organic ratio can be adjusted through the use of appropriate additives or by modifying the anions in ionic liquid electrolytes. This ratio can serve as a reference for designing a stable CEI layer to enhance the cycling performance of PTCDA electrodes. For example, KFSI/[Pyr_{13}FSI] and KFSI/ECPC with 10% ionic liquid both demonstrate excellent capacity retention and rate capability, with high K/C ratios of 40% and 43%, respectively. This suggests that a more inorganic CEI may be crucial for ensuring long-term cycling stability, consistent with findings from previous studies

Chapter 6 Summary and Conclusions

This thesis focuses on addressing the capacity decay problems in graphite electrodes and PTCDA electrodes for potassium-ion batteries (PIBs).

Through detailed failure analysis of ionic liquid and carbonate electrolytes in Chapter 3, we identify that the capacity failure in graphite electrodes primarily arises from the degradation of graphite materials and the progressive accumulation of the SEI layer. Using nondestructive XPS analysis with an inert environment transfer holder, we examined SEI layer accumulation both qualitatively and quantitatively, leveraging surface SEI analysis and Ar-ion etching XPS techniques.

By comparing cells with good retention to those exhibiting capacity failure, we identified SEI types that promote long-term cycling stability, particularly for KFSI/[Pyr_{13}]FSI and KFSI/[Pyr_{13}]TFSI ionic liquids. These stable SEI layers are distinguished by their inorganic-rich composition and limited accumulation of fluorine species over repeated cycles. This finding provides valuable guidance for designing electrolytes that support stable, long-term cycling performance. Specifically, we propose that the SEI layers formed by the promising 15 mol% KFSI/[Pyr_{13}]FSI ionic liquid electrolytes should serve as a foundation for developing more mixed-anion ionic liquid electrolytes. In addition to XPS surface analysis, other techniques such as SEM, TEM, and XRD were employed in the capacity failure analysis. While these methods provided supplementary chemical insights, the XPS analysis proved to be the most critical tool, particularly for understanding the evolution of SEI layers during cycling.

In **Chapter 4**, we extend the failure analysis to reinforce the conclusions drawn in **Chapter 3**. To modify the SEI layer formed by conventional ECPC electrolytes and enhance its inorganic content, specific additives, including ionic liquids (ILs) and standard additives, were incorporated into the ECPC

formulation to improve interfacial stability. ILs proved to be highly effective in increasing the inorganic content of the SEI layer, resulting in enhanced cycling stability. This finding indicates that incorporating ILs as additives can replicate certain beneficial characteristics of SEI layers formed by the pure FSI ionic liquid electrolyte. Surface XPS analysis played a critical role in identifying and understanding these SEI characteristics, providing key insights into their composition and stability.

In **Chapter 5**, we extend our analysis to PTCDA electrodes as a supplementary study alongside the primary graphite electrodes. The cycling stability of KFSI/[Pyr_{13}]FSI and KFSI/[Pyr_{13}]TFSI is similarly preserved with PTCDA electrodes, with Pyr_{13}FSI demonstrating its effectiveness as an additive in carbonate electrolytes for stabilizing PTCDA cycling performance. We further performed XPS analysis to uncover key characteristics of the CEI layer on PTCDA electrodes, emphasizing the formation of a stable inorganic CEI layer on the organic PTCDA material. These findings offer valuable insights for the future design of electrolytes in PIBs, particularly for enhancing the cycling performance of graphite electrodes and PTCDA electrodes.

References

1. Jian, Z., W. Luo, and X. Ji, *Carbon electrodes for K-ion batteries.* Journal of the American chemical society, 2015. **137**(36): p. 11566-11569.
2. Komaba, S., et al., *Potassium intercalation into graphite to realize high-voltage/high-power potassium-ion batteries and potassium-ion capacitors.* Electrochemistry Communications, 2015. **60**: p. 172-175.
3. Mohan, I., et al., *Potential of potassium and sodium-ion batteries as the future of energy storage: Recent progress in anodic materials.* Journal of Energy Storage, 2022. **55**: p. 105625.
4. Wang, L., et al., *Graphite as a potassium ion battery anode in carbonate-based electrolyte and ether-based electrolyte.* Journal of Power Sources, 2019. **409**: p. 24-30.
5. Zhao, J., et al., *Electrochemical intercalation of potassium into graphite.* Advanced Functional Materials, 2016. **26**(44): p. 8103-8110.
6. Lei, Y., et al., *Unveiling the influence of electrode/electrolyte interface on the capacity fading for typical graphite-based potassium-ion batteries.* Energy Storage Materials, 2020. **24**: p. 319-328.
7. Liu, Q., et al., *Artificial SEI for superhigh-performance K-graphite anode.* Advanced Science, 2021. **8**(9): p. 2003639.
8. Deng, D., *Li-ion batteries: basics, progress, and challenges.* Energy Science & Engineering, 2015. **3**(5): p. 385-418.
9. Wang, D., X. Du, and B. Zhang, *Solvent Molecular Design to Regulate the Intercalation Behavior in Ether Electrolyte for Stable Graphite Anodes in Potassium-Ion Batteries.* Small Structures, 2022. **3**(10): p. 2200078.
10. Du, X. and B. Zhang, *Robust solid electrolyte interphases in localized high concentration electrolytes boosting black phosphorus anode for potassium-ion batteries.* ACS nano, 2021. **15**(10): p. 16851-16860.
11. Fan, L., et al., *Graphite anode for a potassium-ion battery with unprecedented performance.* Angewandte Chemie, 2019. **131**(31): p. 10610-10615.
12. Xu, Z., et al., *Dispersion-corrected DFT investigation on defect chemistry and potassium migration in potassium-graphite intercalation compounds for potassium ion batteries anode materials.* Carbon, 2016. **107**: p. 885-894.
13. Peled, E. and S. Menkin, *SEI: past, present and future.* Journal of The Electrochemical Society, 2017. **164**(7): p. A1703.
14. An, Y., et al., *Commercial expanded graphite as a low–cost, long-cycling life anode for potassium–ion batteries with conventional carbonate electrolyte.* Journal of Power Sources, 2018. **378**: p. 66-72.
15. Fiore, M., et al., *Paving the way toward highly efficient, high-energy potassium-ion batteries with ionic liquid electrolytes.* Chemistry of Materials, 2020. **32**(18): p. 7653-7661.
16. Yoshii, K., et al., *Sulfonylamide-based ionic liquids for high-voltage potassium-ion batteries with honeycomb layered cathode oxides.* ChemElectroChem, 2019. **6**(15): p. 3901-3910.
17. Chen, Y., et al., *Organic electrode for non-aqueous potassium-ion batteries.* Nano Energy, 2015. **18**: p. 205-211.
18. Mohammadiroudbari, M., et al., *Porous bipolar polymers as organic cathodes for sustainable*

sodium/potassium-ion batteries. Journal of Materials Chemistry A, 2023. **11**(31): p. 16636-16647.
19. Wen, J., et al., *Nonfluorinated antisolvents for ultrastable potassium-ion batteries.* ACS nano, 2023. **17**(16): p. 16135-16146.
20. Jiang, Y., et al., *Optimized solid electrolyte interphase and solvation structure of potassium ions in carbonate electrolytes for high-performance potassium metal batteries.* Small, 2023. **19**(29): p. 2300411.
21. Jo, C.H. and S.T. Myung, *Role of Ether-Based Electrolytes in Enhancing Potential of Potassium-ion Batteries.* Advanced Energy Materials, 2024. **14**(21): p. 2400217.
22. Liu, S., et al., *An intrinsically non-flammable electrolyte for high-performance potassium batteries.* Angewandte Chemie International Edition, 2020. **59**(9): p. 3638-3644.
23. Fei, H., et al., *Stable all-solid-state potassium battery operating at room temperature with a composite polymer electrolyte and a sustainable organic cathode.* Journal of Power Sources, 2018. **399**: p. 294-298.
24. Xu, K., *Nonaqueous liquid electrolytes for lithium-based rechargeable batteries.* Chemical reviews, 2004. **104**(10): p. 4303-4418.
25. Aurbach, D., et al., *On the correlation between surface chemistry and performance of graphite negative electrodes for Li ion batteries.* Electrochimica acta, 1999. **45**(1-2): p. 67-86.
26. Lei, Y., et al., *Exploring stability of nonaqueous electrolytes for potassium-ion batteries.* ACS Applied Energy Materials, 2018. **1**(5): p. 1828-1833.
27. Sun, J., et al., *Anion-derived solid-electrolyte interphase enables long life Na-ion batteries using superconcentrated ionic liquid electrolytes.* ACS Energy Letters, 2021. **6**(7): p. 2481-2490.
28. Li, L., et al., *Developing better ester-and ether-based electrolytes for potassium-ion batteries.* Chemical Science, 2021. **12**(7): p. 2345-2356.
29. Qin, L., et al., *Localized high-concentration electrolytes boost potassium storage in high-loading graphite.* Advanced Energy Materials, 2019. **9**(44): p. 1902618.
30. Li, J., et al., *Weak cation–solvent interactions in ether-based electrolytes stabilizing potassium-ion batteries.* Angewandte Chemie International Edition, 2022. **61**(33): p. e202208291.
31. Lu, P., et al., *Chemistry, impedance, and morphology evolution in solid electrolyte interphase films during formation in lithium ion batteries.* The Journal of Physical Chemistry C, 2014. **118**(2): p. 896-903.
32. Lian, X., et al., *Dendrite-Free and High-Rate Potassium Metal Batteries Sustained by an Inorganic-Rich SEI.* Advanced Materials, 2024. **36**(9): p. 2306992.
33. Ozawa, K., *Lithium-ion rechargeable batteries with LiCoO2 and carbon electrodes: the LiCoO2/C system.* Solid State Ionics, 1994. **69**(3-4): p. 212-221.
34. Aurbach, D., et al., *A comparative study of synthetic graphite and Li electrodes in electrolyte solutions based on ethylene carbonate-dimethyl carbonate mixtures.* Journal of the Electrochemical Society, 1996. **143**(12): p. 3809.
35. Tarascon, J., et al., *Synthesis conditions and oxygen stoichiometry effects on Li insertion into the spinel LiMn2 O 4.* Journal of The Electrochemical Society, 1994. **141**(6): p. 1421.
36. Tarascon, J. and D. Guyomard, *New electrolyte compositions stable over the 0 to 5 V voltage*

range and compatible with the Li1+ xMn2O4/carbon Li-ion cells. Solid State Ionics, 1994. **69**(3-4): p. 293-305.

37. Ue, M., et al., *Electrochemical properties of quaternary ammonium salts for electrochemical capacitors.* Journal of the Electrochemical Society, 1997. **144**(8): p. 2684.
38. Aurbach, D., *Review of selected electrode–solution interactions which determine the performance of Li and Li ion batteries.* Journal of Power Sources, 2000. **89**(2): p. 206-218.
39. Shimizu, M., et al., *Kinetics study and degradation analysis through raman spectroscopy of graphite as a negative-electrode material for potassium-ion batteries.* The Journal of Physical Chemistry C, 2020. **124**(24): p. 13008-13016.
40. Eshetu, G.G., et al., *Impact of the electrolyte salt anion on the solid electrolyte interphase formation in sodium ion batteries.* Nano Energy, 2019. **55**: p. 327-340.
41. Qin, L., et al., *Pursuing graphite-based K-ion O 2 batteries: a lesson from Li-ion batteries.* Energy & Environmental Science, 2020. **13**(10): p. 3656-3662.
42. Xiao, N., W.D. McCulloch, and Y. Wu, *Reversible dendrite-free potassium plating and stripping electrochemistry for potassium secondary batteries.* Journal of the American Chemical Society, 2017. **139**(28): p. 9475-9478.
43. Onuma, H., et al., *Application of ionic liquid as K-ion electrolyte of graphite//K2Mn [Fe (CN) 6] cell.* ACS Energy Letters, 2020. **5**(9): p. 2849-2857.
44. Zhou, M., et al., *Less is more: trace amount of a cyclic sulfate electrolyte additive enable ultra-stable graphite anode for high-performance potassium-ion batteries.* ACS Applied Materials & Interfaces, 2022. **14**(39): p. 44429-44438.
45. Xu, W., et al., *A localized high concentration electrolyte for 4 V-class potassium metal batteries.* Energy Advances, 2022. **1**(4): p. 191-196.
46. Yamada, Y. and A. Yamada, *Superconcentrated electrolytes to create new interfacial chemistry in non-aqueous and aqueous rechargeable batteries.* Chemistry Letters, 2017. **46**(8): p. 1056-1064.
47. Yamada, Y., et al., *Advances and issues in developing salt-concentrated battery electrolytes.* Nature Energy, 2019. **4**(4): p. 269-280.
48. Freemantle, M., *An introduction to ionic liquids.* 2010: Royal Society of chemistry.
49. Yamamoto, T., et al., *Physicochemical and electrochemical properties of K [N (SO2F) 2]–[N-methyl-N-propylpyrrolidinium][N (SO2F) 2] ionic liquids for potassium-ion batteries.* The Journal of Physical Chemistry C, 2017. **121**(34): p. 18450-18458.
50. Yamamoto, T., R. Matsubara, and T. Nohira, *Highly conductive ionic liquid electrolytes for potassium-ion batteries.* Journal of Chemical & Engineering Data, 2021. **66**(2): p. 1081-1088.
51. Gu, M., et al., *In situ formed uniform and elastic SEI for high-performance batteries.* Energy & Environmental Science, 2023. **16**(3): p. 1166-1175.
52. Yamamoto, T., A. Yadav, and T. Nohira, *Charge–Discharge Behavior of Graphite Negative Electrodes in FSA-Based Ionic Liquid Electrolytes: Comparative Study of Li-, Na-, K-Ion Systems.* Journal of The Electrochemical Society, 2022. **169**(5): p. 050507.
53. Jeon, J., et al., *Long-life potassium metal batteries enabled by anion-derived solid electrolyte interphase using concentrated ionic liquid electrolytes.* Journal of Colloid and Interface Science, 2024. **670**: p. 617-625.
54. Beltrop, K., et al., *Alternative electrochemical energy storage: potassium-based dual-graphite batteries.* Energy & Environmental Science, 2017. **10**(10): p. 2090-2094.

55. Arnaiz, M., et al., *Aprotic and protic ionic liquids combined with olive pits derived hard carbon for potassium-ion batteries.* Journal of The Electrochemical Society, 2019. **166**(14): p. A3504.
56. De Vos, N., C. Maton, and C.V. Stevens, *Electrochemical stability of ionic liquids: general influences and degradation mechanisms.* ChemElectroChem, 2014. **1**(8): p. 1258-1270.
57. Kroon, M.C., et al., *Decomposition of ionic liquids in electrochemical processing.* Green Chemistry, 2006. **8**(3): p. 241-245.
58. Forsyth, M., et al., *Tuning sodium interfacial chemistry with mixed-anion ionic liquid electrolytes.* ACS applied materials & interfaces, 2019. **11**(46): p. 43093-43106.
59. Nádherná, M., et al., *Lithium bis (fluorosulfonyl) imide–PYR14TFSI ionic liquid electrolyte compatible with graphite.* Journal of power sources, 2011. **196**(18): p. 7700-7706.
60. Chatel, G., et al., *Mixing ionic liquids–"simple mixtures" or "double salts"?* Green Chemistry, 2014. **16**(4): p. 2051-2083.
61. Kerner, M., et al., *Ionic liquid based lithium battery electrolytes: fundamental benefits of utilising both TFSI and FSI anions?* Physical Chemistry Chemical Physics, 2015. **17**(29): p. 19569-19581.
62. Zhang, S.S., *A review on electrolyte additives for lithium-ion batteries.* Journal of Power Sources, 2006. **162**(2): p. 1379-1394.
63. Ryou, M.-H., et al., *Effect of fluoroethylene carbonate on high temperature capacity retention of LiMn2O4/graphite Li-ion cells.* Electrochimica Acta, 2010. **55**(6): p. 2073-2077.
64. Son, H.B., et al., *Effect of reductive cyclic carbonate additives and linear carbonate co-solvents on fast chargeability of LiNi0. 6Co0. 2Mn0. 2O2/graphite cells.* Journal of Power Sources, 2018. **400**: p. 147-156.
65. Wang, D.Y., et al., *A comparative study of vinylene carbonate and fluoroethylene carbonate additives for LiCoO2/graphite pouch cells.* Journal of the Electrochemical Society, 2014. **161**(4): p. A467.
66. Michan, A.L., et al., *Fluoroethylene carbonate and vinylene carbonate reduction: understanding lithium-ion battery electrolyte additives and solid electrolyte interphase formation.* Chemistry of Materials, 2016. **28**(22): p. 8149-8159.
67. Ells, A.W., R. May, and L.E. Marbella, *Potassium fluoride and carbonate lead to cell failure in potassium-ion batteries.* ACS Applied Materials & Interfaces, 2021. **13**(45): p. 53841-53849.
68. Yoon, S.U., et al., *Effects of fluoroethylene carbonate-induced solid-electrolyte-interface layers on carbon-based anode materials for potassium ion batteries.* Applied Surface Science, 2021. **547**: p. 149193.
69. Lowndes, R. and D. Martin, *Dielectric constants of ionic crystals and their variations with temperature and pressure.* Proceedings of the Royal Society of London. A. Mathematical and Physical Sciences, 1970. **316**(1526): p. 351-375.
70. Li, A., et al., *Effects of ethylene sulfite as a supplementary film-forming additive on the electrochemical performance of graphite anode in EC-based electrolyte.* Ionics, 2015. **21**: p. 2431-2438.
71. Li, X., et al., *Ethylene sulfate as film formation additive to improve the compatibility of graphite electrode for lithium-ion battery.* Ionics, 2014. **20**: p. 795-801.
72. Tong, B., et al., *Sulfur-containing compounds as electrolyte additives for lithium-ion batteries.* InfoMat, 2021. **3**(12): p. 1364-1392.

73. Haregewoin, A.M., A.S. Wotango, and B.-J. Hwang, *Electrolyte additives for lithium ion battery electrodes: progress and perspectives.* Energy & Environmental Science, 2016. **9**(6): p. 1955-1988.
74. Zhao, W., et al., *Recent advances in the research of functional electrolyte additives for lithium-ion batteries.* Current Opinion in Electrochemistry, 2017. **6**(1): p. 84-91.
75. Plylahan, N., et al., *Ionic liquid and hybrid ionic liquid/organic electrolytes for high temperature lithium-ion battery application.* Electrochimica Acta, 2016. **216**: p. 24-34.
76. Bae, S.-Y., E.-G. Shim, and D.-W. Kim, *Effect of ionic liquid as a flame-retarding additive on the cycling performance and thermal stability of lithium-ion batteries.* Journal of power sources, 2013. **244**: p. 266-271.
77. Javadian, S., et al., *Effect of imidazolium-based ionic liquid as electrolyte additive on electrochemical performance of 18650 cylindrical Li-ion batteries at room and 60° C temperatures.* Journal of the Iranian Chemical Society, 2019. **16**: p. 2123-2134.
78. Nakagawa, H., *Electrolytes containing ionic liquids for improved safety of lithium-ion batteries.* Electrochemistry, 2015. **83**(9): p. 707-710.
79. Yang, H., et al., *Potassium difluorophosphate as an electrolyte additive for potassium-ion batteries.* ACS applied materials & interfaces, 2020. **12**(32): p. 36168-36176.
80. Yuan, F., et al., *Key factor determining the cyclic stability of the graphite anode in Potassium-Ion batteries.* ACS nano, 2022. **16**(8): p. 12511-12519.
81. Nyman, A., et al., *Analysis of the polarization in a Li-ion battery cell by numerical simulations.* Journal of The Electrochemical Society, 2010. **157**(11): p. A1236.
82. Kim, D.-H., et al., *Toward fast operation of lithium batteries: ion activity as the factor to determine the concentration polarization.* ACS Energy Letters, 2019. **4**(6): p. 1265-1270.
83. Aurbach, D., et al., *A short review of failure mechanisms of lithium metal and lithiated graphite anodes in liquid electrolyte solutions.* Solid state ionics, 2002. **148**(3-4): p. 405-416.
84. Wang, H., et al., *A depth-profiling study on the solid electrolyte interface: Bis (fluorosulfuryl) imide anion toward improved K+ storage.* ACS Applied Energy Materials, 2019. **2**(11): p. 7942-7951.
85. Zhou, M., et al., *Electrolytes and interphases in potassium ion batteries.* Advanced materials, 2021. **33**(7): p. 2003741.
86. Wang, H., D. Zhai, and F. Kang, *Solid electrolyte interphase (SEI) in potassium ion batteries.* Energy & Environmental Science, 2020. **13**(12): p. 4583-4608.
87. Zhang, J., et al., *Stabilizing SEI by cyclic ethers toward enhanced K+ storage in graphite.* Journal of Energy Chemistry, 2022. **71**: p. 344-350.
88. Huang, J., et al., *Bismuth microparticles as advanced anodes for potassium-ion battery.* Advanced Energy Materials, 2018. **8**(19): p. 1703496.
89. Zeng, G., et al., *Non-flammable phosphate electrolyte with high salt-to-solvent ratios for safe potassium-ion battery.* Journal of The Electrochemical Society, 2019. **166**(6): p. A1217-A1222.
90. Shan, X., et al., *A brief review on solid electrolyte interphase composition characterization technology for lithium metal batteries: challenges and perspectives.* The Journal of Physical Chemistry C, 2021. **125**(35): p. 19060-19080.
91. Chu, Y., et al., *Advanced characterizations of solid electrolyte interphases in lithium-ion batteries.* Electrochemical energy reviews, 2020. **3**: p. 187-219.

92. Fadley, C.S., *X-ray photoelectron spectroscopy: Progress and perspectives*. Journal of Electron Spectroscopy and Related Phenomena, 2010. **178**: p. 2-32.
93. Powell, C. and A. Jablonski, *Surface sensitivity of X-ray photoelectron spectroscopy.* Nuclear Instruments and Methods in Physics Research Section A: Accelerators, Spectrometers, Detectors and Associated Equipment, 2009. **601**(1-2): p. 54-65.
94. Matthew, J., *Surface analysis by Auger and x-ray photoelectron spectroscopy. D. Briggs and JT Grant (eds). IMPublications, Chichester, UK and SurfaceSpectra, Manchester, UK, 2003. 900 pp., ISBN 1-901019-04-7, 900 pp*. 2004, Wiley Online Library.
95. Gu, M., et al., *Regulating solvent molecule coordination with KPF6 for superstable graphite potassium anodes.* ACS nano, 2021. **15**(5): p. 9167-9175.
96. Li, J., et al., *Weak cation–solvent interactions in ether-based electrolytes stabilizing potassium-ion batteries.* Angewandte Chemie, 2022. **134**(33): p. e202208291.
97. Yu, D., et al., *Unraveling the role of ion-solvent chemistry in stabilizing small-molecule organic cathode for potassium-ion batteries.* Energy Storage Materials, 2021. **43**: p. 172-181.
98. Chen, H., et al., *Use of a water-in-salt electrolyte to avoid organic material dissolution and enhance the kinetics of aqueous potassium ion batteries.* Sustainable Energy & Fuels, 2020. **4**(1): p. 128-131.
99. Zheng, J., et al., *Recent Advances in Potassium-Ion Batteries: From Material Design to Electrolyte Engineering.* Advanced Materials Technologies, 2023. **8**(8): p. 2201591.
100. Xu, C. and Z. Cheng, *Thermal stability of ionic liquids: Current status and prospects for future development.* Processes, 2021. **9**(2): p. 337.
101. Arbizzani, C., G. Gabrielli, and M. Mastragostino, *Thermal stability and flammability of electrolytes for lithium-ion batteries.* Journal of Power Sources, 2011. **196**(10): p. 4801-4805.
102. Rothermel, S., et al., *Dual-graphite cells based on the reversible intercalation of bis (trifluoromethanesulfonyl) imide anions from an ionic liquid electrolyte.* Energy & Environmental Science, 2014. **7**(10): p. 3412-3423.
103. Verma, P., P. Maire, and P. Novák, *A review of the features and analyses of the solid electrolyte interphase in Li-ion batteries*. Electrochimica Acta, 2010. **55**(22): p. 6332-6341.
104. Edstroem, K., T. Gustafsson, and J.O. Thomas, *The cathode–electrolyte interface in the Li-ion battery.* Electrochimica Acta, 2004. **50**(2-3): p. 397-403.
105. Giffin, G.A., *The role of concentration in electrolyte solutions for non-aqueous lithium-based batteries*. nature communications, 2022. **13**(1): p. 5250.
106. Ravikumar, B., M. Mynam, and B. Rai, *Effect of salt concentration on properties of lithium ion battery electrolytes: a molecular dynamics study.* The Journal of Physical Chemistry C, 2018. **122**(15): p. 8173-8181.
107. Zhang, X., et al., *Electrochemical impedance spectroscopy study of lithium-ion capacitors: Modeling and capacity fading mechanism.* Journal of Power Sources, 2021. **488**: p. 229454.
108. Bouchet, R., S. Lascaud, and M. Rosso, *An EIS study of the anode Li/PEO-LiTFSI of a Li polymer battery.* Journal of the electrochemical society, 2003. **150**(10): p. A1385.
109. Zhu, Y., et al., *Comparison of electrochemical performances of olivine NaFePO 4 in sodium-ion batteries and olivine LiFePO 4 in lithium-ion batteries.* Nanoscale, 2013. **5**(2): p. 780-787.
110. Zhang, S.S., K. Xu, and T. Jow, *EIS study on the formation of solid electrolyte interface in Li-ion battery.* Electrochimica acta, 2006. **51**(8-9): p. 1636-1640.

111. Randles, J.E.B., *Kinetics of rapid electrode reactions.* Discussions of the faraday society, 1947. **1**: p. 11-19.
112. Cruz-Manzo, S. and P. Greenwood, *An impedance model based on a transmission line circuit and a frequency dispersion Warburg component for the study of EIS in Li-ion batteries*. Journal of Electroanalytical Chemistry, 2020. **871**: p. 114305.
113. Grulke, E.A., et al., *Size and shape distributions of carbon black aggregates by transmission electron microscopy.* Carbon, 2018. **130**: p. 822-833.
114. Perdigao, J., P. Lambrechts, and G. Vanherle, *Microscopy investigations: techniques, results, limitations*. Am. J. Dent, 2000. **13**: p. 3D18D.
115. Warren, B., *X-ray Diffraction*. Vol. 208. 1990: Dover.
116. Igarashi, D., et al., *Effect of crystallinity of synthetic graphite on electrochemical potassium intercalation into graphite.* Electrochemistry, 2021. **89**(5): p. 433-438.
117. Smart, M., et al., *Irreversible capacities of graphite in low-temperature electrolytes for lithium-ion batteries.* Journal of The Electrochemical Society, 1999. **146**(11): p. 3963.
118. Han, B., et al., *Additive stabilization of SEI on graphite observed using cryo-electron microscopy.* Energy & Environmental Science, 2021. **14**(9): p. 4882-4889.
119. Unocic, R.R., et al., *Direct visualization of solid electrolyte interphase formation in lithium-ion batteries with in situ electrochemical transmission electron microscopy.* Microscopy and Microanalysis, 2014. **20**(4): p. 1029-1037.
120. Chen, X., X. Wang, and D. Fang, *A review on C1s XPS-spectra for some kinds of carbon materials.* Fullerenes, Nanotubes and Carbon Nanostructures, 2020. **28**(12): p. 1048-1058.
121. Zhang, S.S., *A review on the separators of liquid electrolyte Li-ion batteries.* Journal of power sources, 2007. **164**(1): p. 351-364.
122. Henderson, J., *The raw materials of early glass production.* Oxford Journal of Archaeology, 1985. **4**(3): p. 267-291.
123. Song, J., et al., *Interphases in sodium-ion batteries.* Advanced Energy Materials, 2018. **8**(17): p. 1703082.
124. Santos, A.R., R.K. Blundell, and P. Licence, *XPS of guanidinium ionic liquids: a comparison of charge distribution in nitrogenous cations*. Physical Chemistry Chemical Physics, 2015. **17**(17): p. 11839-11847.
125. Hurisso, B.B., K.R. Lovelock, and P. Licence, *Amino acid-based ionic liquids: using XPS to probe the electronic environment via binding energies.* Physical Chemistry Chemical Physics, 2011. **13**(39): p. 17737-17748.
126. Morales-Ugarte, J., et al., *EIS and XPS investigation on SEI layer formation during first discharge on graphite electrode with a vinylene carbonate doped imidazolium based ionic liquid electrolyte.* The Journal of Physical Chemistry C, 2018. **122**(32): p. 18223-18230.
127. Zhuang, Q.-C., J. Li, and L.-L. Tian, *Potassium carbonate as film forming electrolyte additive for lithium-ion batteries.* Journal of power sources, 2013. **222**: p. 177-183.
128. Wang, D., et al., *Cyclic Ether-Based Electrolyte with a Weak Solvation Structure for Advanced Potassium Metal Batteries*. Small, 2024: p. 2403642.
129. Dhir, S., et al., *Fundamental investigations on the ionic transport and thermodynamic properties of non-aqueous potassium-ion electrolytes*. Nature communications, 2023. **14**(1): p. 3833.
130. Greczynski, G. and L. Hultman, *X-ray photoelectron spectroscopy: towards reliable binding*

energy referencing. Progress in Materials Science, 2020. **107**: p. 100591.

131. Qiu, L., K. Zou, and G. Xu, *Investigation on the sulfur state and phase transformation of spent and regenerated S zorb sorbents using XPS and XRD.* Applied surface science, 2013. **266**: p. 230-234.
132. Liao, F., et al., *Electrochemical lithiation and passivation mechanisms of iron monosulfide thin film as negative electrode material for lithium-ion batteries studied by surface analytical techniques.* Applied surface science, 2013. **283**: p. 888-899.
133. Jiang, X., et al., *A Nonflammable Na+-Based Dual-Carbon Battery with Low-Cost, High Voltage, and Long Cycle Life.* Advanced Energy Materials, 2018. **8**(36): p. 1802176.
134. Sacci, R.L., et al., *Nanoscale imaging of fundamental Li battery chemistry: solid-electrolyte interphase formation and preferential growth of lithium metal nanoclusters.* Nano letters, 2015. **15**(3): p. 2011-2018.
135. Sun, H.-H., et al., *In situ formation of a multicomponent inorganic-rich SEI layer provides a fast charging and high specific energy Li-metal battery.* Journal of Materials Chemistry A, 2019. **7**(30): p. 17782-17789.
136. Wang, H., et al., *Flame-Retardant Nonaqueous Electrolytes for High-Safety Potassium-Ion Batteries.* Small Methods, 2024. **8**(7): p. 2301104.
137. Lei, Y., et al., *Achieving ultralong cycle life graphite binary intercalation in intermediate-concentration ether-based electrolyte for potassium-ion batteries.* Carbon, 2022. **196**: p. 229-235.
138. Zhao, Y., et al., *Electrolyte-Induced Morphology Evolution to Boost Potassium Storage Performance of Perylene-3, 4, 9, 10-tetracarboxylic Dianhydride.* Nano Letters, 2024. **24**(15): p. 4546-4553.
139. Wang, H., et al., *Highly stable potassium metal batteries enabled by regulating surface chemistry in ether electrolyte.* Energy Storage Materials, 2021. **42**: p. 526-532.
140. Xia, L., et al., *Oxidation Decomposition Mechanism of Fluoroethylene Carbonate-Based Electrolytes for High-Voltage Lithium Ion Batteries: A DFT Calculation and Experimental Study.* ChemistrySelect, 2017. **2**(24): p. 7353-7361.
141. Lingappan, N., et al., *A comprehensive review of separator membranes in lithium-ion batteries.* Renewable and Sustainable Energy Reviews, 2023. **187**: p. 113726.
142. Torcheux, L., A. Mayeux, and M. Chemla, *Electrochemical coupling effects on the corrosion of silicon samples in HF solutions.* Journal of The Electrochemical Society, 1995. **142**(6): p. 2037.
143. Han, X., et al., *CEI Optimization: Enable the High Capacity and Reversible Sodium-Ion Batteries for Future Massive Energy Storage*. Advanced Energy and Sustainability Research, 2024. **5**(1): p. 2300166.